2022

Bipolar Electroactive Conducting Polymers for Wireless Cell Stimulation

Chunyan Qin

UNIVERSITY
OF WOLLONGONG
AUSTRALIA

Bipolar Electroactive Conducting Polymers for Wireless Cell Stimulation

Chunyan Qin, B.A., B.Eng., M.Sc.

Supervisors:

Prof Jun Chen, Prof Gordon G. Wallace, Dr Zhilian Yue and Prof Xu-Feng Huang

This thesis is presented as part of the requirement for the conferral of the degree:

Doctor of Philosophy

University of Wollongong

School of Chemistry and Molecular Bioscience

February 2022

Abstract

Electrochemical stimulation (ES) promotes wound healing and tissue regeneration in biomedical applications and clinical studies and is central to the emerging field of electroceuticals. Traditional ES such as deep brain stimulation for Parkinson's disease, utilises metal electrodes that are "hard wired" to a power supply to deliver the stimulation. Bipolar electrochemistry (BPE) introduces an innovative approach to cell stimulation that is wireless. Developing conducting polymers (CPs)-based stimulation platforms wireless powdered by BPE bipolar will provide an exciting new dimension to medical bionics. In this project, Chapter 2 deals with development of a bipolar electrochemical activity testing system and bipolar electrochemical stimulation (BPES) system. Then, bipolar electroactive and biocompatible CPs grown on FTO substrate are successfully synthesised, modified, and characterised in Chapter 3 and Chapter 4 using the above systems prior to using for wireless cell stimulation. Furthermore, free standing and soft CP templates are developed (Chapter 5). More importantly, all these bipolar electroactive CPs have been applied to wireless cell stimulation using BPE (all research Chapters). Significant increase in both cell number and neurite growth has been demonstated, suggesting that the BPES system is highly efficient for stimulation of animal PC 12 cell and human SH-SY5Y cell. More specific information is presented in each chapter as below.

In Chapter 3, a CP-based bipolar electrochemical stimulation (BPES) system for cell stimulation was present. Polypyrrole (PPy) films with different dopants have demonstrated reversible and recoverable bipolar electrochemical activity under a low driving DC voltage (<5.5 V). This BPES system enabling wireless and programmable

cell stimulation has been devised using PPy co-doped with dextran sulfate (DS) and collagen (PPy-DS-collagen/FTO) as a bipolar electrode and rat pheochromocytoma cells as a model cell line. Significantly, wireless BPES enhances cell proliferation and differentiation, evidenced by increased PC 12 cells number and extensive neurites outgrowth. The work establishes a new paradigm for the wireless electrochemical stimulation of cells using a CP as the bipolar electrode.

In Chapter 4, redox active CP dopants were integrated into the CP backbone to address the poor bipolar electroactivity. Poly (2-methoxyaniline-5-sulfonic acid) (PMAS) was utilised to enhance the electrochemical properties of the PPy matrix, evidenced by *in situ* spectroscopy and electrochemistry. Significantly, *in vitro* cultivation and BPES of rat PC 12 cells on PPy-PMAS-DS-collagen/FTO showed a significant increase in cell growth and neurites extension. This opens the avenues of using highly conducting PMAS modified PPy to create soft templates without electroactivity loss.

In Chapter 5, a soft template (PPy-PMAS-collagen/PEDOT-PSS) comprises poly(3,4-ethylenedioxythiophene)-poly(styrenesulfonate) (PEDOT-PSS) that provides mechanical and structural support to a blend of highly conducting PMAS modified PPy. *In vitro* cultivation and BPES of PC 12 cells on the prepared soft templates showed a significant increase in cell growth and neurites extension. Furthermore, the potential application of the soft CP-based BPES system to human cells was reported. Significantly, the new BPES platform greatly encouraged human neuroblastoma SH-SY5Y cells to differentiate and form extensive neuronal phenotypes and neural networks. This represents the possibility of using the soft template based BPES system

in vivo and clinical applications related to translational models of human mental disorders.

In summary, this thesis provides insights into the fundamental bipolar electroactive CPs for living cell stimulation in a wireless way. At this stage, translation of soft CP templates based BPES systems from animal cell lines to human cell lines measurement and operation is not straightforward and requires further dedicated investigations.

Acknowledgments

With the end of my pursuing PhD journey in sight, I would like to express sincere gratitude to all people who offer me countless support since July 2017.

First of all, I am extremely grateful to my supervisors Prof Jun Chen, Prof Gordon G. Wallace, Dr Zhilian Yue and Prof Xu-Feng Huang for the opportunity to carry out my brand-new research, and for their invaluable advice, continuous support and patient mentoring during this interdisciplinary project all along the way. I would like to thank to Prof. Jun Chen on telling me both the scientific investigation and communication as clearly as possible. Thanks to Prof. Gordon G. Wallace, whose dynamism, perspective and charming work motivation and enthusiasm have deeply inspired me. I would also like to thank to Dr. Zhilian Yue and Prof. Xu-Feng Huang. Their warm encouragement, immense knowledge and plentiful experience have been of great mental and technical help. My special thanks to Prof. Robert J. Forster from Dublin City University who has been closely following this work through monthly conference calls since I commenced my PhD. He has been always motivated and helped me instantly. Thanks for his invitation to give me a wonderful research period in Dublin, making my life colourful.

I appreciate all the technical support from the members of IPRI, TRICEP, ANFF-Material Node and EMC. I am very much thankful to Dr Andrew Nattestad, Dr Patricia Hayes, Dr Kerry Gilmore and Dr Gregory Ryder for support with spectra measurements, cell culture/imaging training and PMAS synthesis. Without all the support, it would be impossible for me to complete this project smoothly. Thanks to Dr. Tian Zheng, Dr.

Yuqing Liu, Dr. Yuyang Hou, Dr. Yu Ge, Dr. Yong Zhao, Dr. Changchun Yu, Dr. Dan Yang, Dr. Dandan Cui, Dr. Yunfeng Chao… and my teammates (Shuai Zhang, Lisha jia, Yuetong Zhou…) for providing a fantastic working environment and spending your cherished time with me in the lab and social life over the past few years. I am honoured to witness most of you were awarded the doctoral degree. I am looking forward to mine.

Huge thanks to my beloved friends Dr. Yuqing Liu, Dr. Tian Zheng, Ms. Sha He, Ms. Zhidan Wu and Ms. Fenglin Liu for their regular checking on me, chatting and constant encouragement. I am also extending my thanks to Mr. Zhihui Ma who is the one to tell me to push myself and be brave to embrace new things. Additionally, I express my sincere appreciation to Mr. Murray Dunne, for your coming, your recognition, your encouragement, and your care. You always tell me to stay positive, stay strong, think the best of things and be good. Carrying these with me, a light against my daily darkness, I struggle to renew passion and expectations in life. Great thanks to Mr. & Mrs. Dunne as well, you are cute, funny, and warm-hearted. Thanks for your gorgeous flowers, tulips, orchids, chrysanthemum etc., I love them.

My most appreciation goes to my family, to my parents who have nothing about what I am doing but never doubt my choice on my study and life. To my big sister, Ms. Chunqin Qin, you have been staying and taking care of our parents since I left China. Although you are always in trouble, I am in your debt. Thanks to my cute and naughty nephews for the happiness they bring to my parents. At last, I want to thank myself, for not giving up all these years. Please keep believe that science can teach you more about what is out there.

Certification

I, Chunyan Qin, declare that this thesis submitted in fulfilment of the requirements for the conferral of the degree Doctor of Philosophy, from the University of Wollongong, is wholly my own work unless otherwise referenced or acknowledged. This document has not been submitted for qualifications at any other academic institution.

_____

Chunyan Qin
1st February 2022

Publications

1. **Chunyan Qin**, Zhilian Yue, Xu-Feng Huang, Gordon G. Wallace, and Jun Chen. "Emerging bipolar electroactive conducting polymer architectures toward wireless electrostimulation - bipolar electrostimulation". (Under final revision).

2. **Chunyan Qin**, Zhilian Yue, Yunfeng Chao, Robert J. Forster, Fionn Ó. Maolmhuaidh, Xu-Feng Huang, Stephen Beirne, Gordon G. Wallace, and Jun Chen. "Data on the bipolar electroactive conducting polymers for wireless cell stimulation". Data in Brief 33 (2020) 106406.

3. **Chunyan Qin**, Zhilian Yue, Yunfeng Chao, Robert J. Forster, Fionn Ó. Maolmhuaidh, Xu-Feng Huang, Stephen Beirne, Gordon G. Wallace, and Jun Chen. "Data on the bipolar electroactive conducting polymers for wireless cell stimulation". Mendeley Data, V1, doi: 10.17632/4zgkyfxhcd.1.

4. **Chunyan Qin**, Zhilian Yue, Yunfeng Chao, Robert J. Forster, Fionn Ó. Maolmhuaidh, Xu-Feng Huang, Stephen Beirne, Gordon G. Wallace, and Jun Chen. "Bipolar electroactive conducting polymers for wireless cell stimulation". Applied Materials Today 21 (2020) 100804.

5. **Chunyan Qin**, Zhilian Yue, Xu-Feng Huang, Robert J. Forster, Gordon G. Wallace, and Jun Chen. "Enhanced wireless cell stimulation using soft and improved bipolar electroactive conducting polymer templates". Applied Materials Today 27 (2022) 101481.

6. **Chunyan Qin**, Zhilian Yue, Xu-Feng Huang, Robert J. Forster, Gordon G. Wallace, and Jun Chen. "Data on enhanced wireless cell stimulation using soft and improved bipolar electroactive conducting polymer templates". Data in Brief, under revision.

7. **Chunyan Qin**, Zhilian Yue, Xu-Feng Huang, Robert J. Forster, Gordon G. Wallace,

and Jun Chen. “Data on enhanced wireless cell stimulation using soft and improved bipolar electroactive conducting polymer templates”. Mendeley Data, V1, doi: 10.17632/j8cxgm5d9k.1.

8. Yunfeng Chao, Yu Ge, Yong Zhao, Jicheng Jiang, Caiyun Wang, **Chunyan Qin**, Amruthalakshmi Vijayakumar, Changchun Yu, and Gordon G. Wallace. “Tuning the structure of three dimensional nanostructured molybdenum disulfide/nitrogen-doped carbon composite for high lithium storage”. Electrochimica Acta 291 (2018) 197-205.

9. Yunfeng Chao, Kezhong Wang, Rouhollah Jalili, Alexander Morlando, **Chunyan Qin**, Amruthalakshmi Vijayakumar, Caiyun Wang, and Gordon G. Wallace. “Scalable Solution Processing MoS2 Powders with Liquid Crystalline Graphene Oxide for Flexible Freestanding Films with High Areal Lithium Storage Capacity”. *ACS Applied Materials & Interfaces* 2019 *11* (50), 46746-46755.

10. Yuqing Liu, Shuai Zhang, Stephen Beirne, Kyuman Kim, **Chunyan Qin**, Yumeng Du, Yuetong Zhou, Zhenxiang Cheng, Gordon G. Wallace, and Jun Chen. “Wearable Photo-Thermo-Electrochemical Cells (PTECs) Harvesting Solar Energy”. Macromolecular Rapid Communications 2022, 43, 2200001.

Conference Presentations

1. Oral presentation: “Bipolar electroactive conducting polymers for wireless cell stimulation” at the Virtual International Conference on Biofabrication 2021 (27 - 29 September 2021).

2. Oral presentation about “Bipolar electroactive conducting polymers for wireless cell stimulation” at the 72nd Annual Virtual Meeting of the International Society of Electrochemistry (29 August - 3 September 2021).

3. Oral presentation: “Bipolar electroactive conducting polymer for wireless cell stimulation” at 2021 ACES Full Virtual Centre Meeting (7 - 8 June 2021).

4. Oral presentation: “Bipolar electroactive conducting polymers for wireless cell stimulation” at the 15th Annual Virtual Electromaterials Science Symposium (3 - 5 February 2021).

5. Oral presentation: “Conducting polymer based bipolar electrochemistry for potential wireless cell stimulation” at the 11th Virtual World Biomaterials Congress 2020 (11-15 December 2020).

6. Oral presentation: “Bipolar electroactive conducting polymers for wireless cell stimulation” at the Virtual Bill Wheeler Community Symposium 2020 (22 September 2020).

7. Oral presentation: “Bipolar electroactive conducting polymers - a wireless stimulation” at 2020 ACES Full Virtual Centre Meeting (20 - 21 August 2020).

8. Oral presentation: “Update of bipolar electroactive conducting polymers for wireless cell stimulation” at ACES_All Virtual Meeting (July 2020).

9. Oral presentation: “Bipolar electroactive conducting polymers for wireless cell stimulation” at IPRI seminar (23 April 2020).

10. Poster presentation: “Bipolar electrostimulation - a wireless platform for cell stimulation enabled by conducting polymers” at the 14th Annual Electromaterials Science Symposium, Australian National University, Canberra (5 - 7 February 2020).

11. Oral presentation: “Conducting polymer based bipolar electrochemistry for wireless stimulation” at the IHMRI-ACES NSW Office Health and Medical Research Funding Workshop, University of Wollongong, Wollongong (17 September 2019).

12. Oral presentation: “Bipolar electroactive conducting polymers for wireless cell stimulation” at the Bill Wheeler Community Symposium 2019, University of Wollongong, Wollongong (15 August 2019).

13. Oral presentation: “Update of bipolar electroactive conducting polymers for wireless cell stimulation” at ACES_All Virtual Meeting (July 2019).

14. Oral presentation: “Conducting polymer based bipolar electrochemistry for wireless stimulation” at the Materials in Medicine: ACES/IHMRI Joint Workshop 2019, University of Wollongong, Wollongong (26 February 2019).

15. Poster presentation: “Wireless cell stimulation enabled by conducting polymers based bipolar electrochemistry” at the 13th Annual Electromaterials Science Symposium, Geelong (11 - 13 February 2019).

16. Poster presentation: “Bipolar electrochemistry: concepts and applications” at the International Conference on Nanoscience and Nanotechnology 2018, University of Wollongong, Wollongong (29 January - 2 February 2018).

17. Oral presentation “Introduction of bipolar electroactive conducting polymers for wireless cell stimulation” at ACES SBS Workshop Program (4 October 2017).

18. Poster presentation: “Bipolar electrochemistry: concepts and applications” at 2017 ACES Full Centre Meeting, University of Wollongong, Wollongong (20 - 21 August 2017).

List of Names or Abbreviations

AC	alternating current
Ag	silver
Al	alginate
AuNPs	gold nanoparticles
Au	gold
BDNF	brain-derived neurotrophic factor
BPES	bipolar electrochemical stimulation
Bu_4NPF_6	Tetrabutylammonium hexafluorophosphate
CABPE	capillary-assisted bipolar electrochemistry
cm	centimetre
CMC	carboxymethyl-chitosan
CNC	cellulose nanocrystal
ColMA	collagen methacryolyl
CO_2	carbon dioxide
CPs	conducting polymers
Cr	Chromium
CV	cyclic voltammetry
DAPI	4, 6-diamidino-2-phenylindole
DC	direct current
DDS	drug delivery systems
DEG	Diethylene glycol

ΔE_{elec}	the fraction of E_{tot} dropped over the bipolar electrode
DI	deionized
DMEM	Gibco Dulbecco's Modified Eagle's Medium
DMEM/F-12	Dulbecco's Modified Eagle Medium: Nutrient Mixture F-12
DS	dextran sulfate sodium salt from Leuconostoc spp.
eATRP	electrochemically mediated atom transfer radical polymerisation
ECL	electrochemiluminescence
EF	electric field
EIS	electrochemical impedance spectroscopy
ES	electrochemical stimulation
E_{tot}	the external applied voltage between the two driving electrodes
η_{an}	anodic overpotentials
η_{cat}	cathodic overpotentials
FBS	fetal bovine serum
FTIR	fourier-transform infrared spectroscopy
FTO	fluorine-doped tin oxide
GelMA	gelatin methacrylate
h	hour
HAMA	hyaluronic acid methacrylate
H_2SO_4	sulphuric acid
Hz	hertz
iPSCs	induced pluripotent stem cells
IrOx	iridium oxide
ITO	Indium tin oxide
JPs	Janus particles

kV	kilovolt
L_{BE}	the length of the bipolar electrode
L_{DE}	the distance of driving electrodes
M	Molar
mA	milliampere
mg	milligram
min	minute
ml	millilitre
mm	millimetre
mM	millimolar
MRI	magnetic resonance imaging
mV	millivolt
mW	milliwatt
µg	microgram
µL	microlitre
µm	micrometre
µM	micromolar
ng	nanogram
NGF	nerve growth factor
nm	nanometre
NT3	neurotrophins
Ω	Ohm
O_2	oxygen
ORR	oxygen reduction reaction
PANI	Polyaniline

PBS	phosphate buffered saline
PEDOT	Poly(3,4-ethylenedioxythiophene)
PEDOT-PSS	Poly(3,4-ethylenedioxythiophene)- polystyrene sulfonate
PDMS	Polydimethylsiloxane
PI	propidium iodide
PMAS	Poly (2-methoxy-5 aniline sulfonic acid)
PPy	Polypyrrole
PSA	prostate specific antigen
P/S	penicillin/streptomycin
Pt	Platinum
*p*TS	*para*-toluenesulfonic acid monohydrate
P3MT	Poly(3-methylthiophene)
Py	Pyrrole
PVA	Poly(vinyl alcohol)
PVDF	Poly(vinylidene fluoride)
RA	retinoic acid
R_{elec}	the total resistance to electronic current posed by bipolar electrode
rpm	revolutions per minute
R_S	the resistance of the solution posed on the left of bipolar electrode
R_{S2}	the resistance of the solution posed on the above of bipolar electrode
R_{S3}	the resistance of the solution posed on the right of bipolar electrode
RT	room temperature
$Ru(bpy)_3^{2+}$	Tris(bipyridine)ruthenium(II) chloride
s	second
SCBPE	spatially coupled bipolar electrochemistry

SD	standard deviation
SEM	scanning electron microscope
SGN	spiral ganglion neuron
SSM	stainless steel mesh
TENGs	triboelectric nanogenerators
2D	two dimensional
3D	three dimensional
TPA	Tripropylamine
UV	UV-vis spectroscopy
V	volt
X_0	zero overpotential

List of Figures

List of Tables

Table of Contents

Chapter 1

Introduction

1.1 Motivation of this thesis

Traditional wired electrochemical stimulation (ES) systems have been developed as powerful strategies to modulate cellular behaviour and biological activity by manipulating electrical signals [1–6]. Subsequent electrical stimulus-responsive conducting polymers (CPs) have greatly boosted the development of these ES systems due to their electroconductivity, biocompatibility, stability, and flexibility [7–12]. They have become one of the most promising neural electrode materials to influence proliferation, differentiation, and migration-associated cell behaviour and advance studies on medical bionics. To date, the key shortcoming of traditional ES is that it requires the working electrodes to be "hard wired" to a potentiostatic to employ the controlled stimulation, which constrains to intra-operative use and practical biomedical deployment, and limits potential therapeutic benefits. Bipolar electrochemistry (BPE) [13,14] offers an effective pathway to modify these ES systems into a desirable contactless mode. However, current BPE studies focus on metals, which have several limitations like risky high driving voltage, plastic deformation and cytotoxic effects etc, and are unacceptable in wireless cell stimulation. This project aims to find bipolar electroactive, biocompatible CPs and employ BPE to establish and develop an attractive and innovative non-contact approach, known as bipolar electrochemical stimulation (BPES). BPES is expected to transform the wired ES system into a wireless system, maintaining the advantages of ES but removing the need for a physical connection to control the applied potential. This project will also focus on developing CP-based BPES

systems enabling wireless and programmable living cell stimulation with enhanced cell proliferation and differentiation, and establish a new paradigm that provides an attractive wireless approach to advance the field of medical applications.

1.2 Backgrounds of this thesis

1.2.1 Traditional wired ES

Traditional wired ES promotes healing [1,15,16], tissue regeneration/rehabilitation [2,17,18] in both neuroscience and clinical studies and is central in the emerging field of electroceuticals [3] due to its non-pharmacological approach. Electrochemical approaches have been extensively utilised to produce electrical signals and demonstrate the functional recovery and integration of neurones *in vitro* and *in vivo* [19]. The merits of these techniques lie in electrochemistry, which allows reversible and on-demand electrochemical event manipulation by safe potential through the expression of electrochemical sensitive ion channels, thus stimulating electroactive molecules, cells, and organs [5]. Therefore, electrochemistry has become an increasingly apparent and important component of biological cell polarity [20,21]. Exogenous electric fields direct cell polarisation in several ways, thus illustrating the relevance of electrochemistry to cell polarisation and provides a fascinating glimpse into how the cell-surrounding electric field could coordinate cellular behaviours in multicellular situations. Recent findings suggest that electrotactic signals contribute to steering cellular activity, guiding cell polarization, orientation, and directions, thus highlighting the potent importance of the existence of electrochemical cues in competing cell stimulation fields [6,22–25].

The success of culturing cells on CPs has verified their biocompatibility. The latest interest in electrical stimuli can be applied directly to the attached biomolecules and

cells through CPs (Figure 1.1), for *in vivo* therapeutics, including wound healing stimulation or functional nerve tissue restoration [26–33] for *in vitro*, thus enhancing neurite outgrowth and recording nerve cell activities. Though the mechanism of the underlying cellular response to ES is unclear, it is still desirable to change the ES application mode. ES regulates cell adhesion [30], proliferation [31], migration [32], and protein production [33]. CPs can self-covalently bind and incorporate biomolecules to improve their self-biocompatibility and promote cell viability [34]. Neurite extension and neurone growth were significantly enhanced due to ES when cultured on biomolecule-doped CP coatings with physical wire connections [28–31,34].

Although traditional wired ES technologies have been well established, the challenges caused by wired electrodes on a targeted area have not been effectively addressed [4]. Therefore, invasiveness is a continuing issue because the long leads must be "hard-wired" from the power supply to the stimulation site. The presented wires are also a source of infection and limit the capability of the power supply to move with the tissue, leading to loss of efficacy because of foreign body response or loss of contact with the target tissue [35–37]. Chronic fatigue on wires can cause device failure either in the wire itself or its connection to the power supply [10,38]. Furthermore, the wires used to power neural stimulation electrodes can interfere with animal behaviour as observed when studying social interaction between rodents [39]. Moreover, the surgical procedures used to remove implanted electrodes and wires can cause secondary tissue damage and pain burdens in patients [40]. Therefore, a wireless, biocompatible, and safe system capable of providing precise and effective ES is highly desirable to meet the demands of intraoperative use, practical biomedical deployment, and potential therapeutic benefits.

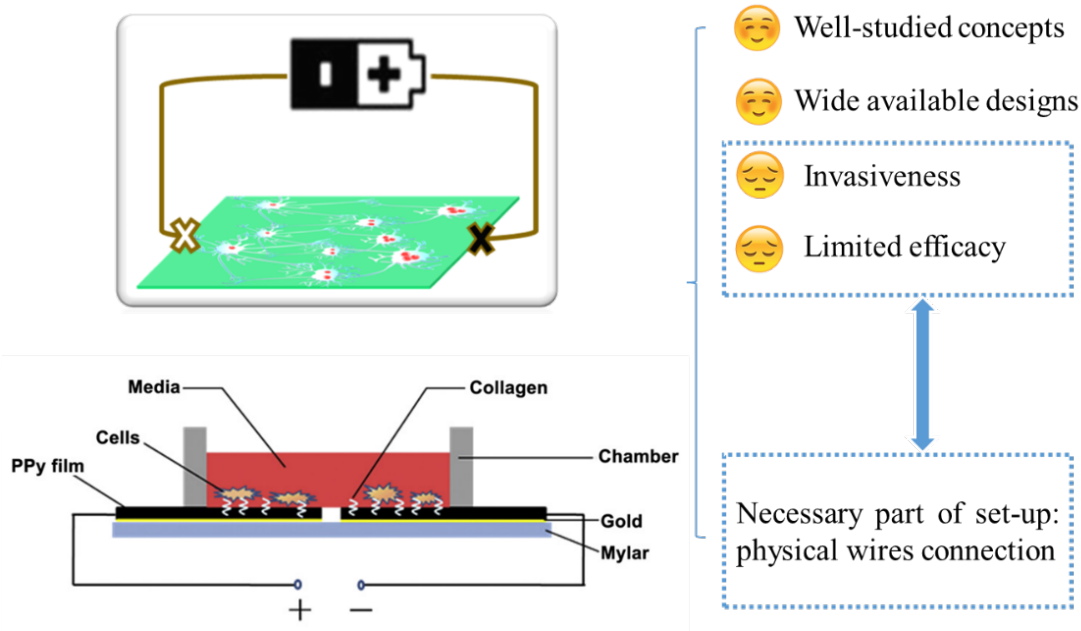

Figure 1.1 Schematic illustration of a typical configuration of traditional wired electrochemical stimulation (ES) setup and demonstration of its advantages and disadvantages.

1.2.2 Bipolar electrochemistry (BPE)

In this part, the fundamentals and applications of BPE have been introduced, and the gap between metals- and CP-based BPE has been compared.

1.2.2.1 General introduction of BPE

BPE, a phenomenon that concurrently generates a pair of oxidation and reduction reactions on the two extremities of conductive objects without any direct ohmic contact, has been known as a basic concept for a long time. The typical bipolar electrochemical cell configuration includes an external power source, two driving electrodes (also called feeding electrodes), one bipolar electrode, and an aqueous supporting electrolyte solution (Figure 1.2a). Bipolar electrochemical reaction occurs when a uniform electric field emerges between the driving electrodes across the electrolyte solution. This creates

sufficient voltage makes it possible to result redox reactions at the anodic (oxidation reaction) and cathodic (reduction reaction) poles of the bipolar electrode [41–44]. Direct contact is not required between the power supply and the isolated bipolar electrode.

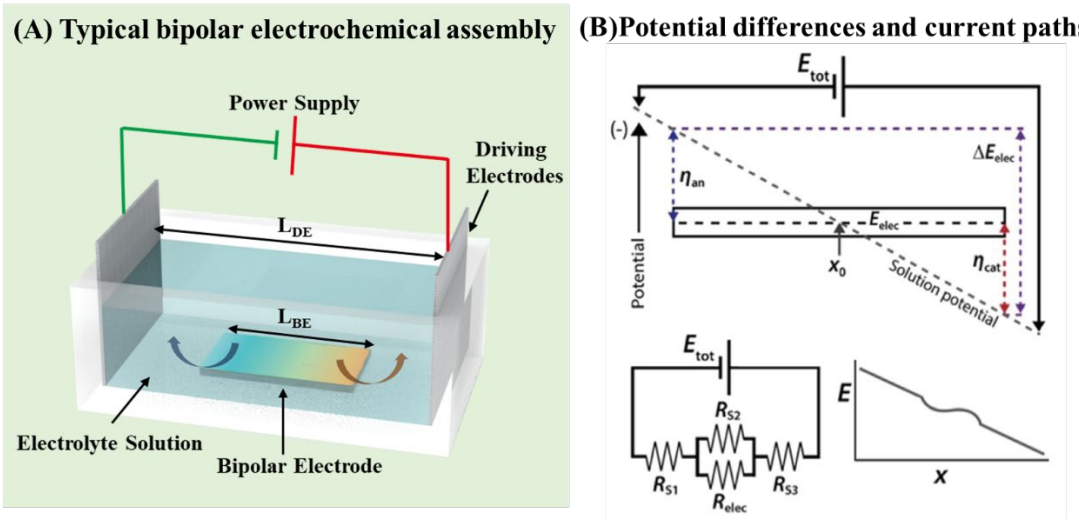

Figure 1.2 (A) Schematic illustration of a typical bipolar electrochemical system including power supply, driving electrodes, bipolar electrode, and electrolyte solution. (B) The according potential differences and equivalent circuits.

This isolated bipolar electrode remains immersed in a suitable supporting electrolyte and an electric field with the required magnitude must be applied to support redox reactions. It can be of any shape or size, but must be a material with sufficient conductivity, varying from various forms of metals [45], carbon [46], coated semiconductor, or insulators [47], which shows no difference when compared to materials used for conventional electrochemistry. However, a fundamental difference is the need for a physical wire connection between the working electrode and the power source.

In BPE, the ion in the electrolyte is an invisible wire that connects the driving electrodes with the bipolar electrode. The intensity of the electricity produced from ionised particles in this electrolyte should separately support the oxidation and reduction reactions on the isolated bipolar electrode. Thus, the conductivity of the electrolyte is relatively important, which is determined by its composition and concentration [48–51]. The large amounts of free mobile ions in high electrolyte concentration may not support the electric fields and cannot trigger bipolar electrochemical reaction. On the contrary, low electrolyte concentration does not produce enough free mobile ions to achieve the electric fields required for bipolar electrochemical reaction. This difference in conductivity is a driving force for current movement through the isolated bipolar electrode.

A minimum value of the applied electrical field, which depends on bipolar electrode size, must be reached to onset redox reactions on the isolated bipolar electrode. Cell geometry and supporting electrolyte conductivity also play important roles in the nature of the electric field formed between the driving electrodes. These parameters for controlling bipolar electrochemical processes have been discussed in multiple studies [52–57]. Briefly, they include the external applied voltage between the two driving electrodes (E_{tot}), the distance between the driving electrodes (L_{DE}), and the length of the bipolar electrode (L_{BE}). Equation (1) identifies the E_{tot} fraction dropped over the bipolar electrode (ΔE_{elec}).

$$\Delta E_{\mathrm{elec}} = E_{\mathrm{tot}}\left(\frac{L_{\mathrm{BE}}}{L_{\mathrm{DE}}}\right) \qquad \text{equation (1)}$$

An electric field in the electrolyte solution resulting from E_{tot} causes the bipolar electrode to reach an equilibrium potential (E_{elec}), which depends on both bipolar electrode position in the field and solution composition. E_{elec} is approximately same everywhere on bipolar surface as it is a conductor. However, the presence of an electric field in solution causes a different interfacial potential between the bipolar electrode and the electrolyte solution, which varies along with the L_{BE}. Therefore, the reactivity of the electroactive species at the poles of the polarised interface is driven by the anodic and cathodic overpotentials (ηan and ηcat, respectively). In other words, $\Delta E_{\mathrm{elec}}/E_{\mathrm{tot}}$ is approximately equal to L_{BE}/L_{DE}. Figure 1.1b shows that E_{tot} and L_{BE} determine the overpotentials magnitudes. The boundary between two poles is defined by the location on the bipolar electrode; therefore, it has zero overpotential (X_0) regarding to the solution. Although X_0 is defined as the centre of the bipolar electrode, its site in a real setting is up to the nature of the faradaic processes occurred at the poles.

The equivalent circuits (reasonable approximations of the resistances (bottom left)) are shown in Figure 1.2b. In open bipolar electrochemistry, the current flows through the system in two different fractions: faradaic current through the bipolar electrode via electronic and bypass current through the solution via ionic (migration of charged species). Therefore, we define the parameter R_{elec} [55] (containing the charge transfer resistance and relevant mass transfer) as the total resistance to the electronic current posed by the bipolar electrode. The resistance of the solution posed on the left, above, and right of the bipolar electrode are R_{S1}, R_{S2} and R_{S3}, respectively. If R_{S2} is significantly lower than R_{elec}, most current passes through the solution instead of the bipolar electrode, which means that the electric field is not significantly influenced by the bipolar electrode. However, when R_{S2} is significantly higher than R_{elec}, most current

passes through the bipolar electrode, which increases or decreases the strength of the local electric field in the solution and generates a nonlinear electric field above the bipolar electrode. Duval et al have named this effect “faradaic depolarisation” [58–61]. The magnitude of this effect is determined by applied electric field strength, the electrochemical properties of electroactive species, and the supporting electrolyte concentration. It is noteworthy that equation (1) indicates no potential drop at the driving electrodes.

1.2.2.2 Metal-based BPE

Metals have been used as conductive objects for a very long time because of their good electrical conductivities, which originates from the fact that they readily lose their outer shell electrons. Along with their use in conventional electrochemistry, metals have also become popular candidates for BPE. During the last two decades, many new metal-based bipolar electrochemical systems have been reported [22-59].

Crooks et al first controlled electrochemical reactions, created various widths, lengths, and geometries gradients, and then simultaneously displayed numerous catalysts from a single substrate to a patterned array by changing the anodic identity to Cr (which oxidises at anodic pole, while the oxygen reduction reaction (ORR) occurs at the cathodic pole). Three bimetallic systems (Pd-Au, Pd-Co and Pd-W) were also evaluated using the same bipolar electrochemical screening system (Figure 1.3) [62–66].

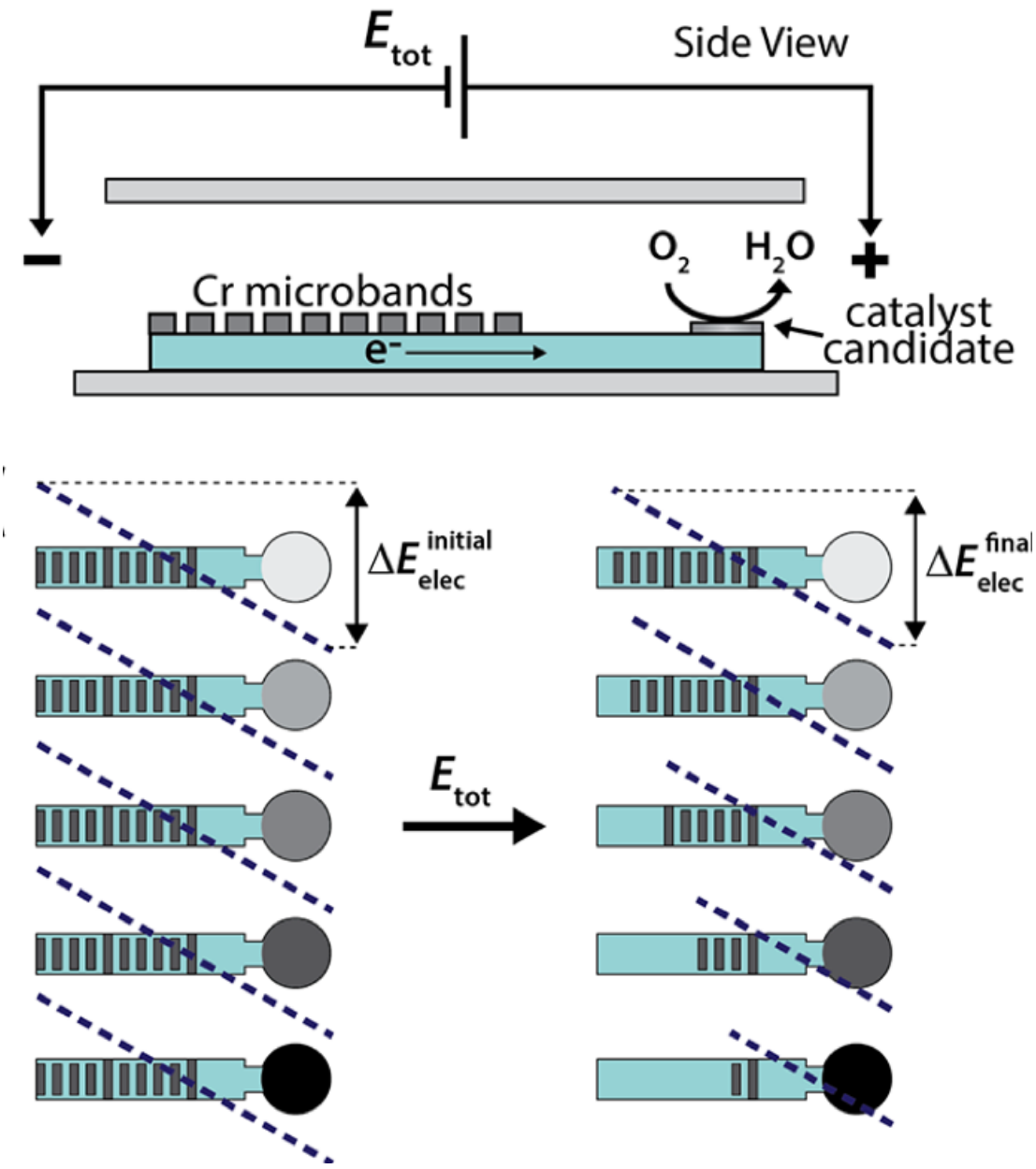

Figure 1.3 The illustration of bipolar electrochemical screening devices. Cr microbands deposited indium tin oxide (ITO) are used as anodic poles, while catalyst candidates are used as cathodic poles [62].

Bradley et al developed a noncontact method known as spatially coupled bipolar electrochemistry (SCBPE) [67] (Figure 1.4), which connects isolated metal as a bipolar electrode. In SCBPE, redox reactions are induced by an applied electrical field on

isolated metal bipolar electrode. Metal ions are provided through the oxidation reaction in the system. The forces that originate from the electrical field or electro- and gravitic-convective motion preferentially drive these metal ions towards the nearest metal, thus, fine-tuning of centred and non-centred metal deposition and growth. Moreover, they demonstrated the potential of certain morphologies on a single substrate, as well as the structure of different metal deposits [67–73].

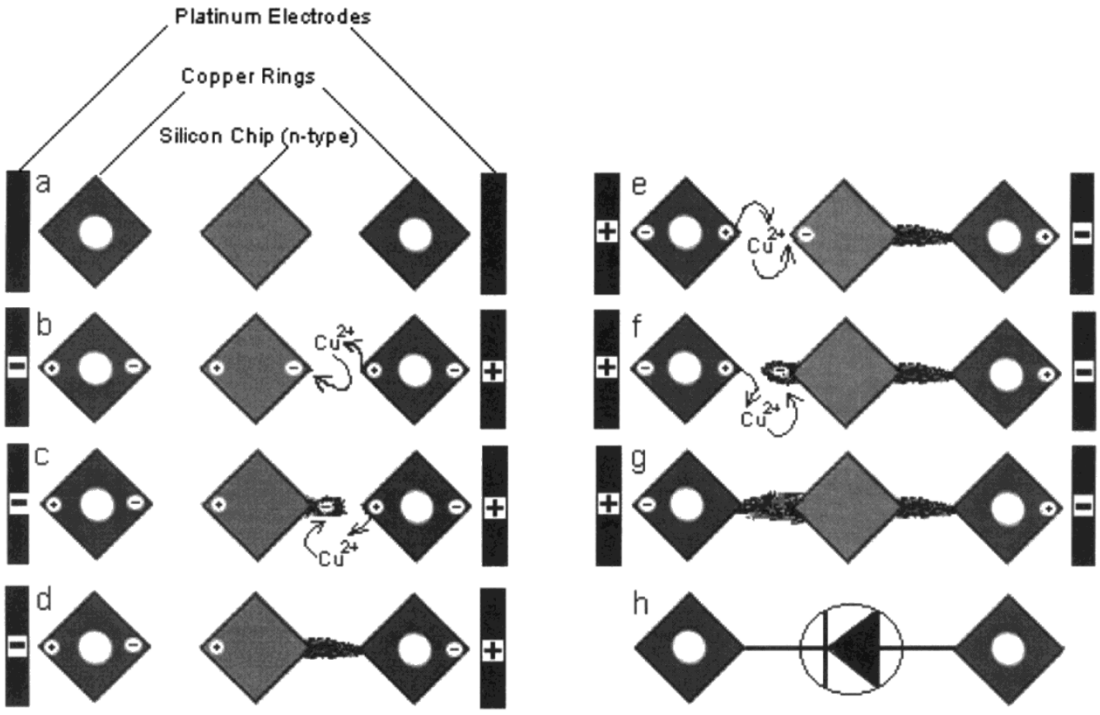

Figure 1.4 Schematic diagram of the formation of a rectifying device using spatially coupled bipolar electrochemistry (SCBPE). (a-d) Generated electric field polarizes two electrodes, copper electro-dissolves at the anodic region of the right copper ring and copper wire begins to electroplate at cathodic region of the silicon chip until it reaches the right copper ring. (e-g) The field polarity is reversed and the same wire-like deposition grows to connect the left copper ring and the silicon chip. (h) Rectification properties for n-Si [67].

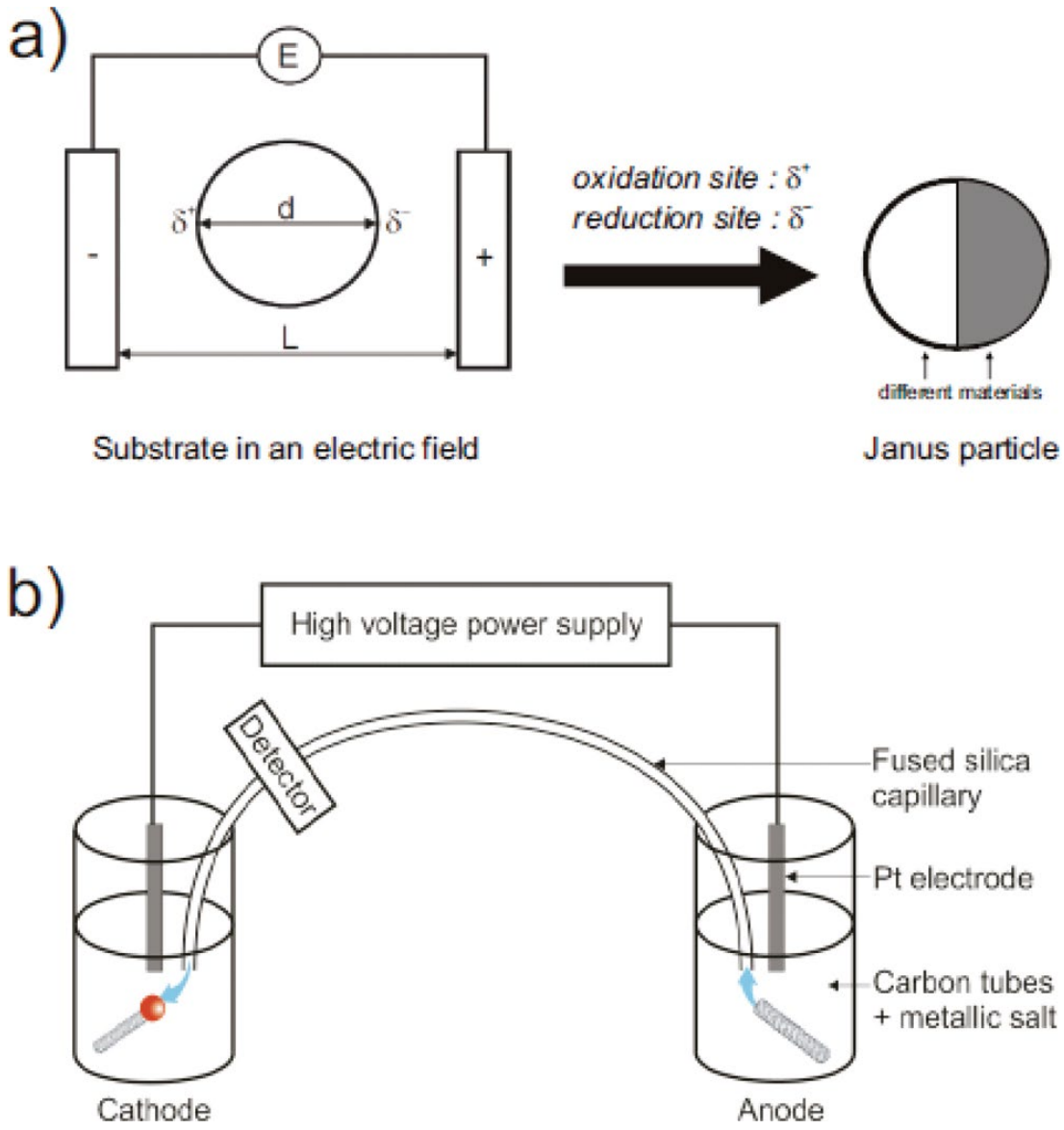

Figure 1.5 (a) Concept of bipolar electrochemistry for synthesis of Janus-Type objects; (b) Setup for the asymmetrical objects preparation using capillary-assisted bipolar electrochemistry (CABPE) [74].

Another popular application is the bulk synthesis of dissymmetric and Janus particles (JPs) via capillary-assisted bipolar electrochemistry (CABPE) [74] (Figure 1.5), and relevant fabrication of metal bipolar surfaces to control mass transfer by electro-migration by Kuhn et al. This CABPE system depends on a “polarization” that occurs

on a conducting object when a high and strong electric field exists between two feeding electrodes, which catalyses the redox reactions at the opposite poles of the object (Figure 1.5a). In this case, the capillary separates the strong potential (approximately several tens of kV) between the two feeding electrodes and promotes bipolar electrodeposition (Figure 1.5b). Under this influence, the conductive objects (bipolar electrode) are polarised and move from the anodic reservoir to the cathodic reservoir owing to the electro-osmotic flow through the capillary as well. Finally, bipolar electrodeposition is achieved in the CABPE system. Furthermore, metal electrodeposition on anisotropic/isotropic micro- and nanoparticles and material modification at the molecular level are realised in this system [46,74–78].

Joseph et al have used external magnetic fields or chemical fuelling, even self-generated power to propel different motors, employing them to isolate and capture nucleic acids or cancer cells in complex media. They coupled metal-based bipolar electrochemical screening device with electrochemiluminescence (ECL) to construct sensing and reporting analysis platforms for biorelevant analytes widely produced by other groups [79–84]. This system is a microfluidic chip comprising a polydimethylsiloxane (PDMS) chip with two microchannels and a glass slice with two indium tin oxide (ITO) bands (Figure 1.6a). The electrical conductivity of the gap between the ITO bands in the channel could be bridged and tuned by prostate-specific antigen (PSA)-guided Ag particle deposition on the gold nanoparticle (AuNP) surface (Figure 1.6b). Here, at “on” state of the gap switch, PSA-induced Ag particle deposition forms an electronic circuit to connect the adjacent bipolar electrodes and produces a continuous H-shaped bipolar electrode. When sufficient external voltage (E_{tot}) is applied to channel b, $Ru(bpy)_3^{2+}$ and tripropylamine (TPA) are oxidised at the anodic pole of the bipolar electrode and emit only one ECL signal. Simultaneously, O_2 is reduced at the cathodic pole of the bipolar

electrode. However, at the "off" state, same redox reactions occur on both separated ITO bands in channel b. Regarding analysis aspect, Crooks et al have used bipolar electrochemical systems in several studies such as specific ion concentration enrichment for seawater desalination [85–91] or enrichment of drug candidates from biologically relevant molecules [92–99].

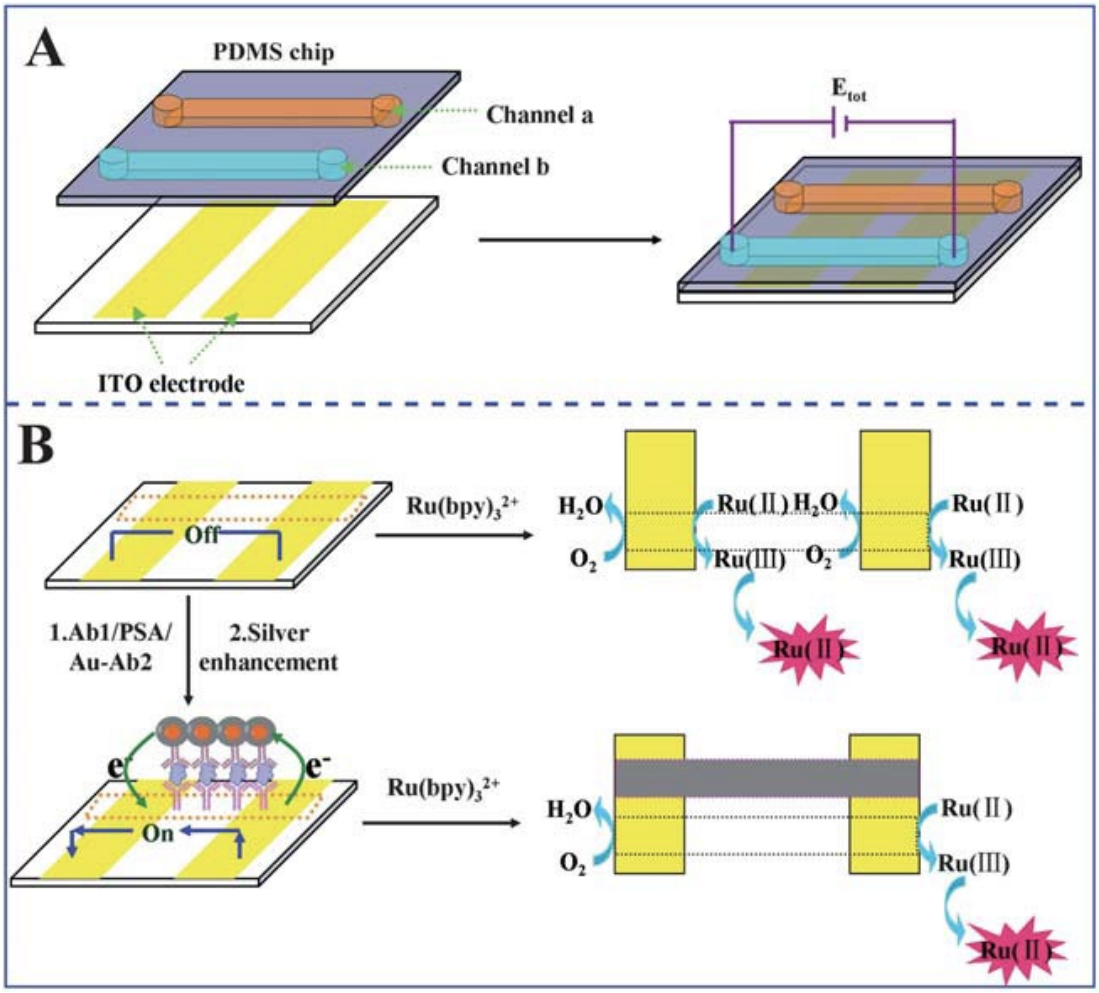

Figure 1.6 (A) Configuration of the microfluidic chip containing sensing channel a and reporting channel b. (B) Schematic illustration of the metal-based bipolar electrochemical screening device with electrochemiluminescence (ECL) for biorelevant analytes [79].

Although metal-based bipolar electrochemical systems have been widely used such as above-mentioned material synthesis and modification, screening, and analytes, it has several limitations. First, the required voltage applied by the external power supply to drive the oxidation and reduction reactions on two ends of the bipolar electrode is extremely high, even reaching ~kV. This increases power supply cost and risk as the researchers might get a fatal electric shock. The high voltage applied also increases the forces and thermal energy of the metal bipolar electrode. Once these forces and heats cross the elastic limit of the metal, it may cause “plastic deformation” or “plasticity”, which is a permanent (irreversible) deformation of the metal object. Additionally, after electron loss, cationic metals are usually inclined to react with O_2 in the air to form metal oxides over time. This induces another challenge: how to eliminate corrosion and electrolysis. Last but not the least, long-term metal biostability constrains its applications *in vitro*, hardly *in vivo*. Therefore, integrating metal-based bipolar electrochemical system into biologic point-of-care applications or other complicated biological environments is stagnant.

1.2.2.3 CP-based BPE

Polyacetylene can achieve a high electrical conductivity of several orders of magnitude by doping with anions [100–102]. CPs have grown enormously due to their good processability by dispersion, coupled with good electrical/physical properties and low costs, particularly as electronic materials because of light weight and flexibility. In most cases, CPs are insulators in their neutral state as their balanced charges, whilst they become semi-conductive or conductive by altering the double bond in the conjugated polymer backbone. The charged species are formed upon introduction of electron

acceptors/donors by a process known as “doping” (“p-type” oxidation doping or “n-type” reduction doping), followed by the insertion of anions or cations respectively. These charged species move along the carbon chain (delocalisation) allowing electron transport [103]. CP doping is often accompanied by a redox process. Therefore, CP oxidation or reduction (coupled with the integration of counterions present in the electrolyte) affects the band gap of the material and transfers electrons on the electrode surface to form polarons and bipolarons in the repeating structure (doping/de-doping), producing considerable colour change and electrical conductivity [104,105].

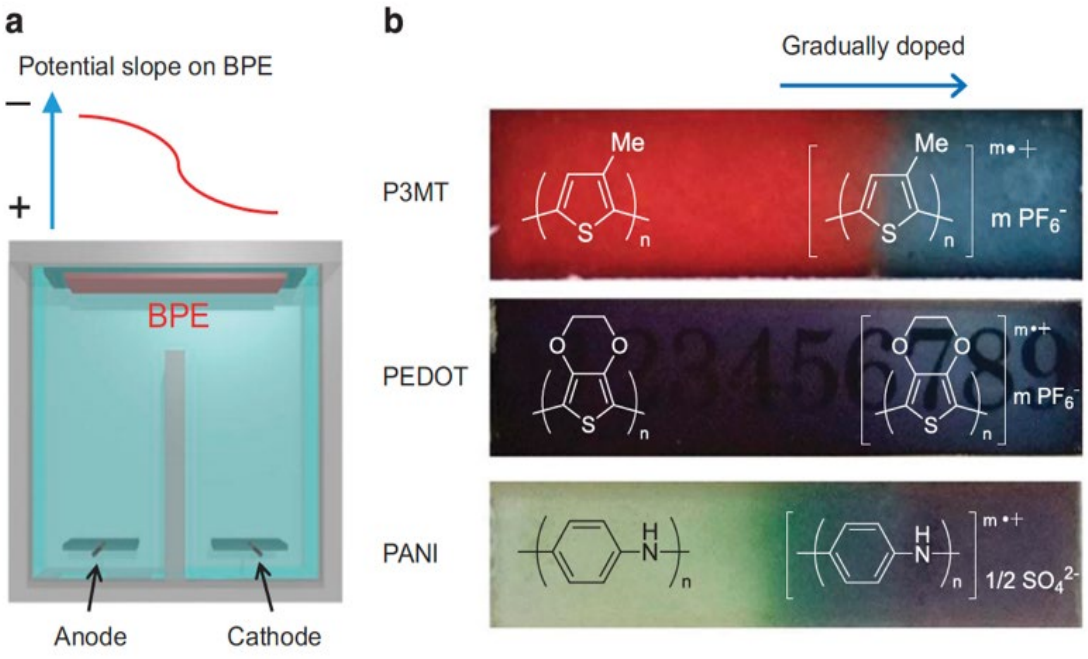

Figure 1.7 (a) U-type electrolytic cell with a pair of driving anode and cathode, as well as a conducting polymer (CP) as bipolar electrode. (b) Images of the gradually doped poly(3-methylthiophene) (P3MT), poly(3,4-ethylenedioxythiophene) (PEDOT), and polyaniline (PANI) films [106].

To date, only few studies have reported the CP-based bipolar electrochemical systems.

Inagi et al have demonstrated the bipolar patterning of CPs [106–108]. They used poly(3-methylthiophene) (P3MT) as a bipolar electrode, resulting in visually and spectroscopically asymmetric doping and reversibility in non-aqueous solvents using a U-type cell. The P3MT film on ITO was subjected to a U-type electrolytic cell, which was equipped with a pair of Pt wires (10 mm × 10 mm) as driving electrodes connected to an external power source (Figure 1.7a). The bipolar electrochemical doping of the P3MT film was carried out by electrolysis using constant current (1 mA) in 0.005 M tetrabutylammonium hexafluorophosphate (Bu_4NPF_6)/acetonitrile as the supporting electrolyte. P3MT was reduced at the pole opposite to the anode driving electrode, while it was oxidised at the pole opposite the cathode driving electrode. Finally, this resulted in a gradually doped film. The same process to generate composition-gradient CPs was extended to poly(3,4-ethylenedioxythiophene) (PEDOT) and polyaniline (PANI) (Figure 1.7b). In addition, the parallel bipolar electrolysis of an oxidisable and reducible CP (P(CHOH)) successfully generated a new class of composition gradient films [109–113]. In terms of selective modification, site-controlled electric potential on CPs "canvas", electro-click, electrochemically mediated atom transfer radical polymerisation (eATRP) are used for doping and patterning [114–116]. Moreover, they have recently succeeded in synthesising dendritic and linear PEDOT fibres by alternating current (AC)-bipolar electropolymerisation for material preparation and fabrication [117,118].

1.2.3 Combining BPE and ES into BPES

1.2.3.1 Benefits of BPES

BPES could serve as an outstanding wireless platform to enable programmable living cell stimulation, bridging the gap between electrochemistry and biology. Unlike

traditional ES, such as deep brain stimulation for Parkinson's disease utilising metal electrodes that are "hard-wired" to a power supply to deliver the stimulation. BPE introduces an innovative wireless approach to cell stimulation wherein redox reactions are driven by an electric field. BPES employs BPE, which does not require wires between the driving electrodes and the bipolar electrode, becoming a new face in wireless cell stimulation technologies (Figure 1.8). It offers an effective pathway to modify the conventional wire-dependent ES systems into a desirable contactless mode that retains the benefits of ES while eliminating the requirement for a physical connection to control the imposed driving potential.

In addition to being wireless, the BPES system is similar to traditional wired ES systems because it depends on electrochemical cues from redox reactions. As the bipolar electrochemical reaction continues, the action potentials in neurones are generated and the cells are polarised for processes such as cell proliferation, differentiation, and cell migration. This differs from the current wireless cell stimulation systems, which manipulate the external magnetic field, ultrasonic sound, and light to control cell physiology.

These wireless cell stimulation systems are constructed from electrical stimulus-responsive materials such as magnetoelectric, piezoelectric, and optoelectronic materials [11,12,119,120]. Stimulus is triggered through an internal energy conversion mechanism underlying the materials, where the general primary driving force, such as a magnetic field, ultrasound, and light is converted into bioelectricity, which has been most commonly used to study cell functions both *in vitro* and *in vivo* [11,121,122]. All these wireless ES methods are appealing, safe and non-invasive. Moreover, they display

strong cell/tissue penetration depth, enhanced spatial localization/ resolution, and depth targeting in the neuromodulation field when the stimuli passing through cell/tissue are undiminished and have no harmful effects [12,36,123–127].

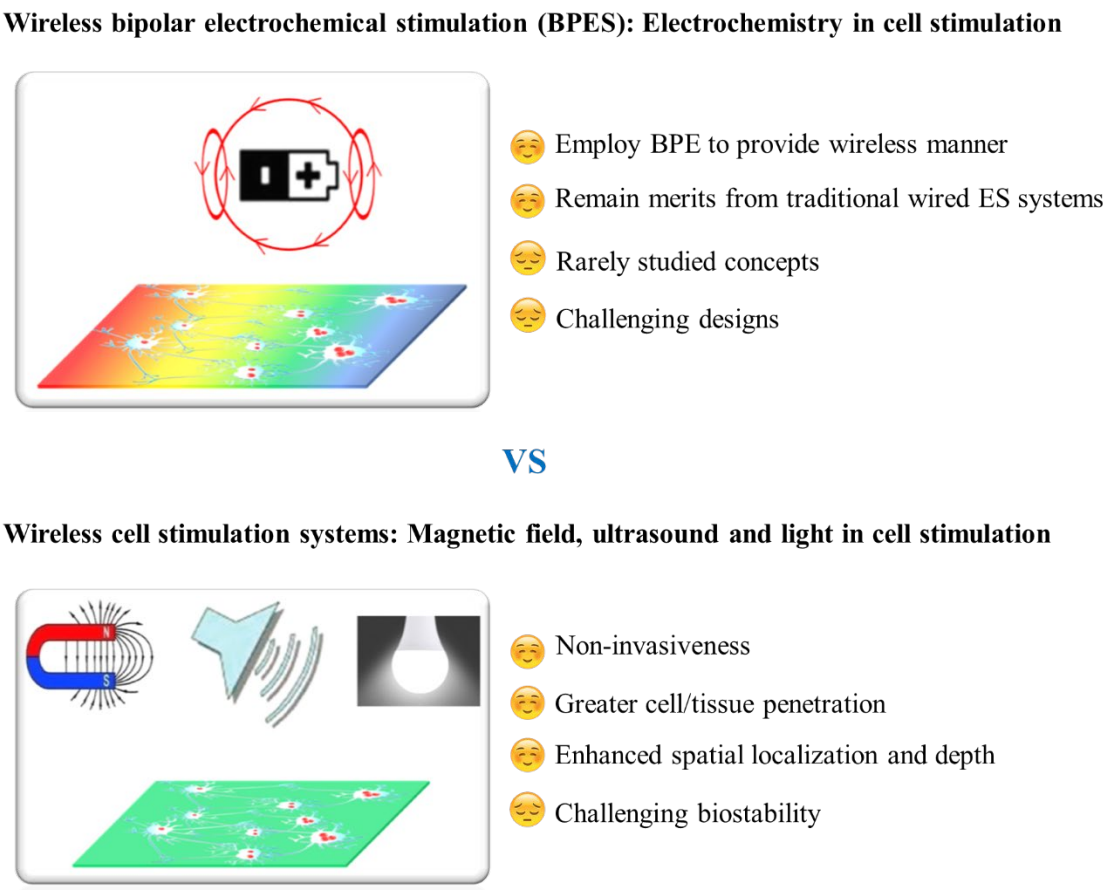

Figure 1.8 Wireless bipolar electrochemical stimulation (BPES) systems combine many advantages of traditional wired ES systems and wireless cell stimulation systems toward becoming a promising strategy for neurological function study.

However, materials selection for the fabrication of electronic implants is critically important, particularly when the implanted electrode is exposed to the patient body. To protect the user, implantable materials must possess biocompatibility and biochemical and mechanical stability. All materials must be resistant to sterilisation procedures,

mechanically robust, and sufficiently biochemically inert for long term continuous operation. Furthermore, the use of lead in the piezoelectric component raises toxicity issues for deployment in biological environments [128]. Thus, many studies have investigated new materials to remove or replace this component. Poly(vinylidene difluoride) (PVDF), for example, is one of the most popular non-lead piezoelectric materials, which have offered same mechanism but eliminated the need of lead [130,131]. This highlights the necessity of evaluating the biostability of interfaces, spatiotemporal selectivity and accuracy, and electrophysiological evidence of cellular regulation. Several reviews have discussed the details of recently developed material-based wireless cell stimulation systems for regulating neurones and neural activity in the central and peripheral nervous systems [126,129–134].

Both traditional wired ES systems and existing wireless cell stimulation systems have been fully developed to study cells grown in culture or treat neurological dysfunction. However, these approaches have been considered independently. The use of electrochemistry to induce cell stimulation wirelessly has not been fully explored yet. BPES systems that employ BPE combine the advantages of these two systems with a view toward becoming a promising strategy for studying neurological functions. It establishes a new paradigm that provides an attractive wireless approach to advance the field of medical applications, and this emerging interdisciplinary field will significantly progress in the future.

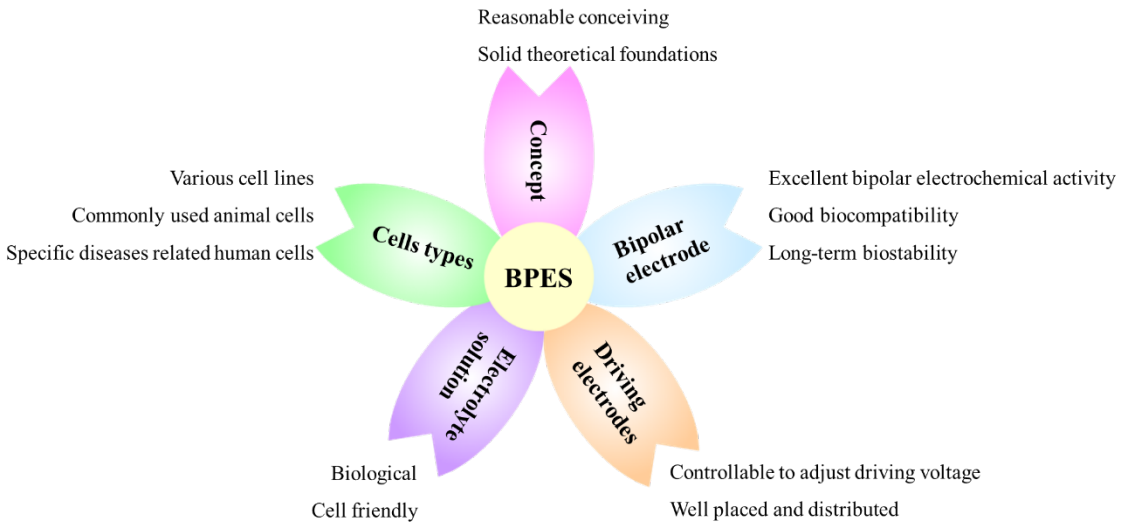

Figure 1.9 Key factors and relevant properties to establish the bipolar electrochemical stimulation (BPES) platform.

1.2.3.2 Challenges to establish BPES

Several critical factors should be addressed for each component of the entire setup used for BPES in real cell stimulation. Herein, we discuss five main components, namely concept, bipolar electrode, driving electrode, electrolyte solution, and cells, to demonstrate the establishment of such a wireless BPES platform (Figure 1.9).

Concept - reasonable design/development: The appreciation of BPE in cell stimulation is still in its infancy. For the success of the beginning of this project, researchers should have a solid theoretical foundation and relevant experience in BPE, electromaterials, electrostimulation, cell culture, tissue engineering, electro/biointerface, and biofabrication. The fundamental elements of the setup are built upon the combination of key expertise. Further development is ensured by the capability of the researchers, research facilities, and multi-pronged approach of new materials use/devices design/development.

Bipolar electrode - excellent bipolar electrochemical activity, biocompatibility, and biostability: To serve as a bipolar electrode, the synthetic materials should possess and maintain bipolar electrochemical activity in non-biological or biological environments within the stimulation period. Moreover, they should be biocompatible, harmless, and nontoxic, and stable in biological solutions. To avoid the release of hazardous chemicals, they must retain their structures and functions without disintegration. Thus, investigations and instruments to monitor and evaluate the bipolar electrochemical activity, biocompatibility, and biostability should be prepared.

Driving electrode - adjustable driving voltage: Overall, driving electrodes should be carefully controlled, as their placement, distance, and distribution determine the intensity and efficacy of the external electric field. Referring to the principle of BPE, the typical assembly encompasses two driving electrodes connected to an external direct current (DC) power source and an isolated conducting object (also called the bipolar electrode) (Figure 1.2a). When an external electric field is applied across the electrolyte, a potential difference is generated between the two ends of the conductive object, that is, the conductive object becomes bipolar. Typically, a minimum applied electric field strength must be reached to onset the bipolar electrochemical reaction; thus, the potential differences and current paths (Figure 1.2b) in the bipolar electrode become the key points for activating the bipolar electrode without electrical wiring [13,135]. The presence of an electric field in solution results in different interfacial potentials between the bipolar electrode and the electrolyte solution, which varies along with the L_{BE}. The magnitude of this effect is determined by three main factors: applied electric field strength, the electrochemical properties of electroactive species, and the supporting

electrolyte concentration [60,61,136,137]. Therefore, it is essential to modulate the driving voltage to trigger the bipolar electrochemical activity of materials and ensure cell survival simultaneously.

Electrolyte solution - biological environment: To realise living cell stimulation, the electrolyte solution must be physiologically favourable to cells. Phosphate buffered saline (PBS) solution and different cell culture media were used to ensure cell survival. High cell viability is of the essence within the BPES period, which means that the safe driving voltage for living cells should be obtained in the biological environment, and the bipolar electrochemical activity of materials could be induced by the same safe driving voltage and biological environment.

Cells - various cell types: Easily cultured cell lines such as PC 12 and HL-1 cells are recommended for setting up the BPES platform. They both are neural cell lines, and the former is derived from a pheochromocytoma of the rat adrenal medulla, while the latter is derived from an AT-1 subcutaneous tumour excised from an adult mouse. Human neural stem cells and primary cortical neurones could be good options to verify the feasibility and universality of the BPES platform. To promote the recent investigations of BPES from animal to human, *in vitro* to *in vivo*, it is certainly preferable to use the human disease-specific cell lines. Human neuroblastoma cell lines, SH-SY5Y cells, have been studied widely to allow researchers to perform translational experiments that accurately model the human nervous system, which has a major influence on treating schizophrenia and other mental disorders [138,139].

1.2.3.3 Limits and barriers to overcome from metal-based BPES

As reviewed in section 1.2.2.2, several studies on BPE have focused on the use of metal-based electrodes and their applications in materials synthesis and modification as well as chemical and bioanalytical detection, known as SCBPE or CABPE [65,140,141]. However, the intrinsic limitation of classic BPE is related to the bipolar electrode size. High applied potential is required to polarise a short bipolar electrode and induce electrochemical reactions at its extremities. Thus, extremely high potentials (on the order of tens of kV or more), are required to polarise micrometric and nanometric metal and semiconductor materials by BPE [142,143]. Although the increase in the external electric field strength could favour their bipolar electrochemical activities, the challenge is that it will simultaneously lead to the cellular membrane electroporation and cell lysis. It is noteworthy that a recent study has successfully demonstrated a decrease in the driving voltage to ~ 30 V at Pt nanopore for intracellular wireless analysis of a single cell (Figure 1.10) [144]. Researchers spatially confined the voltage drop at the nanopores, resulting in a remarkably low applied potential restricted inside the nanopipette and minimises the potential bias of the voltage on the cellular activity. However, it is very difficult to use rigid bipolar electroactive metal and semiconductor material-based BPES in a living cell for wireless stimulation under this driving voltage.

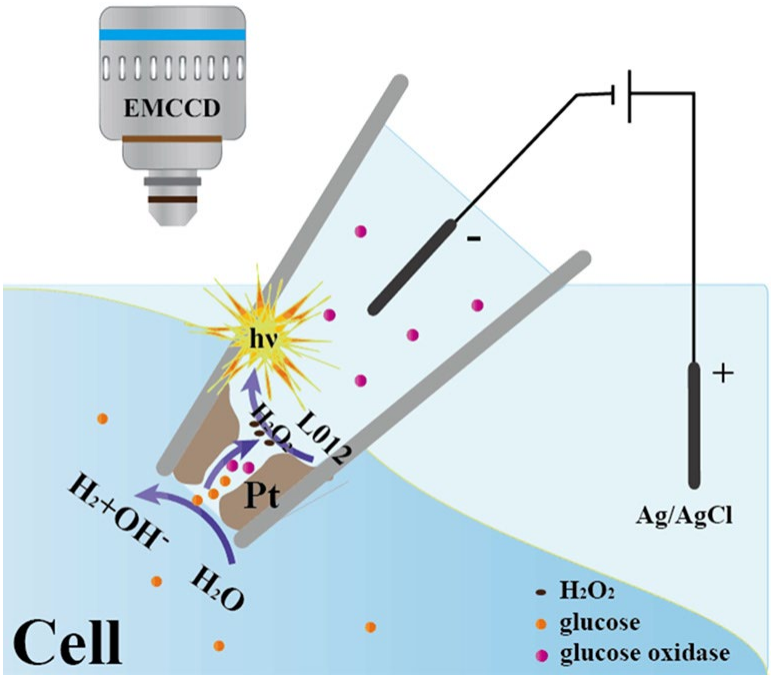

Figure 1.10 Illustration of the bipolar electrochemiluminescence (ECL) detection at the porous Pt deposit within the nanopipette inserted into the cytosol for intracellular wireless electroanalysis. [144]

One early setup introducing BPE based on metal and semiconductor materials in ES mainly used a dipole (Figure 1.11) [145]. Stimulation induces a dipole in all conductive materials such as Au and Pt, and semiconductor materials such as iridium oxide (IrOx), and mixed oxide (Ir-Ti)Ox. The length of each neurite and the angle of its growth cone (distal tip of neurite) relative to the electric field were determined from phase-contrast images captured hourly for 3 h. The results show that slow stimulation steers neurite extension on Au but not on Pt. Neurites grow rapidly and in random directions on IrOx and (Ir-Ti)Ox. Although the electric dipole induced in conductive materials controls nerve growth, several issues are unclear in this setup: (i) the bipolar electrochemical activity of materials and the driving voltage were not investigated, it is difficult to determine whether the bipolar electrochemical activity of materials is induced under the

applied driving voltage, (ii) the cells are stimulated in a short time (3 h), which is not enough for practical applications, and (iii) the transparency of bipolar materials is required, which constrains the useable materials.

Other limitations include irreversible “plastic deformation”, and cytotoxic effects arising from metal electrode corrosion and electrolysis have not been addressed as well [146]. Additionally, further investigations *in vivo* are difficult to perform in the clinic due to the rigid properties of the materials. Therefore, it is urgent to develop biocompatible bipolar electrochemical systems that can be used under biologically relevant conditions, where the voltage is sufficient for the electrochemical reactions of interest/direct potential stimulation, but does not damage the biological cells.

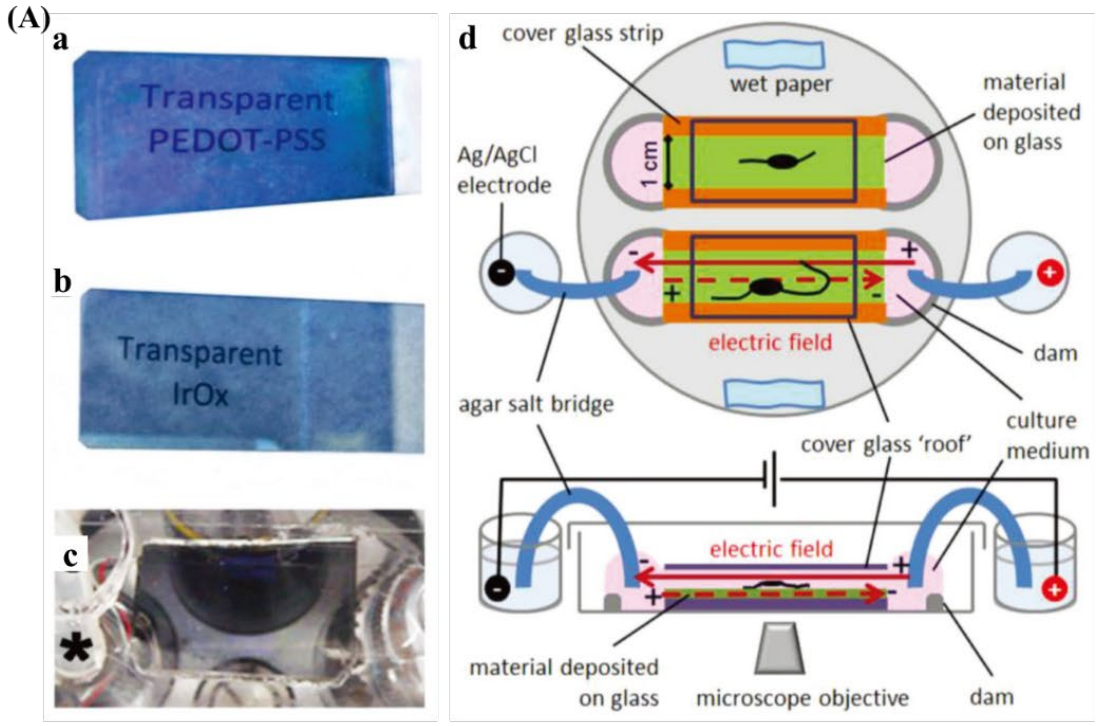
(A)
a
Transparent PEDOT-PSS
b
Transparent IrOx
c
d
cover glass strip
wet paper
material deposited on glass
Ag/AgCl electrode
1 cm
electric field
dam
agar salt bridge
culture medium
cover glass 'roof'
material deposited on glass
microscope objective
dam

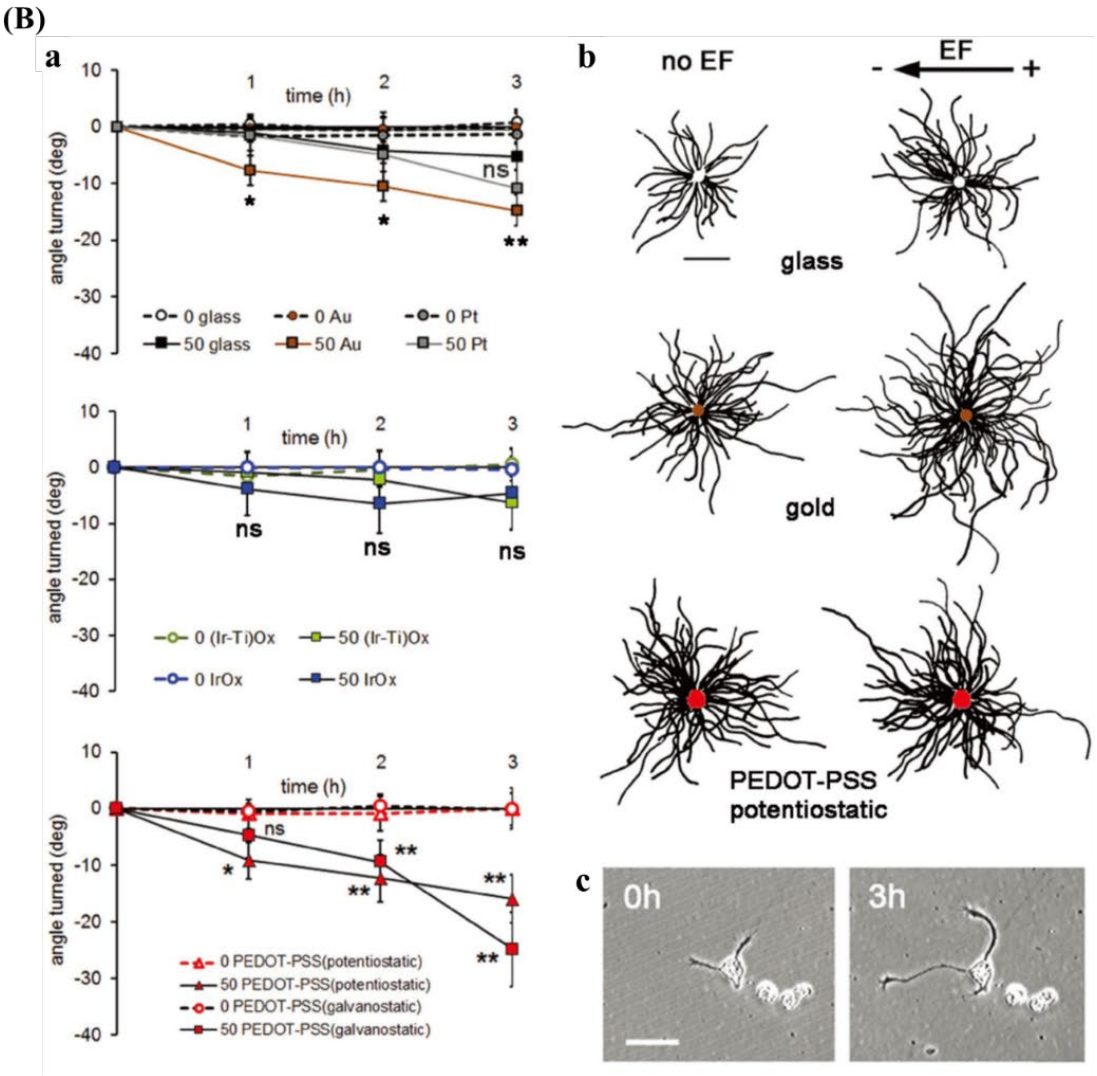
(B)
a
angle turned (deg)
time (h)
0 glass
0 Au
0 Pt
50 glass
50 Au
50 Pt
ns
0 (Ir-Ti)Ox
50 (Ir-Ti)Ox
0 IrOx
50 IrOx
0 PEDOT-PSS(potentiostatic)
50 PEDOT-PSS(potentiostatic)
0 PEDOT-PSS(galvanostatic)
50 PEDOT-PSS(galvanostatic)
b
no EF
EF
glass
gold
PEDOT-PSS potentiostatic
c
0h
3h

Figure 1.11 (A) Experimental scheme. (A-a,b) Transparency of materials (blue) electrodeposited onto glass. (A-c) IrOx during an electric field experiment. The end of an agar bridge is visible (asterisk) and the microscope objective turret can be seen through the material. (A-d) The electric field setup. Control (no electric field) and electric field conditions were run in parallel. Materials were not "wired" directly to the power supply. Arrows indicate the imposed external electric field (solid red arrow) in the culture medium and the dipole (dotted red arrow) of opposite polarity induced within the materials on which the neurons grew. For some experiments, the cells grew directly on the plastic and the materials were omitted. (B) Neuron growth during 50 mV/mm external electric field (EF) stimulation. (B-a) The angle of growth cone migration. Negative values indicate migration toward the external cathode; zero indicates randomly directed migration. Statistics compared to the same substrates but without an EF (Student's 2-tailed t-test). *$p \leq 0.05$, **$p \leq 0.005$, and ns = no significant difference. (B-b) Composite drawings made by superimposing the cell bodies and tracing each neurite. Scale 100 μm. The electric field vector represents the external field imposed within the culture medium. (B-c) A neuron growing on poly(3,4-ethylenedioxythiophene)–poly(styrenesulfonate) (PEDOT-PSS) (galvanostatic). Scale 50 μm.[145]

1.2.3.4 BPES concept proved by CPs

In tandem with recent advances in the development of easily fabricable CPs with highly tuneable electrochemical properties, mechanical flexibility, and biocompatibility with various cell lines, well-defined CP-based electrodes provide a unique conduit for electrical communication with living cells [147–150]. It has already been clearly demonstrated that electrical stimulation through hard-wired CPs can influence cell

proliferation, differentiation, migration, and connectivity, which are the central aspects of medical bionics [34,151–154]. The impact of using CPs for ES has been particularly profound with neural systems [155–157].

It is clear that switching from conventional rigid metal and semiconductor materials to softer polymers helps mitigate tissue reactions and promotes biostability. Utilising CPs with a bipolar stimulation approach will provide an exciting new dimension. Apart from the benefit of the principal "wireless" manner of bipolar electrochemical reaction to realise a new non-invasive method for electrically communicating with the internal environment of a cell, using CP as a bipolar electrode will overcome the limitations mentioned above. Thus, it is advantageous to use CP-based ES systems in biology (both electrically sensing and actuating cell behaviour) effectively [147,158,159]. To realise the possibility of CP-based bipolar electrochemical systems in wireless cell stimulation, the above-mentioned factors (bipolar electroactivity, driving voltage, environment suitable for biostability, biosafety, and cell viability) need to be fully considered.

Since Inagi et al have successfully demonstrated the novel bipolar patterning of P3MT film in Bu_4NPF_6/acetonitrile, studies have extended to gradient doping of other CPs such as PEDOT and PANI (Figure 1.7) [106,160]. These studies provide evidence of the bipolar electroactivity of CPs. Thus, CPs could be alternative bipolar electrode materials to replace metals when performing bipolar electrochemical reactions. The driving voltage is critical for bipolar electrochemical platforms to trigger bipolar reactions and ensure high cell viability concurrently. As the existing CP-based bipolar electrochemical systems have primarily used organic solvent (Bu_4NPF_6/acetonitrile) and sulphuric acid (H_2SO_4) [106,160], they are incompatible with living cells. We need to demonstrate that

the reversible and recoverable bipolar electrochemical activity of CPs could be achieved in a biological environment (such as PBS buffer) under a low driving voltage. Moreover, the CPs maintained stable activity in cell culture media without leaking toxicity within the BPES period. Furthermore, in the abovementioned dipole setup, researchers also stimulated the cells in conductive PEDOT-PSS materials within 3 h (Figure 1.11b).

Therefore, although CP-based BPES systems have begun to appear and earn an important place in wireless ES field, it should be noted that the current research on BPES systems with CPs is still in its early stages, and several issues are yet to be fully addressed.

1.2.4 Soft material templates

The existing CPs that act as bipolar electrodes comprise a rigid supporting substrate that is incompatible with cells. This may lead to destructive tissue damage and inevitable inflammatory risks *in vivo*. Moreover, recent studies underscore the feasibility of this BPES approach using simple two dimensional (2D) CP films on a non-flexible substrate [145]. This also has hindered its further applications because the whole BPES system is oversimplified and limits cell culture lifespan, which lacks the complexity of an *in vivo* microenvironment, cannot be representative of a native cell environment, and is unable to function well in living tissue.

One possible method for overcoming this constraint is to transfer the CP from a rigid substrate to a soft, biocompatible template. PDMS [161,162] is the most commonly used silicon-based organic polymer, and can be used in combination with water and

alcohol solvents without material deformation. Therefore, it is one of the most widely used materials as a stamp resin in soft lithography for flow delivery in microfluidic chips and biomedical microelectromechanical systems [163]. A soft PPy/PDMS electrode might be developed by the easy attachment and detachment of physically attached PDMS hydrogel coating. An alternative option, poly(vinyl alcohol) (PVA) [164,165] that is hydrophilic, biocompatible, and innoxious, has been used in a variety of medical and commercial applications including eye drops, contact lenses, and cartilage replacements. The crosslinked PVA hydrogel offers stable and lower interfacial toughness, polymerising the oxidants and pyrrole monomer permeable to the PVA surface. Therefore, a biocompatible PPy/PVA electrode with a high content of water was constructed. Both soft electrodes provided evidence of a CP shift [164].

The CPs on soft supporting substrates mentioned above have been reported as distinct types of bioelectronic devices because of their powerful flexibilities in functional integration [166]. Their high-performance operation is confined by the intrinsic insulation of the non-conductive layer. Using high loading volume of active electronic components to improve the comparatively poor charge transport characteristics within the material is one possible approach. Here, we propose an alternative method to fabricate completely active CP films, enabling high-performance operation of all electronic components within the active materials. The ability to dope with synergistic electronic conductors such as a sulfonated polyaniline, poly (2-methoxyaniline-5-sulfonic acid) (PMAS) [32,151,167] develops a unique biocompatible system that can undergo multiple redox reactions. CPs can undergo redox processes dictated by their unique reversible electrochemical activity and large charge injection capacities, providing effective conductivity for direct cell activity [26,156,168–172]. Poly(3,4-

ethylenedioxythiophene)-poly(styrenesulfonate) (PEDOT-PSS) is considered an ideal material due to its high conductivity, good chemical and electrochemical stability, excellent dispersibility in various solvents**,** interface functionality, and associated schemes in materials processing and assembly [126,173]. A large free-standing PPy/PEDOT-PSS film was prepared using the well-dispersed conductive ink solutions with a simple bar-coating method as described previously [174], where diethylene glycol (DEG) was used as both a dispersing agent and a secondary dopant to improve the conductivity of PEDOT-PSS. This composite film, which combines the effects of high bipolar electroactivity and mechanically compliant architectures, might represent one of the most flexible, and active materials with a high-performance operation and chronic stability in bioelectronic systems.

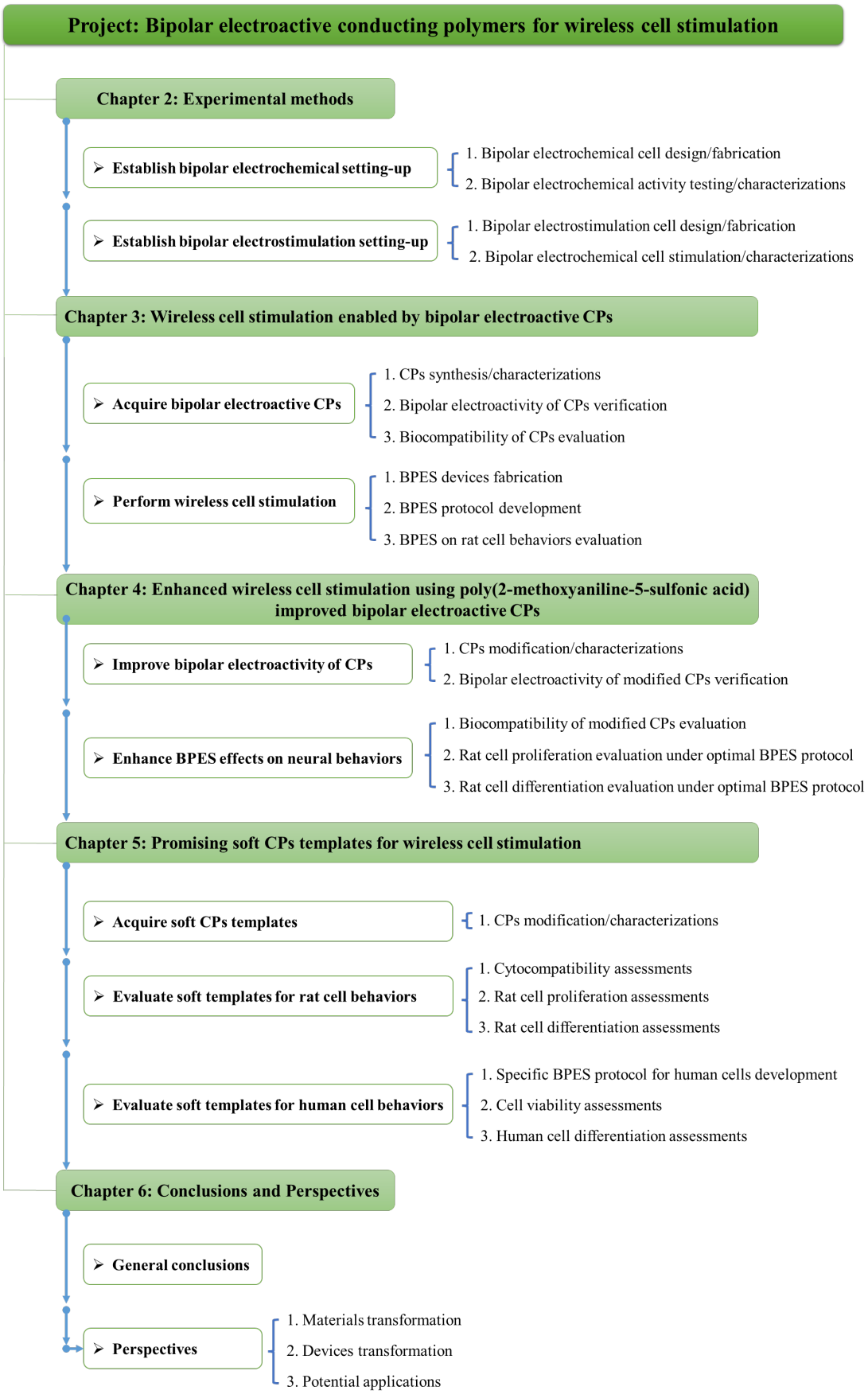

Figure 1.12 Illustrated overview of this project.

1.3 Objectives of this thesis

As discussed in section 1.2, few studies have reported wireless living cell stimulation on conducting polymers (CPs) via bipolar electrochemistry (BPE). Therefore, in this thesis, we aim to investigate bipolar electroactive and biocompatible CPs, explore their capability for living cell stimulation using BPE, and build a wireless CP-based bipolar electrochemical stimulation (BPES) system with a view towards suiting for human disease-related electroceutical therapies.

Specific aims/milestones/experiments are outlined and listed in Figure 1.12.

Objective 1: Obtain bipolar electroactive CPs, verify the bipolar electrochemical activity of CPs in a biological environment, establish CP-based BPES system, and perform wireless general cell stimulation in Chapter 3.

Objective 2: Modify CPs, test the improved bipolar electrochemical activity of CPs in a biological environment, and evaluate the effects of modified CP-based BPES on wireless general cell stimulation in Chapter 4.

Objective 3: Synthesise and characterise soft and free-standing CP templates, evaluate the effects of soft CP-based BPES on wireless general cell stimulation, develop BPES protocol for specific human cells, and evaluate the effects of soft CP-based BPES on wireless human cell stimulation in Chapter 5.

1.4 References

[1] P. Hunter Peckham, Functional electrical stimulation: Current status and future prospects of applications to the neuromuscular system in spinal cord injury, Paraplegia. 25 (1987) 279–288. https://doi.org/10.1038/sc.1987.52.

[2] H. Madersbacher, Intravesical electrical stimulation for the rehabilitation of the neuropathic bladder, Paraplegia. 28 (1990) 349–352. https://doi.org/10.1038/sc.1990.47.

[3] M. (2013) Famm, K., Litt, B., Tracey, K.J., Boyden, E.S., Slaoui, Drug discovery: a jump-start for electroceuticals, Nature. 496 (2013) 159–161.

[4] S. Zhao, A.S. Mehta, M. Zhao, Biomedical applications of electrical stimulation, Cell. Mol. Life Sci. 77 (2020) 2681–2699. https://doi.org/10.1007/s00018-019-03446-1.

[5] G. Dijk, H.J. Ruigrok, R.P. O'Connor, PEDOT:PSS-Coated Stimulation Electrodes Attenuate Irreversible Electrochemical Events and Reduce Cell Electropermeabilization, Adv. Mater. Interfaces. 8 (2021) 1–8. https://doi.org/10.1002/admi.202100214.

[6] A.F. Quigley, J.M. Razal, M. Kita, R. Jalili, A. Gelmi, A. Penington, R. Ovalle-Robles, R.H. Baughman, G.M. Clark, G.G. Wallace, R.M.I. Kapsa, Electrical Stimulation of Myoblast Proliferation and Differentiation on Aligned Nanostructured Conductive Polymer Platforms, Adv. Healthc. Mater. 1 (2012) 801–808. https://doi.org/10.1002/adhm.201200102.

[7] M.J. Higgins, P.J. Molino, Z. Yue, G.G. Wallace, Organic conducting polymer-protein interactions, Chem. Mater. 24 (2012) 828–839. https://doi.org/10.1021/cm203138j.

[8] X. Liu, Z. Yue, M.J. Higgins, G.G. Wallace, Conducting polymers with immobilised fibrillar collagen for enhanced neural interfacing, Biomaterials. 32 (2011) 7309–7317. https://doi.org/10.1016/j.biomaterials.2011.06.047.

[9] R.A. Green, N.H. Lovell, G.G. Wallace, L.A. Poole-Warren, Conducting polymers for neural interfaces: Challenges in developing an effective long-term implant, Biomaterials. 29 (2008) 3393–3399. https://doi.org/10.1016/j.biomaterials.2008.04.047.

[10] V.P. Mesut Sahin, Wireless microstimulators for neural prosthetics, Crit Rev Biomed Eng. 39 (2011) 63–77.

[11] K. Kapat, Q.T.H. Shubhra, M. Zhou, S. Leeuwenburgh, Piezoelectric Nano-Biomaterials for Biomedicine and Tissue Regeneration, Adv. Funct. Mater. 30 (2020). https://doi.org/10.1002/adfm.201909045.

[12] A. Singer, S. Dutta, E. Lewis, Z. Chen, J.C. Chen, N. Verma, B. Avants, A.K. Feldman, J. O'Malley, M. Beierlein, C. Kemere, J.T. Robinson, Magnetoelectric Materials for Miniature, Wireless Neural Stimulation at Therapeutic Frequencies, Neuron. 107 (2020) 631-643.e5. https://doi.org/10.1016/j.neuron.2020.05.019.

[13] N. Shida, Y. Zhou, S. Inagi, Bipolar Electrochemistry: A Powerful Tool for Electrifying Functional Material Synthesis, Acc. Chem. Res. (2019). https://doi.org/10.1021/acs.accounts.9b00337.

[14] S.E. Fosdick, K.N. Knust, K. Scida, R.M. Crooks, Bipolar electrochemistry, Angew. Chemie - Int. Ed. 52 (2013) 10438–10456. https://doi.org/10.1002/anie.201300947.

[15] J.K. Krauss, N. Lipsman, T. Aziz, A. Boutet, P. Brown, J.W. Chang, B. Davidson, W.M. Grill, M.I. Hariz, A. Horn, M. Schulder, A. Mammis, P.A. Tass, J. Volkmann, A.M. Lozano, Technology of deep brain stimulation: current status and future directions, Nat. Rev. Neurol. (2020). https://doi.org/10.1038/s41582-020-00426-z.

[16] M. Hopkin, Implant boosts activity in injured brain, Nature. 448 (2007) 522. https://doi.org/10.1038/448522a.

[17] X. Yu, Z. Xie, Y. Yu, J. Lee, A. Vazquez-Guardado, H. Luan, J. Ruban, X. Ning, A. Akhtar, D. Li, B. Ji, Y. Liu, R. Sun, J. Cao, Q. Huo, Y. Zhong, C.M. Lee, S.Y. Kim, P. Gutruf, C. Zhang, Y. Xue, Q. Guo, A. Chempakasseril, P. Tian, W. Lu, J.Y. Jeong, Y.J. Yu, J. Cornman, C.S. Tan, B.H. Kim, K.H. Lee, X. Feng, Y. Huang, J.A. Rogers, Skin-integrated wireless haptic interfaces for virtual and augmented reality, Nature. 575 (2019) 473–479. https://doi.org/10.1038/s41586-019-1687-0.

[18] S. Mura, J. Nicolas, P. Couvreur, Stimuli-responsive nanocarriers for drug delivery, Nat. Mater. 12 (2013) 991–1003. https://doi.org/10.1038/nmat3776.

[19] J.A. Steinbeck, S.J. Choi, A. Mrejeru, Y. Ganat, K. Deisseroth, D. Sulzer, E. V. Mosharov, L. Studer, Optogenetics enables functional analysis of human embryonic stem cell-derived grafts in a Parkinson's disease model, Nat. Biotechnol. 33 (2015) 204–209. https://doi.org/10.1038/nbt.3124.

[20] A. Kotwal, C.E. Schmidt, Electrical stimulation alters protein adsorption and nerve cell interactions with electrically conducting biomaterials, Biomaterials. 22 (2001) 1055–1064. https://doi.org/10.1016/S0142-9612(00)00344-6.

[21] Y. Wei, X. Mo, P. Zhang, Y. Li, J. Liao, Y. Li, J. Zhang, C. Ning, S. Wang, X. Deng, L. Jiang, Directing Stem Cell Differentiation via Electrochemical Reversible Switching between Nanotubes and Nanotips of Polypyrrole Array, ACS Nano. 11 (2017) 5915–5924. https://doi.org/10.1021/acsnano.7b01661.

[22] B. Zhu, S.C. Luo, H. Zhao, H.A. Lin, J. Sekine, A. Nakao, C. Chen, Y. Yamashita, H.H. Yu, Large enhancement in neurite outgrowth on a cell membrane-mimicking conducting polymer, Nat. Commun. 5 (2014). https://doi.org/10.1038/ncomms5523.

[23] X. Liu, J. Chen, K.J. Gilmore, M.J. Higgins, Y. Liu, G.G. Wallace, Guidance of neurite outgrowth on aligned electrospun polypyrrole/ poly(styrene-β-isobutylene-β-

styrene) fiber platforms, J. Biomed. Mater. Res. - Part A. 94 (2010) 1004–1011. https://doi.org/10.1002/jbm.a.32675.

[24] J. Li, X. Liu, J.M. Crook, G.G. Wallace, Electrical stimulation-induced osteogenesis of human adipose derived stem cells using a conductive graphene-cellulose scaffold, Mater. Sci. Eng. C. 107 (2020) 110312. https://doi.org/10.1016/j.msec.2019.110312.

[25] K. Lynch, O. Skalli, F. Sabri, Growing Neural PC-12 Cell on Crosslinked Silica Aerogels Increases Neurite Extension in the Presence of an Electric Field, J. Funct. Biomater. 9 (2018) 30. https://doi.org/10.3390/jfb9020030.

[26] B. Song, Nerve regeneration and wound healing are stimulated and directed by an endogenous electrical field in vivo, J. Cell Sci. 117 (2004) 4681–4690. https://doi.org/10.1242/jcs.01341.

[27] Y. Ito, T. Yagi, Y. Ohnishi, K. Kiuchi, Y. Uchikawa, A study on conductive polymer electrodes for stimulating the nervous system, Int. J. Appl. Electromagn. Mech. 14 (2001) 347–352.

[28] W.R. Stauffer, X.T. Cui, Polypyrrole doped with 2 peptide sequences from laminin, Biomaterials. 27 (2006) 2405–2413.

[29] D. Kim, S.M. Richardson-Burns, J.L. Hendricks, C. Sequera, D.C. Martin, Effect of immobilized nerve growth factor on conductive polymers: electrical properties and cellular response, Adv. Funct. Mater. 17 (2007) 79–86.

[30] K.-H. Park, E.A. Jo, K. Na, Heparin/polypyrrole (PPy) composite on gold-coated matrix for the neurite outgrowth of PC12 cells by electrical stimulation, Biotechnol. Bioprocess Eng. 12 (2007) 463.

[31] X. Cui, J. Wiler, M. Dzaman, R.A. Altschuler, D.C. Martin, In vivo studies of polypyrrole/peptide coated neural probes, Biomaterials. 24 (2003) 777–787.

[32] X. Liu, K.J. Gilmore, S.E. Moulton, G.G. Wallace, Electrical stimulation promotes nerve cell differentiation on polypyrrole/poly (2-methoxy-5 aniline sulfonic acid) composites, J. Neural Eng. 6 (2009). https://doi.org/10.1088/1741-2560/6/6/065002.

[33] Z. Yue, X. Liu, P.J. Molino, G.G. Wallace, Bio-functionalisation of polydimethylsiloxane with hyaluronic acid and hyaluronic acid - Collagen conjugate for neural interfacing, Biomaterials. 32 (2011) 4714–4724. https://doi.org/10.1016/j.biomaterials.2011.03.032.

[34] Z. Yue, X. Liu, P.J. Molino, G.G. Wallace, Bio-functionalisation of polydimethylsiloxane with hyaluronic acid and hyaluronic acid–collagen conjugate for neural interfacing, Biomaterials. 32 (2011) 4714–4724.

[35] E. Moro, Neurosurgery: Complications of DBS surgery-insights from large databases, Nat. Rev. Neurol. 12 (2016) 617–618. https://doi.org/10.1038/nrneurol.2016.163.

[36] D.K. Piech, B.C. Johnson, K. Shen, M.M. Ghanbari, K.Y. Li, R.M. Neely, J.E. Kay, J.M. Carmena, M.M. Maharbiz, R. Muller, A wireless millimetre-scale implantable neural stimulator with ultrasonically powered bidirectional communication, 2020. https://doi.org/10.1038/s41551-020-0518-9.

[37] N.T. Markwardt, J. Stokol, R.L. Rennaker, Sub-meninges implantation reduces immune response to neural implants, J. Neurosci. Methods. 214 (2013) 119–125. https://doi.org/10.1016/j.jneumeth.2013.01.020.

[38] A.E. Pena, S.S. Kuntaegowdanahalli, J.J. Abbas, J. Patrick, K.W. Horch, R. Jung, Mechanical fatigue resistance of an implantable branched lead system for a distributed set of longitudinal intrafascicular electrodes, J. Neural Eng. 14 (2017). https://doi.org/10.1088/1741-2552/aa814d.

[39] R.C. Pinnell, A.P. de Vasconcelos, J.C. Cassel, U.G. Hofmann, A miniaturized, programmable deep-brain stimulator for group-housing and water maze use, Front. Neurosci. 12 (2018) 1–11. https://doi.org/10.3389/fnins.2018.00231.

[40] Y. Wang, S. Vaddiraju, B. Gu, F. Papadimitrakopoulos, D.J. Burgess, Foreign body reaction to implantable biosensors: Effects of tissue trauma and implant size, J. Diabetes Sci. Technol. 9 (2015) 966–977. https://doi.org/10.1177/1932296815601869.

[41] S.E. Fosdick, K.N. Knust, K. Scida, R.M. Crooks, Bipolar electrochemistry, Angew. Chemie - Int. Ed. 52 (2013) 10438–10456. https://doi.org/10.1002/anie.201300947.

[42] W. Zhan, J. Alvarez, R.M. Crooks, Electrochemical sensing in microfluidic systems using electrogenerated chemiluminescence as a photonic reporter of redox reactions, J. Am. Chem. Soc. 124 (2002) 13265–13270.

[43] K.F. Chow, F. Mavré, R.M. Crooks, Wireless electrochemical DNA microarray sensor, J. Am. Chem. Soc. 130 (2008) 7544–7545. https://doi.org/10.1021/ja802013q.

[44] R.M. Crooks, Principles of Bipolar Electrochemistry, ChemElectroChem. 3 (2016) 357–359. https://doi.org/10.1002/celc.201500549.

[45] S.E. Fosdick, S.P. Berglund, C.B. Mullins, R.M. Crooks, Parallel screening of electrocatalyst candidates using bipolar electrochemistry, Anal. Chem. 85 (2013) 2493–2499. https://doi.org/10.1021/ac303581b.

[46] G. Loget, G. Larcade, V. Lapeyre, P. Garrigue, C. Warakulwit, J. Limtrakul, M.-H. Delville, V. Ravaine, A. Kuhn, Single point electrodeposition of nickel for the dissymmetric decoration of carbon tubes, Electrochim. Acta. 55 (2010) 8116–8120.

[47] L. Bouffier, N. Sojic, A. Kuhn, Capillary-assisted bipolar electrochemistry: A focused mini review, Electrophoresis. 38 (2017) 2687–2694.

[48] A.J. Bard, L.R. Faulkner, J. Leddy, C.G. Zoski, Electrochemical methods:

fundamentals and applications, wiley New York, 1980.

[49] D.C. Eardley, D. Handley, S.P.S. Andrew, Bipolar electrolysis with intra phase conduction in two phase media, Electrochim. Acta. 18 (1973) 839–848.

[50] F. Goodridge, Some recent developments of monopolar and bipolar fluidized bed electrodes, Electrochim. Acta. 22 (1977) 929–933.

[51] J. Yang, Q. Zhang, H. Wang, Y. Liu, Establishment and verification of mathematical model for current leakage in bipolar multi-compartment cell, Trans. Nonferrous Met. Soc. China(China). 5 (1995) 29–35.

[52] R. Dhopeshwarkar, D. Hlushkou, M. Nguyen, U. Tallarek, R.M. Crooks, Electrokinetics in microfluidic channels containing a floating electrode, J. Am. Chem. Soc. 130 (2008) 10480–10481. https://doi.org/10.1021/ja8036405.

[53] R.K. Anand, E. Sheridan, D. Hlushkou, U. Tallarek, R.M. Crooks, Bipolar electrode focusing: tuning the electric field gradient, Lab Chip. 11 (2011) 518–527.

[54] G. Loget, D. Zigah, L. Bouffier, N. Sojic, A. Kuhn, Bipolar electrochemistry: from materials science to motion and beyond, Acc. Chem. Res. 46 (2013) 2513–2523.

[55] L. Koefoed, K. Shimizu, S.U. Pedersen, K. Daasbjerg, A. Kuhn, D. Zigah, One-step preparation of bifunctionalized surfaces by bipolar electrografting, Rsc Adv. 6 (2016) 3882–3887.

[56] L. Bouffier, S. Arbault, A. Kuhn, N. Sojic, Generation of electrochemiluminescence at bipolar electrodes: concepts and applications, Anal. Bioanal. Chem. 408 (2016) 7003–7011. https://doi.org/10.1007/s00216-016-9606-9.

[57] L. Bouffier, T. Doneux, B. Goudeau, A. Kuhn, Imaging redox activity at bipolar electrodes by indirect fluorescence modulation, Anal. Chem. 86 (2014) 3708–3711.

[58] J.F.L. Duval, Electrokinetics of the amphifunctional metal/electrolyte solution interface in the presence of a redox couple, J. Colloid Interface Sci. 269 (2004) 211–

223. https://doi.org/10.1016/j.jcis.2003.07.025.

[59] J.F.L. Duval, H.P. Van Leeuwen, J. Cecilia, J. Galceran, Rigorous analysis of reversible faradaic depolarization processes in the electrokinetics of the metal/electrolyte solution interface, J. Phys. Chem. B. 107 (2003) 6782–6800.

[60] J.F.L. Duval, J. Buffle, H.P. Van Leeuwen, Quasi-reversible faradaic depolarization processes in the electrokinetics of the metal/solution interface, J. Phys. Chem. B. 110 (2006) 6081–6094. https://doi.org/10.1021/jp055650+.

[61] J.F.L. Duval, M. Minor, J. Cecilia, H.P. Van Leeuwen, Coupling of lateral electric field and transversal faradaic processes at the conductor/electrolyte solution interface, J. Phys. Chem. B. 107 (2003) 4143–4155. https://doi.org/10.1021/jp022459g.

[62] S.E. Fosdick, S.P. Berglund, C.B. Mullins, R.M. Crooks, Parallel screening of electrocatalyst candidates using bipolar electrochemistry, Anal. Chem. 85 (2013) 2493–2499.

[63] K.-F. Chow, F. Mavré, J.A. Crooks, B.-Y. Chang, R.M. Crooks, A Large-Scale, Wireless Electrochemical Bipolar Electrode Microarray, J. Am. Chem. Soc. 131 (2009) 8364–8365. https://doi.org/10.1021/ja902683f.

[64] I. Dumitrescu, R.K. Anand, S.E. Fosdick, R.M. Crooks, Pressure-driven bipolar electrochemistry, J. Am. Chem. Soc. 133 (2011) 4687–4689.

[65] K.F. Chow, B.Y. Chang, B.A. Zaccheo, F. Mavré, R.M. Crooks, A sensing platform based on electrodissolution of a Ag bipolar electrode, J. Am. Chem. Soc. 132 (2010) 9228–9229. https://doi.org/10.1021/ja103715u.

[66] S.E. Fosdick, R.M. Crooks, Bipolar electrodes for rapid screening of electrocatalysts, J. Am. Chem. Soc. 134 (2011) 863–866.

[67] J.C. Bradley, Z. Ma, S.G. Stephens, Electric field directed construction of diodes using free-standing three-dimensional components, Adv. Mater. 11 (1999) 374–378.

https://doi.org/10.1002/(SICI)1521-4095(199903)11:5<374::AID-ADMA374>3.0.CO;2-Q.

[68] J.C. Bradley, S. Dengra, G.A. Gonzalez, G. Marshall, F. V Molina, Ion transport and deposit growth in spatially coupled bipolar electrochemistry, J. Electroanal. Chem. 478 (1999) 128–139. https://doi.org/10.1016/S0022-0728(99)00424-6.

[69] and S.G.S. Jean-Claude Bradley,*, z Zhongming Ma, Ed Clark, Jeffrey Crawford, Programmable Hard-Wiring of Circuitry Using Spatially Coupled Bipolar Electrochemistry, J. Electrochem. Soc. 146 (1999) 194–198. https://doi.org/10.1149/1.1391586.

[70] J. Bradley, Z. Ma, Contactless electrodeposition of palladium catalysts, Angew. Chemie Int. Ed. 38 (1999) 1663–1666.

[71] J. Bradley, J. Crawford, K. Ernazarova, M. McGee, S.G. Stephens, Wire formation on circuit boards using spatially coupled bipolar electrochemistry, Adv. Mater. 9 (1997) 1168–1171.

[72] J. Bradley, J. Crawford, M. McGee, S.G. Stephens, A contactless method for the directed formation of submicrometer copper wires, J. Electrochem. Soc. 145 (1998) L45–L47.

[73] J.-C. Bradley, H.-M. Chen, J. Crawford, J. Eckert, K. Ernazarova, T. Kurzeja, M. Lin, M. McGee, W. Nadler, S.G. Stephens, Creating electrical contacts between metal particles using directed electrochemical growth, Nature. 389 (1997) 268.

[74] G. Loget, V. Lapeyre, P. Garrigue, C. Warakulwit, J. Limtrakul, M.H. Delville, A. Kuhn, Versatile procedure for synthesis of janus-type carbon tubes, Chem. Mater. 23 (2011) 2595–2599. https://doi.org/10.1021/cm2001573.

[75] G. Loget, A. Kuhn, Propulsion of microobjects by dynamic bipolar self-regeneration, J. Am. Chem. Soc. 132 (2010) 15918–15919.

https://doi.org/10.1021/ja107644x.

[76] I. Malytska, C. Mézière, M. Kielar, L. Hirsch, G. Wantz, N. Avarvari, A. Kuhn, L. Bouffier, Bipolar Electrochemistry with Organic Single Crystals for Wireless Synthesis of Metal-Organic Janus Objects and Asymmetric Photovoltage Generation, J. Phys. Chem. C. 121 (2017) 12921–12927. https://doi.org/10.1021/acs.jpcc.7b02678.

[77] Z. Fattah, P. Garrigue, V. Lapeyre, A. Kuhn, L. Bouffier, Controlled orientation of asymmetric copper deposits on carbon microobjects by bipolar electrochemistry, J. Phys. Chem. C. 116 (2012) 22021–22027.

[78] L. Bouffier, N. Sojic, A. Kuhn, Capillary-assisted bipolar electrochemistry: A focused mini review, Electrophoresis. 00 (2017) 1–8. https://doi.org/10.1002/elps.201600568.

[79] M.-S. Wu, D.-J. Yuan, J.-J. Xu, H.-Y. Chen, Electrochemiluminescence on bipolar electrodes for visual bioanalysis, Chem. Sci. 4 (2013) 1182. https://doi.org/10.1039/c2sc22055e.

[80] M.-S. Wu, D.-J. Yuan, J.-J. Xu, H.-Y. Chen, Sensitive electrochemiluminescence biosensor based on Au-ITO hybrid bipolar electrode amplification system for cell surface protein detection, Anal. Chem. 85 (2013) 11960–11965.

[81] S. Campuzano, D. Kagan, J. Orozco, J. Wang, Motion-driven sensing and biosensing using electrochemically propelled nanomotors, Analyst. 136 (2011) 4621. https://doi.org/10.1039/c1an15599g.

[82] J. Wang, Can man-made nanomachines compete with nature biomotors?, ACS Nano. 3 (2009) 4–9.

[83] S. Balasubramanian, D. Kagan, C. Jack Hu, S. Campuzano, M.J. Lobo-Castañon, N. Lim, D.Y. Kang, M. Zimmerman, L. Zhang, J. Wang, Micromachine-enabled capture and isolation of cancer cells in complex media, Angew. Chemie. 123

(2011) 4247–4250.

[84] D. Kagan, S. Campuzano, S. Balasubramanian, F. Kuralay, G.-U. Flechsig, J. Wang, Functionalized micromachines for selective and rapid isolation of nucleic acid targets from complex samples, Nano Lett. 11 (2011) 2083–2087.

[85] K.N. Knust, D. Hlushkou, R.K. Anand, U. Tallarek, R.M. Crooks, Electrochemically mediated seawater desalination, Angew. Chemie - Int. Ed. 52 (2013) 8107–8110. https://doi.org/10.1002/anie.201302577.

[86] W. Zhan, R.M. Crooks, Microelectrochemical logic circuits, J. Am. Chem. Soc. 125 (2003) 9934–9935. https://doi.org/10.1021/ja0366585.

[87] B.-Y. Chang, K.-F. Chow, J.A. Crooks, F. Mavré, R.M. Crooks, Two-channel microelectrochemical bipolar electrode sensor array, Analyst. 137 (2012) 2827. https://doi.org/10.1039/c2an35382b.

[88] S.E. Fosdick, J.A. Crooks, B.-Y. Chang, R.M. Crooks, Two-dimensional bipolar electrochemistry, J. Am. Chem. Soc. 132 (2010) 9226–9227.

[89] E. Sheridan, D. Hlushkou, K.N. Knust, U. Tallarek, R.M. Crooks, Enrichment of Cations via Bipolar Electrode Focusing, Anal. Chem. 84 (2012) 7393–7399. https://doi.org/10.1021/ac301101b.

[90] E. Sheridan, D. Hlushkou, R.K. Anand, D.R. Laws, U. Tallarek, R.M. Crooks, Label-free electrochemical monitoring of concentration enrichment during bipolar electrode focusing, Anal. Chem. 83 (2011) 6746–6753.

[91] B.Y. Chang, F. Mavré, K.F. Chow, J.A. Crooks, R.M. Crooks, Snapshot voltammetry using a triangular bipolar microelectrode, Anal. Chem. 82 (2010) 5317–5322. https://doi.org/10.1021/ac100846v.

[92] R.K. Anand, E. Sheridan, K.N. Knust, R.M. Crooks, Bipolar electrode focusing: Faradaic ion concentration polarization, Anal. Chem. 83 (2011) 2351–2358.

https://doi.org/10.1021/ac103302j.

[93] B.Y. Chang, J.A. Crooks, K.F. Chow, F. Mavré, R.M. Crooks, Design and operation of microelectrochemical gates and integrated circuits, J. Am. Chem. Soc. 132 (2010) 15404–15409. https://doi.org/10.1021/ja107095z.

[94] D.R. Laws, D. Hlushkou, R.K. Perdue, U. Tallarek, R.M. Crooks, Bipolar electrode focusing: simultaneous concentration enrichment and separation in a microfluidic channel containing a bipolar electrode, Anal. Chem. 81 (2009) 8923–8929.

[95] K.N. Knust, E. Sheridan, R.K. Anand, R.M. Crooks, Dual-channel bipolar electrode focusing: simultaneous separation and enrichment of both anions and cations, Lab Chip. 12 (2012) 4107. https://doi.org/10.1039/c2lc40660h.

[96] R.K. Perdue, D.R. Laws, D. Hlushkou, U. Tallarek, R.M. Crooks, Bipolar electrode focusing: The effect of current and electric field on concentration enrichment, Anal. Chem. 81 (2009) 10149–10155. https://doi.org/10.1021/ac901913r.

[97] D. Hlushkou, R.K. Perdue, R. Dhopeshwarkar, R.M. Crooks, U. Tallarek, Electric field gradient focusing in microchannels with embedded bipolar electrode, Lab Chip. 9 (2009) 1903. https://doi.org/10.1039/b822404h.

[98] E. Sheridan, K.N. Knust, R.M. Crooks, Bipolar electrode depletion: membraneless filtration of charged species using an electrogenerated electric field gradient, Analyst. 136 (2011) 4134–4137.

[99] K. Scida, E. Sheridan, R.M. Crooks, Electrochemically-gated delivery of analyte bands in microfluidic devices using bipolar electrodes, Lab Chip. 13 (2013) 2292. https://doi.org/10.1039/c3lc50321f.

[100] C.K. Chiang, C.R. Fincher Jr, Y.W. Park, A.J. Heeger, H. Shirakawa, E.J. Louis, S.C. Gau, A.G. MacDiarmid, Electrical conductivity in doped polyacetylene, Phys. Rev. Lett. 39 (1977) 1098.

[101] H. Shirakawa, E.J. Louis, A.G. MacDiarmid, C.K. Chiang, AJ Heeger J. Chem. Soc, Chem. Commun. 578 (1977) 31.

[102] S. Sadki, P. Schottland, N. Brodie, G. Sabouraud, The mechanisms of pyrrole electropolymerization, Chem. Soc. Rev. 29 (2000) 283–293.

[103] C.K. Chiang, M.A. Druy, S.C. Gau, A.J. Heeger, E.J. Louis, A.G. MacDiarmid, Y.W. Park, H. Shirakawa, Synthesis of highly conducting films of derivatives of polyacetylene,(CH) x, J. Am. Chem. Soc. 100 (1978) 1013–1015.

[104] J. Heinze, B.A. Frontana-Uribe, S. Ludwigs, Electrochemistry of Conducting Polymers□Persistent Models and New Concepts, Chem. Rev. 110 (2010) 4724–4771.

[105] P.M. Beaujuge, J.R. Reynolds, Color control in π-conjugated organic polymers for use in electrochromic devices, Chem. Rev. 110 (2010) 268–320.

[106] Y. Ishiguro, S. Inagi, T. Fuchigami, Gradient doping of conducting polymer films by means of bipolar electrochemistry, Langmuir. 27 (2011) 7158–7162. https://doi.org/10.1021/la200464t.

[107] S. Inagi, T. Fuchigami, Electrochemical Post-Functionalization of Conducting Polymers, Macromol. Rapid Commun. 35 (2014) 854–867.

[108] S. Inagi, Y. Ishiguro, M. Atobe, T. Fuchigami, Bipolar patterning of conducting polymers by electrochemical doping and reaction, Angew. Chemie - Int. Ed. 49 (2010) 10136–10139. https://doi.org/10.1002/anie.201005671.

[109] S. Inagi, S. Hayashi, T. Fuchigami, Electrochemical polymer reaction: selective fluorination of a poly (fluorene) derivative, Chem. Commun. (2009) 1718–1720.

[110] S. Hayashi, S. Inagi, T. Fuchigami, Synthesis of 9-substituted fluorene copolymers via chemical and electrochemical polymer reaction and their optoelectronic properties, Macromolecules. 42 (2009) 3755–3760.

[111] S. Inagi, K. Koseki, S. Hayashi, T. Fuchigami, Electrochemical tuning of the

optoelectronic properties of a fluorene-based conjugated polymer, Langmuir. 26 (2010) 18631–18633.

[112] S. Inagi, S. Hayashi, K. Hosaka, T. Fuchigami, Facile Functionalization of a Thiophene− Fluorene Alternating Copolymer via Electrochemical Polymer Reaction, Macromolecules. 42 (2009) 3881–3883.

[113] S. Inagi, H. Nagai, I. Tomita, T. Fuchigami, Parallel polymer reactions of a polyfluorene derivative by electrochemical oxidation and reduction, Angew. Chemie - Int. Ed. 52 (2013) 6616–6619. https://doi.org/10.1002/anie.201302251.

[114] Y. Ishiguro, S. Inagi, T. Fuchigami, Site-controlled application of electric potential on a conducting polymer "canvas," J. Am. Chem. Soc. 134 (2012) 4034–4036. https://doi.org/10.1021/ja211774z.

[115] N. Shida, Y. Ishiguro, M. Atobe, T. Fuchigami, S. Inagi, Electro-click modification of conducting polymer surface using Cu (I) species generated on a bipolar electrode in a gradient manner, ACS Macro Lett. 1 (2012) 656–659.

[116] N. Shida, Y. Koizumi, H. Nishiyama, I. Tomita, S. Inagi, Electrochemically mediated atom transfer radical polymerization from a substrate surface manipulated by bipolar electrolysis: Fabrication of gradient and patterned polymer brushes, Angew. Chemie Int. Ed. 54 (2015) 3922–3926.

[117] Y. Koizumi, N. Shida, M. Ohira, H. Nishiyama, I. Tomita, S. Inagi, Electropolymerization on wireless electrodes towards conducting polymer microfibre networks, Nat. Commun. 7 (2016) 10404.

[118] M. Ohira, Y. Koizumi, H. Nishiyama, I. Tomita, S. Inagi, Synthesis of linear PEDOT fibers by AC-bipolar electropolymerization in a micro-space, Polym. J. 49 (2017) 163.

[119] G.G. Genchi, E. Sinibaldi, L. Ceseracciu, M. Labardi, A. Marino, S. Marras, G.

De Simoni, V. Mattoli, G. Ciofani, Ultrasound-activated piezoelectric P(VDF-TrFE)/boron nitride nanotube composite films promote differentiation of human SaOS-2 osteoblast-like cells, Nanomedicine Nanotechnology, Biol. Med. 14 (2018) 2421–2432. https://doi.org/10.1016/j.nano.2017.05.006.

[120] M. Jakešová, M. Silverå Ejneby, V. Đerek, T. Schmidt, M. Gryszel, J. Brask, R. Schindl, D.T. Simon, M. Berggren, F. Elinder, E.D. Głowacki, Optoelectronic control of single cells using organic photocapacitors, Sci. Adv. 5 (2019) eaav5265. https://doi.org/10.1126/sciadv.aav5265.

[121] R. Guduru, P. Liang, J. Hong, A. Rodzinski, A. Hadjikhani, J. Horstmyer, E. Levister, S. Khizroev, Magnetoelectric "spin" on stimulating the brain, Nanomedicine. 10 (2015) 2051–2061. https://doi.org/10.2217/nnm.15.52.

[122] Y. Wang, K. Xie, H. Yue, X. Chen, X. Luo, Q. Liao, M. Liu, F. Wang, P. Shi, Flexible and fully implantable upconversion device for wireless optogenetic stimulation of the spinal cord in behaving animals, Nanoscale. 12 (2020) 2406–2414. https://doi.org/10.1039/c9nr07583f.

[123] J. Hopkins, L. Travaglini, A. Lauto, T. Cramer, B. Fraboni, J. Seidel, D. Mawad, Photoactive Organic Substrates for Cell Stimulation: Progress and Perspectives, Adv. Mater. Technol. 4 (2019) 1–10. https://doi.org/10.1002/admt.201800744.

[124] N.A. Repina, A. Rosenbloom, A. Mukherjee, D. V. Schaffer, R.S. Kane, At light speed: Advances in optogenetic systems for regulating cell signaling and behavior, Annu. Rev. Chem. Biomol. Eng. 8 (2017) 13–39. https://doi.org/10.1146/annurev-chembioeng-060816-101254.

[125] P.K. Wright, Medical Applications of Thermoelectrics, Modul. Syst. Appl. Thermoelectr. (2012) 535–564. https://doi.org/10.1201/b11892-30.

[126] M. Zhu, Q. Shi, T. He, Z. Yi, Y. Ma, B. Yang, T. Chen, C. Lee, Self-Powered and

Self-Functional Cotton Sock Using Piezoelectric and Triboelectric Hybrid Mechanism for Healthcare and Sports Monitoring, ACS Nano. (2019). https://doi.org/10.1021/acsnano.8b08329.

[127] M. Jakešová, Wireless Bioelectronic Devices Driven by Deep Red Light, n.d.

[128] H. Wang, A.J.F. Tampio, Y. Xu, B.D. Nicholas, D. Ren, Noninvasive Control of Bacterial Biofilms by Wireless Electrostimulation, ACS Biomater. Sci. Eng. 6 (2020) 727–738. https://doi.org/10.1021/acsbiomaterials.9b01199.

[129] M.N. Sardoiwala, A.K. Srivastava, S. Karmakar, S. Roy Choudhury, Nanostructure Endows Neurotherapeutic Potential in Optogenetics: Current Development and Future Prospects, ACS Chem. Neurosci. 10 (2019) 3375–3385. https://doi.org/10.1021/acschemneuro.9b00246.

[130] A. Marino, G.G. Genchi, M. Pisano, P. Massobrio, M. Tedesco, S. Martinoia, R. Raiteri, G. Ciofani, Nanomaterial-Assisted Acoustic Neural Stimulation, Neural Interface Eng. (2020) 347–363. https://doi.org/10.1007/978-3-030-41854-0_15.

[131] J. Blackmore, S. Shrivastava, J. Sallet, C.R. Butler, R.O. Cleveland, Ultrasound Neuromodulation: A Review of Results, Mechanisms and Safety, Ultrasound Med. Biol. 45 (2019) 1509–1536. https://doi.org/10.1016/j.ultrasmedbio.2018.12.015.

[132] X. Wang, J. Law, M. Luo, Z. Gong, J. Yu, W. Tang, Z. Zhang, X. Mei, Z. Huang, L. You, Y. Sun, Magnetic Measurement and Stimulation of Cellular and Intracellular Structures, ACS Nano. 14 (2020) 3805–3821. https://doi.org/10.1021/acsnano.0c00959.

[133] W. Hu, Q. Li, B. Li, K. Ma, C. Zhang, X. Fu, Optogenetics sheds new light on tissue engineering and regenerative medicine, Biomaterials. 227 (2020). https://doi.org/10.1016/j.biomaterials.2019.119546.

[134] L. Bareket-Keren, Y. Hanein, Novel interfaces for light directed neuronal stimulation: Advances and challenges, Int. J. Nanomedicine. 9 (2014) 65–83.

https://doi.org/10.2147/IJN.S51193.

[135] G. Loget, D. Zigah, L. Bouffier, N. Sojic, A. Kuhn, Bipolar electrochemistry: from materials science to motion and beyond, Acc. Chem. Res. 46 (2013) 2513–2523. https://doi.org/10.1021/ar400039k.

[136] J.F.L. Duval, Electrokinetics of the amphifunctional metal/electrolyte solution interface in the presence of a redox couple, J. Colloid Interface Sci. 269 (2004) 211–223.

[137] J.F.L. Duval, H.P. van Leeuwen, J. Cecilia, J. Galceran, Rigorous Analysis of Reversible Faradaic Depolarization Processes in the Electrokinetics of the Metal/Electrolyte Solution Interface, J. Phys. Chem. B. 107 (2003) 6782–6800. https://doi.org/10.1021/jp030278o.

[138] X.F. Huang, X. Song, Effects of antipsychotic drugs on neurites relevant to schizophrenia treatment, Med. Res. Rev. 39 (2019) 386–403. https://doi.org/10.1002/med.21512.

[139] M. Hu, P. Zheng, Y. Xie, Z. Boz, Y. Yu, R. Tang, A. Jones, K. Zheng, X.F. Huang, Propionate protects haloperidol-induced neurite lesions mediated by neuropeptide Y, Front. Neurosci. 12 (2018) 1–10. https://doi.org/10.3389/fnins.2018.00743.

[140] S.E. Fosdick, R.M. Crooks, Bipolar electrodes for rapid screening of electrocatalysts, J. Am. Chem. Soc. 134 (2012) 863–866. https://doi.org/10.1021/ja210354m.

[141] K.-F. Chow, F. Mavré, J.A. Crooks, B.-Y. Chang, R.M. Crooks, A large-scale, wireless electrochemical bipolar electrode microarray, J. Am. Chem. Soc. 131 (2009) 8364–8365.

[142] G. Loget, J. Roche, A. Kuhn, True bulk synthesis of Janus objects by bipolar

electrochemistry, Adv. Mater. 24 (2012) 5111–5116. https://doi.org/10.1002/adma.201201623.

[143] L. Koefoed, S.Us. Pedersen, K. Daasbjerg, Grafting of Aryl Diazonium, Iodonium, and Sulfonium Salts in Unusual Patterns by Exploiting the Potential Gradient in Bipolar Electrochemistry, ChemElectroChem. 3 (2016) 495–501. https://doi.org/10.1002/celc.201500512.

[144] Y. Wang, R. Jin, N. Sojic, D. Jiang, H.Y. Chen, Intracellular Wireless Analysis of Single Cells by Bipolar Electrochemiluminescence Confined in a Nanopipette, Angew. Chemie - Int. Ed. 59 (2020) 10416–10420. https://doi.org/10.1002/anie.202002323.

[145] A.M. Rajnicek, Z. Zhao, J. Moral-Vico, A.M. Cruz, C.D. McCaig, N. Casañ-Pastor, Controlling Nerve Growth with an Electric Field Induced Indirectly in Transparent Conductive Substrate Materials, Adv. Healthc. Mater. 7 (2018). https://doi.org/10.1002/adhm.201800473.

[146] L. Bouffier, N. Sojic, A. Kuhn, Capillary-assisted bipolar electrochemistry: A focused mini review, Electrophoresis. 38 (2017) 2687–2694. https://doi.org/10.1002/elps.201600568.

[147] E. Zeglio, A.L. Rutz, T.E. Winkler, G.G. Malliaras, A. Herland, Conjugated Polymers for Assessing and Controlling Biological Functions, Adv. Mater. 31 (2019). https://doi.org/10.1002/adma.201806712.

[148] R. Ravichandran, S. Sundarrajan, J.R. Venugopal, S. Mukherjee, S. Ramakrishna, Applications of conducting polymers and their issues in biomedical engineering, J. R. Soc. Interface. 7 (2010). https://doi.org/10.1098/rsif.2010.0120.focus.

[149] E.A. Cuttaz, C.A.R. Chapman, O. Syed, J.A. Goding, R.A. Green, Stretchable, Fully Polymeric Electrode Arrays for Peripheral Nerve Stimulation, Adv. Sci. 2004033 (2021) 1–14. https://doi.org/10.1002/advs.202004033.

[150] J.F. Maya-Vetencourt, D. Ghezzi, M.R. Antognazza, E. Colombo, M. Mete, P. Feyen, A. Desii, A. Buschiazzo, M. Di Paolo, S. Di Marco, F. Ticconi, L. Emionite, D. Shmal, C. Marini, I. Donelli, G. Freddi, R. MacCarone, S. Bisti, G. Sambuceti, G. Pertile, G. Lanzani, F. Benfenati, A fully organic retinal prosthesis restores vision in a rat model of degenerative blindness, Nat. Mater. 16 (2017) 681–689. https://doi.org/10.1038/nmat4874.

[151] E.M. Stewart, X. Liu, G.M. Clark, R.M.I. Kapsa, G.G. Wallace, Inhibition of smooth muscle cell adhesion and proliferation on heparin-doped polypyrrole, Acta Biomater. 8 (2012) 194–200. https://doi.org/10.1016/j.actbio.2011.07.029.

[152] X. Liu, Z. Yue, M.J. Higgins, G.G. Wallace, Conducting polymers with immobilised fibrillar collagen for enhanced neural interfacing, Biomaterials. 32 (2011) 7309–7317. https://doi.org/10.1016/j.biomaterials.2011.06.047.

[153] P.J. Molino, B.B. Zhang, G.G. Wallace, T.W. Hanks, Surface modification of polypyrrole/biopolymer composites for controlled protein and cellular adhesion, Biofouling. 29 (2013) 1155–1167. https://doi.org/10.1080/08927014.2013.830110.

[154] K.J. Gilmore, M. Kita, Y. Han, A. Gelmi, M.J. Higgins, S.E. Moulton, G.M. Clark, R. Kapsa, G.G. Wallace, Skeletal muscle cell proliferation and differentiation on polypyrrole substrates doped with extracellular matrix components, Biomaterials. 30 (2009) 5292–5304. https://doi.org/10.1016/j.biomaterials.2009.06.059.

[155] N. Wenger, E.M. Moraud, J. Gandar, P. Musienko, M. Capogrosso, L. Baud, C.G. Le Goff, Q. Barraud, N. Pavlova, N. Dominici, I.R. Minev, L. Asboth, A. Hirsch, S. Duis, J. Kreider, A. Mortera, O. Haverbeck, S. Kraus, F. Schmitz, J. DiGiovanna, R. Van Den Brand, J. Bloch, P. Detemple, S.P. Lacour, E. Bézard, S. Micera, G. Courtine, Spatiotemporal neuromodulation therapies engaging muscle synergies improve motor control after spinal cord injury, Nat. Med. 22 (2016) 138–145.

https://doi.org/10.1038/nm.4025.

[156] Z. Aqrawe, J. Montgomery, J. Travas-sejdic, D. Svirskis, Chemical Conducting polymers for neuronal microelectrode array recording and stimulation, Sensors Actuators B. Chem. 257 (2018) 753–765. https://doi.org/10.1016/j.snb.2017.11.023.

[157] E. Song, J. Li, S.M. Won, W. Bai, J.A. Rogers, Materials for flexible bioelectronic systems as chronic neural interfaces, Nat. Mater. 19 (2020) 590–603. https://doi.org/10.1038/s41563-020-0679-7.

[158] B.P. Ruddy, Conducting polymer wires for intravascular neural recording, 2006.

[159] Y. Long, J. Li, F. Yang, J. Wang, X. Wang, Wearable and Implantable Electroceuticals for Therapeutic Electrostimulations, Adv. Sci. 2004023 (2021) 1–22. https://doi.org/10.1002/advs.202004023.

[160] S. Inagi, Y. Ishiguro, M. Atobe, T. Fuchigami, Bipolar patterning of conducting polymers by electrochemical doping and reaction, Angew. Chemie. 122 (2010) 10334–10337.

[161] F. Sarvi, Z. Yue, K. Hourigan, M.C. Thompson, P.P.Y. Chan, Surface-functionalization of PDMS for potential micro-bioreactor and embryonic stem cell culture applications, J. Mater. Chem. B. 1 (2013) 987–996. https://doi.org/10.1039/c2tb00019a.

[162] J. Li, X. Liu, J.M. Crook, G.G. Wallace, Development of a porous 3D graphene-PDMS scaffold for improved osseointegration, Colloids Surfaces B Biointerfaces. 159 (2017) 386–393. https://doi.org/10.1016/j.colsurfb.2017.07.087.

[163] Y. Liu, J. Li, S. Song, J. Kang, Y. Tsao, S. Chen, V. Mottini, K. McConnell, W. Xu, Y.Q. Zheng, J.B.H. Tok, P.M. George, Z. Bao, Morphing electronics enable neuromodulation in growing tissue, Nat. Biotechnol. 38 (2020) 1031–1036. https://doi.org/10.1038/s41587-020-0495-2.

[164] C. Zhao, C. Wang, Z. Yue, K. Shu, G.G. Wallace, Intrinsically stretchable supercapacitors composed of polypyrrole electrodes and highly stretchable gel electrolyte, ACS Appl. Mater. Interfaces. 5 (2013) 9008–9014. https://doi.org/10.1021/am402130j.

[165] Z. Shi, X. Gao, M.W. Ullah, S. Li, Q. Wang, G. Yang, Electroconductive natural polymer-based hydrogels, Biomaterials. 111 (2016) 40–54. https://doi.org/10.1016/j.biomaterials.2016.09.020.

[166] C. Liao, M. Zhang, M.Y. Yao, T. Hua, L. Li, F. Yan, Flexible Organic Electronics in Biology: Materials and Devices, Adv. Mater. 27 (2015) 7493–7527. https://doi.org/10.1002/adma.201402625.

[167] G.J. Wilson, M.G. Looney, A.G. Pandolfo, Enhanced capacitance textile fibres for supercapacitors via an interfacial molecular templating process, Synth. Met. 160 (2010) 655–663. https://doi.org/10.1016/j.synthmet.2009.12.022.

[168] N. Gomez, C.E. Schmidt, Nerve growth factor-immobilized polypyrrole: Bioactive electrically conducting polymer for enhanced neurite extension, J. Biomed. Mater. Res. - Part A. 81 (2007) 135–149. https://doi.org/10.1002/jbm.a.31047.

[169] S. Vandghanooni, M. Eskandani, Electrically conductive biomaterials based on natural polysaccharides : Challenges and applications in tissue engineering, Int. J. Biol. Macromol. 141 (2019) 636–662. https://doi.org/10.1016/j.ijbiomac.2019.09.020.

[170] Y. Wang, H. Zhu, H. Yang, A.D. Argall, L. Luan, C. Xie, Nano functional neural interfaces, Nano Res. 11 (2018) 5065–5106.

[171] H. Palza, P.A. Zapata, C. Angulo-pineda, Electroactive Smart Polymers for Biomedical Applications, Materials (Basel). 12 (2019) 227.

[172] L. Guo, M. Ma, N. Zhang, R. Langer, D.G. Anderson, Stretchable polymeric multielectrode array for conformal neural interfacing, Adv. Mater. (2014).

https://doi.org/10.1002/adma.201304140.

[173] A. Inoue, H. Yuk, B. Lu, X. Zhao, Strong adhesion of wet conducting polymers on diverse substrates, Sci. Adv. 6 (2020) 1–11. https://doi.org/10.1126/sciadv.aay5394.

[174] Y. Liu, B. Weng, J.M. Razal, Q. Xu, C. Zhao, Y. Hou, S. Seyedin, R. Jalili, G.G. Wallace, J. Chen, High-Performance Flexible All-Solid-State Supercapacitor from Large Free-Standing Graphene-PEDOT/PSS Films, Sci. Rep. 5 (2015) 17045. https://doi.org/10.1038/srep17045.

Chapter 2

Experimental Methods

This chapter is partially adapted from the article, "Data on the bipolar electroactive conducting polymers for wireless cell stimulation" that was published in Data in Brief 33 (2020) 106406, by Chunyan Qin, Zhilian Yue, Yunfeng Chao, Robert J. Forster, Fionn Ó. Maolmhuaidh, Xu-Feng Huang, Stephen Beirne, Gordon G. Wallace, and Jun Chen, with permission from Elsevier.

2.1 Introduction

This chapter describes all materials, reagents, apparatus, techniques and procedures utilised throughout the project. It concentrates on bipolar electrochemical testing system, bipolar electroactivity characterisations, bipolar electrostimulation system, and relevant cells culture and stimulated cells characterisations. Specific information of each chapter is provided in corresponding experimental section.

2.2 Chemicals/reagents lists

The chemicals/reagents used in this project are listed in Table 2.1.

Table 2.1 Lists of chemical reagents and materials.

Item name	Supplier
Pyrrole (Py)	Sigma-Aldrich
Poly(3,4 ethylenedioxythiophene)-poly(styrenesulfonate) (PEDOT-PSS)	Ajax Finechem
p-toluenesulfonic acid monohydrate (*p*TS)	Sigma–Aldrich

Dextran sulfate sodium salt from Leuconostoc spp. (DS)	Sigma-Aldrich
Type collagen I	ThermoFisher
Fe(III) tosylate	Sigma-Aldrich
Phosphate buffered saline (PBS)	Sigma-Aldrich
Rhodamine Red ™ -X succunimidyl ester	Invitrogen
Stainless steel mesh (SSM: 500 × 500 with wire diameter of 0.025 mm)	Stainless Steel Wire & Mesh
Dental LT Clear Resin	LST
Clear RTV silicone adhesive sealant	Permatex
Ethanol	Chem-Supply
Acetone	Sigma-Aldrich
Tween-20	Sigma-Aldrich
Diethylene Glycol (DEG)	Sigma-Aldrich
Dulbecco's Modified Eagle Medium (DMEM)	Invitrogen
Horse serum	Invitrogen
Fetal Bovine Serum (FBS)	Invitrogen
Nerve growth factor (NGF)	Gibco
Dulbecco's Modified Eagle Medium/Nutrient Mixture F-12 (DMEM/F-12)	Invitrogen
Heat-inactivated Fetal Bovine Serum	Invitrogen
Penicillin/Streptomycin (P/S)	Gibco
Donkey serum	Merck
Calcein AM	Invitrogen
Propidium Iodide (PI)	Invitrogen
PicoGreen ™	Santa Cruz

Triton X-100	Sigma
Monoclonal anti- β- tubulin III (neuronal) antibody produced in mouse	Life Technologies
Alexa Fluor 546 (donkey anti-mouse IgG highly cross-adsorbed secondary antibody)	Life Technologies
4, 6-diamidino-2-phenylindole (DAPI)	Invitrogen

2.3 Materials preparation and fabrication techniques

2.3.1 Pyrrole (Py) monomer solution preparation

Various aqueous solution used in this study contained same pyrrole (Py) monomer concentration and different dopant concentrations. Generally, Py monomer was dissolved in deionized (DI) water via continuous hand stirring prior to dopant addition. All dopants were added one by one, that is, a dopant was added after the former dopant was dissolved completely. A well-dispersed solution was prepared after dissolving all dopants.

2.3.2 Electrodeposition polymerisation

All materials, such as solutions, substrates and electrochemical cells, were specifically treated before polymerisation. The prepared solutions were degassed with N_2 for 15 min to remove oxygen. The substrates such as fluorine-doped tin oxide (FTO) were cleaned and subjected to O_2 plasma treatment for increasing their wettability. Potential sweep electro-polymerisation [1–5] was carried out with a CHI-720 electrochemical analyser using a three-electrode cell (Figure 2.1a-b) that consisted of a substrate working electrode, Pt counter electrode, and Ag/AgCl reference electrode in treated solutions. Different doped polymers were deposited on the substrates by sweeping within potential

range at a reasonable rate. A digital photo of the obtained PANI and PPy films is shown in Figure 2.1c.

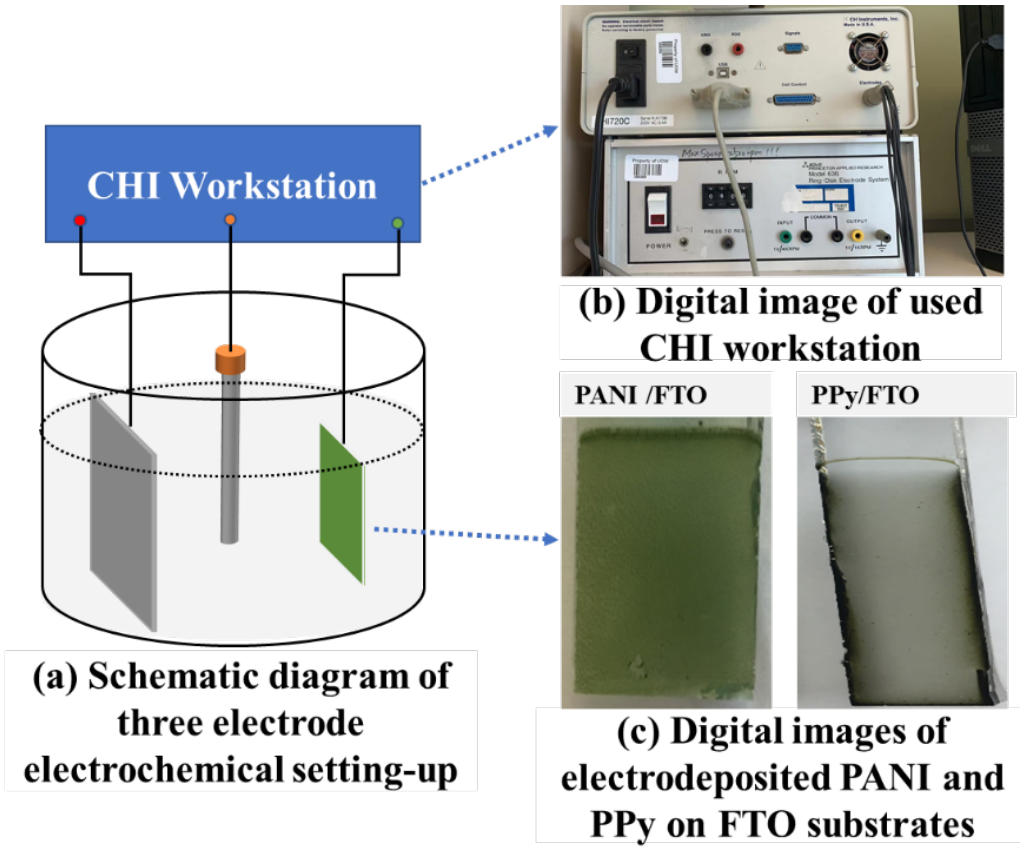

Figure 2.1 (a) Schematic diagram of three electrode electrochemical setting-up. Digital images of (b) used CHI workstation and (c) electrodeposited PANI and PPy on FTO substrates.

2.3.3 Chemical oxidation polymerisation

Chemical oxidation polymerisation [6,7] was performed using the same aqueous solutions with oxidising agent such as like Fe(III) tosylate. This oxidiser was added dropwise to the solutions with continuous magnetic stirring. Stirring lasted over the weekend to ensure the reaction was completed. The resulting mixture was washed and centrifuged (8000 rpm, 15 min) for several times using ethanol and DI water until the

supernatant is colourless. The sediments were freeze-dried to obtain PPy powders. Two centrifuges were used in this work for materials centrifugation: small, low-speed centrifuge (Microcentrifuge, MiniStar silverline) and middle, high-speed centrifuge (Thermoline Dynafuge centrifuge)

2.3.4 Polymer slurry preparation

Diethylene glycol (DEG) [8] was dispersed into DI water by magnetic stirring for 10 min and sonicated for 20 min using a high-power ultrasonic bath (Bandelin SONOREX DIGIPLUS DL 512 H). Equal poly (3,4 ethylenedioxythiophene)-poly(styrenesulfonate) (PEDOT-PSS) pellets and our synthetic PPy powders were added to the DEG solution. The mixed polymers were sonicated in bath sonicator (Branson B5500R-DTH) for 15 min prior to blending using a conditioning mixer (THINKY ARE-250). The PPy/PEDOT-PSS slurry was prepared for further use after going through the mixing (2000 rpm, 20 min) and then defoaming (800 rpm, 5min) programme.

2.4 General characterisation techniques

2.4.1 Spectra characterisation techniques

The Raman spectroscopy utilised in this work is LabRAM HR Evolution system with three different lasers (HORIBA Figure 2.2). It can measure within wide wavenumbers from 0 to 4000 cm^{-1} to confirm the destination of the specific band. The UV-vis spectroscopy (UV-3600, Figure 2.3) involves a broad range of radiation wavelengths and is routinely used for determining the conjugated organic compounds. Fourier transform infrared spectroscopy (FTIR) (IR Prestige-21, Figure 2.4) was used to study the polar bond vibration of different atoms. Raman and FTIR can be complementary to identify molecular vibration of polymers.

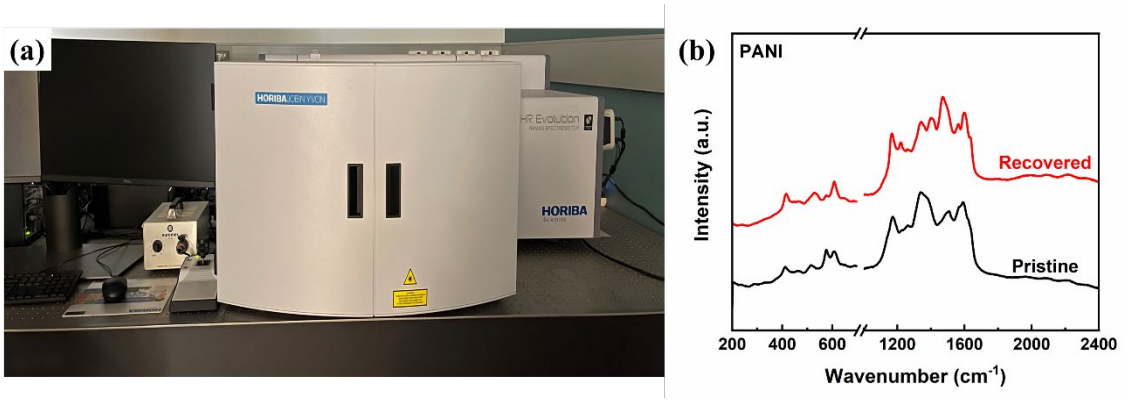

Figure 2.2 (a) Raman spectroscope used throughout this project. (b) Raman spectra of PANI before (pristine) and after (recovered) bipolar electrochemical testing.

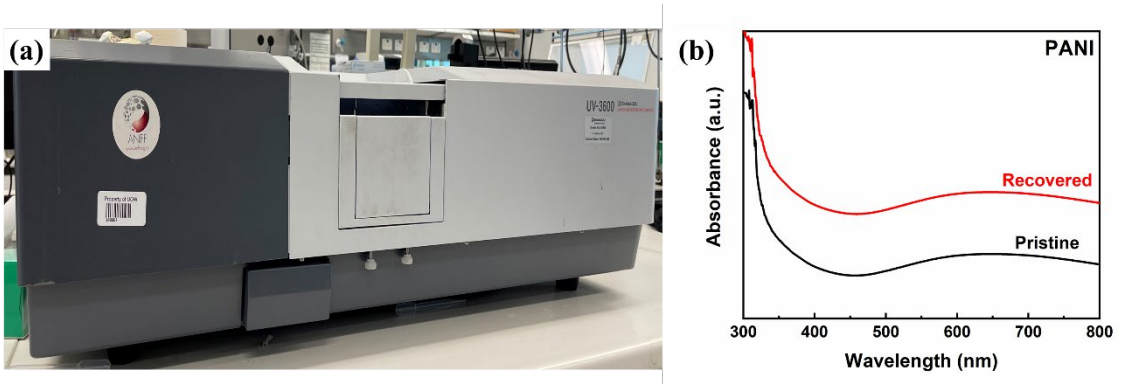

Figure 2.3 (a) UV spectroscope used throughout this project. (b) UV spectra of PANI before (pristine) and after (recovered) bipolar electrochemical testing.

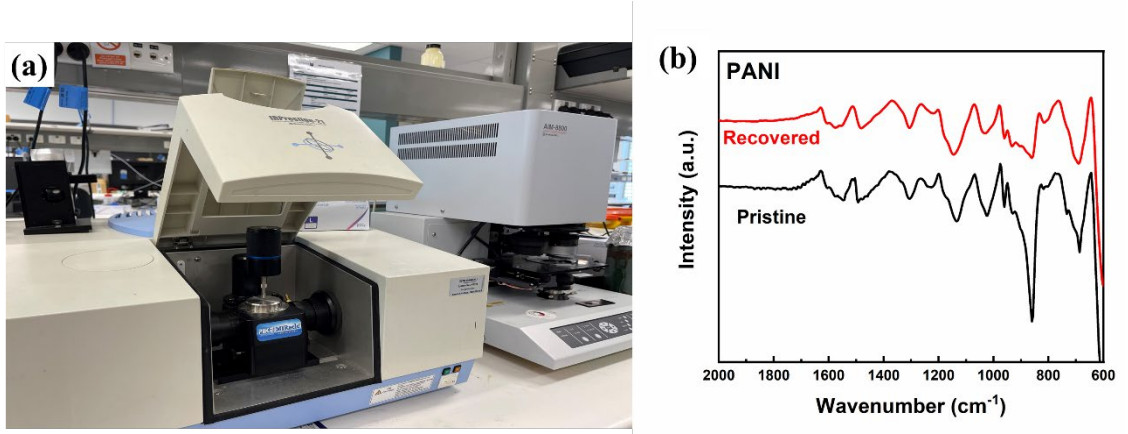

Figure 2.4 (a) Fourier transform infrared (FTIR) spectroscope used throughout this project. (b) FTIR spectra of PANI before (pristine) and after (recovered) bipolar electrochemical testing.

2.4.2 Electrochemical characterisation techniques

Potentiodynamic cyclic voltammetry (CV) was conducted to determine the electrochemical redox state of polymers and electrochemical impedance spectroscopy (EIS) was used to understand the charge transfer between electrode and electrolyte interfaces [9]. In this work, both CV and EIS measurements were carried out in PBS solution (pH = 7.4) using a biological electrochemical platform (Figure 2.5a). The electrical conductivity and resistance of polymers were measured using four-point probe and Agilent multimeter (Figure 2.5b).

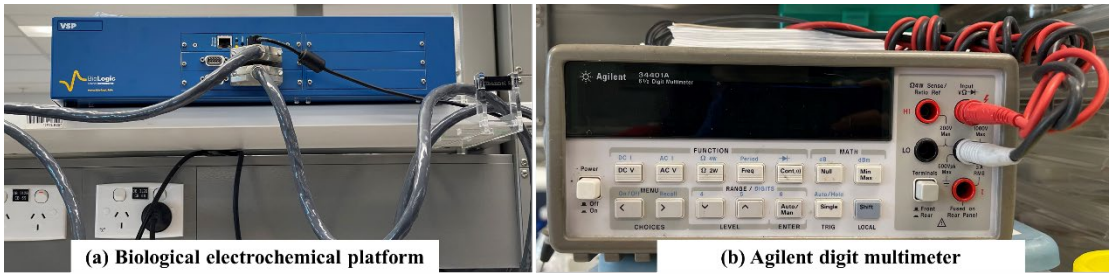

Figure 2.5 Relevant electrochemical characterisations instruments used throughout this project.

2.5 Device preparation/fabrication techniques

2.5.1 Laser cutter

The laser cutter (Figure 2.6) was mainly utilised to prepare sample substrates and parts of bipolar electrochemical cell. The PLS6MW multi-wavelength laser platform was chosen with a 10.6 μm carbon dioxide (CO_2) laser cutting system under ambient conditions. The laser power and cutting speed were varied according to the material thickness.

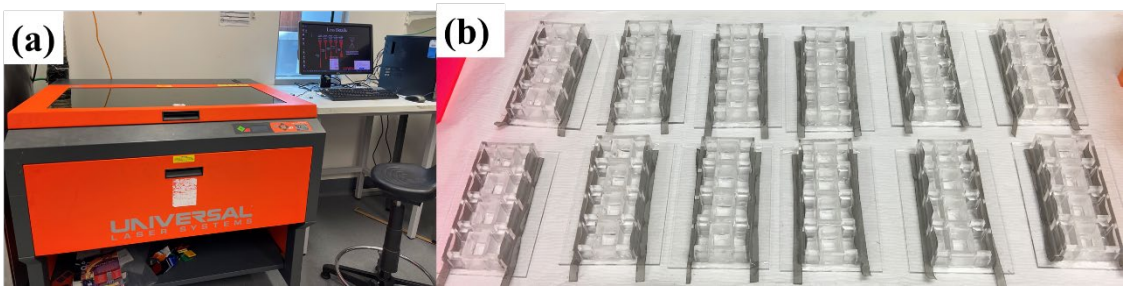

Figure 2.6 (a) Laser cutter system used in this project. (b) Fabricated bipolar electrochemical stimulation (BPES) devices after obtaining components using laser cutter.

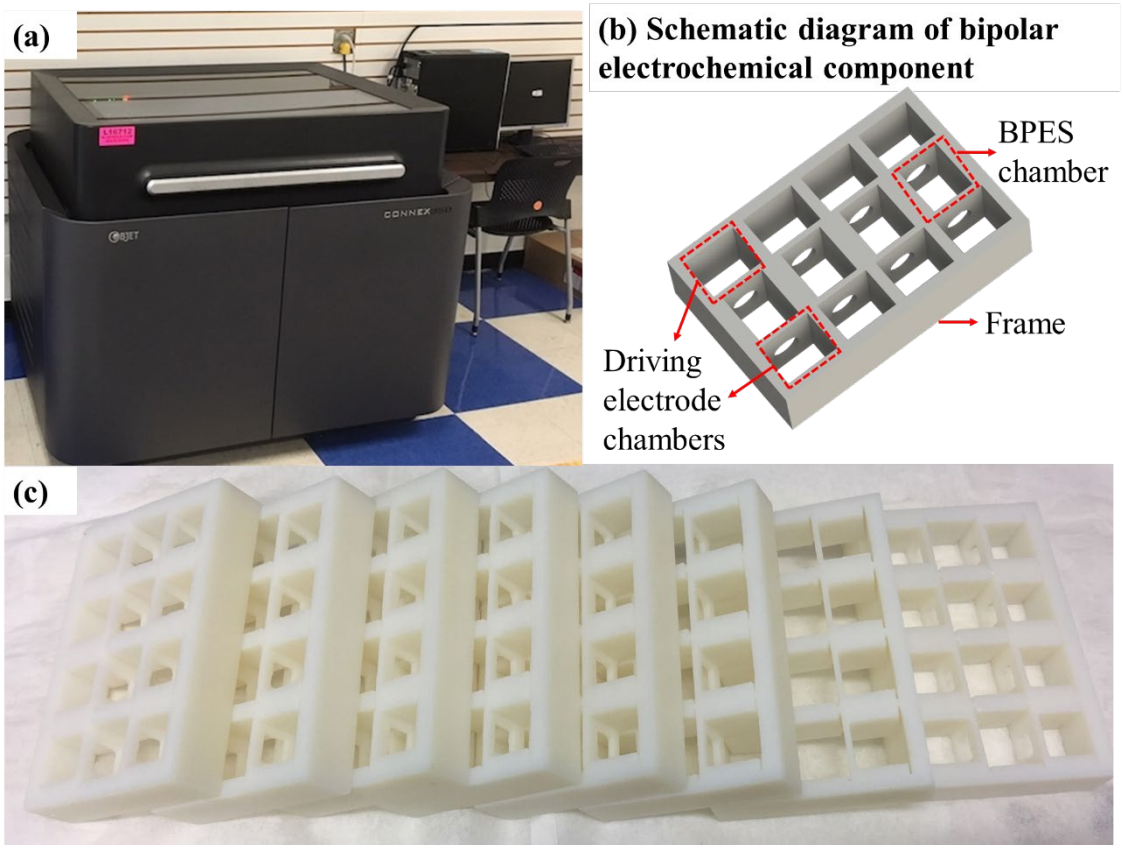

Figure 2.7 (a) Printer used in this project. (b) Schematic diagram and (c) Images of printed bipolar electrochemical component.

2.5.2 Printer

The Objet Connex 350 printer (Figure 2.7a) was used to enable biocompatible polymers and dental LT clear resin to build bipolar electrochemical frameworks and chambers. One bipolar electrochemical component consists of four middle wells as bipolar chambers and eight side wells as driving chambers (Figure 2.7b-c). For further details and printing parameters, please refer to the Translational Research Initiative for Cellular Engineering and Printing (TRICEP).

2.6 Bipolar electrochemical testing system

2.6.1 Bipolar electrochemical cell design and fabrication

The designed bipolar electrochemical cell [10] comprised frame, screw, viton ring and acrylic bottom (Figure 2.8a). The screw and viton ring were used to connect and immobilise the frame to the bottom. The parallel slots were used for tuning the distance, as the potential that triggers the redox reactions depends on the distance between the two driving voltages [11–15]. The fabricated bipolar electrochemical cell was obtained as shown in Figure 2.8b. In addition, for more convenient observation and application in following *in situ* spectroelectrochemical experiments, clear acrylic bottom replaced the opaque one.

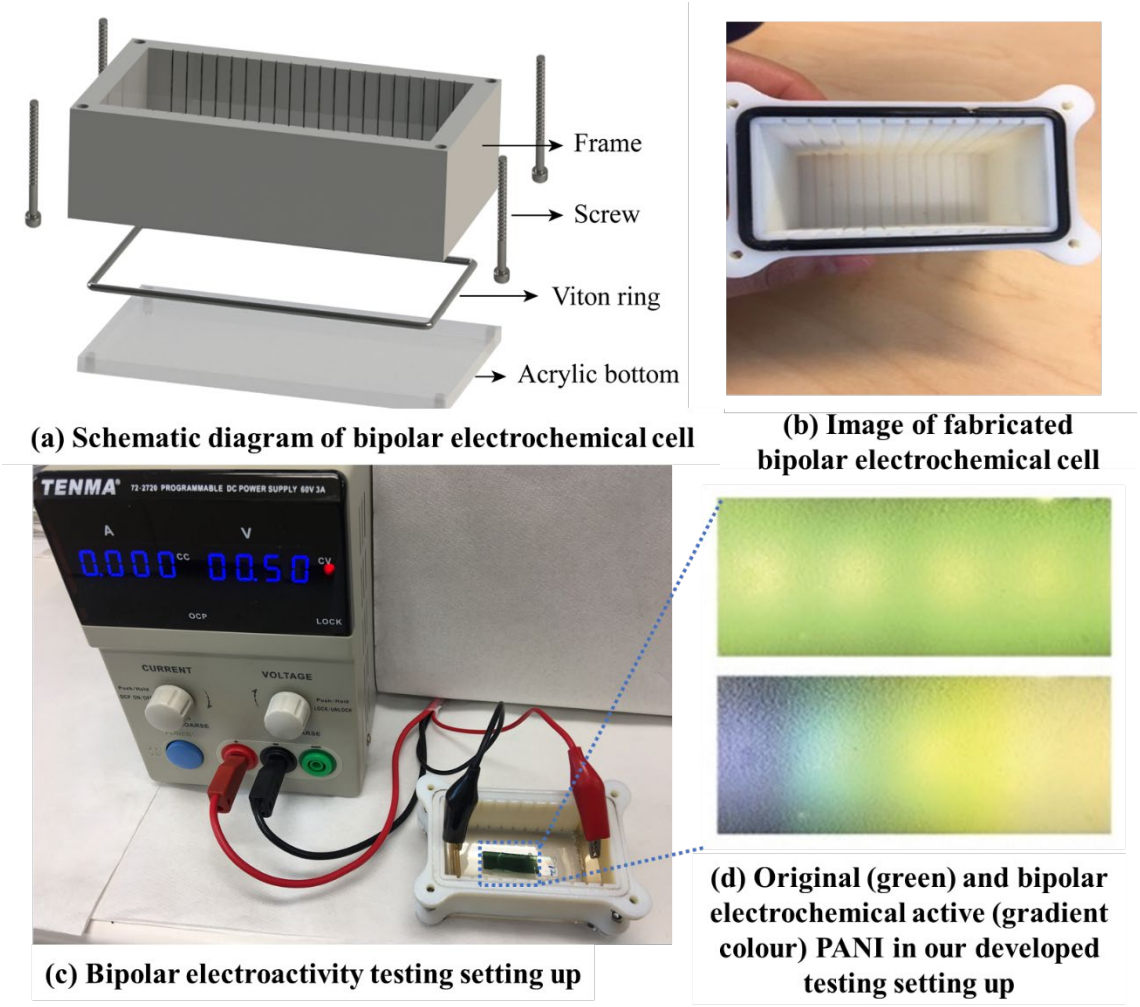

Figure 2.8 (a) Schematic diagram and (b) digital image of bipolar electrochemical cell. (c) Bipolar electroactivity testing setting up and (d) example of bipolar electroactive polymer in it. Images were taken using an iPhone camera.

2.6.2 Bipolar electroactivity testing setup and conditions

A schematic image of the entire bipolar electroactivity testing setup [10] shows that it includes a one channel power supply, fabricated bipolar electrochemical cell, driving electrodes, and two electric wires (Figure 2.8c). PANI was chosen to check the functionality of our setup because it possesses bipolar electroactivity [16–18]. Our setup is proven to be functional as shown in Figure 2.8d.

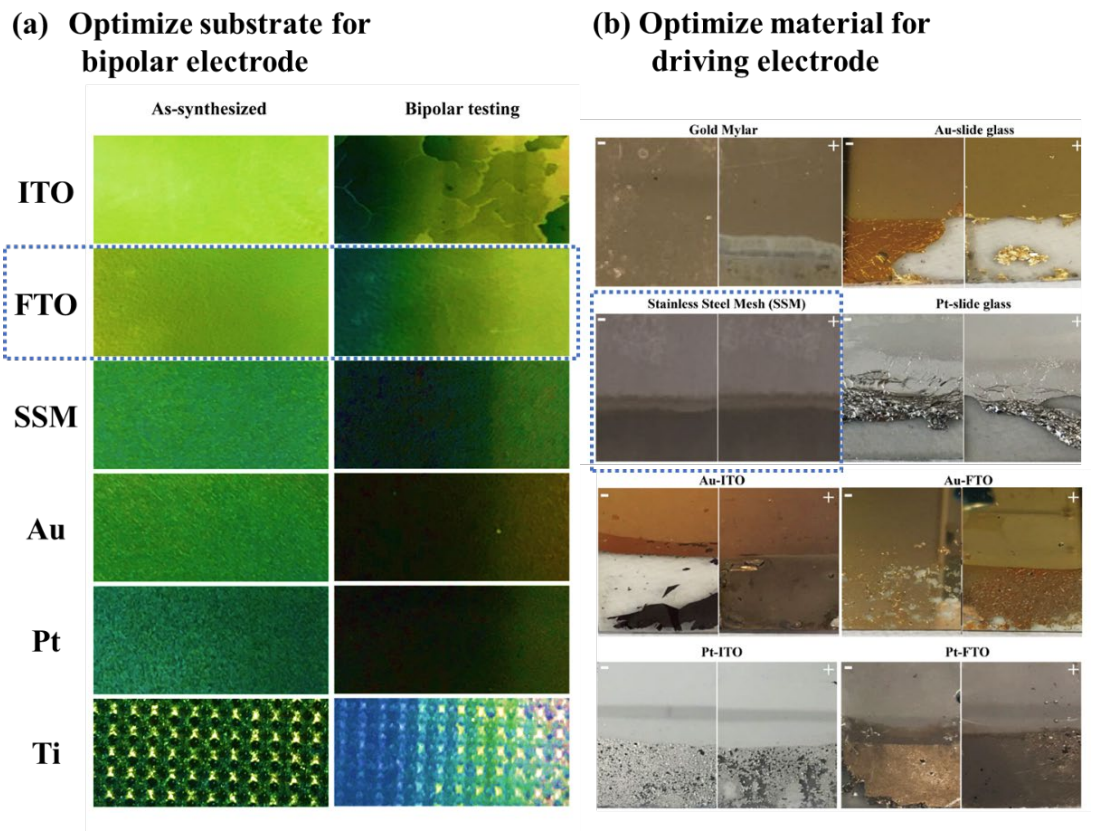

Figure 2.9 The use of PANI polymer on various substrates were evaluated in our bipolar electrochemical system to select suitable substrates and materials for bipolar electrode and driving electrodes. Images were taken using an iPhone camera.

The parameters of testing the bipolar electrochemical activity of the polymers in this system were evaluated. The power supply voltage to provide a sufficient initial voltage is within 0-60 V. Suitable substrates for bipolar electrode were tested to fit our system. Clear FTO (Figure 2.9a) was chosen because of its high conductivity and the ability of growing the supporting polymer on it. Different materials for driving electrodes were tested to ensure their chemical stability, and a stainless steel mesh (SSM) (Figure 2.9b) was selected for the following experiments. The electrolytic solution used is a biological PBS solution (pH = 7.4) because it is compatible with living cells.

2.7 Bipolar electroactivity characterisations

2.7.1 *In situ* Raman-bipolar electrochemical system

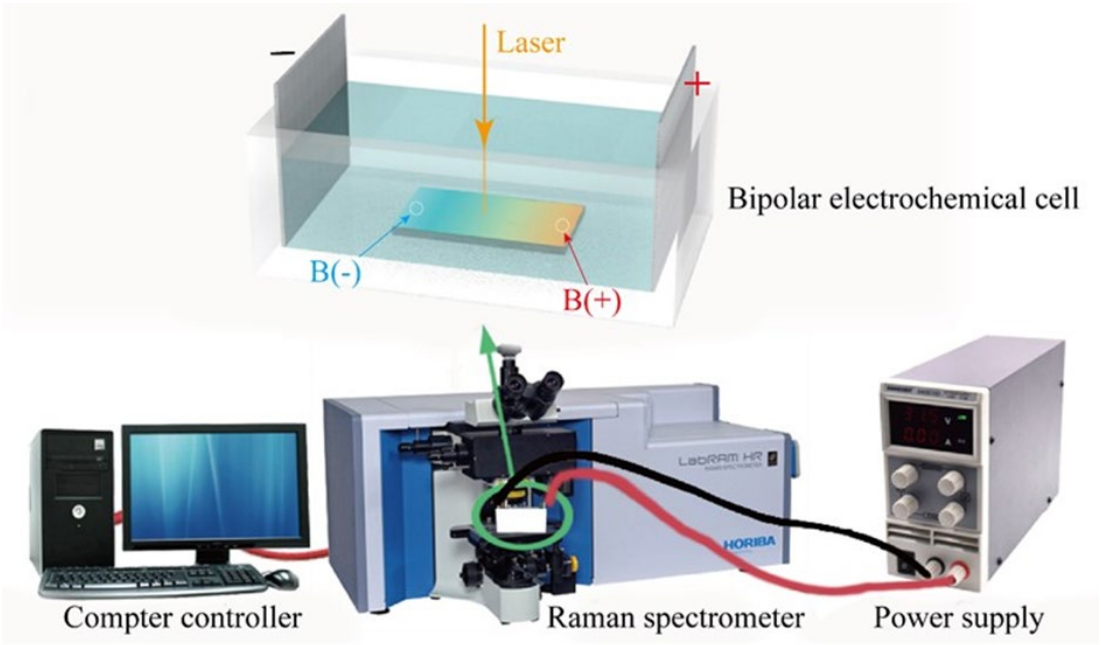

Figure 2.10 *In situ* Raman measurement along with bipolar electrochemical process.

In situ Raman-bipolar electrochemical system [10] is schematically illustrated in Figure 2.10, which consists of our bipolar electrochemical setup, Raman spectrometer, and computer controller. A micro-Raman spectrometer with 632.81 nm diode laser excitation was utilised. The objective lens (× 50 WLD) was positioned directly above the optical window and focused on the bipolar electrode. The laser spot was approximately 1 - 2 μm in diameter with a weak laser power (< 10 mW) to avoid possible laser irradiation damage of the samples. All spectra were acquired by collecting data for 10 s within the wavenumber range of 500 cm^{-1} - 2000 cm^{-1}. All samples were placed in the middle of the designed bipolar cell, and immersed in PBS. For reference, the pristine spectrum was taken from the original film in PBS without the applied driving voltage, and the recovered spectrum shows the Raman spectrum from the film

after bipolar testing in PBS with removed driving voltage. All *in situ* spectra were obtained at different driving voltage. B(-) and B(+) present the Raman spectra from the poles of the bipolar electrode, which are opposite to the cathodic and anodic driving electrodes. According to the principle of BPE, oxidation at the B(-) site and reduction at the B(+) site occurred simultaneously.

2.7.2 *In situ* UV-bipolar electrochemical system

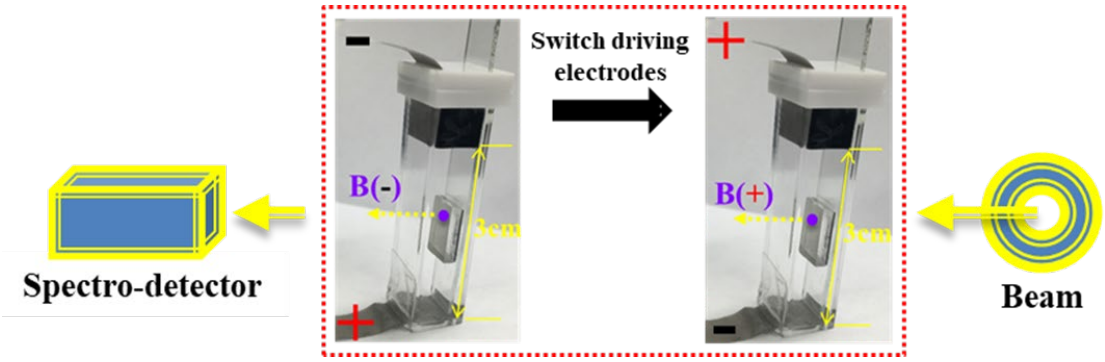

Figure 2.11 *In situ* UV-vis absorption spectra combined with bipolar electrochemical system.

The *in situ* UV-vis absorption spectra combined with bipolar electrochemical system are made up of home-made and fabricated bipolar UV cell, beam, and UV spectrodetector (Figure 2.11). To work with existing UV instruments, the measured spot was fixed in the same position as our polymer samples immersed in PBS. All UV absorption spectra were recorded in the range of 300 nm - 1100 nm. For reference, the pristine spectrum was acquired from the original film in PBS without the applied driving voltage, and the recovered spectrum shows the UV spectrum from the film after bipolar testing in PBS with removed driving voltage. The B(-) spectrum was acquired, followed by obtained B(+) spectrum after switching the driving electrode to change the bipolar electrode

polarity.

2.7.3 *In situ* UV-conventional three electrode electrochemical system

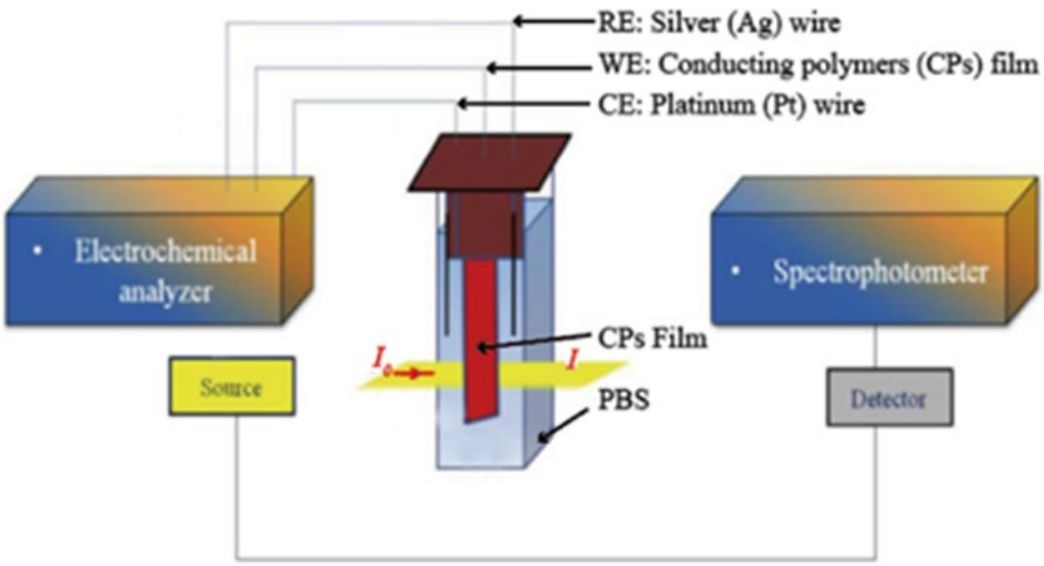

Figure 2.12 *In situ* UV-vis absorption spectra combined with the conventional three-electrode electrochemical system.

A schematic illustration of the *in situ* UV spectra with the conventional three-electrode electrochemical system [10], which constitutes electrochemical platform, a 3-electrode cell, and a UV spectrophotometer is shown in Figure 2.12. The custom-made quartz cuvette acting as an electrochemical reaction cell was equipped with a polymer film (1 cm × 0.8 cm) as the working electrode, an Ag wire as the reference electrode and a Pt wire as the counter electrode. *In situ* UV-visible absorption spectra in the range of 300 nm - 1100 nm was obtained after applying consecutive potentials from -0.6 V to +0.6 V. All potentials are vs. an Ag wire reference electrode and keep 30 s poise time in PBS (pH = 7.4).

2.8 Routine cell culture

2.8.1 Culture of rat pheochromocytoma cell line PC 12

PC 12 cells were seeded and cultured in DMEM growth media supplemented with 2 mM glutamine, 5% (v/v) fetal bovine serum (FBS), and 10% (v/v) horse serum in a humidified 37 °C incubator (Thermo HERA cell 150) with 5% CO_2 atmosphere before further use. For differentiation, a low serum medium (1% horse serum) supplemented with 50 ng/ml nerve growth factor (NGF) was used.

2.8.2 Culture of human neuroblastoma cell line SH-SY5Y

SH-SY5Y cells were cultured in DMEM/F12 growth media supplemented with 2 mM glutamine, 10% (v/v) heated-inactived FBS, and 1% (v/v) penicillin/streptomycin (P/S) in a humidified 37 ℃ incubator (Thermo HERA cell 150) with 5% CO_2 atmosphere before further use. For differentiation, a low heated-inactived FBS serum medium (1%) supplemented with 10 μM retinoic acid (RA) was used.

2.9 Bipolar electrochemical stimulation (BPES) system

2.9.1 BPES device design and fabrication

To conduct BPES, a specific bipolar electrochemical stimulating device [10] was designed with a similar construction to mimic conventional electrochemical cell stimulation one (Figure 2.13a). The tailored PVDF sheets (1.2 cm × 1.0 cm) were inserted into the slots in the cell culture well (1.0 cm^2 /well) acting as the media link. Two parallel SSM strips in the driving wells were used to connect with the external DC power supply to generate an accurately controlled electric field suitable for cell stimulation. All parts were fixed using silicon adhesive overnight. We used a laser cutter

and a 3D printer to obtain all parts, and the fabricated BPES devices are displayed in Figure 2.13b-2.13c. A leakage check was conducted, followed by the capability of inducting bipolar electrochemistry test before cell seeding and the BPES. Gradient PPy films in four middle wells of the fabricated BPES device were observed (Figure 2.13c).

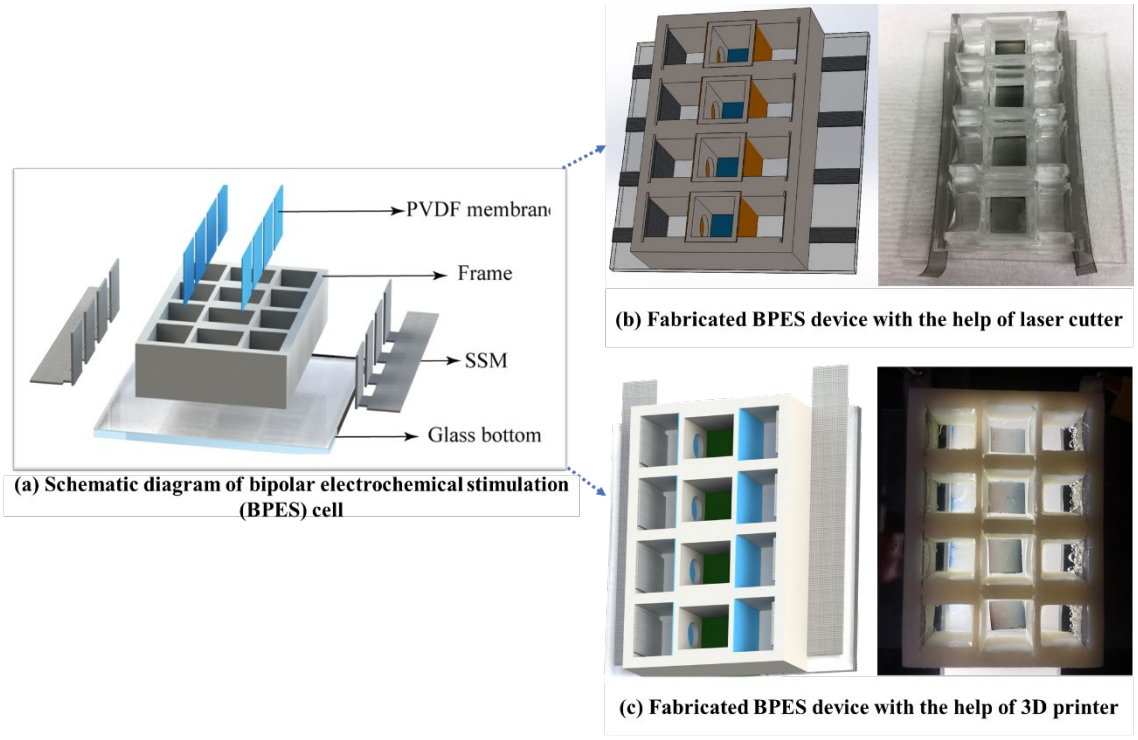

Figure 2.13 (a) Schematic diagram of bipolar electrochemical stimulation (BPES) cell. Relevant devices were fabricated using (b) laser cutter and (c) 3D printer. The gradient bipolar electroactivity of tailored PPy films were observed in fabricated devices.

2.9.2 BPES setup and conditions

To investigate the effects of BPES on nerve cell behaviour, we developed and optimised the BPES parameters (Figure 2.14a). A programmable, multi-channel power supply (Figure 2.14b) was used to meet the requirements of duplicate experiments, and an immunofluorescent image of bipolar electrostimulated neural cells is shown in Figure

2.14c. Both BPES devices and PPy substrates (1 cm × 1 cm) were first immersed in 70% ethanol for 5 min, followed by drying under sterile conditions and exposing to UV light for 20 min (EtOH-UV sterilisation). After sterilisation, four pieces of tailored and sterilised PPy substrates were placed in the middle cell culture wells of each bipolar device individually, followed by UV exposure for another 20 min to ensure thorough sterilisation. Then, an initial density of cells in growth medium were seeded in the middle wells in growth media for at least 24 h to ensure cell attachment. Subsequently, cells were exposed to a BPES pulse mode [10,19].

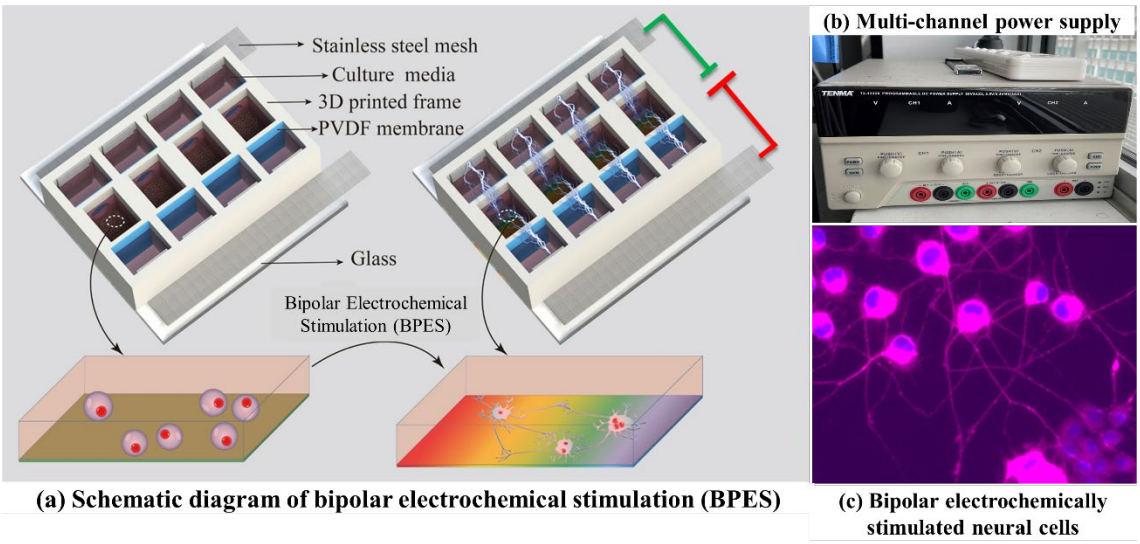

Figure 2.14 (a) Schematic diagram of bipolar electrochemical stimulation (BPES) process. Relevant images of (b) power source and (c) bipolar electrochemically stimulated nerve cells.

The waveform of the applied pulse mode comprised a phase duration of 10 min with an interphase interval of 5 min. Under BPES pulse mode-A, the cells were stimulated for 1 h per day for 7 days. However, under BPES pulse mode-B, the cells were stimulated for 8 h on day 2, and then cultured in the absence of BPSE for the following 5 days. Under

BPES pulse mode-C, the cells were stimulated on day 2 for 8 h, and this pattern was continued until day 5, after which they were cultured as normal in the absence of BPSE until the end of day 7. Under Control Non-BPES, the cells were cultured under identical conditions without BPES (i.e., normal condition). All experiments were conducted for 7 days. BPES pulse mode-C was chosen for the results reported in chapter 4 and chapter 5 because it has been successfully verified to be an optimal and effective protocol, which promotes significant nerve cell differentiation in chapter 3.

2.10 Bipolar stimulated cells characterisation

2.10.1 Live/dead assay

Cyto-compatibility and cell viability studies were conducted using live/dead assay on day 1, day 3, day 5, and day 7. Calcein AM (2×10^{-6} M) and PI (2×10^{-6} M) were used to stain the live and dead cells, respectively. Finally, the cells were visualised and imaged using a ZEISS Axiovert or AxioImager microscope (Figure 2.15).

2.10.2 Cell number assay - PicoGreen

To confirm the effects of BPES on nerve cell proliferation, the adherent cells were counted on day 1, day 3, day 5 and day 7. A Quant-iT ^{TM} PicoGreen dsDNA Assay Kit in accordance with the manufacturer's instructions was used to quantify. The number of triplicate samples was measured using a microplate reader (BMG LABTECH POLARstar Omega, Germany) at 485-12/520 nm.

2.10.3 Fluorescence staining

Immunofluorescence staining was used to investigate the effects of BPES on nerve cell differentiation. The fixed cells were permeabilized with methanol:acetone (50:50) on ice

for 5 min, and washed twice with PBS. The cells were then blocked in 10% donkey serum with 0.1% w/v Tween-20 in PBS at room temperature (RT) for at least 1 h, incubated with mouse anti- β-tubulin III in 10% donkey serum with 0.1% w/v Tween-20 in PBS at 4 °C overnight, and Alexafluo 546 anti-mouse secondary anti- body at 37 °C for another at least 1 h. The nuclei were counterstained with 4-6-diamidino-2-phenylindole (DAPI) for 5 min at RT. Images were acquired using a ZEISS Axiovert or AxioImager microscope (Figure 2.15).

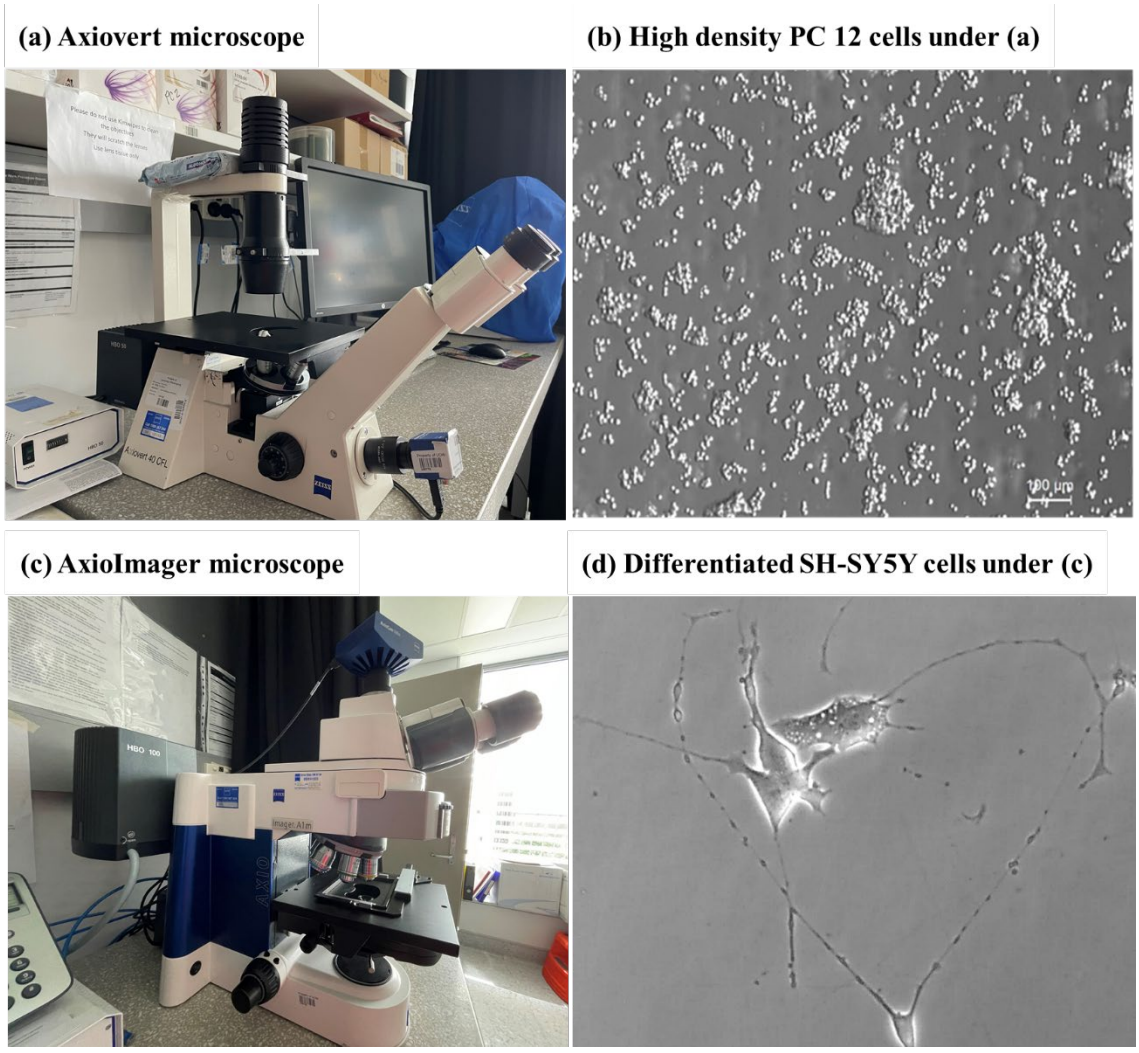

Figure 2.15 (a) ZEISS Axiovert microscope and (b) acquired image of PC 12 cells. (c) AxioImager microscope and (d) image of differentiated SH-SY5Y cells.

2.10.4 Quantitative analysis

ImageJ with NeuriteQuant add-in was used to quantify the neurite numbers by averaging the number of neurites per cell in the observed area from all the samples collected. The software with Neurite length tracer add-in can measure the neurite growth in cells, including the total neurite number per cell, the total neurite length per cell, mean neurite length per cell, and maximum neurite length per cell. Neurites were measured when the length of the projection exceeded a single body length of the cell from which it extended. Data are represented as mean ± standard deviation (SD) unless otherwise indicated. Results were analysed using Origin software using one-way ANOVA or two- way ANOVA with Tukey simultaneous testing method and Bonferroni post hoc test, respectively. A p -value was determined and a maximum value of 0.05 was used to indicate significance.

2.11 Reference

[1] Z. Chen, E. Villani, S. Inagi, Recent progress in bipolar electropolymerization methods toward one-dimensional conducting polymer structures, Curr. Opin. Electrochem. 28 (2021) 100702. https://doi.org/10.1016/j.coelec.2021.100702.

[2] F. Endres, A. Abbott, D.R. MacFarlane, Electrodeposition from ionic liquids, John Wiley & Sons, 2017.

[3] A. Watanabe, K. Mori, Y. Iwasaki, Y. Nakamura, S. Niizuma, Electrochromism of Polyaniline Film Prepared by Electrochemical Polymerization, Macromolecules. 20 (1987) 1793–1796. https://doi.org/10.1021/ma00174a015.

[4] S. Yalçınkaya, C. Demirbilek, C.Ö. Dinç, Preparation and characterization of polypyrrole/dextran sulphate composite: its electrochemical and thermal behaviors, Polym. Bull. 72 (2015) 2843–2855. https://doi.org/10.1007/s00289-015-1439-8.

[5] A.A. Hermas, S.S. Al-Juaid, S.A. Al-Thabaiti, A.H. Qusti, M. Abdel Salam, In situ electropolymerization of conducting polypyrrole/carbon nanotubes composites on stainless steel: Role of carbon nanotubes types, Prog. Org. Coatings. 75 (2012) 404–410. https://doi.org/10.1016/j.porgcoat.2012.07.006.

[6] M.A. Ali, H. Kim, C. Lee, H. Nam, J. Lee, Effects of iron(III) p-toluenesulfonate hexahydrate oxidant on the growth of conductive poly(3,4-ethylenedioxythiophene) (PEDOT) nanofilms by vapor phase polymerization, Synth. Met. 161 (2011) 1347–1352. https://doi.org/10.1016/j.synthmet.2011.04.036.

[7] J.R. and L.R. Demoustier-Champagne Sophie, Ferain Etienne Jerome Christine, Electrochemically synthesized polypyrrole nanotubules:effects of different experimental cnditions, Eur. Polym. J. 34 (1998) 1767–1774.

[8] Y. Liu, B. Weng, J.M. Razal, Q. Xu, C. Zhao, Y. Hou, S. Seyedin, R. Jalili, G.G. Wallace, J. Chen, High-Performance Flexible All-Solid-State Supercapacitor from Large Free-Standing Graphene-PEDOT/PSS Films, Sci. Rep. 5 (2015) 17045. https://doi.org/10.1038/srep17045.

[9] Y. Chao, Y. Ge, Y. Zhao, J. Jiang, C. Wang, C. Qin, A. Vijayakumar, C. Yu, G.G. Wallace, Tuning the structure of three dimensional nanostructured molybdenum disulfide/nitrogen-doped carbon composite for high lithium storage, Electrochim. Acta. 291 (2018) 197–205. https://doi.org/10.1016/j.electacta.2018.08.148.

[10] Qin Chunyan, Yue Zhilian, Chao Yunfeng, Forster Robert, Maolmhuaidh Fionn, Huang Xu-Feng, Beirne Stephen, Wallance Gordon, Chen Jun, Data on the bipolar electroactive conducting polymers for wireless cell stimulation, Data Br. 33 (2020) 106406-undefined. https://doi.org/10.17632/4zgkyfxhcd.1.

[11] S.E. Fosdick, K.N. Knust, K. Scida, R.M. Crooks, Bipolar electrochemistry, Angew. Chemie Int. Ed. 52 (2013) 10438–10456.

[12] R.M. Crooks, Principles of bipolar electrochemistry, ChemElectroChem. 3 (2016) 357–359.

[13] C.A.C. Sequeira, D.S.P. Cardoso, M.L.F. Gameiro, Bipolar Electrochemistry, a Focal Point of Future Research, Chem. Eng. Commun. 203 (2016) 1001–1008. https://doi.org/10.1080/00986445.2016.1147031.

[14] V. Eßmann, J. Clausmeyer, W. Schuhmann, Alternating current-bipolar electrochemistry, Electrochem. Commun. 75 (2017) 82–85. https://doi.org/10.1016/j.elecom.2017.01.006.

[15] L. Koefoed, S.U. Pedersen, K. Daasbjerg, Bipolar electrochemistry—A wireless approach for electrode reactions, Curr. Opin. Electrochem. 2 (2017) 13–17. https://doi.org/10.1016/j.coelec.2017.02.001.

[16] Y. Ishiguro, S. Inagi, T. Fuchigami, Gradient doping of conducting polymer films by means of bipolar electrochemistry, Langmuir. 27 (2011) 7158–7162. https://doi.org/10.1021/la200464t.

[17] S. Inagi, Fabrication of gradient polymer surfaces using bipolar electrochemistry, Polym. J. 48 (2016) 39–44. https://doi.org/10.1038/pj.2015.73.

[18] N. Shida, Y. Zhou, S. Inagi, Bipolar Electrochemistry: A Powerful Tool for Electrifying Functional Material Synthesis, Acc. Chem. Res. (2019). https://doi.org/10.1021/acs.accounts.9b00337.

[19] C. Qin, Z. Yue, Y. Chao, R.J. Forster, F. Maolmhuaidh, X.F. Huang, S. Beirne, G.G. Wallace, J. Chen, Bipolar electroactive conducting polymers for wireless cell stimulation, Appl. Mater. Today. 21 (2020). https://doi.org/10.1016/j.apmt.2020.100804.

Chapter 3

Wireless cell stimulation enabled by bipolar electroactive conducting polymers

This chapter is adapted from the article, "Bipolar electroactive conducting polymers for wireless cell stimulation" that was published in Applied Materials Today 21 (2020) 100804, and partially adapted from the article, "Data on the bipolar electroactive conducting polymers for wireless cell stimulation" that was published in Data in Brief 33 (2020) 106406, both by Chunyan Qin, Zhilian Yue, Yunfeng Chao, Robert J. Forster, Fionn Ó. Maolmhuaidh, Xu-Feng Huang, Stephen Beirne, Gordon G.Wallace and Jun Chen, with permission from Elsevier.

3.1 Introduction

The use of electrochemical stimulation (ES) to influence the proliferation and differentiation of living cells offers a means to understanding of fundamental biological processes and for developing many clinical applications [1]. Conducting polymers (CPs) are increasingly recognized as highly attractive materials for bioapplications due to their tuneable cytocompatibility as well as stable mechanical and chemical properties [2–4]. Specifically, CPs enable highly efficient delivery of the electrical stimulus to achieve effective cell stimulation [5,6]. Moreover, driving redox processes within the polymer matrix allows the surface properties and composition to be altered *in situ* delivering secondary effects to the adhering cells that can be controlled over time [7–11]. Conventional CP-based ES protocols usually contain coated electrodes with cells attached acting as the working electrode, *directly* connected to a potentiostat [12]. This

approach requires the working electrode to be “hard wired” to a potentiostat so that the voltage, and thus charge injection and the interfacial properties of the CPs can be controlled. This direct connection constrains practical clinical deployment [13–16]. An implantable system that could be activated via the imposition of a non-contact electric field is highly likely to be a powerful platform and a transformative technology in electroceutical development [17,18].

Bipolar electrochemistry (BPE), could offer an alternative non-contact pathway to be able to transform the traditional ES system to a wireless platform, known as bipolar electrochemical stimulation (BPES), maintaining the advantages of ES but removing the need for a physical wire to control the applied potential. In BPES system, the electronically conducting bipolar electrode is placed in an electric field induced indirectly by the driving electrodes (also known as “feeder electrodes”) without any direct ohmic contact [19–21]. The electric field, which is uniform across the electrolyte, could activate the bipolar electrode without electrical wiring via generating a potential difference between the two ends (or “anodic / cathodic poles”) of the bipolar electrode. The electrode size and electric field strength/distribution control the magnitude of this potential difference making it possible to concurrently activate oxidation and reduction processes at opposite ends of the bipolar electrode, typically by controlling the voltage difference between the two feeder electrodes [22,23]. To date, the focus has been on electroanalytical applications, the creation of Janus-type structures and imaging [24–31]. In this contribution, we report on the use of BPES where the bipolar electrode is functionalised with a cytocompatible CP to enable electrical stimulation of living cells. The electric field strength required to switch the redox composition of the CPs must not damage adherent cells, and so CPs with low switching potentials are required [32,33].

Here, we present for the first time the development of polypyrrole (PPy)-based bipolar electrochemical stimulation (BPES) system for wireless stimulation of nerve cells. Specifically, our synthetic PPy-DS/collagen film demonstrated reversible and recoverable bipolar electrochemical activity in phosphate buffered saline (PBS) buffer solution, as supported by *in situ* and *ex situ* spectro-electrochemical techniques. For the first time we demonstrate a fully functional, custom designed bipolar electrochemical stimulation device in which neural cells are actively growing on a PPy-DS/collagen film. Significantly, these cells respond to applied wireless electrical stimulation which induces enhanced cell proliferation and neurite outgrowth (number and length). These observations highlight the effect of wireless electrical stimulation and suggest that the BPES prototype system is a promising platform for programmable wireless electrostimulation. This work represents an important first step towards *in vivo* wireless stimulation of biocompatible implants, for site-selective stimulation of neural cells for traumatic injury repair.

3.2 Experiments

3.2.1 Materials

Pyrrole (Py) was purchased from Merck, purified by reduced pressure distillation and stored at -20 ºC. Other chemicals for synthesis, such as sulfuric acid (H_2SO_4), *p*-toluenesulfonic acid monohydrate (*p*TS), dextran sulfate sodium salt from Leuconostoc spp. (DS), phosphate buffered saline (PBS) and Nunc® Lab-Tek® chambered coverglass (polystyrene) were supplied from Sigma-Aldrich (Sydney, Australia). Stainless steel mesh (SSM-500x500 with wire DIM of 0.025 mm) was from Stainless Steel Wire & Mesh Pty Ltd. (Melbourne, Australia). Gibco Dulbecco's Modified

Eagle's Medium (DMEM), horse serum, fetal bovine serum (FBS), collagen (Type I from rat tail), nerve growth factor (NGF), calcein AM, propidium iodide (PI), PicoGreen™, Alexa Fluor 546 (Donkey anti-Mouse IgG Highly Cross-Adsorbed Secondary Antibody), monoclonal anti-β-tubulin III (neuronal) antibody produced in mouse, 4'-6-diamidino-2-phenylindole (DAPI) and rhodamine Red™-X succunimidyl ester were from Invitrogen (Melbourne, Australia). Dental LT Clear Resin was obtained from LST Sydney (a reseller for Formlabs) and clear RTV silicone adhesive sealant was purchased from Permatex (USA).

3.2.2 Preparation of polypyrrole (PPy) films

The preparation of polypyrrole (PPy) films were carried out by cyclic voltammetry (CV) from an aqueous solution containing 0.2 M distilled pyrrole (Py) with 0.1 M *p*TS, 2 mg/ml DS without or with 2 µg/ml collagen within a potential range of 0 - 0.65 V at a scan rate of 20 mV/s. After polymerisation, all films were thoroughly rinsed with Milli-Q water and allowed to dry under ambient conditions before further characterisation and investigation.

3.2.3 Bipolar electrochemistry (BPE)

3.2.3.1 In-house designed bipolar cells

The detailed set-up for the evaluation of bipolar electrochemistry (BPE) has been reported in Chapter 2 (Figure 2.8), which consists of a DC power supply system connected to a bespoke bipolar cell. This 3D printed cell has a rectangle frame closely connected with acrylic bottom (transparent) through viton ring and tightened screws. The parallel slots are designed to insert stainless steel mesh (SSM) for controlled

adjustment of the distance between SSM and test PPy films (placed in the centre of printed cell) to optimise the testing conditions.

3.2.3.2 Bipolar electrochemical activity evaluation

The bipolar electrochemical activity of the PPy films with different dopants was evaluated using the fluidic platform with integrated feeder electrodes by applying a programmable DC voltage to the feeder electrodes using TENMA DC supply system. All bipolar electrochemical activity tests were conducted in standard PBS buffer solution with a pH of 7.4, simulating that of the normal biological environment. In a typical testing set-up, the CP films deposited on FTO (0.5 cm × 0.5 cm - 3.0 cm × 3.0 cm) were immersed into the PBS buffer and placed in the centre of the bipolar cell. The separation of the SSMs as feeder electrodes were adjustable from 1 cm to 5 cm depending on the size of PPy film being tested. This bipolar electrochemical activity evaluation was mainly used to investigate the reversibility of the PPy redox switching and stability towards repeated cycling.

3.2.4 Materials characterisations

3.2.4.1 *In situ* confocal Raman spectrometry

In situ confocal Raman spectrometry (HR800 Raman spectrometer, Japan), as reported in Chapter 2 (Figure 2.10), was utilised to identify the reversible and recoverable bipolar electrochemical activity. Spectra were acquired by 10 s data collection within the wavenumber range of 500 cm^{-1} - 2000 cm^{-1} using excitation laser at 632.81 nm. The objective lens (× 50 WLD) was positioned directly above the optical window and focused on the particular region of interest on the PPy film under BPE activation with a low laser power (less than 10 mW).

3.2.4.2 *In situ* UV-vis spectra spectrometry with the conventional electrochemical system

To identify the electrochromic behaviour in response to the wireless electric field, *in situ* UV-vis spectra (Shimadzu UV-vis 3600) were recorded simultaneously with the conventional three-electrodes electrochemical system [34] within the range of 300 nm - 1100 nm under different applied potentials (from -0.6 V to +0.6 V) in PBS (pH = 7.4) (reported in Chapter 2: Figure 2.12).

3.2.4.3 Other physical characterisation techniques

Other physical characterisation techniques were also employed to further confirm the bipolar electrochemical activity of the prepared PPy films independent of dopants. A field emission scanning electron microscopy (JEOL JSM-7500FA) were utilised to probe the surface morphology. For chemical stability, *ex situ* Raman spectra were obtained within the wavenumber range of 500 cm^{-1} - 2000 cm^{-1}, while FTIR spectra were collected using a FT-IR spectrometer (IRpretige-21, Shimadzu) over a range of 600 cm^{-1} - 2000 cm^{-1}. To ensure the successful incorporation of collagen with uniform distribution into PPy films, fluorescence (rhodamine red^{TM}-X succunimidyl ester) labelling and ZEISS Axiovert microscope (Carl Zeiss, Germany) were utilised to check the surface morphology of treated PPy-DS and PPy-DS/collagen films [35].

3.2.4.4 Electrochemical characterisation techniques

Cyclic voltammetry (CV) and electrochemical impedance spectroscopy (EIS) with a conventional direct wire connection were employed to investigate the electrochemical activity of the prepared PPy films with different dopants in PBS (pH = 7.4). CVs were

carried out with a potential range of -0.7 V to +0.7 V at a scan rate of 100 mV/s, while EIS were performed over the frequency range of 0.1 Hz to 100 kHz using an AC signal with +50.0 mV vs the reference electrode.

3.2.5 Standard cell culture and cytocompatibility studies

3.2.5.1 Cell culture of PC 12 cells

PC 12 cells were seeded and cultured in DMEM growth media supplemented with 2 mM glutamine, 5% (v/v) fetal bovine serum (FBS) and 10% (v/v) horse serum in a humidified 37 ℃ incubator with 5% CO_2 atmosphere before further use. For differentiation, a low serum medium (1% horse serum) supplemented with 50 ng/ml nerve growth factor (NGF) was used.

3.2.5.2 Cytocompatibility study

For cyto-compatibility studies, different PPy substrates were prepared and sterilized by firstly being immersed in 70% ethanol for 5 min, followed by drying under sterile conditions and exposing to UV light for 20 min (EtOH-UV sterilisation). PC 12 cells were cultured on the substrates at a density of 20000 cells/cm^2 in growth media and 2000 cells/cm^2 in differentiation media. Cyto-compatibility test was conducted using live/dead assay after day 1, day 3, day 5 and day 7. Calcein AM (2×10^{-6} M) and PI (2×10^{-6} M) were used to stain the live and dead cells respectively. Finally, cells were visualised and images were obtained using a ZEISS Axiovert microscope.

3.2.6 Bipolar electrochemical stimulation (BPES)

3.2.6.1 In-house designed bipolar devices

In order to conduct bipolar electrostimulation (BPES), a specific bipolar device was designed with a similar construction to mimic conventional electrochemical cell stimulation one as reported in Chapter 2 (Figure 2.13). The tailored PVDF sheets (1.2 cm × 1.0 cm) are inserted into the slots at the cell culture well (1.0 cm^2/well) acting as the media link. Two paralleled strips of SSM in the driving wells are used to connect with the external DC power supply to generate an accurately controlled electric field suitable for cell stimulation. All parts were fixed using silicon adhesive overnight, followed by a leakage check and sterilisation before cells seeding and the BPES.

3.2.6.2 Optimisation of BPES parameters

Both bipolar devices and PPy-coated FTO glassy slides (1 cm × 1 cm) were first immersed in 70% ethanol for 5 min, followed by drying under sterile conditions and exposing to UV light for 20 min (EtOH-UV sterilisation). After sterilisation treatment, four pieces of tailored and sterilized PPy-DS/collagen films were placed into the middle cell culture wells of each bipolar device individually, followed by another 20 min' UV exposure to make sure thorough sterilisation. Then cells were seeded in the middle wells, which have the PPy-DS/collagen substrates, at an initial density of 6000 cells/cm^2 in growth media. Data shows the applied pulse mode (phase duration of 10 min + interphase interval of 5 min, repeated 6 times per day) over 7 consecutive days, was to investigate the impact of different DC stimulation voltages from 0.5 V to 5.5 V. In order to evaluate the BPES performance, the cells were sampled and assessed by live/dead analysis on day 7.

3.2.7 BPES performance evaluation

3.2.7.1 BPES on cell proliferation

PC 12 cells were seeded into growth media at 20000 cells/cm^2 in the bipolar devices. BPES pulse mode-A was initiated after cells seeding 22.5 h for continuous 7 days with growth media refreshed every 2 days. Calcein AM and PI staining was used to observe the cell morphology with a ZEISS Axiovert microscope. The numbers of adherent cells on day 1, day 3, day 5 and day 7 were quantified using a Quant-iT^{TM} PicoGreen dsDNA Assay Kit in accordance with the manufacturer's instructions. Numbers of triplicate samples were measured with a microplate reader (POLARstar Omega, Germany) at 485-12/520 nm.

3.2.7.2 BPES on cell differentiation

PC 12 cells at a seeding density of 2000 cells/cm^2 under identical conditions were stimulated with different programmed BPES pulse modes as reported Chapter 2 (section 2.9.2), and finally fixed on day 7 in 3.7% paraformaldehyde at RT for 10 min, and washed with PBS twice and stored in refrigerator at 4 ºC for the following immunofluorescence staining. For the immunofluorescence staining, the fixed cells were permeabilized with methanol:acetone (50:50) on ice for 5 min, and washed with PBS twice. The cells were then blocked in 10% donkey serum with 0.1% w/v Tween-20 in PBS at RT for 1 h, incubated with mouse anti-β-tubulin III (Convance, Australia) in 10% donkey serum with 0.1% w/v Tween-20 in PBS at 4 ºC overnight, and Alexafluo 546 anti-mouse secondary antibody (Invitrogen, Australia) at 37 ºC for 1 h. The nuclei were counterstained with 4'-6-diamidino-2-phenylindole (DAPI) (Invitrogen, Australia) for 5 min at RT. Images were acquired using a ZEISS Axiovert microscope (Carl Zeiss, Germany).

3.2.7.3 Quantitative analysis

ImageJ with NeuriteQuant add-in was used to quantify the neurite numbers by averaging the number of neurites per cell in the observed area from all the samples collected. The software with Neurite length tracer add-in can measure the neurite growth of cells, including the total neurite number per cell, the sum total length of neurites per cell, mean neurite length per cell, and maximum neurite length per cell. Neurites were measured when the length of the projection exceeded a single body length of the cell from which it extended. Data are represented as mean ± standard deviation (SD) unless otherwise indicated. Results were analysed using Origin 2018b 64Bit using one-way ANOVA or two-way ANOVA with Tukey simultaneous testing method and Bonferroni`s post hoc test respectively. A *p*-value was determined and a maximum value of 0.05 was used to indicate significance.

3.3 Results and Discussion

3.3.1 Preparation of PPy films with various dopants

Polypyrrole (PPy) films with various dopants (*p*TS, DS and collagen) were successfully deposited onto FTO slides via typical cyclic voltammetry approach (Figure 3.1). The thickness of PPy-*p*TS, PPy-DS and PPy-DS/collagen films were 0.26 µm, 0.33 µm and 0.48 µm, respectively. In this study, three dopants were selected to investigate the effect of dopants on bipolar electrochemical activity. *p*TS is a popular low molecular weight dopant often used in PPy preparation. Naturally derived DS is a bioinert high molecular weight dopant. Collagen type I is a major component of extracellular matrix of connective tissue. It was incorporated into the PPy matrix together with DS to improve cell-substrate interactions [13,36,37]. All prepared PPy films were evaluated by cyclic voltammetry (CV) and electrochemical impedance spectroscopy (EIS) in PBS buffer to ascertain their electroactivity (Figure 3.2). No significant difference in electrical

properties amongst different PPy films were observed with the addition of *p*TS, DS and collagen as dopants. The electrochemical results also validated that the co-entrapment of collagen to functionalize PPy-DS did not change the nature of the dominant electrochemical behaviour of PPy films. These films are ready for further investigation and evaluation under bipolar electrostimulation environment.

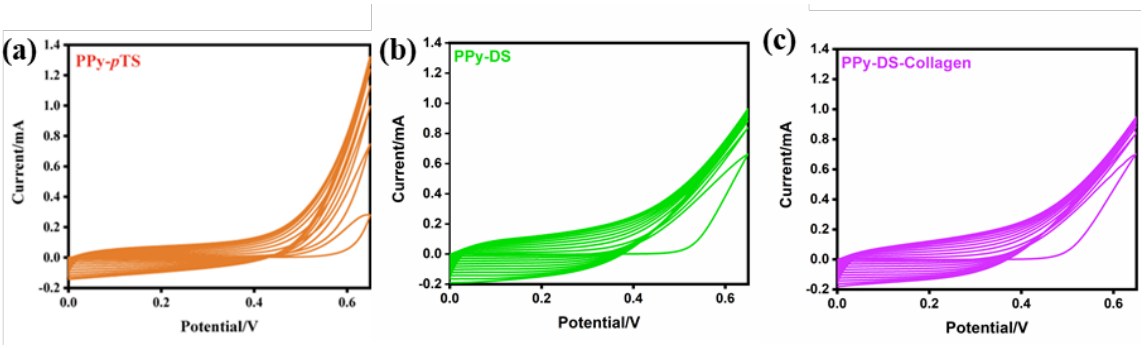

Figure 3.1 Electrodeposition of (a) PPy-*p*TS, (b) PPy-DS and (c) PPy-DS/collagen films onto FTO glass. PPy films were electro-synthesised by cyclic voltammetry (CV) from an aqueous solution containing 0.2 M distilled Py with 0.1 M *p*TS, or with 2 mg/ml DS without or with 2 µg/ml collagen, within a potential range of 0 - 0.65 V at a scan rate of 20 mV/s.

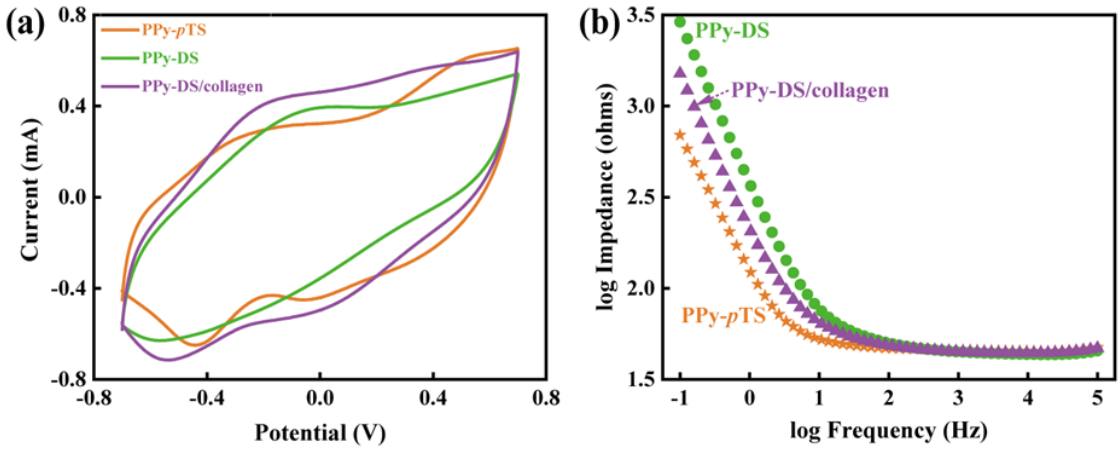

Figure 3.2 Electrochemical activity of PPy films in PBS (pH = 7.4). (a) Cyclic voltammetry (CV) of PPy-DS/collagen, PPy-DS and PPy-*p*TS at a scan rate of 100

mV/s. (b) electrochemical impedance spectroscopy (EIS) of them over a frequency range of 0.1 Hz-10^5 Hz.

3.3.2 Bipolar electrochemical activity of PPy films

The bipolar electrochemical activity of PPy films was investigated using an in-house designed bipolar electrochemical system, as shown in Figure 3.3a and reported in Chapter 2 for completely schematic diagram, in which the PPy-coated FTO glass slide (1 cm × 2 cm) was placed in the centre of bipolar cell. Immediately after applying a DC voltage of 5.5 V to the feeder electrodes (5 cm apart), the PPy films exhibit a colour change gradient (from green to orange, Figure 3.3b) demonstrating the expected redox processes caused by potential difference between two poles (ends) of the PPy films induced by the electric field generated by the feeder electrodes [38,39]. All three PPy films with various dopants display generally similar behaviour and, significantly, changing the polarity of the voltage applied to the feeder electrodes causes the sequences of colours across the BPES to change reversibly (+ / -). This observed relevant colour changes in response to the bipolar electrochemical activation could be explained by a common phenomenon related to the typical electrochemical redox process within PPy films [34,40]. This is further supported by the *in-situ* UV-vis absorption spectroscopy reported in Figure 3.4.

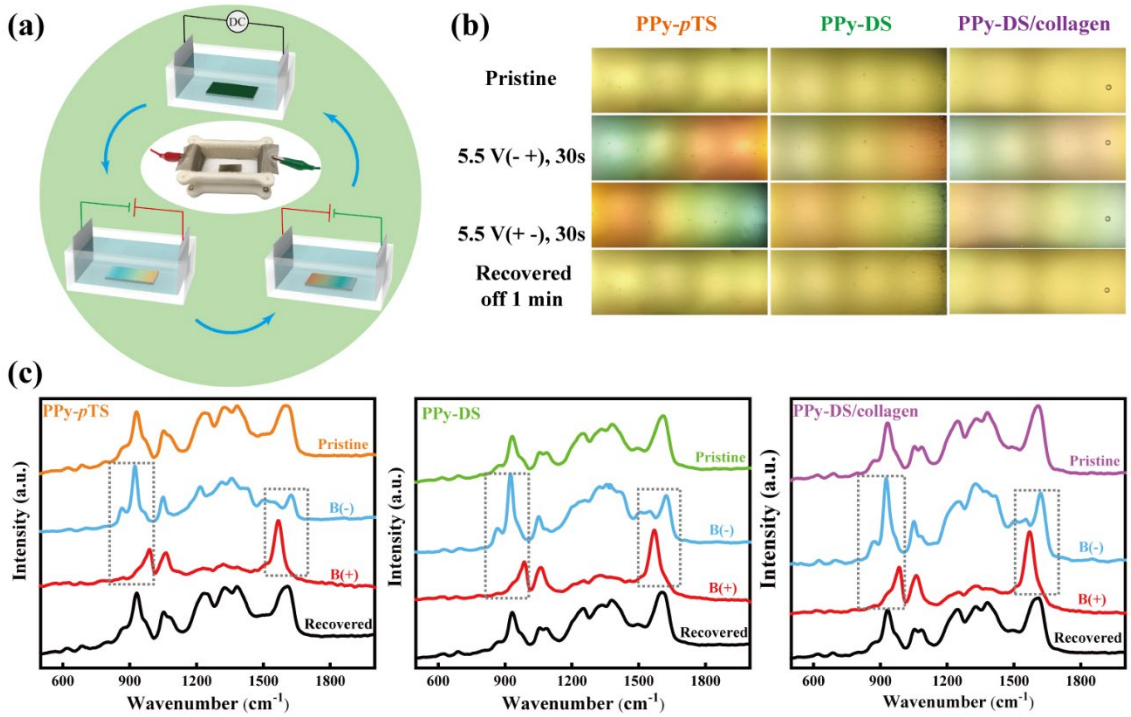

Figure 3.3 Stable bipolar electrochemical activity of PPy films in biological environment under low DC voltage. (a) Schematic of cycled BPES process and bipolar cell. (b) Optical images of the CPs immersed in bipolar cell following application of a voltage to the feeder electrodes. The colour changes correspond to changes in the redox composition of the CP layer due to the electric field potential induced in the BPES (the brighter regions are an imaging artifact). (c) *In situ* Raman spectra obtained when a voltage of 5.5 V is applied to the feeder electrodes. All experiments conducted in PBS. Excitation laser at 632.81 nm and accumulation time was 10 s.

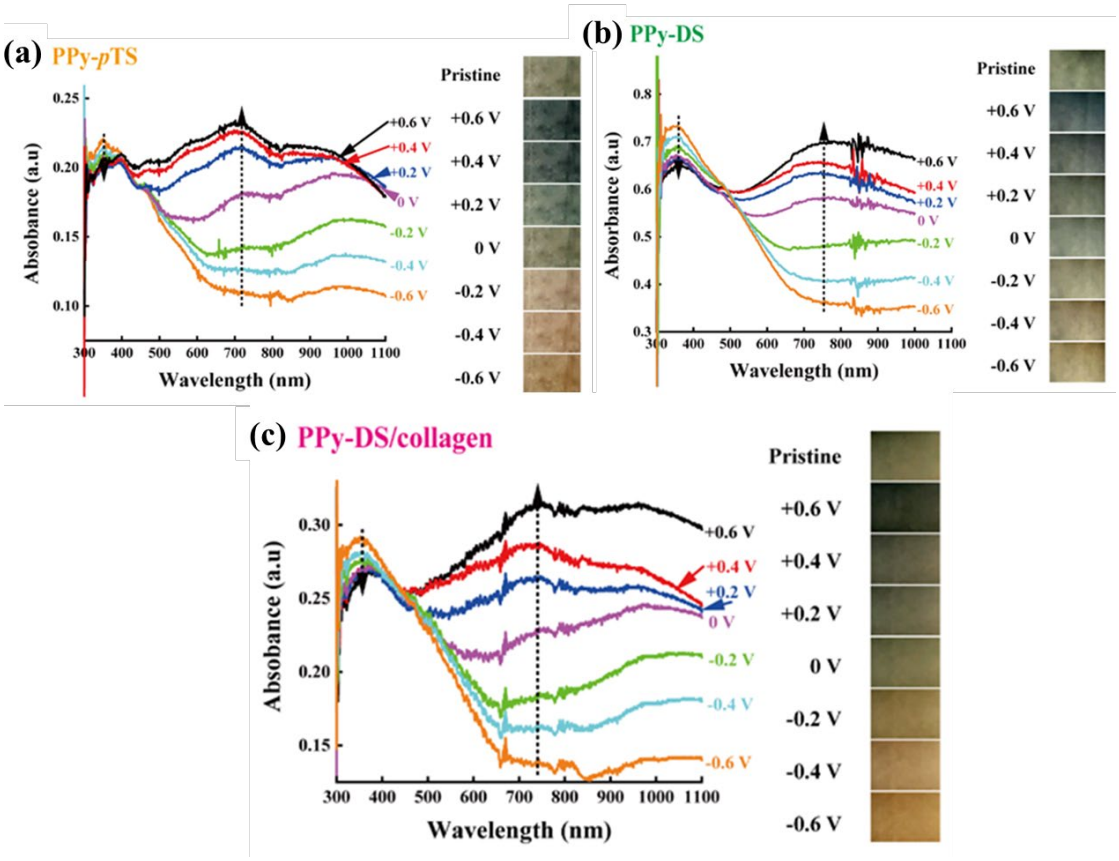

Figure 3.4 *In situ* UV-visible absorption spectra in the range of 300 nm - 1100 nm and according colours of (a) PPy-*p*TS, (b) PPy-DS and (c) PPy-DS/collagen obtained after applied consecutive potentials from -0.6 V to +0.6 V. All potentials are vs. an Ag wire reference electrode and keep 30 s poise time in PBS (pH = 7.4).

Further investigation into the chemical stability and reversibility of the PPy field induced redox switching was carried out using *in situ* Raman spectrometry (see Chapter 2: Figure 2.10 for set-up illustration). As a control, the "pristine" Raman spectrum was taken from the original PPy film before applying a voltage to the feeder electrodes, while the "recovered" Raman spectrum was recorded 1 min after the bipolar electrochemical process. B(-) and B(+) present the Raman spectra where the polarity of the feeder electrodes was switched. All the peaks present in the spectra in Figure 3.3c could be assigned to the characteristic Raman bands of PPy at different redox states, i.e.

oxidation (B(-)), reduction (B(+)) and neutralization ("pristine" and "recovered") [41]. Two specific areas of peaks were clearly distinguished in all Raman spectra. One is from the range of 800 cm^{-1} - 1000 cm^{-1}, which can be attributed to the ring deformation associated with the bipolaron and polaron formed in the main aromatic structure of PPy respectively. While the other is in the range from 1500 cm^{-1} to 1700 cm^{-1}, which is considered to be the C=C backbone stretching in the oxidation and reduction states of PPy. The consistency of the Raman spectra before and after the BPES cycle not only demonstrated that the reversible bipolar electrochemical activity of PPy was independent of dopants, but also showed that the redox phenomenon occurred on both sides (B(-) and B(+)). The reversible bipolar electrochemical property of PPy was further investigated and confirmed by *ex situ* Raman spectrometry, FTIR spectrometry and scanning electron microscopy (SEM) to explore the PPy before ("pristine") and after ("recovered") undergoing the identical bipolar testing (Figure 3.5). The topography measurements (SEM) showed no visible changes in surface morphologies of all PPy films revealing characteristically similar sized nodular features. It is demonstrated that the low applied DC voltage (up to 1.0 V per cm) that could only drive the redox of PPy films to generate the colour gradients without any observable conformational deformation change (shrinking and swelling), which required high electric field (4.0 V per cm) [42–44].

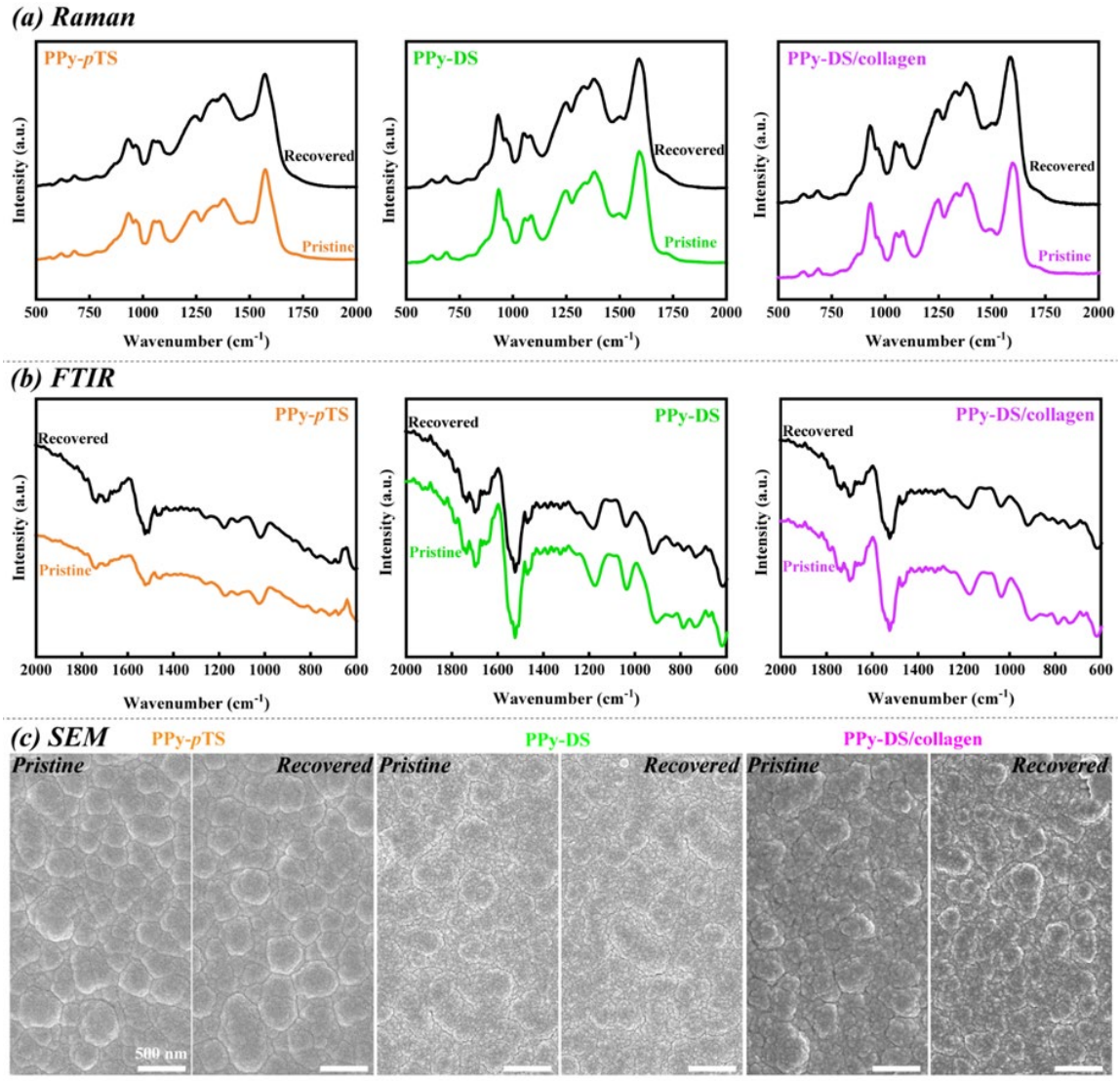

Figure 3.5 Characterisations of synthesised PPy-*p*TS, PPy-DS and PPy-DS/collagen before (pristine) and after (recovered) bipolar electrochemical testing. (a) Raman spectrometry, (b) FTIR spectrometry and (c) scanning electron microscopy (SEM) were performed under identical bipolar testing condition. All samples were tested in PBS under 5.5 V driving voltage for 30 s, and then taken out from PBS, subsequently rinsed with Milli-Q water and allowed to dry before all *ex situ* characterisations.

3.3.3 Cytocompatibility of PPy films as cell supportive substrates

In this work, collagen type I was incorporated into the PPy film matrix as a co-dopant during electropolymerisation to improve cell adhesion and differentiation [45,46]. To confirm the presence and distribution of collagen in PPy film, both PPy-DS (as control) and PPy-DS/collagen films were labelled with fluorescent rhodamine red^{TM}-X succinimidyl ester (Figure 3.6) [35]. PPy-DS/collagen film displayed a clear fluorescent signal assigned to fluorescence-labelled collagen, indicating that collagen was uniformly incorporated into the PPy matrix. Supported by CV and EIS of PPy-DS/collagen, it confirmed that incorporation of collagen into PPy-DS did not change significantly the intrinsic electrochemical activity and behaviour of PPy-DS films, which was consistent with the findings observed during bipolar electrochemical process (Figure 3.3b).

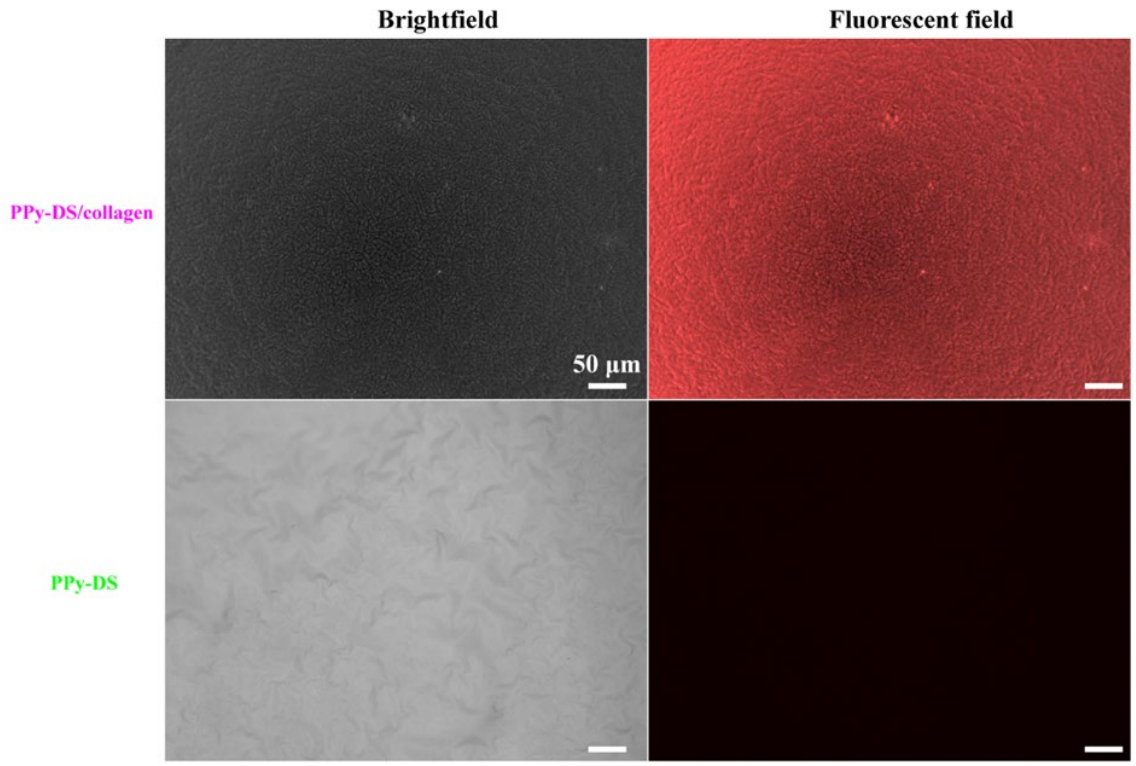

Figure 3.6 Images of PPy-DS and PPy-DS/collagen after fluorescent labelling. PPy-DS and PPy-DS/collagen (1 cm × 1 cm) were firstly soaked in 1.5 ml solution with

isometric PBS and ethanol for 30 min. Then 500 µl rhodamine red^{TM}-X succunimidyl ester/DMSO at a final concentration of 2.5 µg/ml was added into each well, followed by 5 hours' reaction at RT in covered Al foil as darkroom. Finally, replaced with the fresh PBS after thorough washing with isometric PBS and ethanol for 10 min each time, total three times to remove the residue fluorescent dye. The surface morphology of fluorescently labelled samples was examined in using a ZEISS Axiovert microscope.

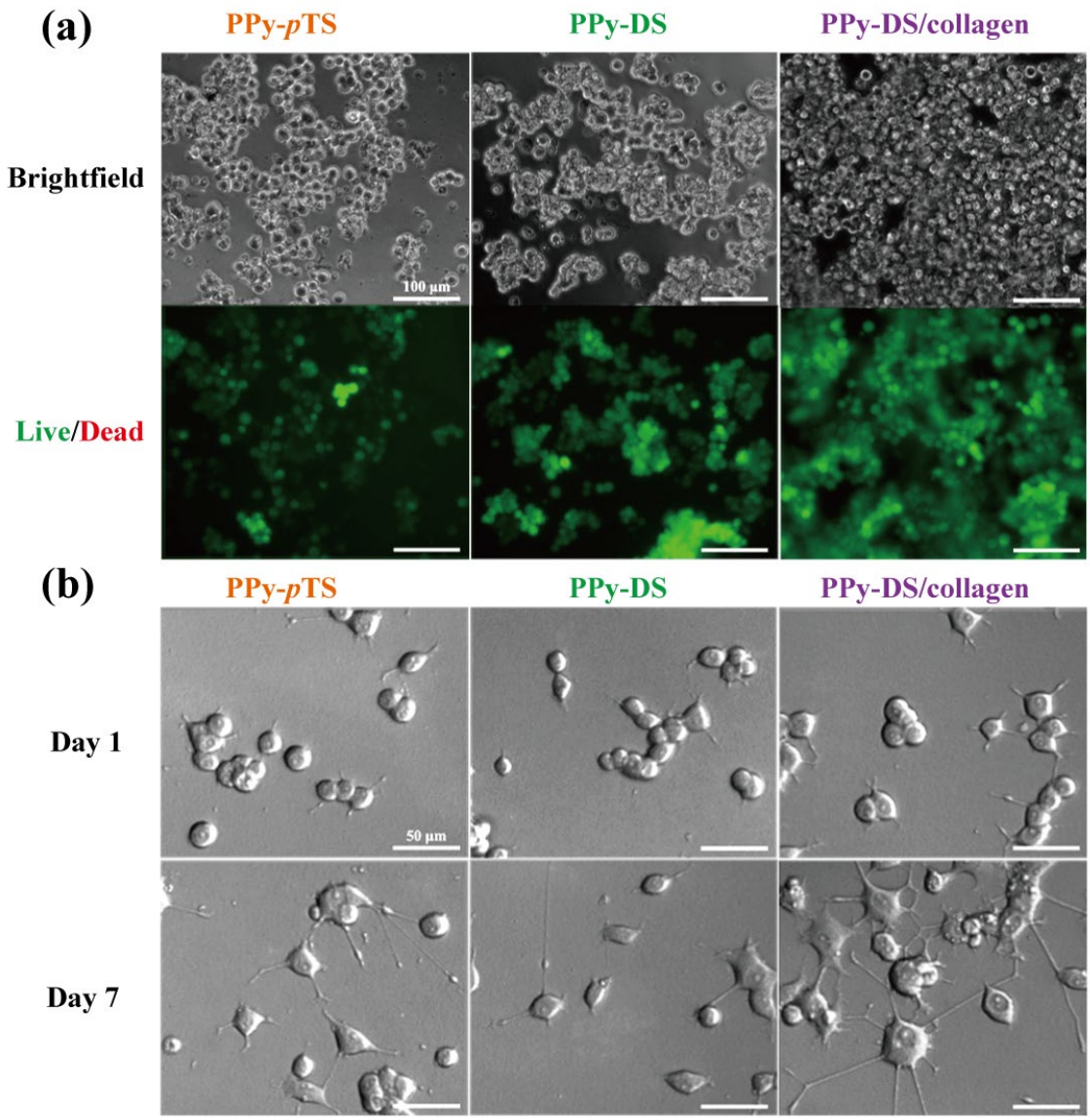

Figure 3.7 Cytocompatibility of PPy films as cell supportive substrates. (a) Bright field and fluorescent images of PC 12 cells on day 7 after cyto-compatibility assessment via

live/dead assay. Calcein-AM was used to stain live cells (green) and propidium iodide (PI) used to stain dead cells (red). (b) Bright field images of PC 12 cells on day 1 and day 7 in the differentiation medium (containing 50 ng/ml NGF) at an initial cell seeding density of 2000 cells/cm^2.

Cytocompatibility of the PPy films was assessed using a rat pheochromocytoma cell line, PC 12, prior to bipolar electrochemical stimulation. PC 12 cells were culture on the 3 types of PPy substrates for one week, during which the cell viability was monitored by live/dead staining at various time points. As shown in Figure 3.7a, PC 12 cells cultured on the three PPy substrates all exhibited rounded morphology with high cell viability and tended to form colonies of cell aggregates, indicating that the PPy films are not cytotoxic irrespective of the dopant used. As shown in Figure 3.7, compared with PPy-*p*TS and PPy-DS, the PPy-DS/collagen demonstrated the best phenomenon of cell proliferation and neurite outgrowth under identical conditions, indicating a promising bio-interfacial material. Therefore, PPy-DS/collagen film was selected as the key bipolar electrode substrate to evaluate the performance of wireless stimulation.

3.3.4 Development of bipolar electrochemical stimulation (BPES) protocols

For the first time, an in-house designed BPES platform for contactless electrical stimulation of living cells has been developed (Figure 3.8). The main bipolar device consisted of three key parts, 3D printed frame, tailored PVDF membrane and laser cut stainless-steel mesh (SSM) as required. The material used for printing 3D frame was a commercial “Dental LT Clear” resin (Formlabs, United States). Printed structures were post processed in accordance with manufacturer’s protocols to ensure suitability for cell culture. Two pieces of etched SSM were employed as driving electrodes to create the

electric field that could induce a voltage in the PPy film so as to generate the redox processes, while the PVDF membrane maintained the proper ion exchange/diffusion and prevented cell migration from the central cell-culture well to side wells (step 1-3). Then, all wells were filled with cell culture media, while the PC 12 cells were only seeded in the four middle replicate cell culture wells where the bipolar substrates (PPy-DS/collagen) were placed, ready for further BPES evaluation.

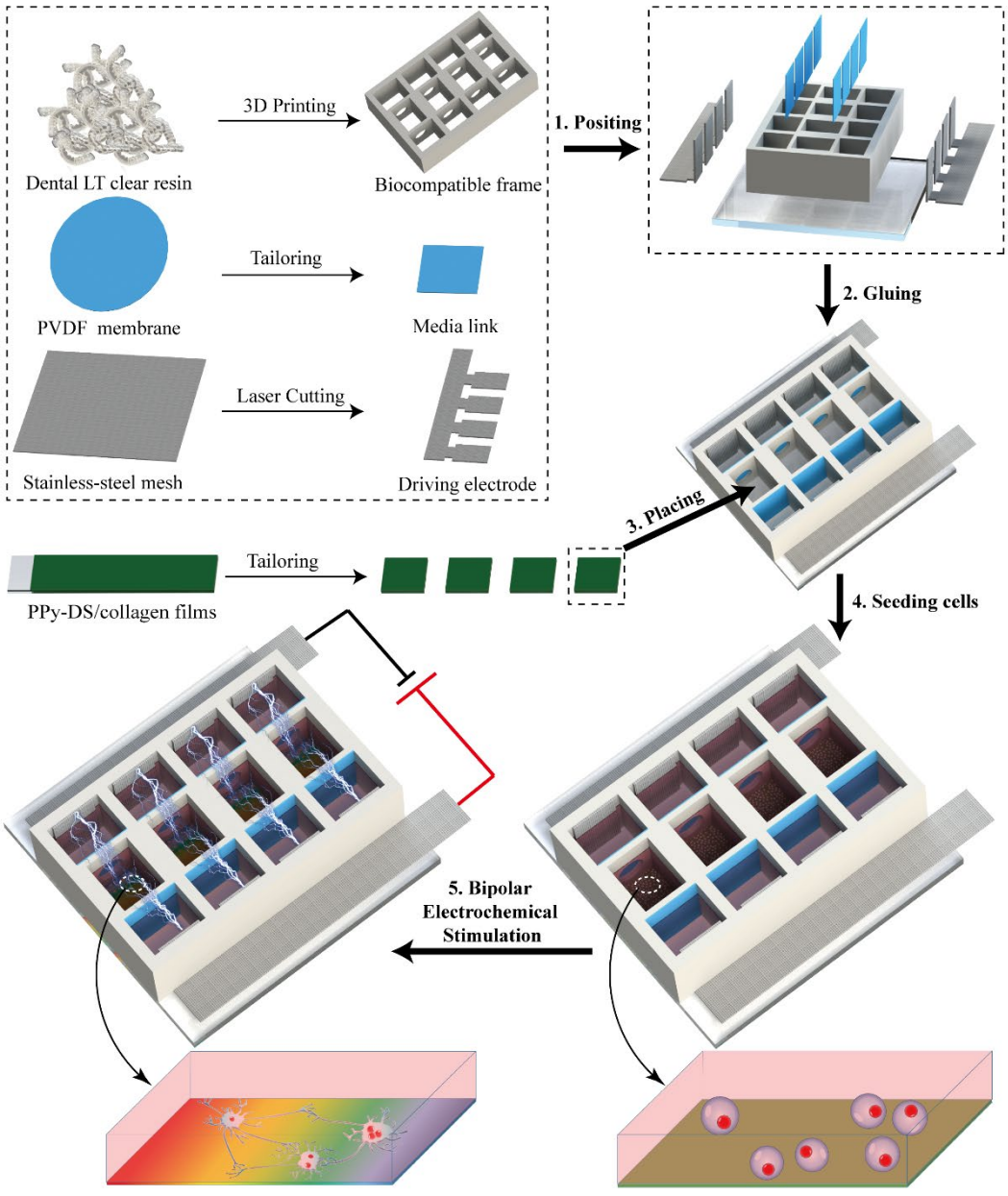

Figure 3.8 Schematic fabrication of bipolar electrochemical stimulation (BPES)

platform. 3D printed frame used dental LT clear resin to ensure biocompatibility. The parallel stainless-steel mesh (SSM) acted as driving electrodes to induce external electric field and tailored PVDF membrane as media link to guarantee ion exchange for smooth bipolar electrochemistry of PPy-DS/collagen and avoid cells migrating to side driving wells. All parts were fixed overnight using silicon adhesive sealant. The tailored PPy-DS/collagen sheets (1 cm × 1 cm) were immersed in the middle cell culture wells, followed with sterilisation process before same density of cells were seeded. Cells were stimulated once the bipolar device was connected with programmable DC power supply.

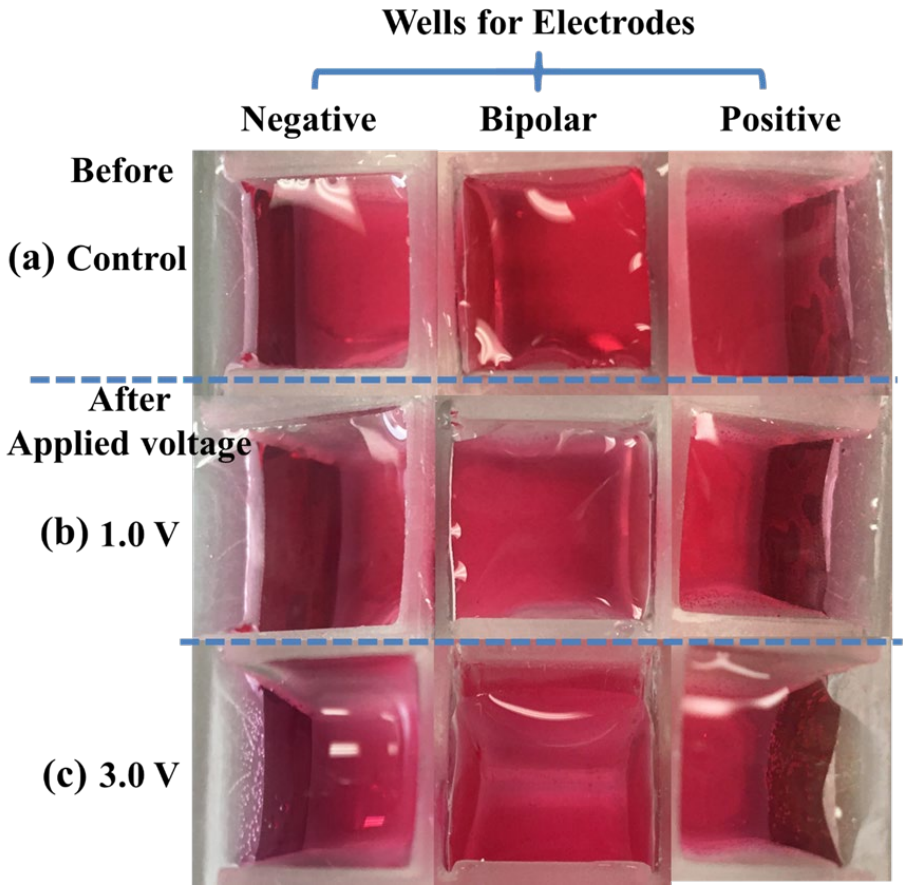

Figure 3.9 Images acquired from different wells for negative feeder electrode, bipolar electrode, and positive feeder electrode, respectively, before (control: (a)) and after applied (b) 1.0 V, (c) 3.0 V.

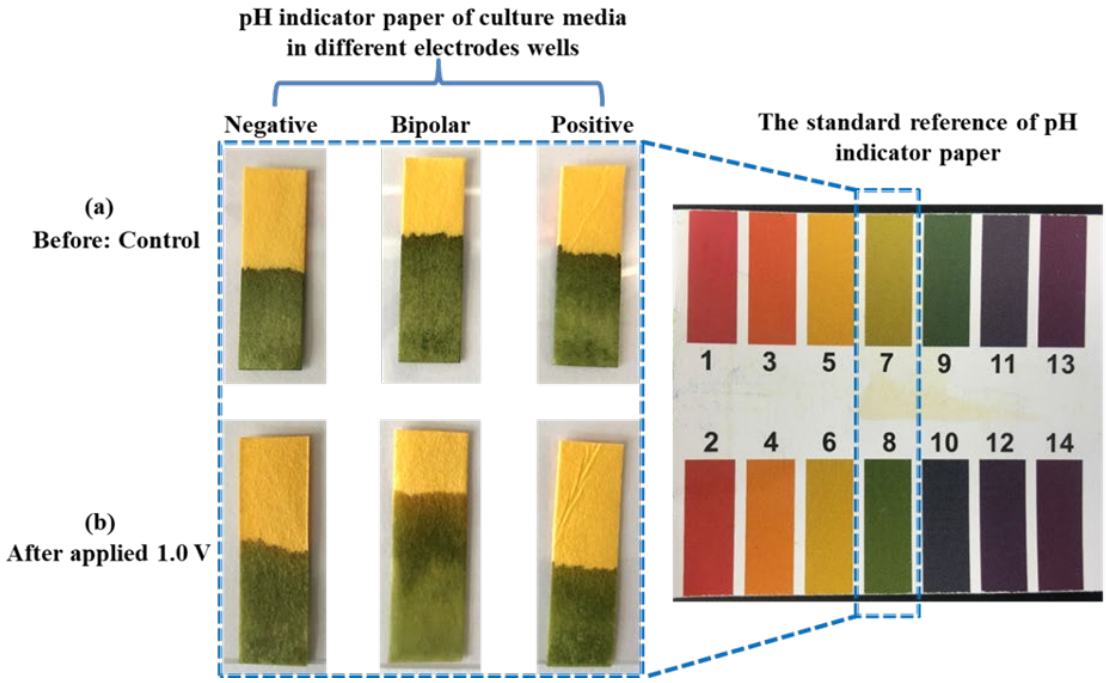

Figure 3.10 Images of pH indicator papers acquired from culture media in different wells for negative feeder electrode, bipolar electrode, and positive feeder electrode respectively, before ((a) control) and after (b) applied 1.0 V underwent identical bipolar electrochemical stimulation process.

The BPES protocol for the specific-designed device was also developed by optimising the applied DC voltage under pulse mode. As the results reported in Figure 3.9, no bubbles were generated on both sites of the "feeder electrodes" under the applied DC voltage of 1.0 V, while clear bubbles generation were observed when the applied DC voltage went over 3.0 V. And referred to the standard pH indicator paper (Figure 3.10), no obvious colour change was observed after immersed in culture media under 1.0 V applied voltage, revealing stable pH value in range of pH 7~ pH 8. These results clearly demonstrated the applied DC voltage of 1.0 V was the safe option to stimulate cells, which could avoid either gas evolution or related pH changes. Further confirmed by the

results of high cell viability following 7 days' treatment (Figure 3.11), optimised pulse mode with magnitude 1.0 V (comprised phase duration of 10 min with interphase interval of 5 min) was selected as the optimal BPES protocol for further study to evaluate the effect of BPES on cell behaviour. Schematic illustrations of the waveform of applied pulse mode and three distinct programmed BPES pulse modes used for studies of cell proliferation and cell differentiation are available in Figure 3.12. Three independent experiments in each BPES pulse mode were performed over a period of one week. Control experiments, standard culturing with no BPES, were also carried out in parallel for proper evaluation and comparison.

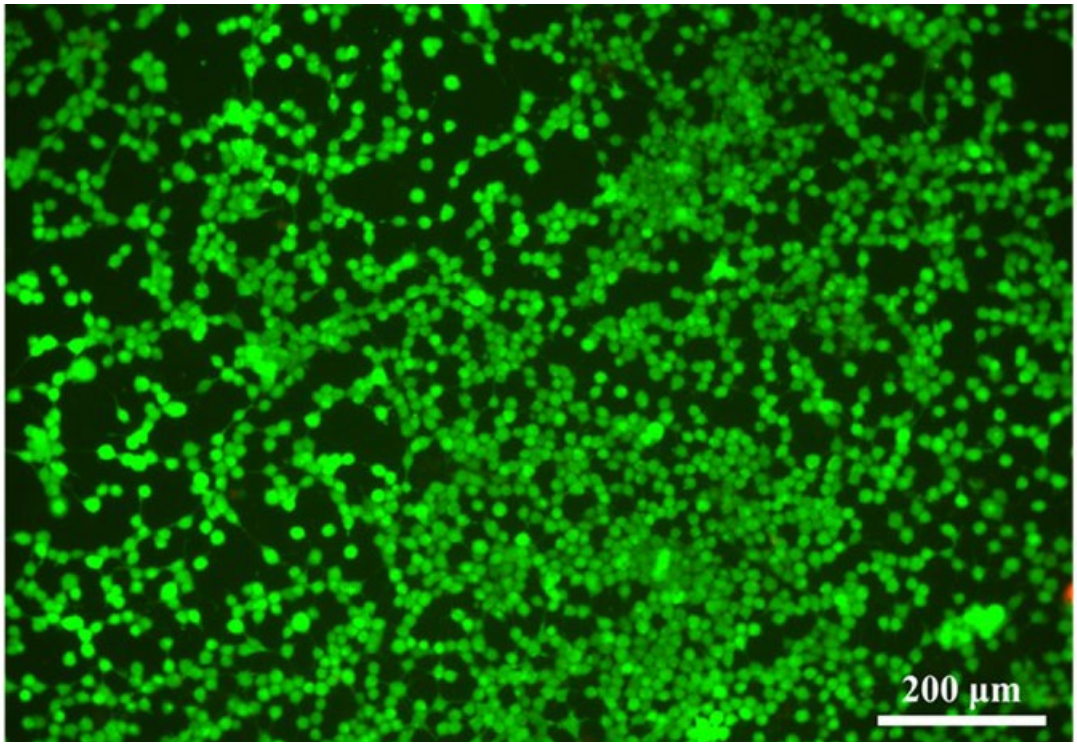

Figure 3.11 Cell viability under BPES. Image of PC 12 cells on day 7 via live (calcein AM; green) and dead (PI; red) staining, after cultured on PPy-DS/collagen with BPES pulse mode-A (Figure 3.12b, 1.0 V DC driving voltage) in growth media.

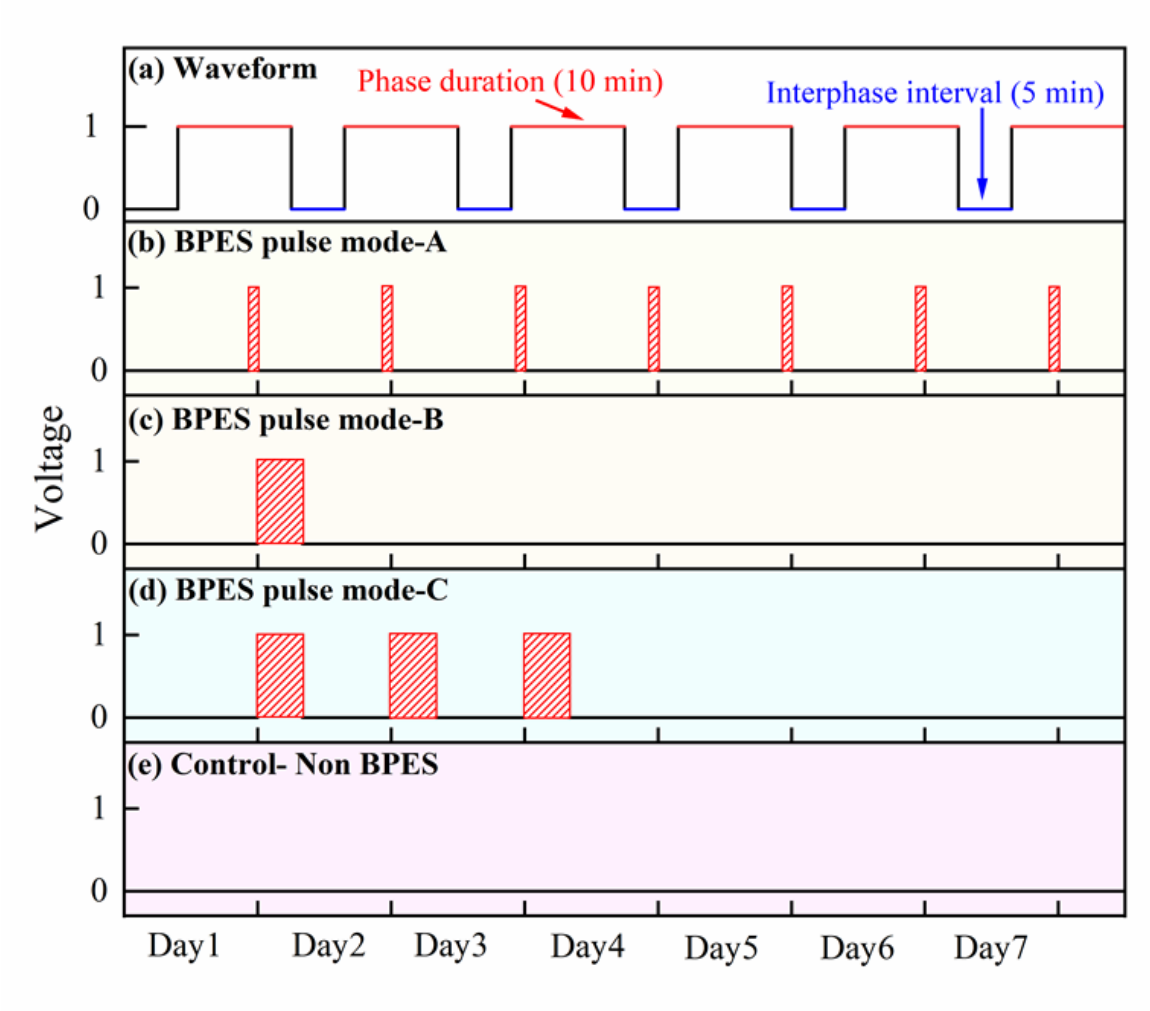

Figure 3.12 Schematic illustration of programmed BPES pulse modes. (a) The waveform of the applied pulse mode comprised phase duration of 10 min with interphase interval of 5 min. (b) BPES pulse mode-A: cells were stimulated for 1 h per day over 7 days. (c) BPES pulse mode-B: cells were stimulated for 8 h on day 2, then cultured as normal in the absence of BPSE for the following 5 days. (d) BPES pulse mode-C: cells were stimulated on day 2 for 8 h, and this pattern was continued until day 5, after which they were cultured as normal in the absence of BPSE to the end of day 7. (e) Control Non-BPES: cells were cultured under identical conditions without BPES (i.e., normal condition).

3.3.5 Evaluation of the BPES platform for wireless stimulation of cells

To assess the effect of BPES on cell proliferation, PC 12 cells cultured on PPy-DS/collagen film was stimulated following developed protocols. BPES pulse mode-A (Figure 3.12b) for 1 h per day in seven consecutive days. A control group under identical culturing conditions with no BPES (Control-Non BPES) was also conducted in parallel. Under BPES, PC 12 cells adhered to the PPy-DS/collagen film and proliferated well over time showing normal morphology. The number of cells at various time points, with or without BPES, were quantified using the PicoGreen assay. Figure 3.13 shows that the number of cells is statistically higher for the BPES stimulated group than the unstimulated control group. Statistical analysis via two-way ANOVA also revealed both BPES and time point with a $P < 0.0001$, indicating significant effects on cell proliferation, and so did the interaction of BPES and time point (with a $P < 0.001$). Particularly, Bonferroni-post hoc analysis indicated that PC 12 cell proliferation with or without BPES treatment was significantly different from each other (with a $P < 0.0001$) (Figure 3.13e-f). These results confirm that BPES treatment promotes cell proliferation with significant positive influence.

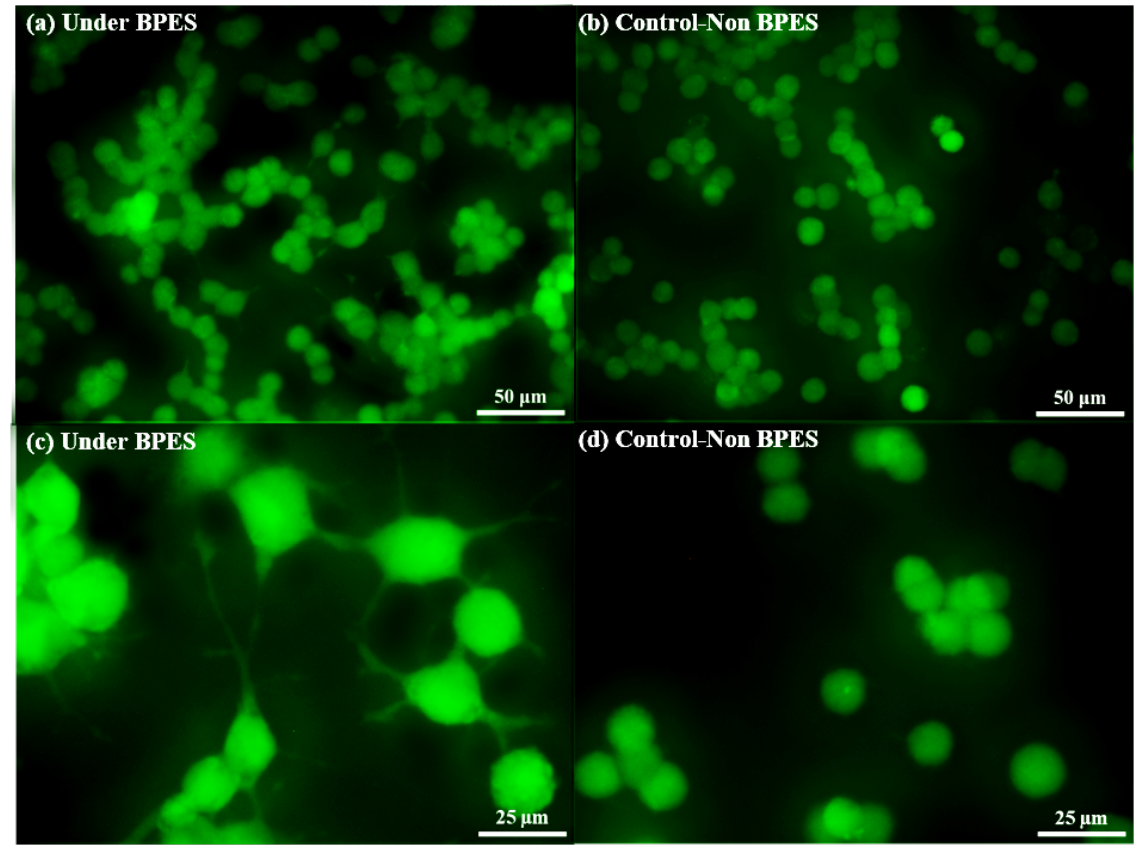

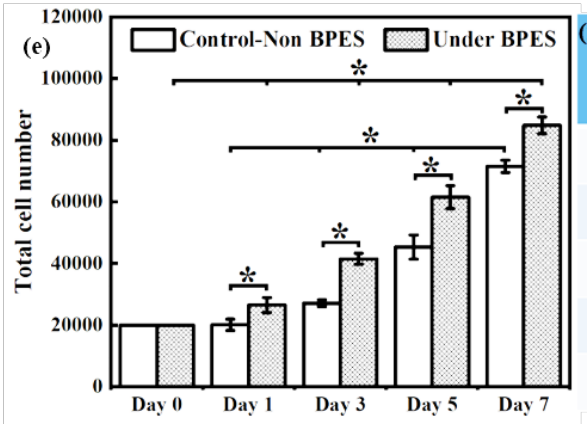

(f)

Time Point	Total Cell Numbers (cells/cm²)	
	Under BPES	Control-Non BPES
Day 0	20000	20000
Day 1	26520.6 ± 2428.4	20090.5 ± 1842.2
Day 3	41519.3 ± 1823.7	27100.8 ± 1098.8
Day 5	61538.2 ± 3699.8	45345.8 ± 3945.9
Day 7	84809.3 ± 2712.1	71523.9 ± 1984.8

Figure 3.13 Evaluation of BPES on cell proliferation. (a)-(d) Images on day 5 via live/dead assay using calcein AM and PI. PC 12 cells were cultured on PPy-DS/collagen at an initial seeding density of 20000 cells/cm^2 in growth media over one week. Under BPES (pulse mode-A): cells were stimulated for 1 h per day with 1 V driving voltage for 7 days. Control (Non-BPES): cells were standard cultured with no BPES. (e)-(f) Numbers of PC 12 cells determined by PicoGreen assay at various time points with statistical analysis using two-way ANOVA. Data are represented as mean ±

standard deviation (SD) and "*" ($P < 0.0001$) was used to indicate significance.

Interestingly, under BPES, the PC 12 cells cultured in the cell growth medium also started early-stage differentiation (Figure 3.13c), indicated by the morphological changes and formation of extended neurites observed on PPy-DS/collagen film. In contrast, the control cells remained undifferentiated with a rounded morphology (Figure 3.13d). This interesting phenomenon suggested that BPES could also initiate neurite sprouting in the absence of nerve growth factor (NGF). Studies have shown that neurite sprouting as an early cellular event of neuronal differentiation could be induced by direct electrical stimulation [15,47]. Here we noted a similar effect using our CP-based wireless BPES, although the specific mechanism remains to be elucidated. This highlights the potential benefits of the proposed BPES system as an alternative therapeutic approach to nerve regeneration to conventional pharmacological approaches.

To investigate the effect of BPES on nerve cell differentiation, PC 12 cells seeded on PPy-DS/collagen films were exposed to NGF (50 ng/ml) in a low serum medium (1% horse serum). Once the cell stimulation devices were established, a BPES pulse mode-A was applied as described above. The PC 12 cells underwent differentiation, exhibiting a typical neural morphology, extending neurites and forming neural networks on PPy-DS/collagen films (Figure 3.14a). Compared with the control group (Figure 3.14d) in the absence of BPES, the stimulated group showed enhanced neurite outgrowth in terms of both lengths and numbers. A ~100% increase in both number and length (Figure 3.14e-f) were observed. Furthermore, statistical analysis using one-way ANOVA combined with Bonferroni-post hoc analysis are summarized, and demonstrate a

significant difference with a $P < 0.0001$ between under BPES and non-BPES. The complete results are available in Figure 3.15 and Table 3.1.

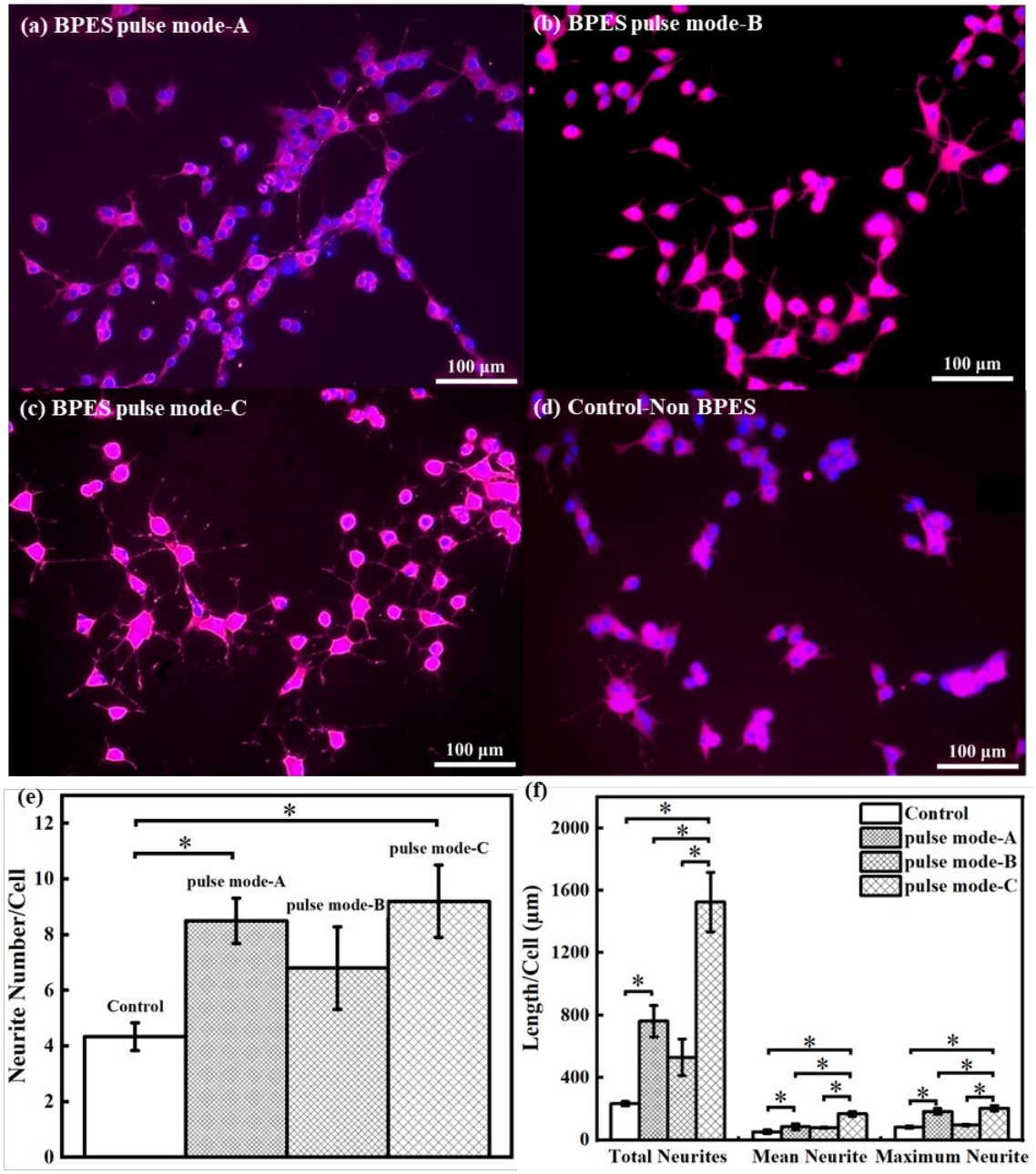

Figure 3.14 Immunofluorescent staining and quantitative analysis of BPES on cell differentiation. (a)-(d) Immunofluorescent images (DAPI: blue, β-tubulin III: red) of the PC 12 cells on day 7 after different BPES pulse modes. Cells were cultured on PPy-DS/collagen over a period of one week at an initial seeding density of 2000 cells/cm^2. (a)

BPES pulse mode-A; (b) BPES pulse mode-B; (c) BPES pulse mode-C; and (d) Control-Non BPES: cells were cultured with no BPES. Assessments of (e) neurite number and (f) neurite growth of cells, including the total neurite number per cell, the sum total length of neurites per cell, mean neurite length per cell, and maximum neurite length per cell. Statistical analysis used one-way ANOVA. Data are represented as mean ± standard deviation (SD) and "*" ($P < 0.0001$) was used to indicate significance.

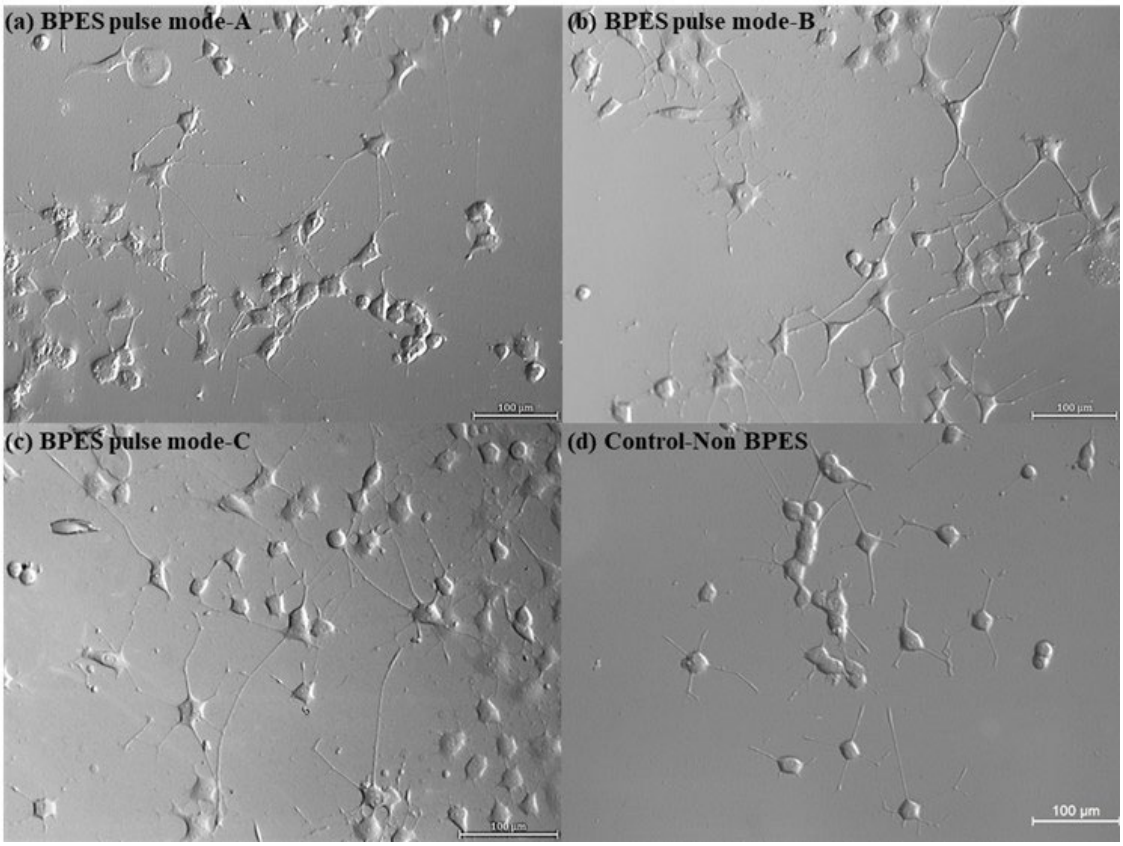

Figure 3.15 Phase-contrast images of PC 12 cells on day 7 after experiencing different BPES pulse modes. Cells were cultured on PPy-DS/collagen over a period of one week at an initial seeding density of 2000 cells/cm^2. (a) BPES pulse mode-A; (b) BPES pulse mode-B; (c) BPES pulse mode-C; and (d) Control-Non BPES: cells were cultured with no BPES.

Table 3.1 Results of different BPES pulse modes on cell differentiation. Data are represented as mean ± standard deviation (SD).

Modes	Neurites Number	Neurite Length (μm)		
		Total	Mean	Max
Control	4.3 ± 0.4	231.9 ± 18.9	52.9 ± 11.7	81.5 ± 12.6
BPES pulse mode-A	8.5 ± 1.0	761.6 ± 166.8	84.6 ± 27.5	182.8 ± 29.3
BPES pulse mode-B	6.8 ± 1.5	529.3 ± 117.5	77.9 ± 3.9	95.6 ± 2.2
BPES pulse mode-C	9.2 ± 1.3	1524.9 ± 191.3	166.5 ± 14.4	203.6 ± 17.7

The effect of different BPES pulse modes as described above were also investigated. Compared with the control group without BPES, all of these BPES pulse modes had a significant effect on neurite elongation (Figure 3.14a-d). Among the three stimulation modes, the BPES pulse mode-C (Figure 3.14c) had the most significant effect on PC 12 cell differentiation. As displayed in Figure 3.14e-f, the PC 12 cells under BPES pulse mode-C displayed a mean neurite length of 166.5 ± 14.4 μm per cell, which is almost twice as much as those under BPES mode-A (84.6 ± 27.5 μm) and mode-B (7.9 ± 3.9 μm). This suggested that the duration of BPES played a key role in modulating the neuronal differentiation, allowing differentiation to be accomplished quickly. Further evaluation showed that there was no significant difference in neurite numbers among three BPES pulse modes.

3.4 Conclusions

Innovative programmable bipolar electrochemical stimulation (BPES), a wireless platform utilising PPy-DS/collagen films, represents an effective approach to promote

neuron growth. The ability to enhance neural cell proliferation and differentiation confirms the delivery of electrical stimulation wirelessly to neurons through this platform. An in-house BPES living cell stimulation prototype has been developed and standardized to be able to replace the conventional direct ES system with a contactless platform. Increased PC 12 cells number and extensive neurites growth were observed in our BPES system. It is noteworthy that the emergence of neurites sprouting in absence of NGF with BPES might have the potential to provide an alternative "electroceutical" therapeutic method to nerve regeneration as opposed to pharmacological approaches.

Further work requires refinement of CPs or finding alternative soft, degradable substrate materials are demanded to reduce or eliminate their dependence on conductive supporting substrates, to achieve truly free-standing flexible structures more suitable for implantation. Furthermore, additional work on the mechanism of BPES is needed to be better understood to promote its potential clinical applications. Our demonstration that weak electric field/low voltages can be used is especially significant and relevant to *in vivo* applications. Together, these findings establish the foundations/framework of CP-based BPES system, a wireless platform for living cell stimulation, paving a way forward to drug free therapy.

3.5 References

[1] J. Kolosnjaj-Tabi, L. Gibot, I. Fourquaux, M. Golzio, M.P. Rols, Electric field-responsive nanoparticles and electric fields: physical, chemical, biological mechanisms and therapeutic prospects, Adv. Drug Deliv. Rev. 138 (2019) 56–67. https://doi.org/10.1016/j.addr.2018.10.017.

[2] V.A. McBain, J. V Forrester, C.D. McCaig, HGF, MAPK, and a small

physiological electric field interact during corneal epithelial cell migration, Investig. Ophthalmol. Vis. Sci. 44 (2003) 540–547. https://doi.org/10.1167/iovs.02-0570.

[3] G. Shi, M. Rouabhia, S. Meng, Z. Zhang, Electrical stimulation enhances viability of human cutaneous fibroblasts on conductive biodegradable substrates, J. Biomed. Mater. Res. - Part A. 84 (2008) 1026–1037. https://doi.org/10.1002/jbm.a.31337.

[4] J. Zhang, K.G. Neoh, E.T. Kang, Electrical stimulation of adipose-derived mesenchymal stem cells and endothelial cells co-cultured in a conductive scaffold for potential orthopaedic applications, J. Tissue Eng. Regen. Med. 12 (2018) 878–889. https://doi.org/10.1002/term.2441.

[5] N. Gomez, C.E. Schmidt, Nerve growth factor-immobilized polypyrrole: Bioactive electrically conducting polymer for enhanced neurite extension, J. Biomed. Mater. Res. - Part A. 81 (2007) 135–149. https://doi.org/10.1002/jbm.a.31047.

[6] B. Song, Nerve regeneration and wound healing are stimulated and directed by an endogenous electrical field in vivo, J. Cell Sci. 117 (2004) 4681–4690. https://doi.org/10.1242/jcs.01341.

[7] S. Vandghanooni, M. Eskandani, Electrically conductive biomaterials based on natural polysaccharides : Challenges and applications in tissue engineering, Int. J. Biol. Macromol. 141 (2019) 636–662. https://doi.org/10.1016/j.ijbiomac.2019.09.020.

[8] Y. Wang, H. Zhu, H. Yang, A.D. Argall, L. Luan, C. Xie, Nano functional neural interfaces, Nano Res. 11 (2018) 5065–5106.

[9] Z. Aqrawe, J. Montgomery, J. Travas-sejdic, D. Svirskis, Chemical Conducting

polymers for neuronal microelectrode array recording and stimulation, Sensors Actuators B. Chem. 257 (2018) 753–765. https://doi.org/10.1016/j.snb.2017.11.023.

[10] H. Palza, P.A. Zapata, C. Angulo-pineda, Electroactive Smart Polymers for Biomedical Applications, Materials (Basel). 12 (2019) 227.

[11] L. Guo, M. Ma, N. Zhang, R. Langer, D.G. Anderson, Stretchable polymeric multielectrode array for conformal neural interfacing, Adv. Mater. (2014). https://doi.org/10.1002/adma.201304140.

[12] J. Black, Electrochemical aspects of d.c. stimulation of osteogenesis, Bioelectrochemistry Bioenerg. 173 (1984) 323–327.

[13] Z. Yue, X. Liu, P.J. Molino, G.G. Wallace, Bio-functionalisation of polydimethylsiloxane with hyaluronic acid and hyaluronic acid–collagen conjugate for neural interfacing, Biomaterials. 32 (2011) 4714–4724.

[14] W.R. Stauffer, X.T. Cui, Polypyrrole doped with 2 peptide sequences from laminin, Biomaterials. 27 (2006) 2405–2413.

[15] X. Liu, K.J. Gilmore, S.E. Moulton, G.G. Wallace, Electrical stimulation promotes nerve cell differentiation on polypyrrole/poly (2-methoxy-5 aniline sulfonic acid) composites, J. Neural Eng. 6 (2009) 65002.

[16] W.Z. Ray, M.A. Mahan, D. Guo, D. Guo, M. Kliot, An update on addressing important peripheral nerve problems: challenges and potential solutions, Acta Neurochir. (Wien). 159 (2017) 1–9. https://doi.org/10.1007/s00701-017-3203-3.

[17] P.M. Rossini, S. Micera, A. Benvenuto, J. Carpaneto, G. Cavallo, L. Citi, C. Cipriani, L. Denaro, V. Denaro, G. Di Pino, F. Ferreri, E. Guglielmelli, K.P. Hoffmann, S. Raspopovic, J. Rigosa, L. Rossini, M. Tombini, P. Dario, Double nerve intraneural interface implant on a human amputee for robotic hand control,

Clin. Neurophysiol. 121 (2010) 777–783. https://doi.org/10.1016/j.clinph.2010.01.001.

[18] J. del Valle, X. Navarro, Interfaces with the peripheral nerve for the control of neuroprostheses, 1st ed., Elsevier Inc., 2013. https://doi.org/10.1016/B978-0-12-420045-6.00002-X.

[19] L. Koefoed, S.U. Pedersen, K. Daasbjerg, Bipolar electrochemistry—A wireless approach for electrode reactions, Curr. Opin. Electrochem. 2 (2017) 13–17. https://doi.org/10.1016/j.coelec.2017.02.001.

[20] C.A.C. Sequeira, D.S.P. Cardoso, M.L.F. Gameiro, Bipolar Electrochemistry, a Focal Point of Future Research, Chem. Eng. Commun. 203 (2016) 1001–1008. https://doi.org/10.1080/00986445.2016.1147031.

[21] N. Shida, Y. Zhou, S. Inagi, Bipolar Electrochemistry: A Powerful Tool for Electrifying Functional Material Synthesis, Acc. Chem. Res. (2019). https://doi.org/10.1021/acs.accounts.9b00337.

[22] S.E. Fosdick, K.N. Knust, K. Scida, R.M. Crooks, Bipolar electrochemistry, Angew. Chemie - Int. Ed. 52 (2013) 10438–10456. https://doi.org/10.1002/anie.201300947.

[23] G. Loget, D. Zigah, L. Bouffier, N. Sojic, A. Kuhn, Bipolar electrochemistry: from materials science to motion and beyond, Acc. Chem. Res. 46 (2013) 2513–2523.

[24] M.S. Wu, G.S. Qian, J.J. Xu, H.Y. Chen, Electrochemiluminescence detection of c-Myc mRNA in breast cancer cells on a wireless bipolar electrode, Methods Mol. Biol. 1039 (2013) 169–179. https://doi.org/10.1007/978-1-62703-535-4_15.

[25] Y.Z. Wang, C.H. Xu, W. Zhao, Q.Y. Guan, H.Y. Chen, J.J. Xu, Bipolar Electrode Based Multicolor Electrochemiluminescence Biosensor, Anal. Chem.

89 (2017) 8050–8056. https://doi.org/10.1021/acs.analchem.7b01494.

[26] W. Gao, K. Muzyka, X. Ma, B. Lou, G. Xu, A single-electrode electrochemical system for multiplex electrochemiluminescence analysis based on a resistance induced potential difference, Chem. Sci. 9 (2018) 3911–3916. https://doi.org/10.1039/c8sc00410b.

[27] K.F. Chow, B.Y. Chang, B.A. Zaccheo, F. Mavré, R.M. Crooks, A sensing platform based on electrodissolution of a Ag bipolar electrode, J. Am. Chem. Soc. 132 (2010) 9228–9229. https://doi.org/10.1021/ja103715u.

[28] M. Hasheminejad, Y. Fang, M. Li, Y. Jiang, W. Wang, Y. Chen, Plasmonic Imaging of the Interfacial Potential Distribution on Bipolar Electrodes, (2017) 1629–1633. https://doi.org/10.1002/anie.201611235.

[29] M.S. Wu, D.J. Yuan, J.J. Xu, H.Y. Chen, Sensitive electrochemiluminescence biosensor based on Au-ITO hybrid bipolar electrode amplification system for cell surface protein detection, Anal. Chem. 85 (2013) 11960–11965. https://doi.org/10.1021/ac402889z.

[30] R. Gao, Y.L. Ying, Y.X. Hu, Y.J. Li, Y.T. Long, Wireless Bipolar Nanopore Electrode for Single Small Molecule Detection, Anal. Chem. 89 (2017) 7382–7387. https://doi.org/10.1021/acs.analchem.7b00729.

[31] P. Sanjuan-Alberte, F.J. Rawson, A. Jain, A. Shaw, S. Abayzeed, R. Rafael Fuentes Dominguez, M.E. Alea-Reyes, M. Clark, M.R. Alexander, R.J.M. Hague, L. Perez-Garcia, Wireless Nanobioelectronics for Electrical Intracellular Sensing, ACS Appl. Nano Mater. (2019). https://doi.org/10.1021/acsanm.9b01374.

[32] C. Bertucci, R. Koppes, C. Dumont, A. Koppes, Neural responses to electrical stimulation in 2D and 3D in vitro environments, Brain Res. Bull. 152 (2019)

265–284. https://doi.org/10.1016/j.brainresbull.2019.07.016.

[33] L. Bouffier, N. Sojic, A. Kuhn, Capillary-assisted bipolar electrochemistry: A focused mini review, Electrophoresis. 00 (2017) 1–8. https://doi.org/10.1002/elps.201600568.

[34] S. Little, S.F. Ralph, C.O. Too, G.G. Wallace, Solvent dependence of electrochromic behaviour of polypyrrole: Rediscovering the effect of molecular oxygen, Synth. Met. 159 (2009) 1950–1955.

[35] X. Liu, Z. Yue, M.J. Higgins, G.G. Wallace, Conducting polymers with immobilised fibrillar collagen for enhanced neural interfacing, Biomaterials. 32 (2011) 7309–7317. https://doi.org/10.1016/j.biomaterials.2011.06.047.

[36] P.J. Molino, M.J. Higgins, P.C. Innis, R.M.I. Kapsa, G.G. Wallace, Fibronectin and bovine serum albumin adsorption and conformational dynamics on inherently conducting polymers: A QCM-D study, Langmuir. 28 (2012) 8433–8445. https://doi.org/10.1021/la300692y.

[37] P.J. Molino, P.C. Innis, M.J. Higgins, R.M.I. Kapsa, G.G. Wallace, Influence of biopolymer loading on the physiochemical and electrochemical properties of inherently conducting polymer biomaterials, Synth. Met. 200 (2015) 40–47. https://doi.org/10.1016/j.synthmet.2014.12.018.

[38] Y. Ishiguro, S. Inagi, T. Fuchigami, Gradient doping of conducting polymer films by means of bipolar electrochemistry, Langmuir. 27 (2011) 7158–7162.

[39] S. Inagi, Y. Ishiguro, M. Atobe, T. Fuchigami, Bipolar patterning of conducting polymers by electrochemical doping and reaction, Angew. Chemie - Int. Ed. 49 (2010) 10136–10139. https://doi.org/10.1002/anie.201005671.

[40] R. Ansari, Polypyrrole Conducting Electroactive Polymers: Synthesis and Stability Studies, E-Journal Chem. 3 (2006) 186–201.

https://doi.org/10.1155/2006/860413.

[41] Y. Hou, L. Zhang, L.Y. Chen, P. Liu, A. Hirata, M.W. Chen, Raman characterization of pseudocapacitive behavior of polypyrrole on nanoporous gold, Phys. Chem. Chem. Phys. 16 (2014) 3523–3528. https://doi.org/10.1039/c3cp54497d.

[42] B. Gupta, B. Goudeau, A. Kuhn, Wireless Electrochemical Actuation of Conducting Polymers, Angew. Chemie - Int. Ed. 56 (2017) 14183–14186. https://doi.org/10.1002/anie.201709038.

[43] B. Gupta, M.C. Afonso, L. Zhang, C. Ayela, P. Garrigue, B. Goudeau, A. Kuhn, Wireless Coupling of Conducting Polymer Actuators with Light Emission, ChemPhysChem. 20 (2019) 941–945. https://doi.org/10.1002/cphc.201900116.

[44] B. Gupta, B. Goudeau, P. Garrigue, A. Kuhn, Bipolar Conducting Polymer Crawlers Based on Triple Symmetry Breaking, Adv. Funct. Mater. (2018). https://doi.org/10.1002/adfm.201705825.

[45] K.J. Gilmore, M. Kita, Y. Han, A. Gelmi, M.J. Higgins, S.E. Moulton, G.M. Clark, R. Kapsa, G.G. Wallace, Skeletal muscle cell proliferation and differentiation on polypyrrole substrates doped with extracellular matrix components, Biomaterials. 30 (2009) 5292–5304. https://doi.org/10.1016/j.biomaterials.2009.06.059.

[46] D. Kim, S.M. Richardson-Burns, J.L. Hendricks, C. Sequera, D.C. Martin, Effect of immobilized nerve growth factor on conductive polymers: electrical properties and cellular response, Adv. Funct. Mater. 17 (2007) 79–86.

[47] S. Manivannan, S. Terakawa, Rapid sprouting of filopodia in nerve terminals of chromaffin cells, PC12 cells, and dorsal root neurons induced by electrical stimulation, J. Neurosci. 14 (1994) 5917–5928.

Chapter 4

Enhanced wireless cell stimulation using poly(2-methoxyaniline-5-sulfonic acid) improved bipolar electroactive conducting polymers

This chapter is partially adapted from the article, "Enhanced wireless cell stimulation using soft and improved bipolar electroactive conducting polymer templates" that was published in Applied Materials Today 27 (2022) 101481 by Chunyan Qin, Zhilian Yue, Xu-Feng Huang, Robert J. Forster, Gordon G. Wallace and Jun Chen, with permission from Elsevier.".

4.1 Introduction

Chapter 2 presented the preliminary work utilising conducting polymers (CPs) with bipolar electrochemical stimulation (BPES) [1,2], which underscores the feasibility of this wireless cell stimulation approach. In these studies, a simple PPy co-doped with dextran sulfate (DS) and collagen (PPy-DS-collagen/FTO) as a bipolar electrode was developed to stimulate rat pheochromocytoma cells. Significantly, this wireless stimulation enhanced neural cell proliferation and differentiation. Despite the progress on CPs based BPES system, rigid, electronically conducting supports such as ITO and FTO are required because the electrochemical activity and conductivity of CPs is not sufficient to create a fully bipolar electrode. Therefore, a significant challenge is to improve the bipolar electroactivity of the modified electrode.

In this context, poly(2-methoxyaniline-5-sulfonic acid) (PMAS), a sulfonated self-doped polyaniline, is attractive due to its unique electrochemical properties and water solubility [3–6]. As a large redox active molecule, PMAS has been extensively studied as a dopant to enhance the electrochemical properties of several materials [7,8]. After chemical or electrochemical polymerisation, the resulting materials typically show significantly lower electrical impedance enabling applications in supercapacitors, batteries, cell culture and tissue engineering [9–12]. Specifically, several studies have reported that incorporating PMAS and appropriate bioactive dopants into PPy creates a PPy-PMAS composite with good conductivity and cyto-compatibility [13,14]. Moreover, it has been shown to support nerve and muscle cell proliferation and differentiation using traditionally wired electrical stimulation [15,16]. Thus, PMAS can be adopted to CPs based BPES to improve the electrochemical activity and enhance wireless cell stimulation.

In this chapter, a PPy-PMAS-DS-collagen/FTO film with enhanced bipolar electrochemical performance under lower driving voltage (~3.0 V in this work, while ~5.5 V in last work) was developed. Its improved bipolar electrochemical activity was confirmed by both *in situ* UV spectroscopy and electrochemistry. Significantly, this material further displays excellent cytocompatibility, and strengthens nerve cell differentiation with BPES treatment compared to the previous set-up. In the future, using different materials preparation methods to get a highly conducting PMAS modified PPy substrates will greatly facilitate a variety of applications of wireless CPs based BPES platform.

4.2 Experiments

4.2.1 Materials

Pyrrole (Py) was purchased from Merck, purified by reduced pressure distillation and stored at -20 ºC. poly (2-methoxy-5 aniline sulfonic acid) (PMAS) was synthesised in-house. Other chemicals for synthesis, such as *p*-toluenesulfonic acid monohydrate (*p*TS), dextran sulfate sodium salt from Leuconostoc spp. (DS), phosphate buffered saline (PBS) and Nunc® Lab-Tek® chambered coverglass (polystyrene) were supplied from Sigma-Aldrich (Sydney, Australia). Stainless steel mesh (SSM-500x500 with wire DIM of 0.025 mm) was from Stainless Steel Wire & Mesh Pty Ltd. (Melbourne, Australia). Gibco Dulbecco's Modified Eagle's Medium (DMEM), horse serum, fetal bovine serum (FBS), collagen (Type I from rat tail), nerve growth factor (NGF), calcein AM, propidium iodide (PI), PicoGreen™, Alexa Fluor 546 (Donkey anti-Mouse IgG Highly Cross-Adsorbed Secondary Antibody), monoclonal anti-β-tubulin III (neuronal) antibody produced in mouse, 4'-6-diamidino-2-phenylindole (DAPI) and rhodamine Red™-X succunimidyl ester were from Invitrogen (Melbourne, Australia). Clear RTV silicone adhesive sealant was purchased from Permatex (USA).

4.2.2 Preparation of PMAS modified PPy films

The preparation of PPy-PMAS/FTO, PPy-PMAS-collagen/FTO and PPy-PMAS-DS-collagen/FTO films were carried out via same synthetic method used in Chapter 3. The electrodeposition was through cyclic voltammetry (CV) from an aqueous solution containing 0.2 M distilled Py with dopants like 2 mg/ml PMAS, 2 mg/ml DS and 2 µg/ml collagen within a potential range of 0 - 0.65 V at a scan rate of 20 mV/s. After polymerisation, all films were thoroughly rinsed with Milli-Q water and allowed to dry under ambient conditions before further characterisation and investigation.

4.2.3 Materials characterisations

To ensure the successful incorporation of PMAS and collagen dopants into PPy matrix, UV spectra were obtained within the range of 300 nm - 1100 nm to check the presence of characteristic peak from PMAS, while fluorescence labelling and microscope (Carl Zeiss, Germany) were utilised to check the collagen distribution. Cyclic voltammetry (CV) and electrochemical impedance spectroscopy (EIS) were employed to investigate the electrochemical activity of the prepared PMAS modified PPy films in PBS (pH = 7.4). CVs were carried out with a potential range of -0.7 V to +0.7 V at a scan rate of 100 mV/s, while EIS were performed over the frequency range of 0.1 Hz to 100 kHz using an AC signal with +50.0 mV vs the reference electrode.

In situ UV spectrometry (Shimadzu UV-vis 3600) along with bipolar electrochemical system as illustrated in Chapter 2 Figure 2.11, was utilised to identify the improved reversible and recoverable bipolar electrochemical activity. Spectra were acquired within the range of 300 nm - 1100 nm under driving voltage of 5.5 V in PBS (pH = 7.4). *In situ* UV were recorded simultaneously with the conventional three-electrodes electrochemical system (Chapter 2 Figure 2.12) within the same range under different applied potentials (from -0.6 V to +0.6 V) in PBS (pH = 7.4) for indirectly support.

Other physical and spectra characterisation techniques were also employed to study the prepared PMAS modified PPy films. A field emission scanning electron microscopy (JEOL JSM-7500FA) were utilised to probe the surface morphology. For chemical stability, *ex situ* UV spectra were obtained within the wavenumber range of 300 nm - 1100 nm, while *ex situ* FTIR spectra were collected using a FT-IR spectrometer (IRpretige-21, Shimadzu) over a range of 600 cm^{-1} - 2000 cm^{-1}.

4.2.4 Bipolar electrochemical activity evaluation

The bipolar electrochemical activity evaluation was mainly used to investigate the PMAS dopant effects on the reversibility of the PPy film redox switching and stability towards repeated cycling. The same testing setting-up and conditions detailed in Chapter 3 were adopted to ensure accurate comparison. Briefly, all bipolar electrochemical activity tests were conducted in standard PBS buffer solution with a pH of 7.4, simulating that of the normal biological environment. The PMAS modified PPy films deposited on FTO were immersed into the PBS buffer and placed in the centre of the in-house designed bipolar cell. The separation of feeder electrodes was adjustable depending on the size of target films being tested.

4.2.5 Standard cell culture and cytocompatibility studies

PC 12 cells continue to be used in this chapter, and standard cultured as descried in Chapter 3.2.5.1. For cyto-compatibility studies, calcein AM (2×10^{-6} M) and PI (2×10^{-6} M) were used to stain the live and dead cells respectively. Please refer to Chapter 3.2.5.2 for details.

4.2.6 Sterilisation preparation of cell substrates and bipolar devices

Same sterilisation procedure was applied to cell substrates and bipolar devices in this chapter. Please review a detailed description in Chapter 3.2.6.2.

4.2.7 Optimised BPES protocol for PC 12 cells

PC 12 cells were seeded on cell substrates at an initial density of 20000 cells/cm^2 for proliferation process and 2000 cells/cm^2 for differentiation process in the bipolar

devices. Cells were treated with or without BPES over one week in growth or differentiation medium refreshed every 2 days. BPES (pulse mode: phase duration of 10 min + interphase interval of 5 min): Cells were stimulated on day 2 for 8 h per day in continuous three days, then standard cultured in the following three days after stimulation finished. Control (Non BPES): cells were standard cultured with no BPES.

4.2.8 BPES performance evaluation

Calcein AM and PI staining (live/dead assay) was used to observe the cell morphology and cell viability on day 7 after BPES treatment. Images were taken using a ZEISS Axiovert microscope. The numbers of adherent cells on day 1, day 3, day 5 and day 7 were quantified using a Quant-iT^{TM} PicoGreen dsDNA Assay Kit in accordance with the manufacturer's instructions. Numbers of triplicate samples were measured with a microplate reader (POLARstar Omega, Germany) at 485-12/520 nm. Tubulin staining was employed to identify specific protein expression of neuronal differentiation. All use the procedures reported in Chapter 3.2.7.

4.2.9 Quantitative analysis

ImageJ software with NeuriteQuant add-in and Neurite length tracer add-in were utilised to quantify the neurite number and measure the neurite growth, using the same procedure as illustrated in Chapter 3.2.7.3. Data are represented as mean ± standard deviation (SD) unless otherwise indicated. Results were analysed using Origin 2019b 34Bit using one-way ANOVA or two-way ANOVA with Tukey simultaneous testing method and Bonferroni`s post hoc test respectively. A *p*-value was determined and a maximum value of 0.05 was used to indicate significance.

4.3 Results and Discussion

4.3.1 Preparation and characterisations of PMAS modified PPy films

PMAS is expected to enhance the polypyrrole (PPy) film's electrochemical property due to its well-defined redox activity [10]. As reported previously, PPy with PMAS and collagen I as dopants was electrodeposited onto FTO slides [2] (Figure 4.1). Collagen type I was used to promoting cell-substrate interactions because of the anchorage-dependent nature of nerve cells [17,18]. After polymerisation, the PMAS modified PPy matrixes were characterised using UV spectra and fluorescent labelling to confirm the presence of dopants. The UV spectra show peaks centered at 350 nm and 470 nm, corresponding to the incorporation of PMAS (Figure 4.2) [7,10,19]. Fluorescent microscopy following labelling of the collagen with Rhodamine red^{TM}-X succinimide ester reveals that the collagen is uniformly distributed across the surface of the PMAS modified PPy layers (Figure 4.3) [1,2,17]. Both techniques confirm successful incorporation of PMAS and collagen into the PPy films. Cyclic voltammetry (CV) and electrochemical impedance spectroscopy (EIS) in PBS buffer reveal a significant increase in conductivity (Figure 4.4a) and lower impedance (Figure 4.4b) for the PPy films with the addition of PMAS compared to the typical *p*TS dopant. These properties make PMAS modified PPy films attractive for BPES experiments presented below.

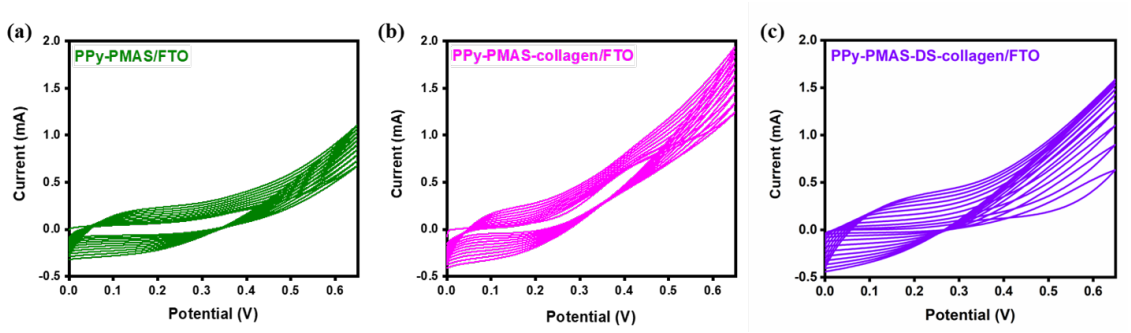

Figure 4.1 Electrodeposition of PMAS modified PPy films. Cyclic voltammograms of

(a) PPy-PMAS, (b) PPy-PMAS-collagen and (c) PPy-PMAS-DS-collagen films grown onto FTO glass obtained during their synthetic process. Aqueous solution contained 0.2 M Py with 2 mg/ml PMAS, 2 µg/ml collagen 2 mg/ml DS, respectively. Potentials were recorded vs. an Ag/AgCl reference electrode under scan range of 0 - 0.65 V at a scan rate of 20 mV/s (10 cycles).

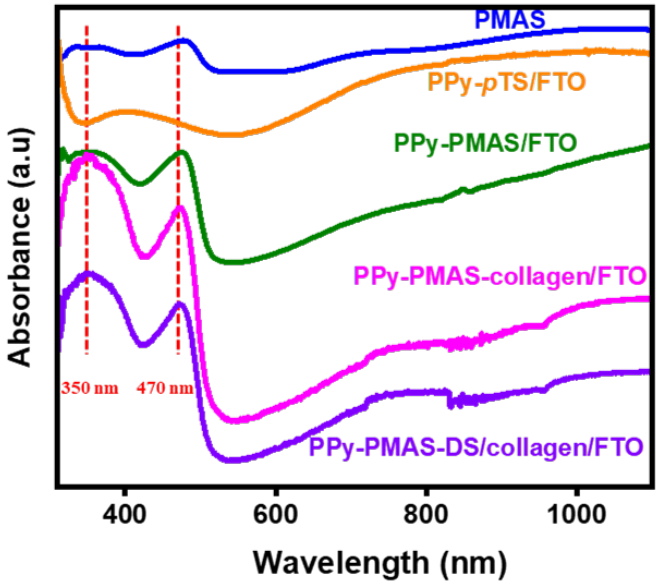

Figure 4.2 UV-vis spectra to identify successful PMAS incorporation within PPy matrixes. Spectra were acquired within the wavelength range of 300 - 1100 nm.

Figure 4.3 Fluorescent labelling to identify successful collagen incorporation within PPy matrixes. Images of the surface morphologies of fluorescently labelled PPy-

PMAS/FTO, PPy-PMAS-collagen/FTO and PPy-PMAS-DS-collagen/FTO were examined in using a ZEISS Axiovert microscope. Samples were treated via the same method used in Chapter 3.

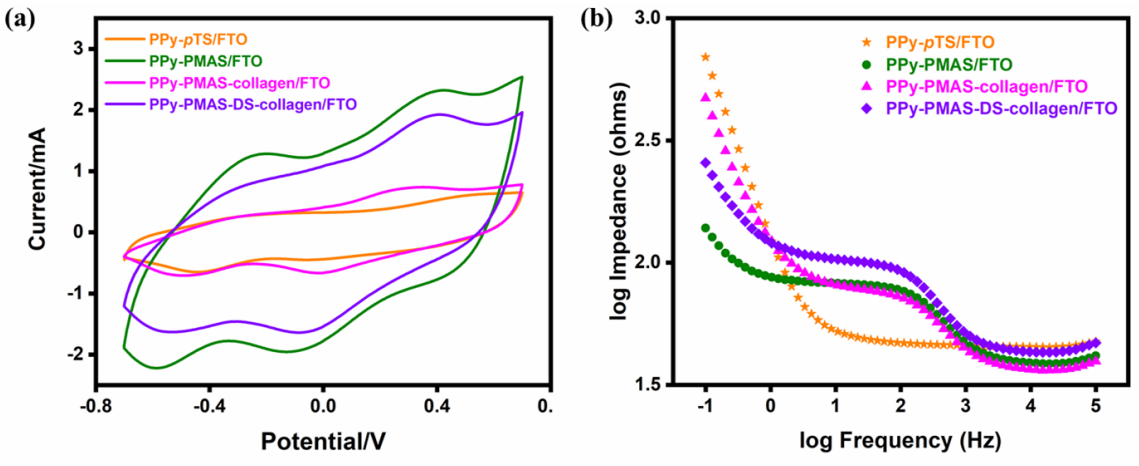

Figure 4.4 Increased electroconductivity of PPy films due to PMAS dopant. (a) Cyclic voltammetry (CV) and (b) Electrochemical impedance spectroscopy (EIS) to identify the electrochemical activity of synthesised PMAS incorporated PPy films in PBS (pH = 7.4). CV of PPy-PMAS-DS-collagen/FTO, PPy-PMAS-collagen/FTO, PPy-PMAS/FTO and PPy-*p*TS/FTO at a scan rate of 100 mV/s. EIS of them over a frequency range of 0.1 Hz-10^5 Hz.

4.3.2 Improvement of bipolar electrochemical activity

To confirm the effects of PMAS incorporation on the bipolar electrochemical activity of PPy, the PMAS modified PPy films was studied using the same bipolar electrochemical system reported in Chapter 2 and 3 [1,2]. As shown in Figure 4.5a, immediately after applying same DC driving voltage of 5.5 V (- / +), a colour change gradient (from dark blue to yellow) is generated across the PPy-PMAS-DS-collagen/FTO film, and reversible colour sequences produced upon changing the polarity of the voltage (+ / -)

applied to the feeder electrodes. This result demonstrates that the potential and hence redox state of the PPy-PMAS-DS-collagen/FTO film can be driven wirelessly. Furthermore, this film exhibits similar bipolar electrochemical redox processes when the driving voltage is decreased to 3.0 V, as do with another two PMAS modified PPy films (PPy-PMAS/FTO and PPy-PMAS-collagen/FTO in Figure 4.6). This ability to switch the redox state using a lower electric field strength (~3.0 V) compared to the PPy-DS-collagen/FTO film (~5.5 V) in Chapter 3 is very significant, suggesting that the bipolar electroactivity of PPy matrix is improved by PMAS doping, most likely through enhanced conductivity which reduces ohmic loss.

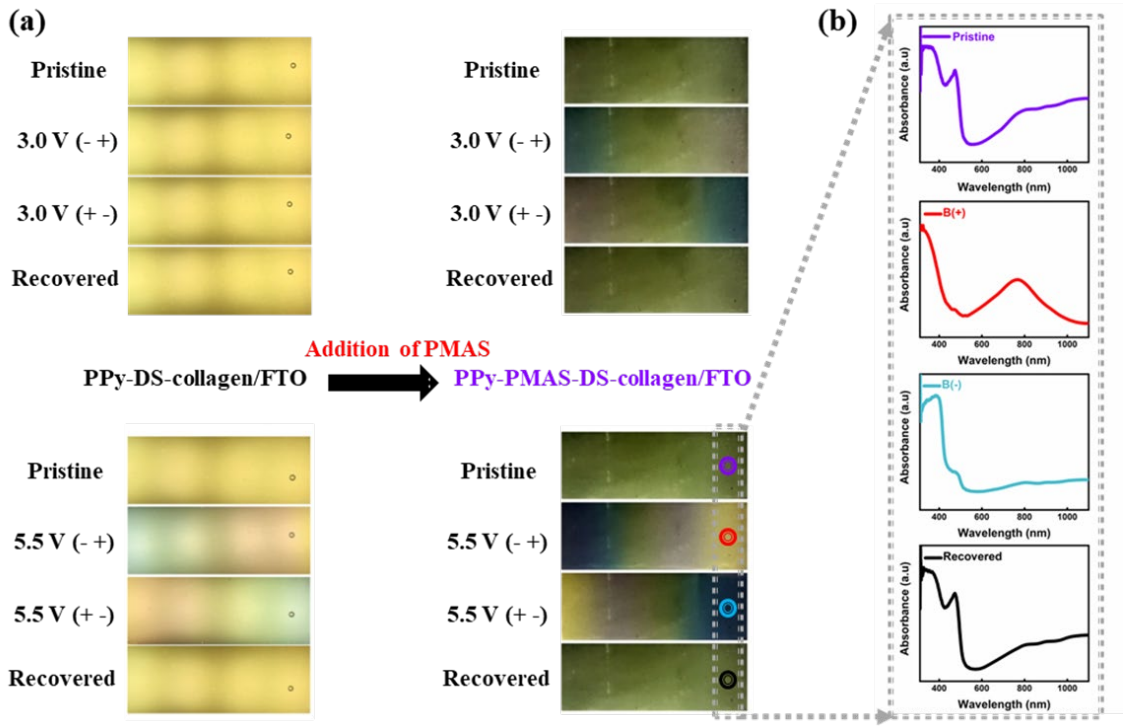

Figure 4.5 (a) Optical images of PPy-DS-collagen matrixes with or without PMAS modification in the previous developed bipolar electrochemical setting up under driving voltage of 5.5 V and 3 V in PBS, revealing its improved bipolar electrochemical activity in PBS due to PMAS incorporation. (b) *In situ* UV spectra under driving voltage of 5.5 V were acquired within the wavelength range of 300 - 1100 nm in PBS. Image at the lower left corner is from the last work reported in Chapter 3, this PPy-DS-collagen/FTO

film exhibited reversible and recoverable bipolar electrochemical redox processes when the driving voltage is 5.5 V.

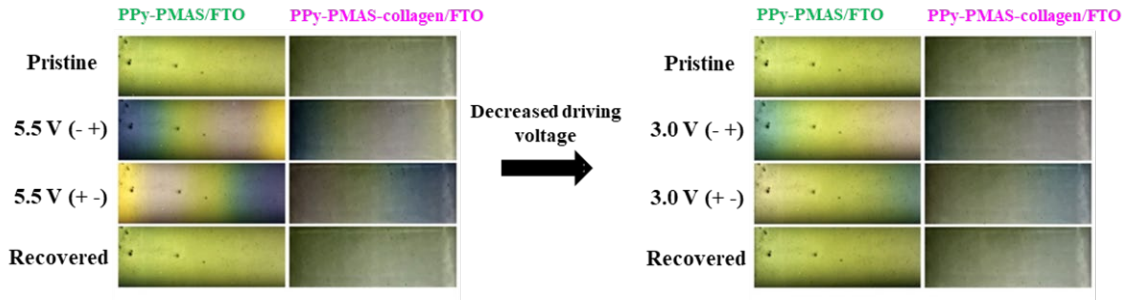

Figure 4.6 Optical images of PPy-PMAS/FTO and PPy-PMAS-collagen/FTO films in the previous developed bipolar electrochemical setting up under driving voltage of 5.5 V (left) and 3.0 V (right).

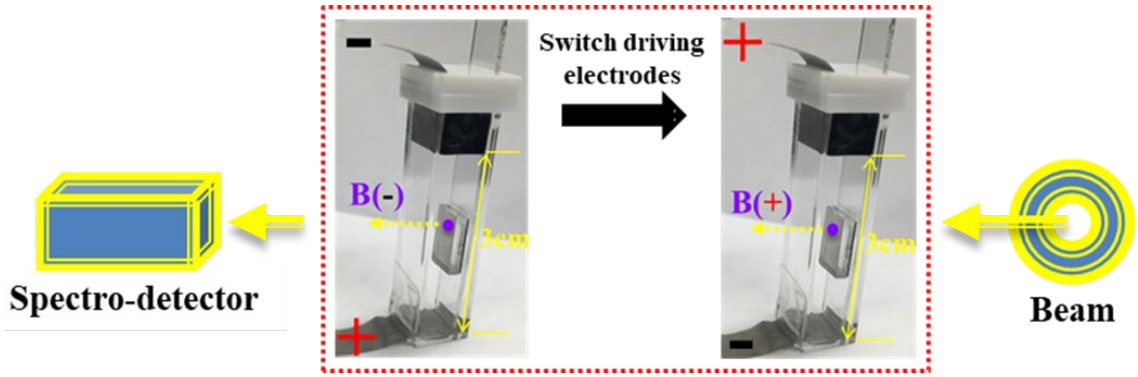

Figure 4.7 *In situ* UV-vis absorption spectra combined with bipolar electrochemical system. Digital image is the home-made bipolar - UV cell.

In situ UV spectrometry (the complete set-up is shown in Figure 4.7) was used to investigate the chemical stability and reversibility of the PPy field induced redox switching. All spectra were consistently recorded at the same spot on the film's surface. As a control, the "pristine" and "recovered" UV spectra were taken from before and after the bipolar stimulation, while B(+) and B(-) present the UV spectra where the

polarity of the feeder electrodes was switched. All the peaks present in the spectra in Figure 4.5b and Figure 4.8 could be assigned to the characteristic UV bands of PMAS modified PPy films at neutralization, reduction, oxidation and back to neutralization state, which has been identified by *in situ* UV in typical electrochemical redox process within PPy [4] (Figure 4.9). The consistency of the UV spectra before and after the bipolar stimulation cycles demonstrates that the contactless electric field induced changes are reversible, and that the gradient redox phenomenon occurred synchronously. The recoverable bipolar electrochemical property was further confirmed by SEM, *ex situ* UV spectrometry and FTIR spectrometry to explore the PMAS modified PPy films before ("pristine") and after ("recovered") undergoing the identical bipolar testing. The topography measurements via SEM (Figure 4.10) showed no visible changes in surface morphologies displaying characteristically similar sized nodular features. The "pristine" and "recovered" spectra (UV and FTIR in Figure 4.11a-4.11b) are indistinguishable indicating that the PMAS modified PPy films are stable with cycling.

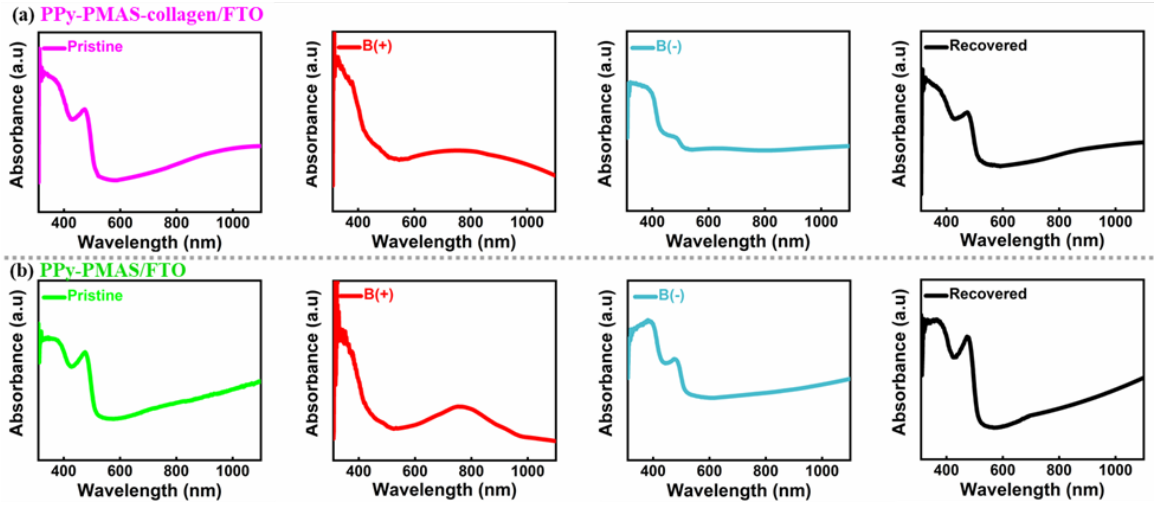

Figure 4.8 *In situ* UV spectra of (a) PPy-PMAS-collagen/FTO and (b) PPy-PMAS/FTO under a driving voltage of 5.5 V were acquired within the wavelength range of 300 - 1100 nm in PBS using a home-made bipolar - UV cell (set-up shown in Figure 4.7).

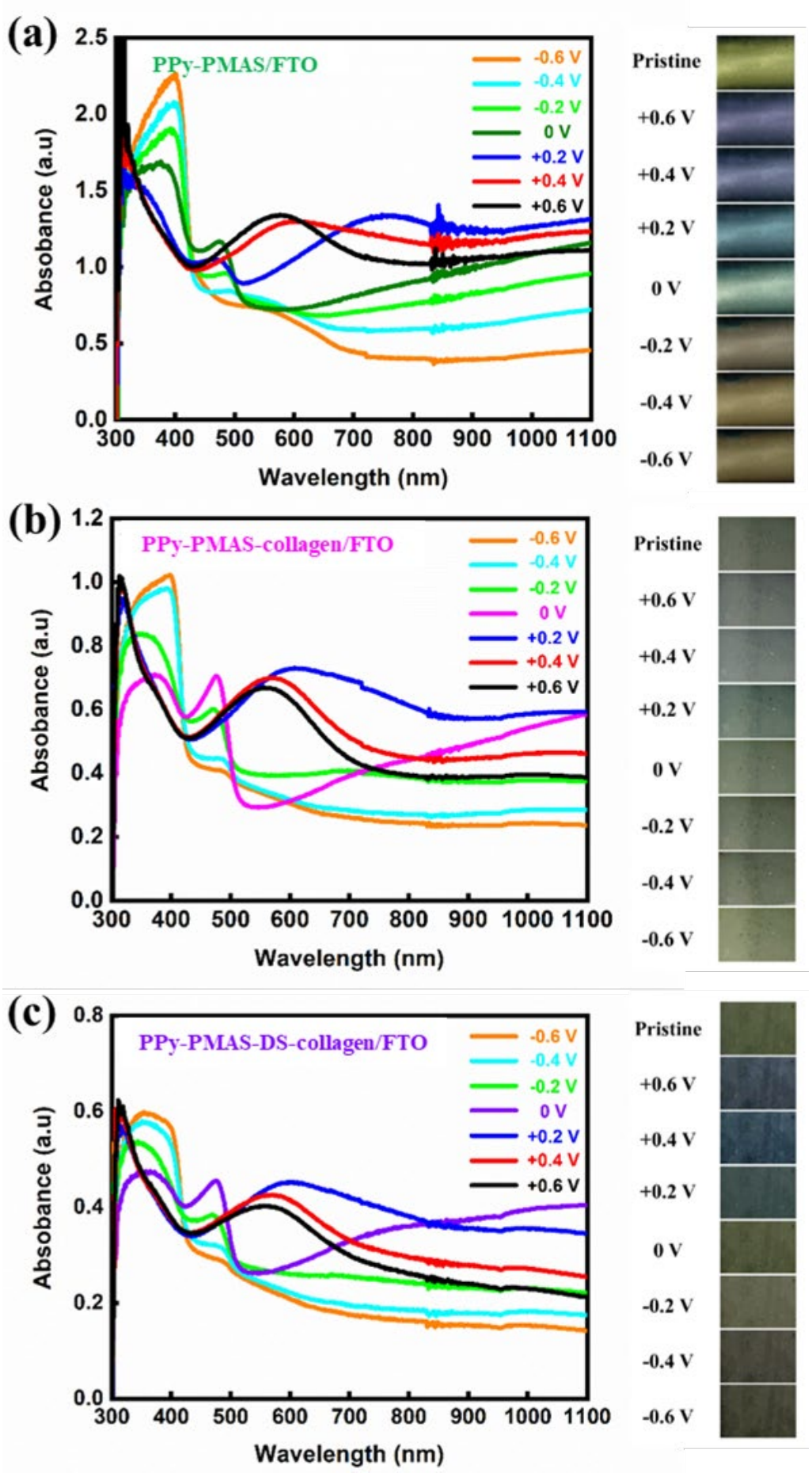
(a)
PPy-PMAS/FTO
-0.6 V
-0.4 V
-0.2 V
0 V
+0.2 V
+0.4 V
+0.6 V
Absobance (a.u)
Wavelength (nm)
Pristine
+0.6 V
+0.4 V
+0.2 V
0 V
-0.2 V
-0.4 V
-0.6 V
(b)
PPy-PMAS-collagen/FTO
-0.6 V
-0.4 V
-0.2 V
0 V
+0.2 V
+0.4 V
+0.6 V
Absobance (a.u)
Wavelength (nm)
Pristine
+0.6 V
+0.4 V
+0.2 V
0 V
-0.2 V
-0.4 V
-0.6 V
(c)
PPy-PMAS-DS-collagen/FTO
-0.6 V
-0.4 V
-0.2 V
0 V
+0.2 V
+0.4 V
+0.6 V
Absobance (a.u)
Wavelength (nm)
Pristine
+0.6 V
+0.4 V
+0.2 V
0 V
-0.2 V
-0.4 V
-0.6 V

Figure 4.9 *In situ* UV-vis absorption spectra combined with the conventional three-electrode electrochemical system. *In situ* UV-visible absorption spectra in the range of 300 - 1100 nm and according colours of (a) PPy-PMAS/FTO, (b) PPy-PMAS-collagen/FTO and (c) PPy-PMAS-DS-collagen/FTO obtained after applied consecutive potentials from -0.6 V to +0.6 V. All potentials are vs. an Ag wire reference electrode and keep 30 s poise time in PBS (pH = 7.4).

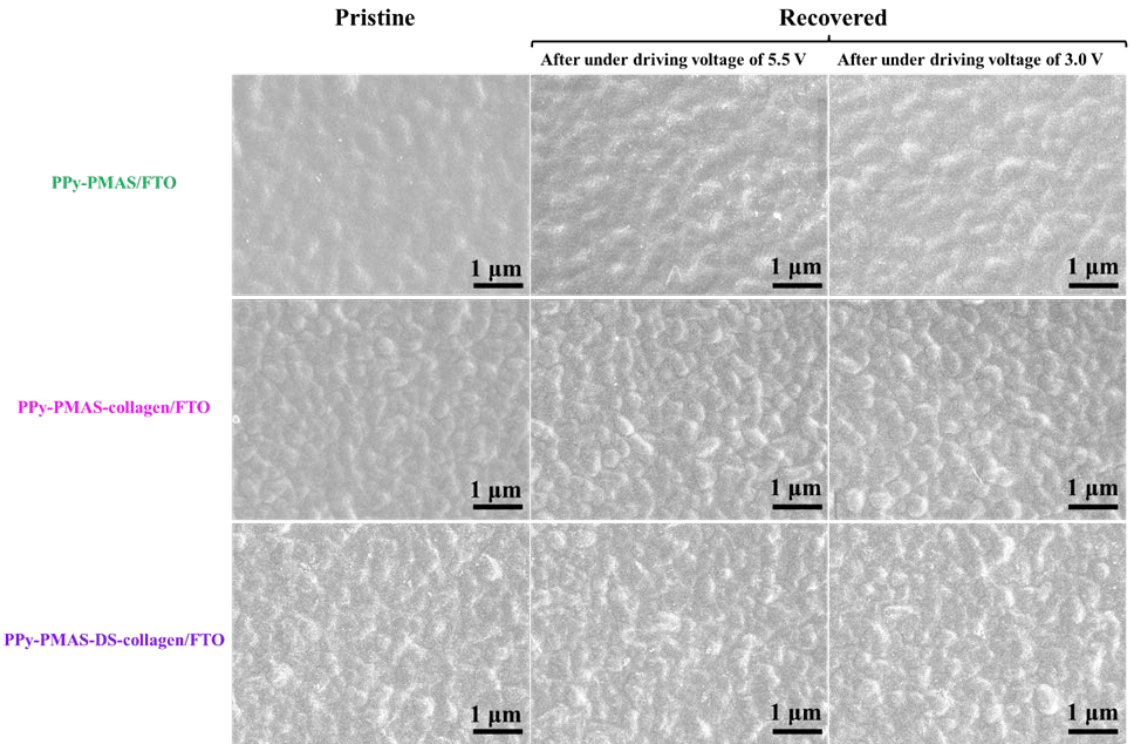

Figure 4.10 Scanning electron microscopy (SEM) images of synthesised PPy-PMAS/FTO, PPy-PMAS-collagen/FTO and PPy-PMAS-DS-collagen/FTO before (pristine) and after (recovered) bipolar testing. All samples were tested in PBS under 5.5 V or 3.0 V driving voltage, and then taken out from electrolyte solution, subsequently rinsed with Milli-Q water and allowed to dry before performing SEM characterisations.

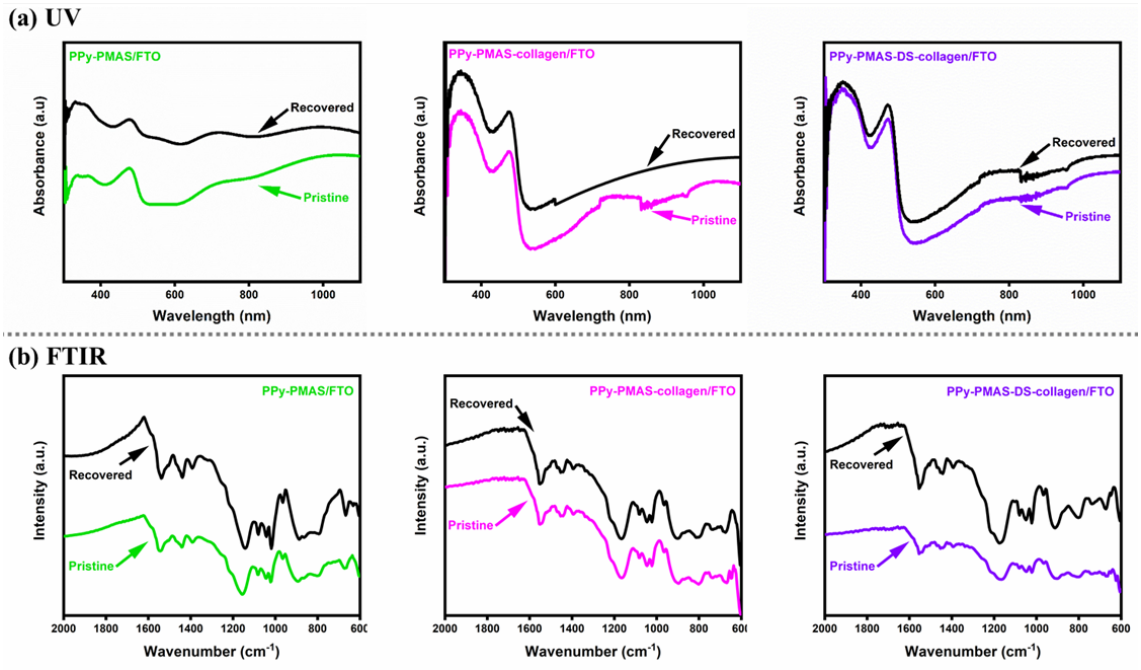

Figure 4.11 Characterisations of synthesised PPy-PMAS/FTO, PPy-PMAS-collagen/FTO and PPy-PMAS-DS-collagen/FTO before (pristine) and after (recovered) bipolar testing. (a) UV and (b) FTIR spectrometry were performed under identical bipolar testing. All samples were tested in PBS under 5.5 V driving voltage, and then taken out from electrolyte solution, subsequently rinsed with Milli-Q water and allowed to dry before all *ex situ* spectra characterisations.

4.3.3 Bipolar electrochemical stimulation (BPES)

As reported in Chapter 2 (Figure 2.13) and Chapter 3 (Figure 3.8), a specific bipolar device was designed with a similar construction to mimic conventional electrochemical cell stimulation. The bipolar electrochemical stimulation (BPES) of PC 12 cells was briefly illustrated in Figure 4.12. All wells of the bipolar device were filled with cell culture media. The tailored bipolar electrochemically active substrates (1 cm × 1 cm) were immersed in the middle cell culture wells, followed with sterilisation process. Then the same density of PC 12 cells were only seeded in four middle replicate cell

culture wells where the bipolar substrates were placed. Once the bipolar device was connected with programmable DC power supply, PC 12 cells were activated to respond to the bipolar electrochemical stimulation. PC 12 cells are likely to differentiate and ready for further immunostaining evaluation.

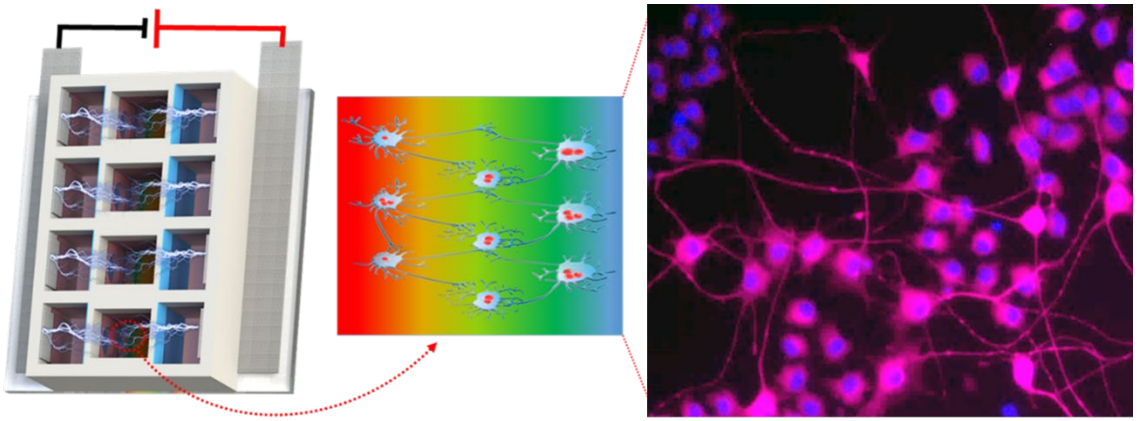

Figure 4.12 Schematic illustration of PC 12 cells differentiation under wireless bipolar electrochemical stimulation (BPES).

4.3.4 Good cytocompatibility and enhanced cell proliferation under BPES

The cytocompatibility of the PMAS modified PPy films was investigated prior to BPES and cell viability after BPES was monitored by live/dead staining. The optimal BPES protocol (BPES pulse mode-c) established in Chapter 3 [1] was used for PC 12 cells stimulation. PPy-PMAS/FTO, PPy-PMAS-collagen/FTO and PPy-PMAS-DS-collagen/FTO showed no cytotoxicity to PC 12 cells (Figure 4.13). A high cell viability was observed for the cells cultured on PPy-PMAS-DS-collagen/FTO even after BPES treatment over one week. The results indicate that the PMAS modified PPy films and the BPES treatment process are both cytocompatible with PC 12 cells culture. Figure 4.13 also suggests PPy-PMAS-DS-collagen/FTO is a better substrate than PPy-

PMAS/FTO and PPy-PMAS-collagen/FTO in promoting cell attachment and proliferation irrespective of with or without BPES.

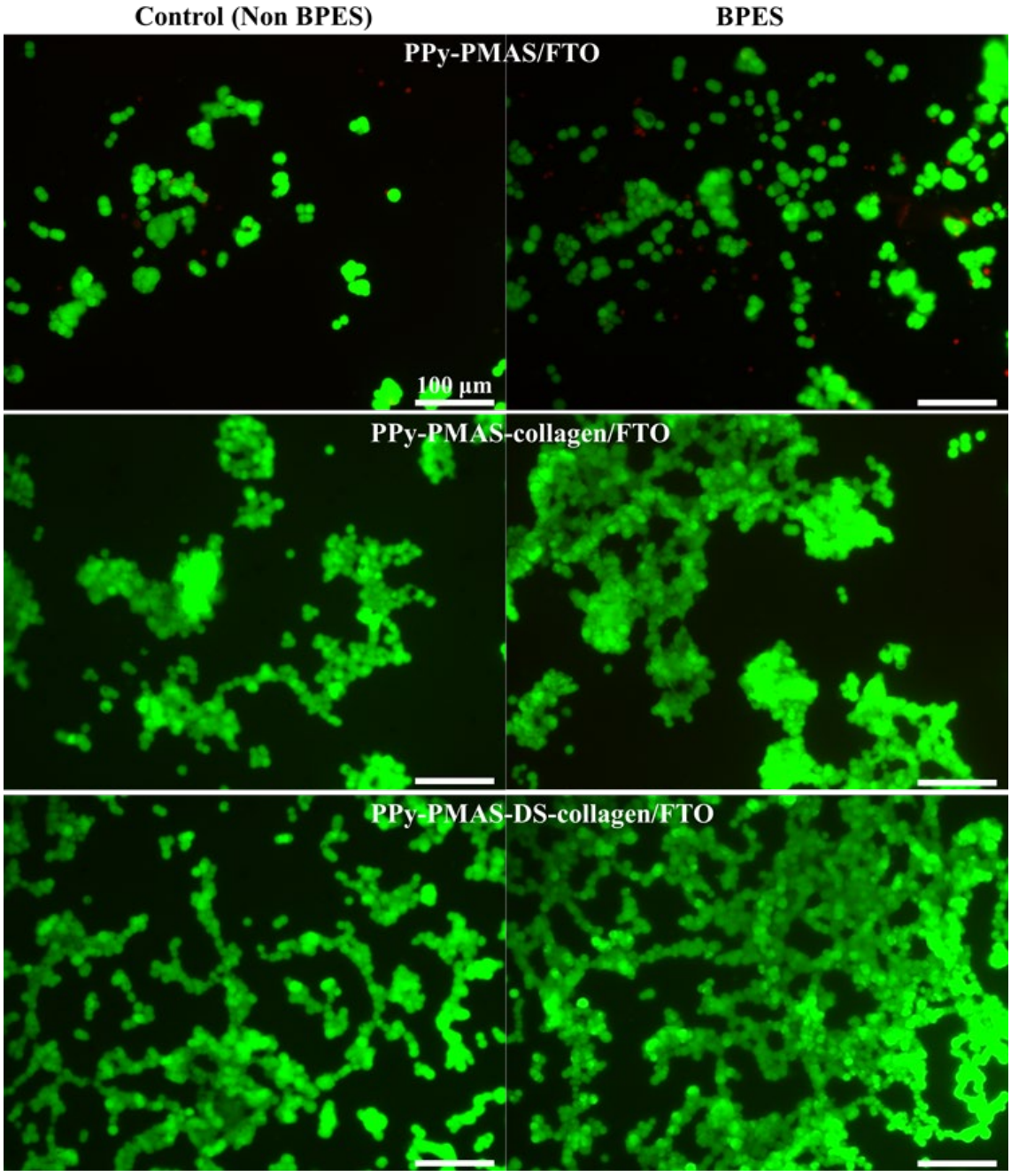

Figure 4.13 Images of PC 12 cells on day 7 via calcein AM and PI staining. Calcein-AM (green) present live cells and PI (red) were on behalf of dead cells. PC 12 cells were cultured on PMAS modified PPy films at an initial seeding density of 20000 cells/cm^2 in growth media over total one week. BPES: Cells were stimulated on day 2

for 8 h per day in continuous three days, then standard cultured in the following three days after stimulation finished. Control (Non BPES): cells were standard cultured with no BPES.

A PicoGreen assay was used to estimate cell numbers on each of the PMAS modified PPy films at different time points (Figure 4.14). When the PC 12 cells cultured on PPy-PMAS/FTO, the cell numbers show a decrease at day 1 with or without BPES treatment while a statistical increase at day 7. For cells cultured on another two substrates, i.e. PPy-PMAS-collagen/FTO and PPy-PMAS-DS-collagen/FTO, the cells display higher viabilities and increased numbers at day 1. Moreover, statistical significance on PC 12 cell numbers was demonstrated at both day 3 and day 7 when cells cultured on PPy-PMAS-collagen/FTO substrate with BPES treatment. Whilst when cells cultured PPy-PMAS-DS-collagen/FTO with BPES treatment, the significance on PC 12 cell numbers were statistically shown at day 3, day 5 and day 7 ($P < 0.0001$). It is well known that the identity of the dopant significantly influences the physicochemical and electrochemical properties of the polymer [20]. Here, the collagen type I, a major component of extracellular matrix, is able to interact with biological DS dopant and enhance the PC 12 cells adhesion. Additionally, these films together with BPES treatment further facilitate cells to proliferate [21–23]. Therefore, these results confirm that the PMAS modified PPy films are cytocompatible with PC 12 cells and support their proliferation. This makes them for further investigation on the effects of BPES on nerve cell differentiation.

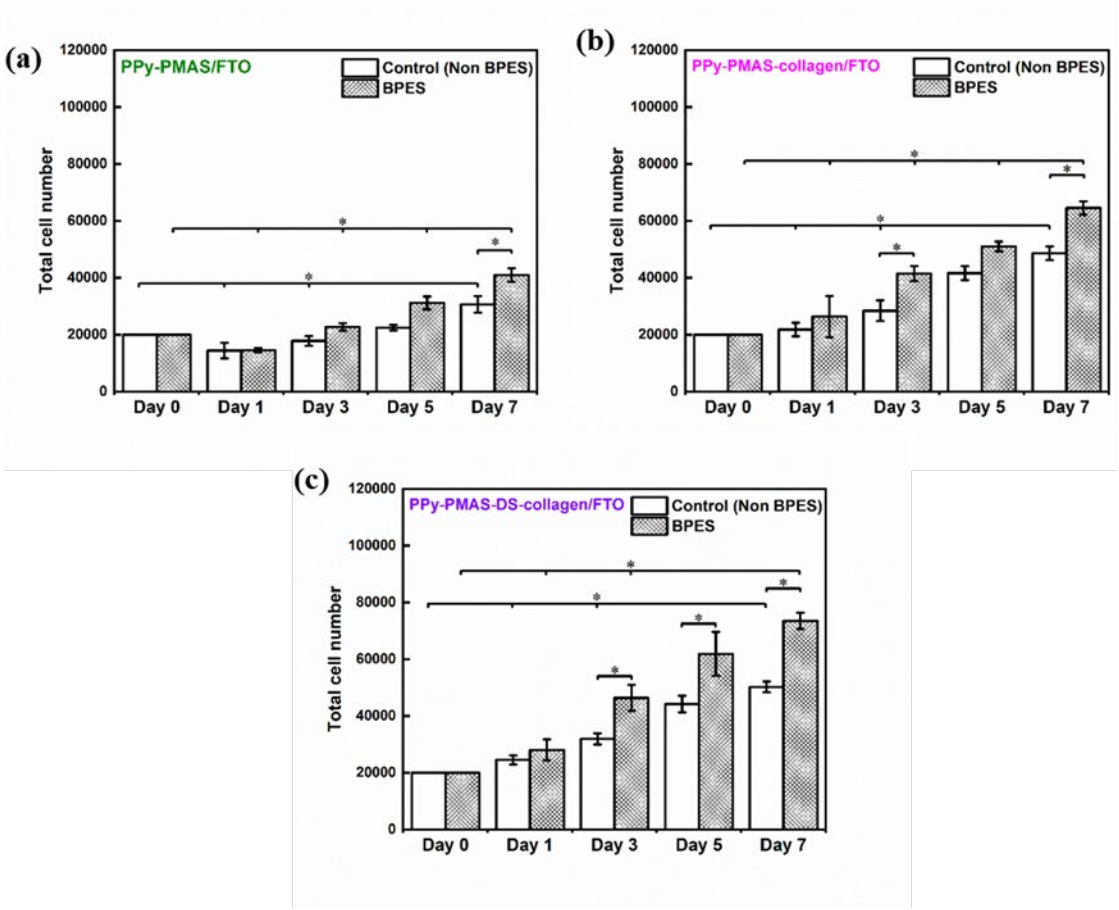

Figure 4.14 Numbers of PC 12 cells calculated via PicoGreen assay at various time points with statistical analysis using two-way ANOVA. PC 12 cells were cultured on PMAS modified PPy films at an initial seeding density of 20000 cells/cm^2 in growth media over a total of one week. BPES: Cells were stimulated on day 2 for 8 h per day over three days, then standard cultured in the following three days after stimulation finished. Control (Non BPES): cells were standard cultured with no BPES. Data are represented as mean ± standard deviation (SD) and "*" ($P < 0.0001$) was used to indicate significance.

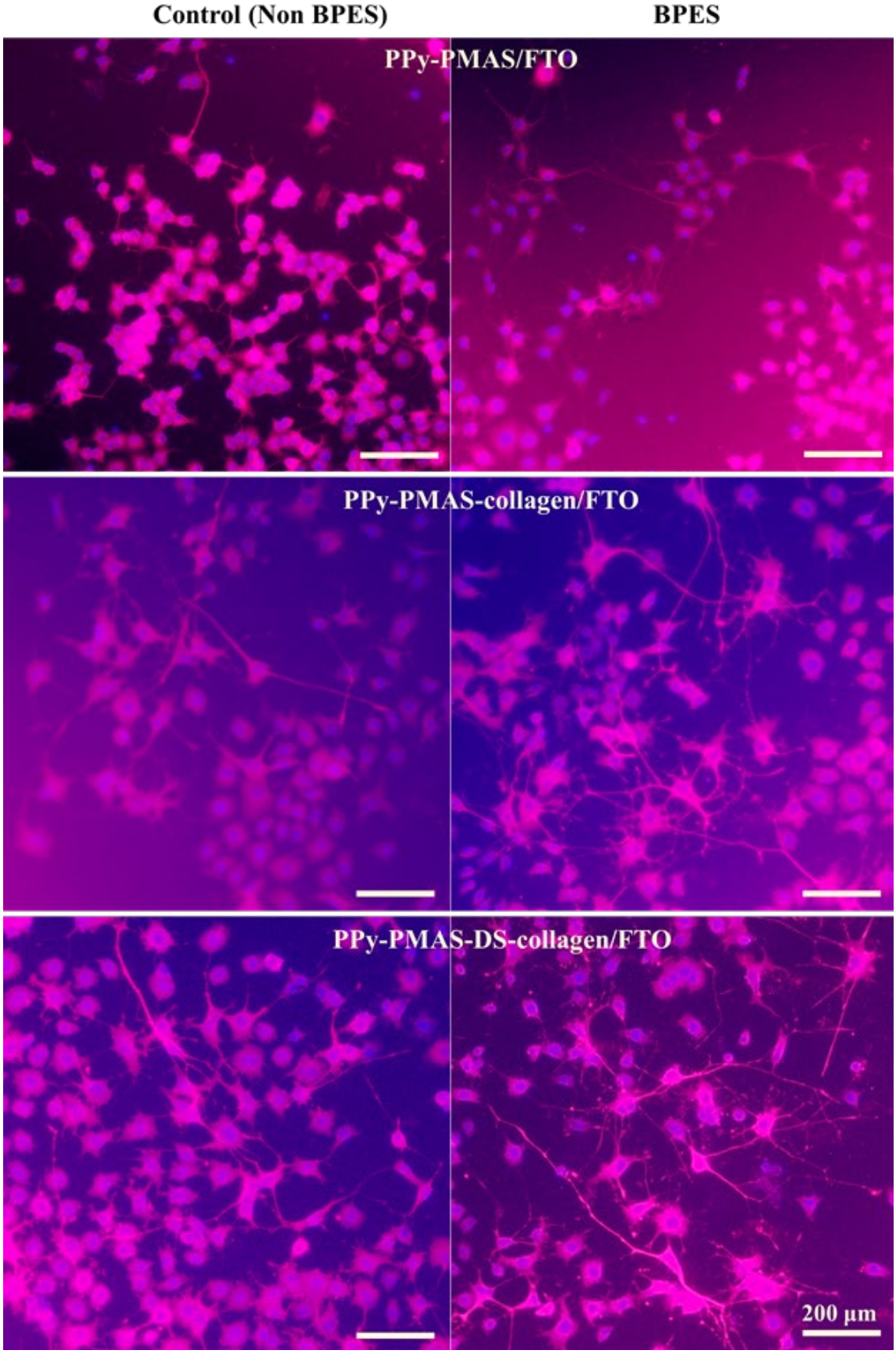
Control (Non BPES)
BPES
PPy-PMAS/FTO
PPy-PMAS-collagen/FTO
PPy-PMAS-DS-collagen/FTO
200 µm

Figure 4.15 Immunofluorescent images of PC 12 cells on day 7 with or without BPES treatment. Cells were cultured on PMAS modified PPy films in differentiation media over one week. BPES: cells were stimulated on day 2 for 8 h per day in continuous three days, then standard cultured in the following three days after stimulation finished. Control (Non BPES): cells were standard cultured with no BPES. Markers of PC 12 cells differentiation: β-tubulin III (red) labels microtubule-associated protein 2, revealing the neuronal soma and proximal portion of neurites. DAPI (blue) labels nucleus.

4.3.5 Enhanced cell differentiation under BPES

To explore the impact of the film composition on the ability of BPES to influence cell differentiation, PC 12 cells were seeded on these three PMAS modified PPy films and exposed to NGF (50 ng/ml) in a low serum medium. Then, the BPES pulse mode programme described above was applied. Compared with control cell groups, the stimulated cell groups on each substrate show more neurites and extensive neurites outgrowth (Figure 4.15). Moreover, under BPES treatment, the PC 12 cells differentiated better when they cultivated on PPy-PMAS-collagen/FTO and PPy-PMAS-DS-collagen/FTO. The subsequent statistical analysis illustrated same phenomenon of cell differentiation in Figure 4.16. Significantly, the cell groups on PPy-PMAS-DS-collagen/FTO showed enhanced neurite outgrowth in terms of both numbers and lengths. And both the neurites number and maximum neurite lengths show statistical enhancement with BPES treatment. All these results indicate that the co-doped biodopants like DS and collagen improved the cell differentiation in combination of BPES treatment.

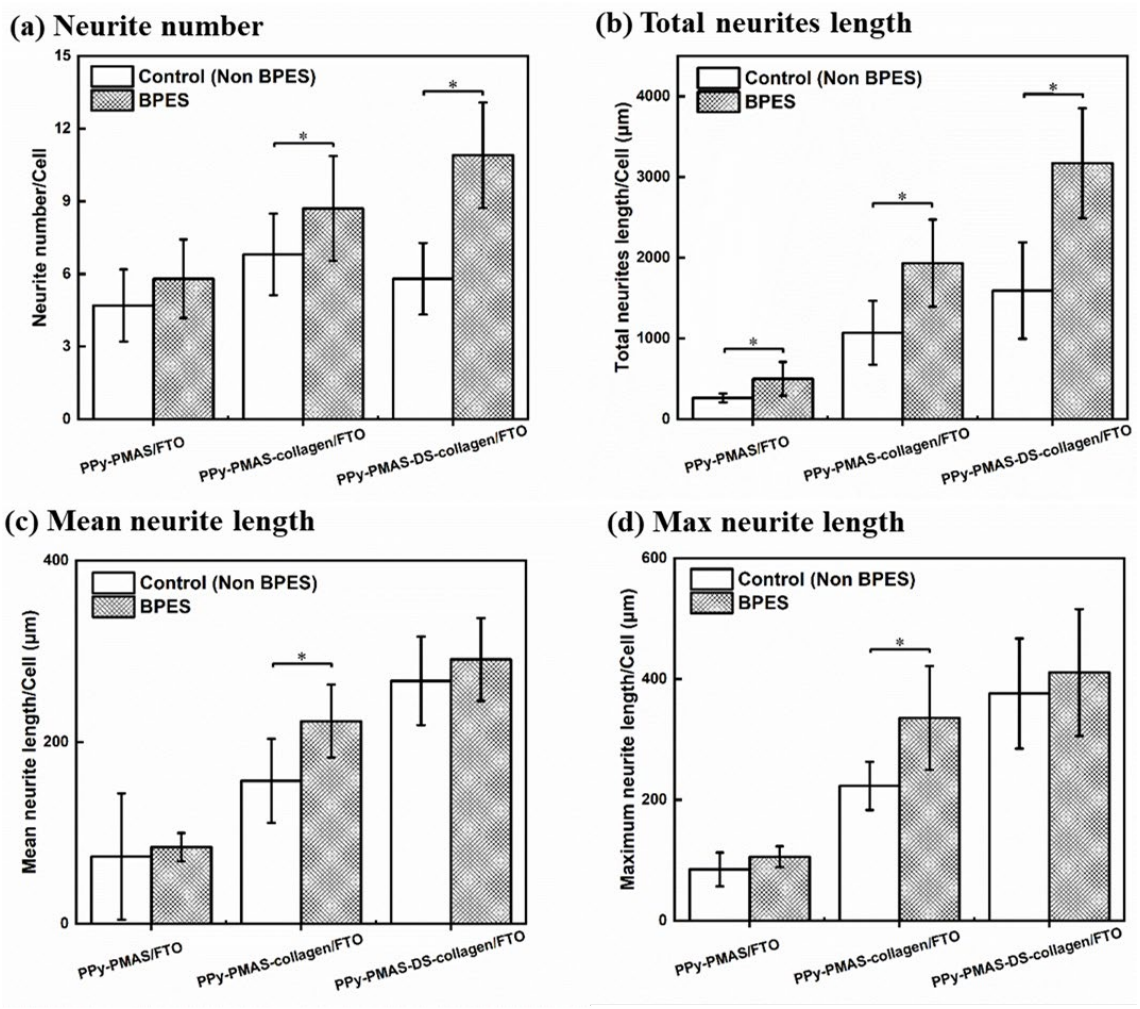

Figure 4.16 Assessments of neurite number and neurite growth of cells cultured on PMAS modified PPy films, including (a) the total neurite number per cell, (b) the total length of neurites per cell, (c) mean neurite length per cell, and (d) maximum neurite length per cell. PC 12 cells were cultured on PMAS modified PPy films at an initial seeding density of 2000 cells/cm^2 in differentiation media over one week. BPES: Cells were stimulated on day 2 for 8 h per day in continuous three days, then standard cultured in the following three days after stimulation finished. Control (Non BPES): cells were standard cultured with no BPES. Statistical analysis used one-way ANOVA. Data are represented as mean ± standard deviation (SD) and "*" ($P < 0.05$) was used to indicate significance.

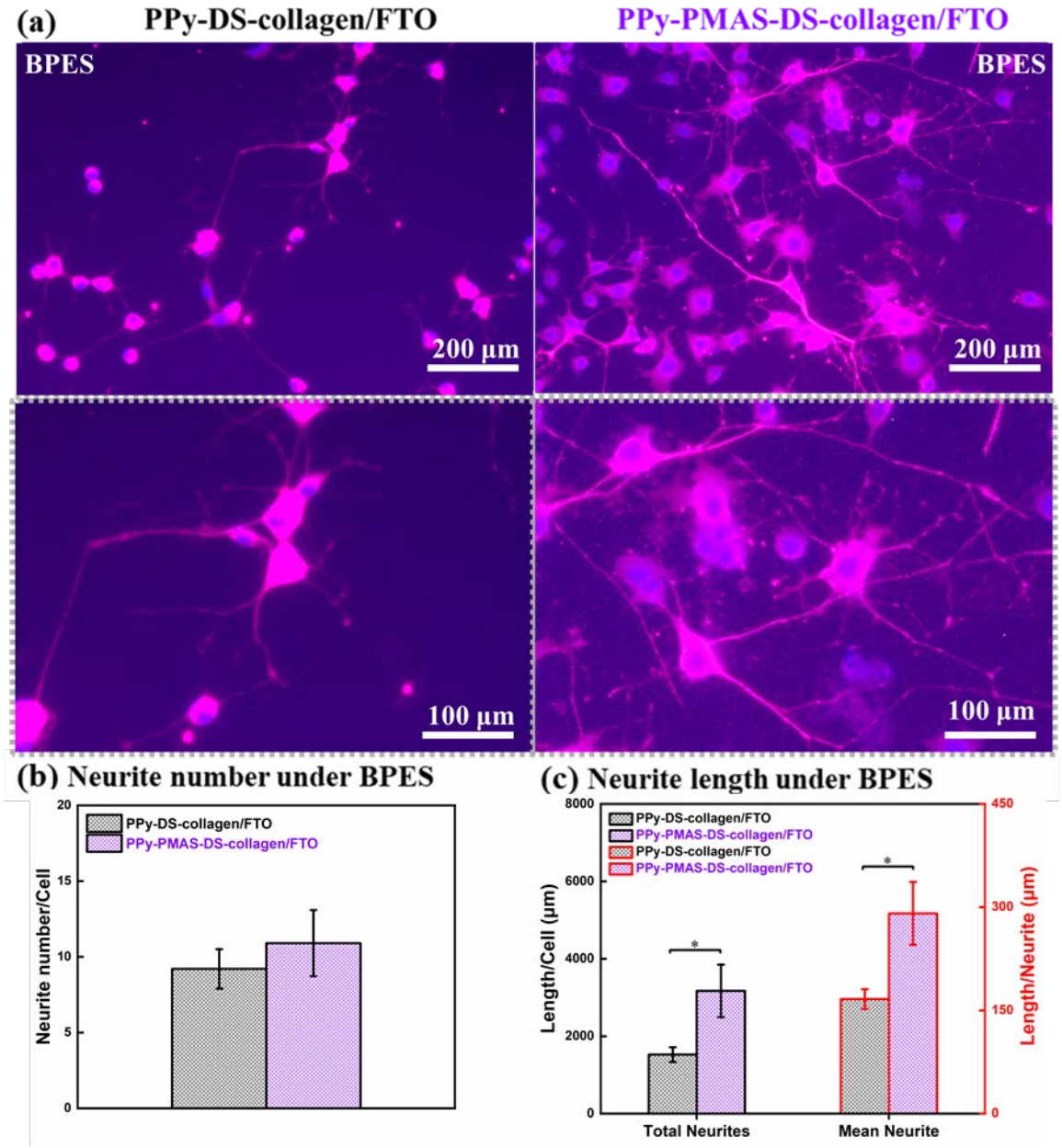

Figure 4.17 (a) Immunofluorescent images of PC 12 cells on day 7 after BPES treatment. (b-c) Assessments of neurite number and neurite growth of cells cultured on PPy-DS-collagen matrixes with or without PMAS modification, including (b) the total neurite number per cell, (c) the total length of neurites per cell, mean neurite length. BPES: cells were stimulated on day 2 for 8 h per day in continuous three days, then standard cultured in the following three days after stimulation finished. β-tubulin III (red) labels microtubule-associated protein 2 and DAPI (blue) labels nucleus. Statistical analysis used one-way ANOVA. Data are represented as mean ± standard deviation

(SD) and "*" ($P < 0.05$) was used to indicate significance. Data about PPy-DS-collagen/FTO is from the last work in Chapter 3.

To assess the effects of BPES on PC 12 cells differentiation, cells were cultured on PPy-DS-collagen matrixes with or without PMAS modification and treated in the same procedure. In the presence of BPES, the PC 12 cells differentiated to typical neural morphologies with extending neurites on both PPy films as immunofluorescent images show in Figure 4.17a. However, more extensive neurite outgrowth and neural network formation was observed on PPy-PMAS-DS-collagen/FTO. This was confirmed by statistical analysis using one-way ANOVA (Figure 4.17b-4.17c). The sum of neurites on PPy-PMAS-DS-collagen/FTO outnumbered those on PPy-DS-collagen/FTO (Figure 4.17b). Moreover, an increase of ~200% in both the total neurites length and the mean neurite length is observed on PPy-PMAS-DS-collagen/FTO (Figure 4.17c). All these findings demonstrate a significant enhancement in nerve cell differentiation is achieved, which is attributed the improved bipolar electroactivity of PPy film when PMAS is used as a dopant. Therefore, it highlights the potential benefits of proposed redox active PMAS doped PPy film to promote cell behaviour.

4.4 Conclusions

Using the redox active polyelectrolyte PMAS as a dopant within PPy matrixes, the bipolar electrochemical properties of CPs have been successfully improved. The resulting PMAS modified PPy films are highly cytocompatible enabling *in vitro* applications of wireless BPES for PC 12 cells. Significantly, efficient and rapid nerve cell differentiation is observed. After addressing the challenge of poor electroactivity of CPs, soft templates with great bipolar electroactivity and cytocompatibility are proposed

to create in the future work. Seeking for soft templates to reduce or remove rigid substrates dependence is highly required to boost BPES development. This will make the CPs based BPES system more suitable for translation from animal cells to human cells.

4.5 References

[1] C. Qin, Z. Yue, Y. Chao, R.J. Forster, F. Maolmhuaidh, X.F. Huang, S. Beirne, G.G. Wallace, J. Chen, Bipolar electroactive conducting polymers for wireless cell stimulation, Appl. Mater. Today. 21 (2020). https://doi.org/10.1016/j.apmt.2020.100804.

[2] C. Qin, Z. Yue, Y. Chao, R.J. Forster, F. Maolmhuaidh, X.F. Huang, S. Beirne, G.G. Wallace, J. Chen, Data on the bipolar electroactive conducting polymers for wireless cell stimulation, Data Br. 33 (2020) 106406. https://doi.org/10.1016/j.apmt.2020.100804.

[3] S. Little, S.F. Ralph, C.O. Too, G.G. Wallace, Solvent dependence of electrochromic behaviour of polypyrrole: Rediscovering the effect of molecular oxygen, Synth. Met. 159 (2009) 1950–1955.

[4] L. Dennany, E.J. O'Reilly, P.C. Innis, G.G. Wallace, R.J. Forster, The influence of poly(2-methoxyaniline-5-sulfonic acid) on the electrochemical and photochemical properties of a highly luminescent ruthenium complex, Electrochim. Acta. 53 (2008) 4599–4605. https://doi.org/10.1016/j.electacta.2007.11.025.

[5] F. Masdarolomoor, P.C. Innis, S. Ashraf, G.G. Wallace, Purification and characterisation of poly(2-methoxyaniline-5-sulfonicacid acid), Synth. Met. 153 (2005) 181–184. https://doi.org/10.1016/j.synthmet.2005.07.249.

[6] D. Zhou, P.C. Innis, G.G. Wallace, S. Shimizu, S.I. Maeda, Electrosynthesis and characterization of poly(2-methoxyaniline-5-sulfonic acid)-effect of pH control, Synth. Met. 114 (2000) 287–293. https://doi.org/10.1016/s0379-6779(00)00249-6.

[7] A. Gelmi, M.J. Higgins, G.G. Wallace, Physical surface and electromechanical properties of doped polypyrrole biomaterials, Biomaterials. 31 (2010) 1974–1983. https://doi.org/10.1016/j.biomaterials.2009.11.040.

[8] W.W. Chan, D.C.L. Yeo, V. Tan, S. Singh, D. Choudhury, M.W. Naing, Additive biomanufacturing with collagen inks, Bioengineering. 7 (2020) 1–23. https://doi.org/10.3390/bioengineering7030066.

[9] G.J. Wilson, M.G. Looney, A.G. Pandolfo, Enhanced capacitance textile fibres for supercapacitors via an interfacial molecular templating process, Synth. Met. 160 (2010) 655–663. https://doi.org/10.1016/j.synthmet.2009.12.022.

[10] Y. Yang, C. Wang, S. Ashraf, G.G. Wallace, Polypyrrole doped with redox-active poly(2-methoxyaniline-5-sulfonic acid) for lithium secondary batteries, RSC Adv. 3 (2013) 5447–5452. https://doi.org/10.1039/c3ra40406d.

[11] E.M. Stewart, X. Liu, G.M. Clark, R.M.I. Kapsa, G.G. Wallace, Inhibition of smooth muscle cell adhesion and proliferation on heparin-doped polypyrrole, Acta Biomater. 8 (2012) 194–200. https://doi.org/10.1016/j.actbio.2011.07.029.

[12] S.S. Nair, S.K. Mishra, D. Kumar, Recent progress in conductive polymeric materials for biomedical applications, Polym. Adv. Technol. 30 (2019) 2932–2953. https://doi.org/10.1002/pat.4725.

[13] B.C. Thompson, S.E. Moulton, R.T. Richardson, G.G. Wallace, Effect of the dopant anion in polypyrrole on nerve growth and release of a neurotrophic protein, Biomaterials. 32 (2011) 3822–3831.

https://doi.org/10.1016/j.biomaterials.2011.01.053.

[14] K.J. Gilmore, M. Kita, Y. Han, A. Gelmi, M.J. Higgins, S.E. Moulton, G.M. Clark, R. Kapsa, G.G. Wallace, Skeletal muscle cell proliferation and differentiation on polypyrrole substrates doped with extracellular matrix components, Biomaterials. 30 (2009) 5292–5304. https://doi.org/10.1016/j.biomaterials.2009.06.059.

[15] X. Liu, K.J. Gilmore, S.E. Moulton, G.G. Wallace, Electrical stimulation promotes nerve cell differentiation on polypyrrole/poly (2-methoxy-5 aniline sulfonic acid) composites, J. Neural Eng. 6 (2009). https://doi.org/10.1088/1741-2560/6/6/065002.

[16] Z. Aqrawe, J. Montgomery, J. Travas-sejdic, D. Svirskis, Chemical Conducting polymers for neuronal microelectrode array recording and stimulation, Sensors Actuators B. Chem. 257 (2018) 753–765. https://doi.org/10.1016/j.snb.2017.11.023.

[17] Z. Yue, X. Liu, P.J. Molino, G.G. Wallace, Bio-functionalisation of polydimethylsiloxane with hyaluronic acid and hyaluronic acid - Collagen conjugate for neural interfacing, Biomaterials. 32 (2011) 4714–4724. https://doi.org/10.1016/j.biomaterials.2011.03.032.

[18] X. Liu, Z. Yue, M.J. Higgins, G.G. Wallace, Conducting polymers with immobilised fibrillar collagen for enhanced neural interfacing, Biomaterials. 32 (2011) 7309–7317. https://doi.org/10.1016/j.biomaterials.2011.06.047.

[19] H. Zhao, G.G. Wallace, Polypyrrole / poly (2-methoxyaniline-5-sulfonic acid) polymer composite, Polym. Gels Networks. 6 (1998) 233–245.

[20] P.J. Molino, Z. Yue, B. Zhang, A. Tibbens, X. Liu, R.M.I. Kapsa, M.J. Higgins, G.G. Wallace, Influence of Biodopants on PEDOT Biomaterial Polymers: Using

QCM-D to Characterize Polymer Interactions with Proteins and Living Cells, Adv. Mater. Interfaces. (2014). https://doi.org/10.1002/admi.201300122.

[21] Z. Yue, X. Liu, P.J. Molino, G.G. Wallace, Bio-functionalisation of polydimethylsiloxane with hyaluronic acid and hyaluronic acid–collagen conjugate for neural interfacing, Biomaterials. 32 (2011) 4714–4724.

[22] P.J. Molino, M.J. Higgins, P.C. Innis, R.M.I. Kapsa, G.G. Wallace, Fibronectin and bovine serum albumin adsorption and conformational dynamics on inherently conducting polymers: A QCM-D study, Langmuir. 28 (2012) 8433–8445. https://doi.org/10.1021/la300692y.

[23] P.J. Molino, P.C. Innis, M.J. Higgins, R.M.I. Kapsa, G.G. Wallace, Influence of biopolymer loading on the physiochemical and electrochemical properties of inherently conducting polymer biomaterials, Synth. Met. 200 (2015) 40–47. https://doi.org/10.1016/j.synthmet.2014.12.018.

Chapter 5

Promising soft conducting polymer templates for wireless cell stimulation

This chapter is partially adapted from the article, "Enhanced wireless cell stimulation using soft and improved bipolar electroactive conducting polymer templates" that was published in Applied Materials Today 27 (2022) 101481 by Chunyan Qin, Zhilian Yue, Xu-Feng Huang, Robert J. Forster, Gordon G. Wallace and Jun Chen, with permission from Elsevier.".

5.1 Introduction

Bipolar electrochemical stimulation (BPES) has recently been explored to be a novel wireless means of modulation of cell behaviour [1–5]. An advantage of this technique is the removal of wired connections as it employs bipolar electrochemistry (BPE) to wirelessly drive electrochemical processes [6–8]. A significant goal is to promote cell growth and differentiation by simply delivering an electrical stimulus to the cultured cells through the bipolar electroactive electrode on which they are growing [2,9]. Metals, metal oxide and conducting polymers (CPs) have all been explored as substrates in both wired and wireless cell stimulation [1,2,9]. Although metals and metal oxide are relatively safe implant materials with acceptable conductivity and electrochemical properties, the adverse secondary effects and mechanical rigidity (i.e. poor mechanical compliance) limits their further biomedical applications [10,11]. Recent studies showed that CPs are attractive bipolar electrodes since they combine electroactivity and

cytocompatibility with many cell types [2,9]. Despite recent progress on CPs based BPES, rigid and electronically conducting supports, such as ITO and FTO, are required because the electrochemical activity and conductivity of CPs are not sufficient to support a fully CP based bipolar electrode. Therefore, a significant challenge is developing free-standing CP-based electrodes with sufficient bipolar electroactivity and mechanical compliance suitable for cell and tissue stimulation.

From a long-term perspective, to pursue *in vivo* implantation of the bipolar active materials into animal models and eventually gain approval for human trials is challenging but would enable diverse applications from tissue repair to on-demand drug release and electroceuticals. For both *in vitro* and *in vivo* applications, it is essential to develop biomimicry BPES systems with mechanical properties simulating the targeted cells and tissues. Therefore, to develop soft substrates to support bipolar electrodes, or to develop soft, free-standing, electronically conducting bipolar electrodes is important. The advent of wearable devices that utilise electroactive, mechanically tuneable and processable poly(3,4-ethylenedioxythiophene)-poly(styrenesulfonate) (PEDOT-PSS) has inspired us [12–14]. It has good bipolar electroactivity [15,16] and is biologically friendly for cell stimulation [17,18] and the PEDOT-PSS could mechanically reinforce the integrated bipolar electrode and promote further wireless BPES system.

In Chapter 4, bipolar electroactive PMAS modified PPy film was developed as neural electrode for wireless supporting nerve cell behaviour. This film has demonstrated both enhanced bipolar electrochemical performance and improved bioactivity because of redox active PMAS dopant and appropriate biomolecules co-dopants. Here, two distinct CPs were introduced: PMAS as a dopant to improve the bipolar electroactivity and

PEDOT-PSS as mechanical support while remaining soft and pliable. Composite bipolar CP integrity PMAS and PEDOT-PSS to unify the benefit of bipolar electroactivity and mechanical compliance. First, we successfully prepared soft, free-standing and large size PPy-PMAS-collagen/PEDOT-PSS film through a simple bar-coating method and tailored it to fabricate BPES devices for subsequent cell stimulation. The enhanced bipolar electrochemical performance and cytocompatibility for cells, results in a significant increase in PC 12 cells number and neurite formation/growth. For future BPES translation, human cell behaviour using SH-SY5Y cells as a model cell type on the same soft template have been evaluated. The developed BPES system facilitates the formation and enhanced expression of specific neuronal proteins associated with mature human neurons. This is an important step to advance neuronal cultures that can be used for subsequent biochemical and molecular analyses, which provides researchers with a more fundamental translational model of human infection and disease.

5.2 Experiments

5.2.1 Materials

Pyrrole (Py) was purchased from Merck, purified by reduced pressure distillation and stored at -20 ^{o}C. poly (2-methoxy-5 aniline sulfonic acid) (PMAS) was synthesised in-house. Other chemicals for synthesis, such as dextran sulfate sodium salt from Leuconostoc spp. (DS), poly(3,4-ethylenedioxythiophene)-poly(styrenesulfonate) (PEDOT-PSS), phosphate buffered saline (PBS) and Nunc® Lab-Tek® chambered coverglass (polystyrene) were supplied from Sigma-Aldrich (Sydney, Australia). Stainless steel mesh (SSM-500x500 with wire DIM of 0.025 mm) was from Stainless Steel Wire & Mesh Pty Ltd. (Melbourne, Australia). Gibco Dulbecco's Modified

Eagle's Medium (DMEM), Nutrient Mixture F-12 (F12), horse serum, fetal bovine serum (FBS), collagen (Type I from rat tail), nerve growth factor (NGF), penicillin, streptomycin, retinoic acid (RA), calcein AM, propidium iodide (PI), PicoGreen™, Alexa Fluor 546 (Donkey anti-Mouse IgG Highly Cross-Adsorbed Secondary Antibody), monoclonal anti-β-tubulin III (neuronal) antibody produced in mouse, 4'-6-diamidino-2-phenylindole (DAPI) and rhodamine Red™-X succunimidyl ester were from Invitrogen (Melbourne, Australia). Clear RTV silicone adhesive sealant was purchased from Permatex (USA).

5.2.2 Preparation of PMAS modified PPy powder

An aqueous solution containing 0.2 M distilled Py with dopants like 2 mg/ml PMAS and 2 μg/ml collagen was prepared. As illustrated in Figure 5.1, with the continuous magnetic stirring, the chemical oxidation polymerisation was initiated with the addition of 0.2 M Fe(III) tosylate oxidizing agent dropwise. The agitation lasted over weekend at room temperature to ensure the reaction completed. The resultant sediments were washed and centrifuged (8000 rpm, 10 min each time) for several times using ethanol and deionized water until the supernatant was colourless. The products were freeze-dried, resulting PPy-PMAS-collagen powder for further test. The other two PMAS modified PPy powder, i.e., PPy-PMAS and PPy-PMAS-DS-collagen powder were prepared using the same procedure.

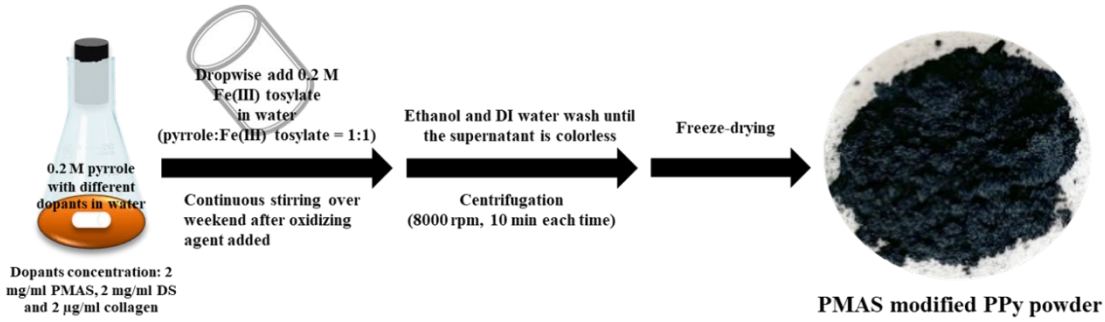

Figure 5.1 Procedure of chemically synthesis to prepare PMAS modified PPy powder.

5.2.3 Preparation of soft bipolar electrodes

The preparation of soft bipolar electrodes using synthetic PMAS modified PPy powders and commercial PEDOT-PSS as mechanical supporting were referred to our previous work [19]. Three soft, free-standing films were prepared using a similar approach, here PPy-PMAS-collagen/PEDOT-PSS film was selected as an example to provide the detailed procedure. Diethylene glycol (DEG) was dissolved in deionized water by magnetic stirring for 10 min and then sonicating for 30 min prior to use. The prepared PPy-PMAS-collagen powder and PEDOT-PSS pellets were equally added to DEG solution, the total concentration (solid content) of mix was kept at 100 mg/ml. The mixed slurry was prepared by blending (2000 rpm, 20 min) and degassing (800 rpm, 5 min). Afterwards, the well-dispersed mixture was simply bar-coated on the homemade glass substrate, dried overnight at room temperature, and then heated in a 60 °C oven (air atmosphere) overnight to evaporate the remaining water and DEG. Finally, a soft, free-standing and flexible PPy-PMAS-collagen/PEDOT-PSS film was peeled off. The resulting film size is depending on the size of designed substrate. And the soft film can be randomly tailored to various shapes to match specific needs. In this work, the square films (1 cm × 1 cm) were used in the bipolar devices for BPES of cells.

5.2.4 Materials characterisations

Physical and spectra characterisation techniques were employed to study our prepared powders and soft bipolar electrodes. A field emission scanning electron microscopy (JEOL JSM-7500FA) were utilised to probe the surface morphology. For chemical stability, *ex situ* Raman spectra and *ex situ* FTIR spectra were adopted. Moreover, the resistance of prepared soft bipolar electrodes were obtained via a multimeter. Please refer the technical details to the Chapter 3 and Chapter 4.2.3.

5.2.5 Cell culture and cytocompatibility studies

Animal cell line: PC 12 cells standard cultured as descried in Chapter 3.2.5.1.

Human cell line: SH-SY5Y cells were cultured in DMEM/F12 growth medium supplemented with 2 mM glutamine, 10% (v/v) heated-inactived FBS and 1% (v/v) penicillin/streptomycin (P/S) in a humidified 37 ℃ incubator with 5% CO_2 atmosphere before further use. For differentiation, a low heated-inactived FBS serum medium (1%) supplemented with 10 μM retinoic acid (RA) was used.

For cyto-compatibility studies, different cell substrates were prepared and sterilized by firstly being immersed in 70% ethanol for 5 min, followed by drying under sterile conditions and exposing to UV light for 20 min (EtOH-UV sterilisation). PC 12 cells and SH-SY5Y cells were cultured on the substrates at a density of 6000 cells/cm^2 in growth media and 5000 cells/cm^2 in differentiation media separately. Cyto-compatibility test was conducted using live/dead assay on day 7. Calcein AM (2×10^{-6} M) and PI (2×10^{-6} M) were used to stain the live and dead cells respectively. Finally, cells were visualised and images were obtained using a ZEISS AxioImager microscope.

5.2.6 Sterilisation preparation of cell substrates and bipolar devices

Bipolar devices and cell substrates were dividually sterilized before integrated together. Synthesised soft bipolar electrodes were washed and sterilized by firstly being immersed in 70% ethanol for 2 hours per time, at least 3 times. Then followed by the same sterilisation procedure as illustrated in Chapter 3.2.6.2.

5.2.7 Optimised BPES protocol for PC 12 cells and SH-SY5Y cells

In this chapter, optimal BPES protocol for PC 12 cells was using the same one in Chapter 4. Please refer to Chapter 4.2.7 for detailed information.

SH-SY5Y cells were seeded on optimal soft bipolar electrode (PPy-PMAS-collagen/PEDOT-PSS) at an initial density of 5000 cells/cm^2 in growth media for differentiation process. Cells were cultured in growth media for two days after seeding, then treated with or without BPES with differentiation media changed every day. BPES (pulse mode: phase duration of 10 min + interphase interval of 5 min): Cells were stimulated on day 3 for 8 h per day for continuous four days. Control (Non BPES): cells were cultured with no BPES.

5.2.8 BPES performance evaluation

Calcein AM and PI staining (live/dead assay) was used to observe the cell morphology and cell viability. Images were taken using a ZEISS AxioImager microscope. The PC 12 cell numbers were quantified using a Quant-iT^{TM} PicoGreen dsDNA Assay Kit in accordance with the manufacturer's instructions and measured with a microplate reader. Tubulin staining was employed to identify specific protein expression of neuronal

differentiation. All use the procedures reported in Chapter 3.2.7.

5.2.9 Quantitative analysis

ImageJ software with NeuriteQuant add-in and Neurite length tracer add-in were utilised to quantify the neurite number and measure the neurite growth, using the same procedure as illustrated in Chapter 3.2.7.3 and Chapter 4.2.9.

5.3 Results and Discussions

5.3.1 Preparation and characterisations of soft CPs templates as bipolar electrodes

Although the bipolar electroactivity of the aforementioned PMAS modified PPy film has been improved and works well on wireless nerve cell stimulation, the bipolar electrode material is attached to a rigid FTO supporting substrate. In this configuration, the FTO electrode potential is controlled by the external electric field and the CP redox composition then reflects this potential distribution. This rigid substrate is incompatible with living cells/tissues, which could cause destructive tissue damage and inevitable inflammatory risks *in vivo*. To address this issue, soft templates were developed for bipolar electrodes which maintain good electrochemical activities. As illustrated in Figure 5.2, PPy-PMAS-collagen powder was synthesised via chemical oxidation polymerisation (step 1) as described in experimental section and in Figure 5.1. As SEM images shown in Figure 5.3, synthetic powders displayed a uniformly sheets structure, and with the high-resolution images they revealed the distinct surface morphologies. PPy-PMAS-collagen powder is tip arrayed surface, while PPy-PMAS has a smooth surface and PPy-PMAS-DS/collagen is full of nodes, like cauliflower surface. Both the Raman and FTIR spectra characteristically show peaks, which is attributed to PPy and PMAS (Figure 5.4). Then, commercial PEDOT-PSS was introduced as a soft

mechanical support due to its physical flexibility and ease of processing [20]. Moreover, its excellent electrochemical activity can act as an electronically conducting support [21]. The confirmed bipolar electrochemical activity [15] and biocompatibility [18] of PEDOT-PSS are key additional features. Here, the synthetic PPy-PMAS-collagen/PEDOT-PSS film is soft, free-standing, and large size (20 cm × 7 cm) and can be tailored for particular applications. In this chapter, this film was cut into squares (1 cm × 1 cm) and fabricated into the specific-made bipolar device (Step 5) for subsequent wireless cell stimulation.

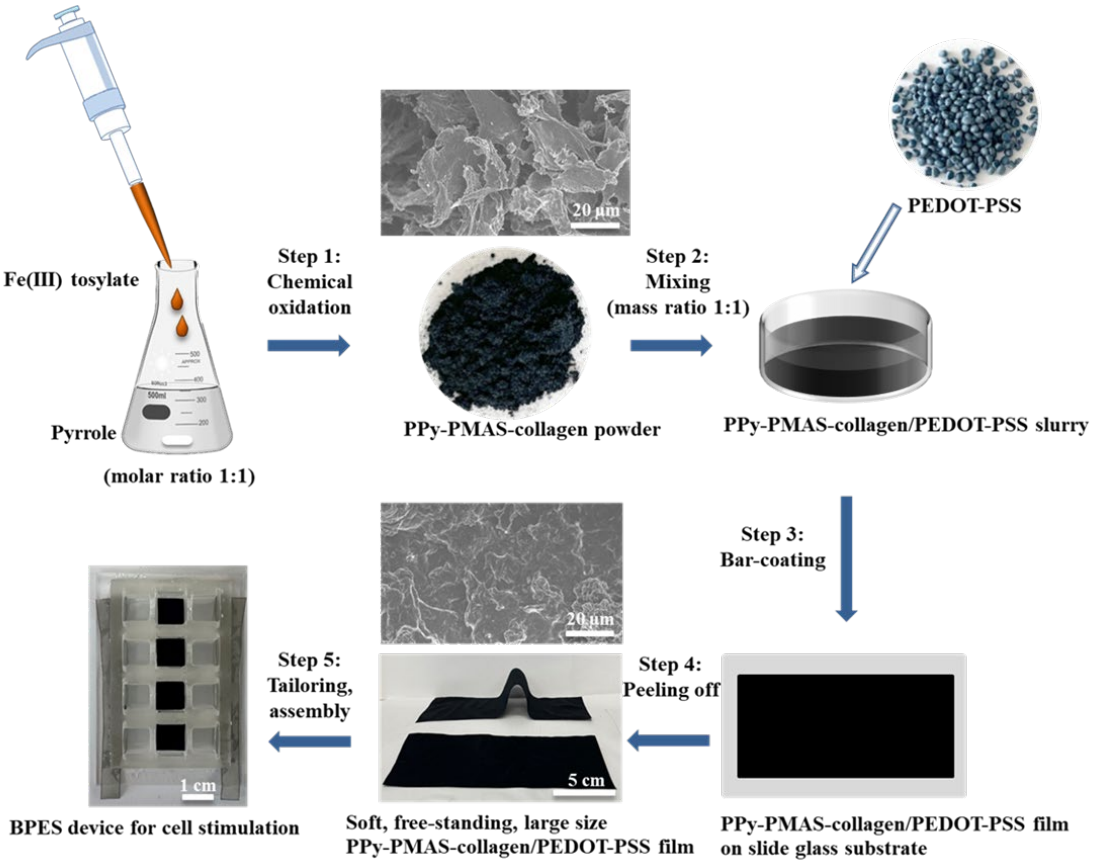

Figure 5.2 Schematic illustration of the preparation process of soft, free-standing PPy-PMAS-collagen/PEDOT-PSS film, and digital photos of large size prepared film and the assembled BPES device. Other soft films were prepared using the similar procedure.

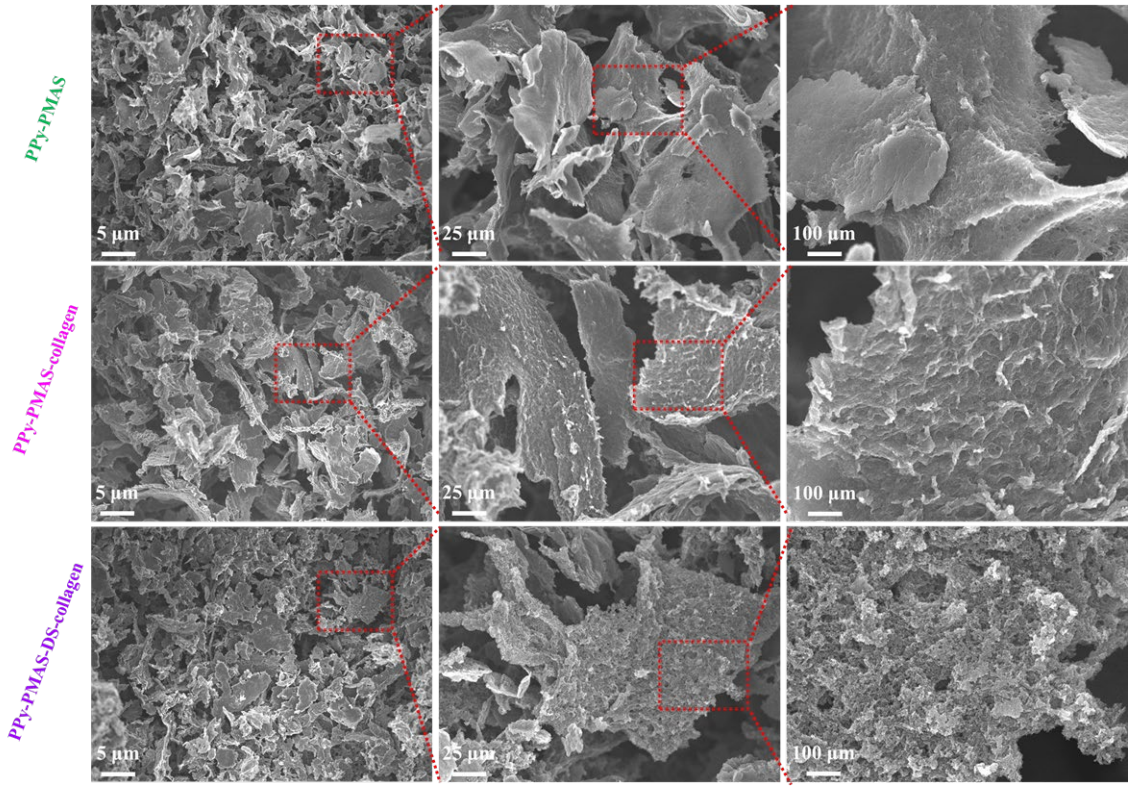

Figure 5.3 SEM characterisation of chemically prepared PMAS modified PPy powders.

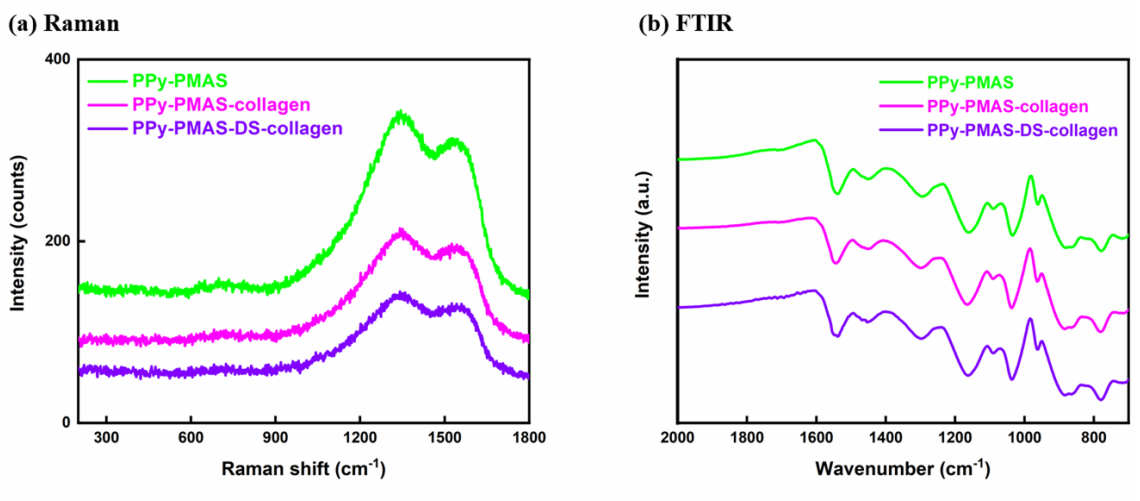

Figure 5.4 (a) Raman and (b) FTIR spectra of as-synthesised PMAS modified PPy powders.

PEDOT-PSS, PPy-PMAS/PEDOT-PSS, and PPy-PMAS-DS-collagen/PEDOT-PSS films were also prepared using the same preparation process. SEM images of the soft films reveal rough surface morphologies compared to the smooth PEDOT-PSS film (Figure 5.5) which may improve cell attachment. All the peaks observed in Raman (Figure 5.6a) and FTIR (Figure 5.6b) spectra matched the characteristic spectra bands of PMAS, PPy and PEDOT-PSS. The lower resistances of soft films are summarized in Figure 5.7, revealing their high electrical conductivities. After 50 cycles of compression testing, the PPy-PMAS-collagen/PEDOT-PSS film preserved their structural integrity (Figure 5.8). A Young's modulus of 29.1 MPa was also demonstrated through a stress-strain curve (Figure 5.9). All the synthesised soft films were tested for their compatibility with PC 12 cells prior to conducting BPES experiments. The live/dead images shown in Figure 5.10 indicate that the soft CPs templates have good cytocompatibilities and the PPy-PMAS-collagen/PEDOT-PSS film shows a more uniform distribution of cells across the surface and higher cell viability. All of the results indicate that the soft template has excellent properties and is suitable for use in cell stimulation investigations.

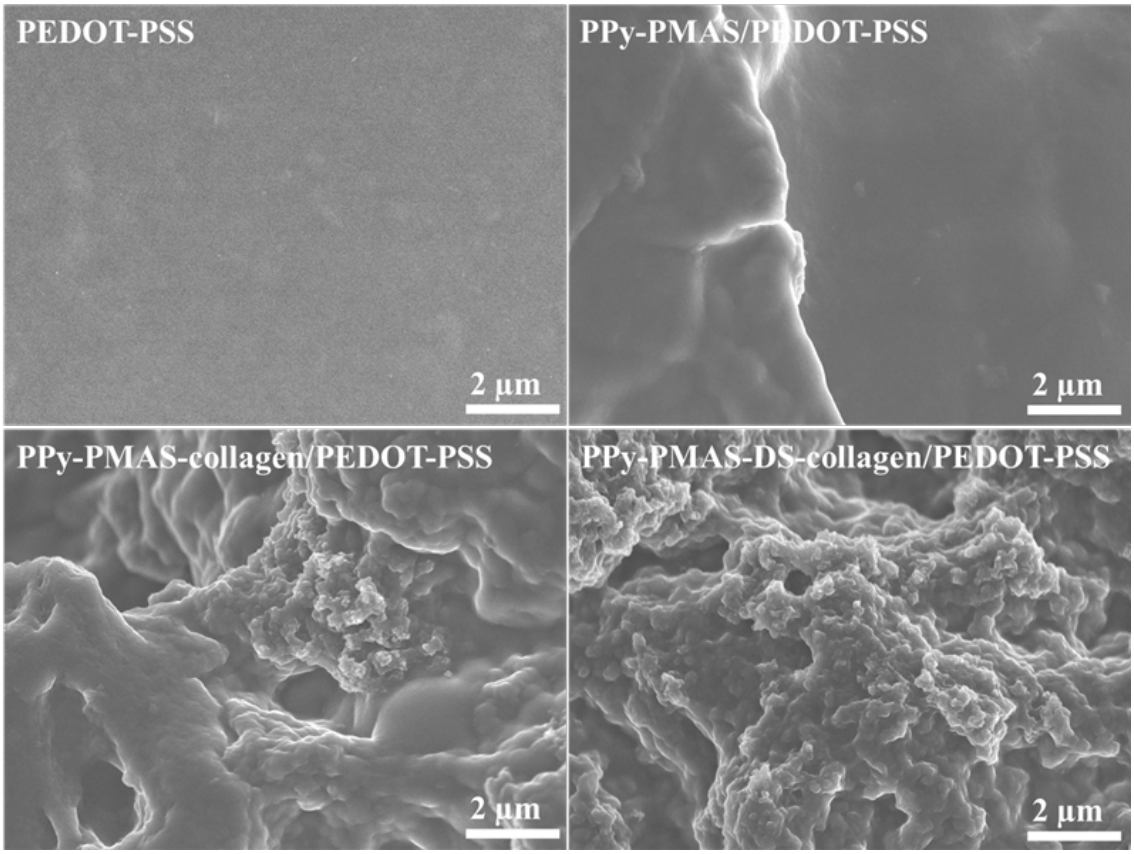

Figure 5.5 SEM characterisation of the prepared soft CPs templates as bipolar electrodes.

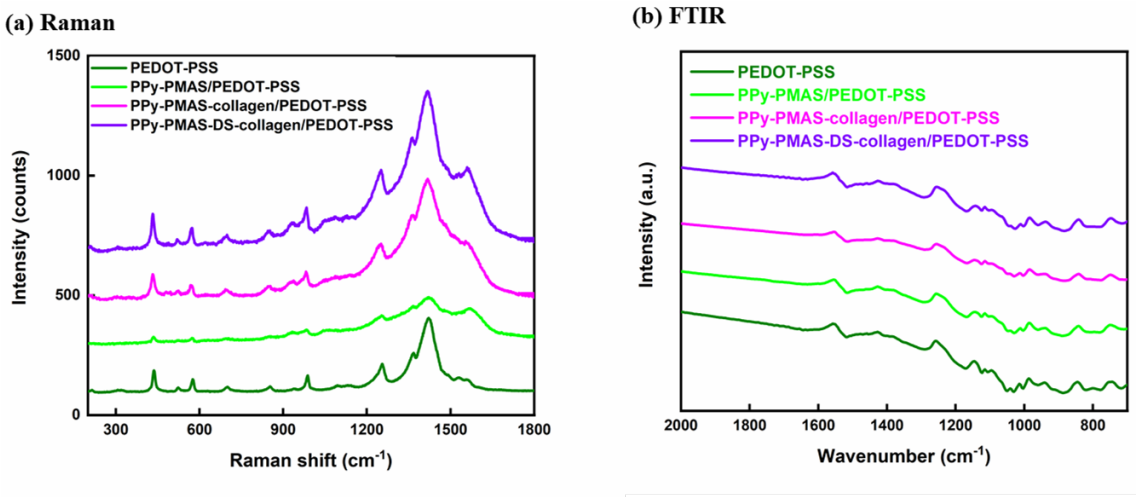

Figure 5.6 (a) Raman and (b) FTIR spectra of all synthesised soft CPs templates as bipolar electrodes.

Soft bipolar electrodes	Resistance (ohm/cm)
PEDOT-PSS	26.4 ± 3.5
PPy-PMAS/PEDOT-PSS	23.8 ± 4.0
PPy-PMAS-collagen/PEDOT-PSS	26.0 ± 3.6
PPy-PMAS-DS-collagen/PEDOT-PSS	48.8 ± 7.4

Figure 5.7 Resistance of the prepared soft CPs templates as bipolar electrodes.

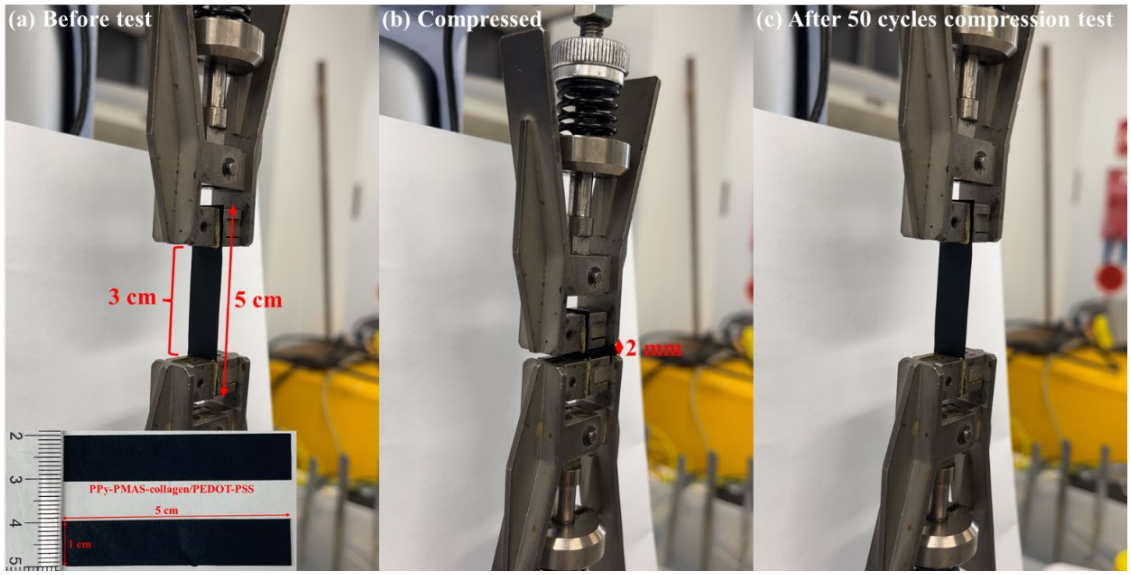

Figure 5.8 Photographs of the different states of PPy-PMAS-collagen/PEDOT-PSS film during a compression cycle test. (a) Original state of the PPy-PMAS-collagen/PEDOT-PSS film before test (test film length was 3 cm). Inserted at bottom left is the image of prepared films (5 cm × 1 cm). (b) Compressed state of the PPy-PMAS-collagen/PEDOT-PSS film during a compression test (compressed to 93.33%). (c) End state of the PPy-PMAS-collagen/PEDOT-PSS film after 50 cycles of compression test.

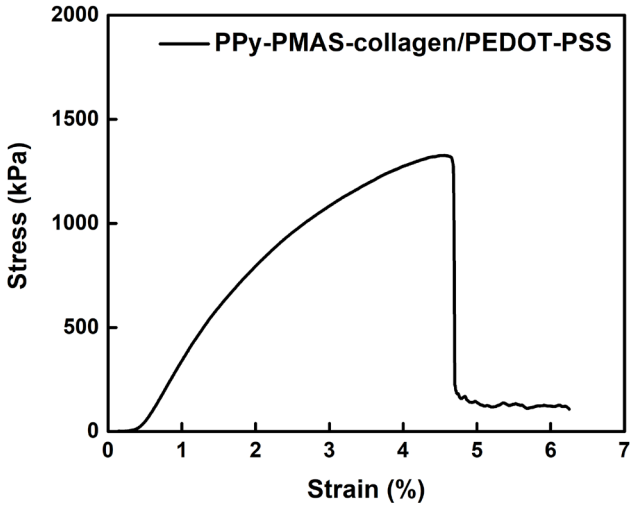

Figure 5.9 Stress-strain curve of PPy-PMAS-collagen/PEDOT-PSS film during a tensile test.

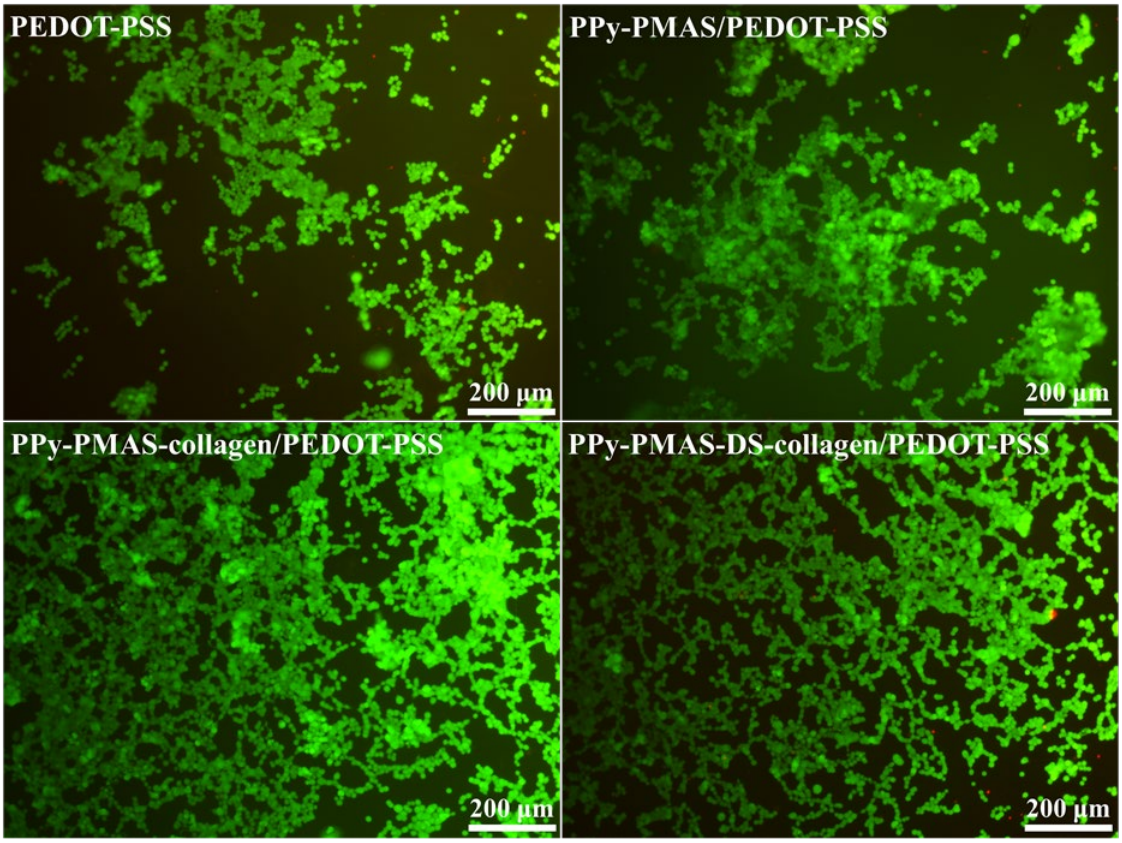

Figure 5.10 Images of PC 12 cells on day 7 after cyto-compatibility assessment via live/dead assay. Calcein-AM (green) present live cells and PI (red) were on behalf of dead cells. Cells were cultured on prepared soft CPs templates as bipolar electrodes in growth media over one week at initial cell seeding density of 6000 cells/cm^2 without

BPES treatment.

5.3.2 Soft CPs templates as bipolar electrodes promote PC 12 cell proliferation

For more insights into the performance of the soft CPs templates as bipolar electrodes, PC 12 cells cultivated on PEDOT-PSS, PPy-PMAS/PEDOT-PSS, and PPy-PMAS-DS-collagen/PEDOT-PSS films were also wirelessly stimulated. Images, numbers, and statistical analysis are shown in Figure 5.11 and Figure 5.12. All soft templates support PC 12 cells growth and exhibit typical neural morphologies. It is clear that for all the groups, BPES promotes PC 12 cells spreading (Figure 5.11). This phenomenon is confirmed by quantified data (Figure 5.12). The number of cells gradually increases over time irrespective of the composition soft templates, and the number of cells was higher for the BPES stimulated group than the unstimulated control group. For PEDOT-PSS, a statistically significant increase in PC 12 cells number was shown at day 7 under BPES treatment. Compared to PEDOT-PSS, when PC 12 cells cultured on PPy-PMAS/PEDOT-PSS, statistically significant increase in their numbers were observed at day 3, day 5 and day 7 under BPES treatment. Furthermore, statistically significant effects on cell numbers were noted at all time points with a $P < 0.0001$ when PC 12 cells were cultured on PPy-PMAS-DS-collagen/PEDOT-PSS. Specifically, the cells number on day 7 after BPES treatment was increased by 5-fold for PPy-PMAS-DS-collagen/PEDOT-PSS, which is still relatively lower than the number of cells on PPy-PMAS-collagen/PEDOT-PSS (Figure 5.13). Although the benefit of DS is not clearly demonstrated, it is possible now not to use it in functionalizing PPy polymer at the presence of PEDOT-PSS. Both PMAS and PEDOT-PSS could enhance the electrochemical activity, and in addition, PEDOT-PSS offers mechanical flexibility and softness. Overall, the combination of PMAS modified PPy films along with PEDOT-

PSS represents a significant advance in BPES platforms due to its biocompatibility, mechanical flexibility, and ability to drive cell differentiation electrically.

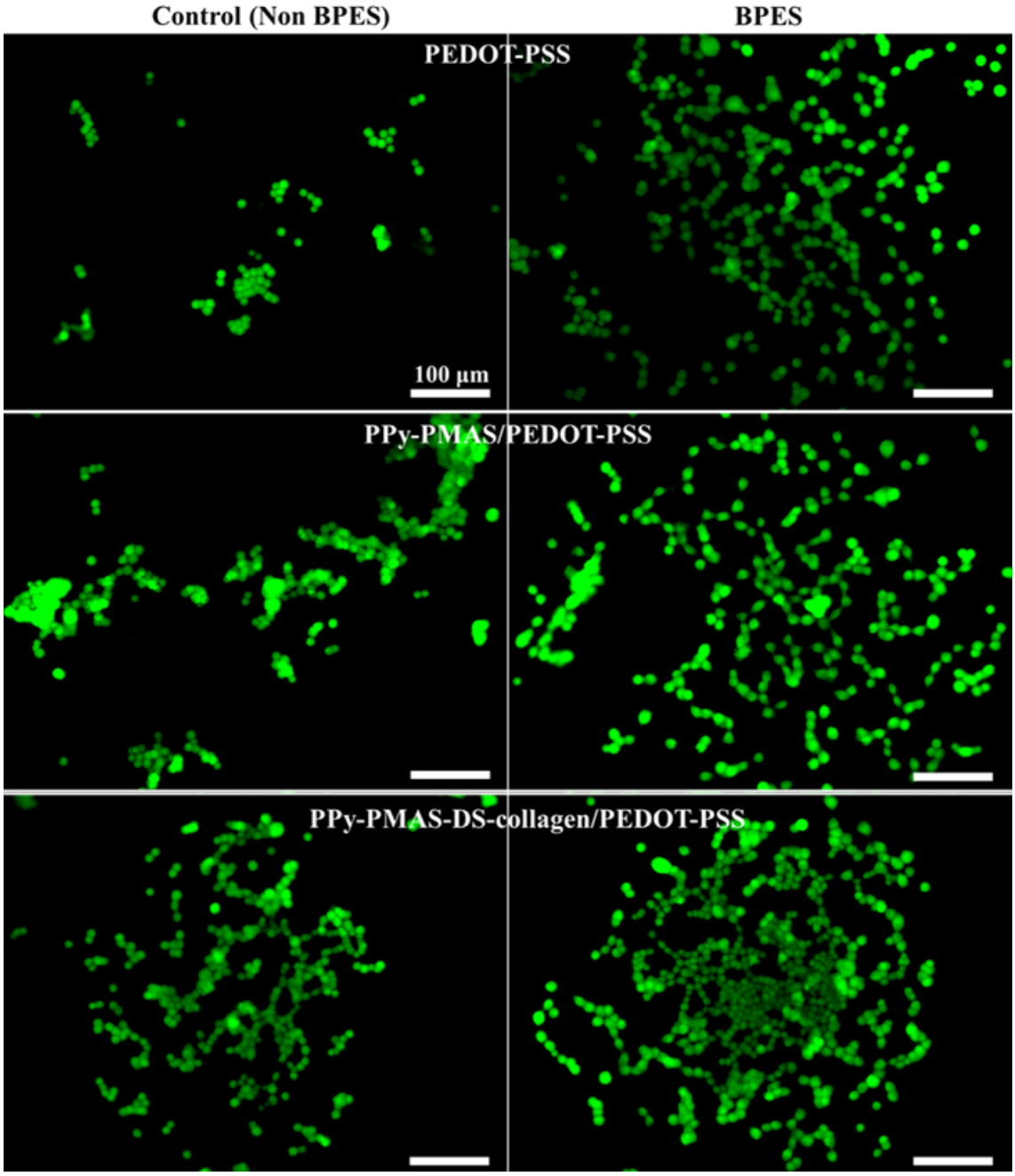

Figure 5.11 Images on day 7 via live/dead assay using calcein AM (green: live) and PI (red: dead) staining. PC 12 cells were cultured on soft CPs templates as bipolar electrodes at an initial seeding density of 20000 cells/cm^2 in growth media over total

one week. BPES: Cells were stimulated on day 2 for 8 h per day in continuous three days, then standard cultured in the following three days after stimulation finished. Control (Non BPES): cells were standard cultured without BPES.

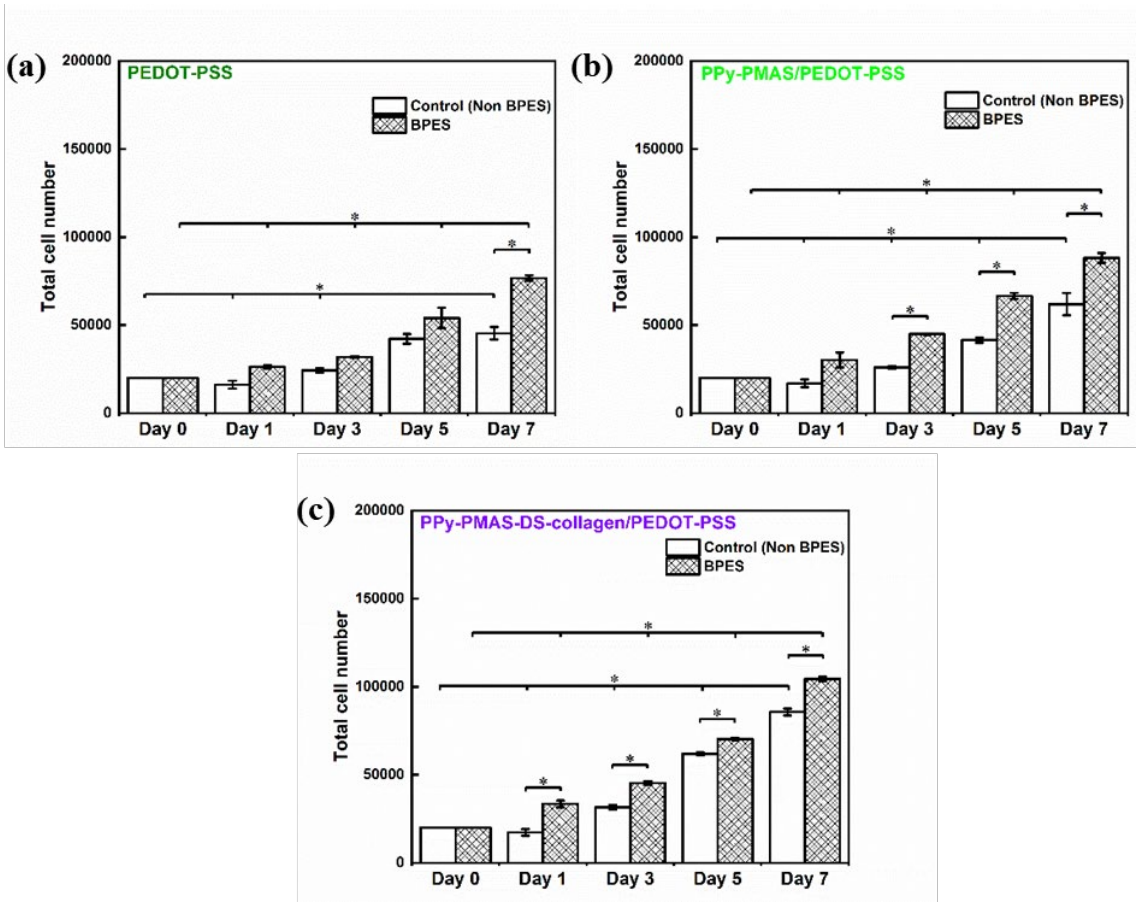

Figure 5.8 Numbers of PC 12 cells calculated via PicoGreen assay at various time points with statistical analysis using two-way ANOVA. PC 12 cells were cultured on soft CPs templates as bipolar electrodes at an initial seeding density of 20000 cells/cm^2 in growth media over total one week. BPES: Cells were stimulated on day 2 for 8 h per day in continuous three days, then standard cultured in the following three days after stimulation finished. Control (Non BPES): cells were standard cultured without BPES. Data are represented as mean ± standard deviation (SD) and "*" ($P < 0.0001$) was used to indicate significance.

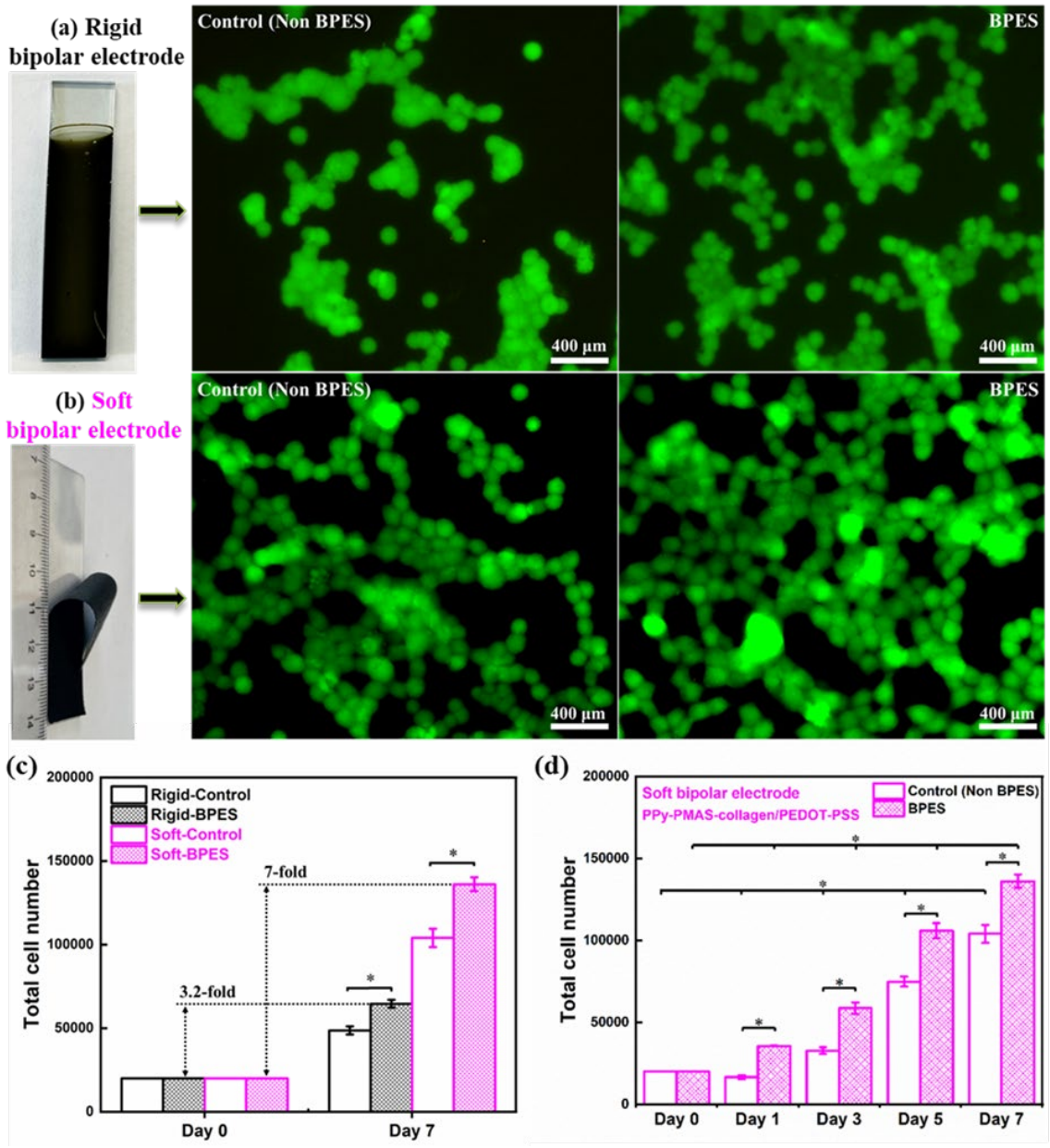

Figure 5.9 Images of (a) rigid and (b) soft bipolar electrodes and accordingly stimulated cells on them via live/dead assay using calcein AM (green: live) and PI (red: dead) staining on day 7. (c-d) Numbers of PC 12 cells calculated via PicoGreen assay at various time points with statistical analysis using Two-way ANOVA. PC 12 cells were cultured on (a) rigid bipolar electrode (PPy-PMAS-collagen/FTO) and (b) soft bipolar electrode (PPy-PMAS-collagen/PEDOT-PSS) at an initial seeding density of 20000 cells/cm^2 in growth media over total one week. BPES: Cells were stimulated on day 2 for 8 h per day in continuous three days, then cultured in the following three days after

stimulation finished. Control (Non BPES): cells were cultured without BPES. Data are represented as mean ± standard deviation (SD) and "*" ($P < 0.0001$) was used to indicate significance.

The prepared PPy-PMAS-collagen/FTO and PPy-PMAS-collagen/PEDOT-PSS film are referred to as rigid and soft bipolar electrode, respectively. Their digital photos were shown in Figure 5.13a and Figure 5.13b. As expected, PC 12 cells grown on rigid and soft bipolar electrodes in proliferation media retained an undifferentiated state with rounded morphologies. This result is important since it indicates that the film's morphology or chemical composition alone do not trigger differentiation. Cells cultured on rigid bipolar electrode were single, round cell and smaller aggregates, whilst cells on soft bipolar electrode were polygonal with larger and more spatially well-dispersed cell clusters (Figure 5.13a-5.13b). Both bipolar electrodes were initially seeded with the same numbers of PC 12 cells. The number of cells on these bipolar electrodes at various time points was quantified using the PicoGreen assay. PC 12 cells cultured on these two bipolar electrodes proliferated well over time, showing statistical significance at day 7 with a $P < 0.0001$ between under BPES and non-BPES (Control) (Figure 5.13c). In particular, the number of cells that grew after BPES treatment was increased by approximately 3.2-fold for the rigid bipolar electrode and 7-fold for the soft bipolar electrode. This indicates that the soft bipolar electrode promotes cell proliferation to a greater extent. It also suggests that the rigid FTO substrate has been successfully removed without influencing the cell behaviour.

From the results of the statistical analysis presented in Figure 5.13d, it is clear to notice that the number of cells is statistically higher for the BPES stimulated group than the unstimulated control group when they were cultured on soft bipolar electrode. Statistical

analysis via two-way ANOVA also revealed both BPES and time point have significant effects on cell proliferation, and so did the interaction of BPES and time (with a $P < 0.0001$). Particularly, Bonferroni-post hoc analysis indicated that PC 12 cell proliferation with or without BPES treatment significantly differed from each other (with a $P < 0.0001$). These results confirm that BPES treatment using soft bipolar electrode promotes more rapid proliferation of PC 12 cells.

5.3.3 Soft CPs templates as bipolar electrodes enhance PC 12 cell differentiation

The role of BPES played in neural cell differentiation on soft CPs templates as bipolar electrodes has also investigated. PC 12 cells were cultivated on PEDOT-PSS, PPy-PMAS/PEDOT-PSS, PPy-PMAS-collagen/PEDOT-PSS and PPy-PMAS-DS-collagen/PEDOT-PSS films under the same conditions. Compared to the control groups, greater neurite outgrowth with BPES was evident on each soft CP template using immunofluorescent staining (Figure 5.14). Confirming this, the neurites number and lengths were assessed with one-way ANOVA (Figure 5.15). The data revealed that the BPES treatment has promote differentiation of nerve cells on these soft CPs templates with statistical significance ($P < 0.05$), exhibiting in both neurites number and lengths. Among all of the soft templates, many more neurites and an increased neurite length were noted on a PPy-PMAS-collagen/PEDOT-PSS film as a bipolar electrode. Specifically, as shown in Figure 5.16, significant and extensive neurites outgrowth was displayed when PC 12 cells were cultured on PPy-PMAS-collagen/PEDOT-PSS film together with BPES treatment. All these findings indicate that the soft CPs templates promote nerve cell differentiation, especially under the significant influence of BPES. PPy-PMAS-collagen/PEDOT-PSS film is preferred soft bipolar electrode for further wireless cell stimulation investigations.

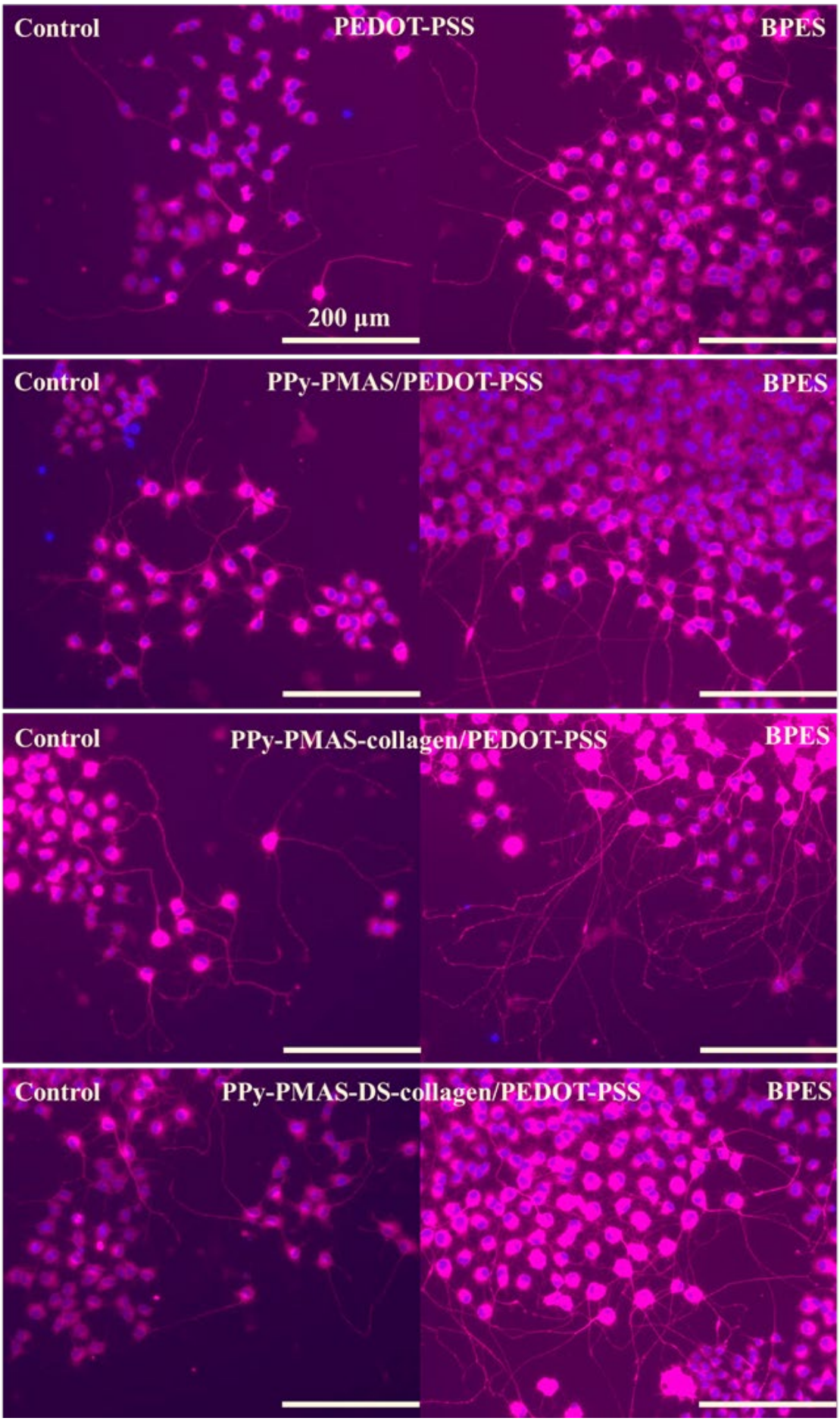
Control
PEDOT-PSS
BPES
200 µm
Control
PPy-PMAS/PEDOT-PSS
BPES
Control
PPy-PMAS-collagen/PEDOT-PSS
BPES
Control
PPy-PMAS-DS-collagen/PEDOT-PSS
BPES

Figure 5.10 Immunofluorescent staining images of PC 12 cells. PC 12 Cells were cultured on soft CPs templates as bipolar electrodes. BPES: Cells were stimulated on day 2 for 8 h per day in continuous three days, then standard cultured in the following three days after stimulation finished. Control (Non BPES): cells were standard cultured with no BPES. β-tubulin III (red) labels microtubule-associated protein 2, and DAPI (blue) labels nucleus.

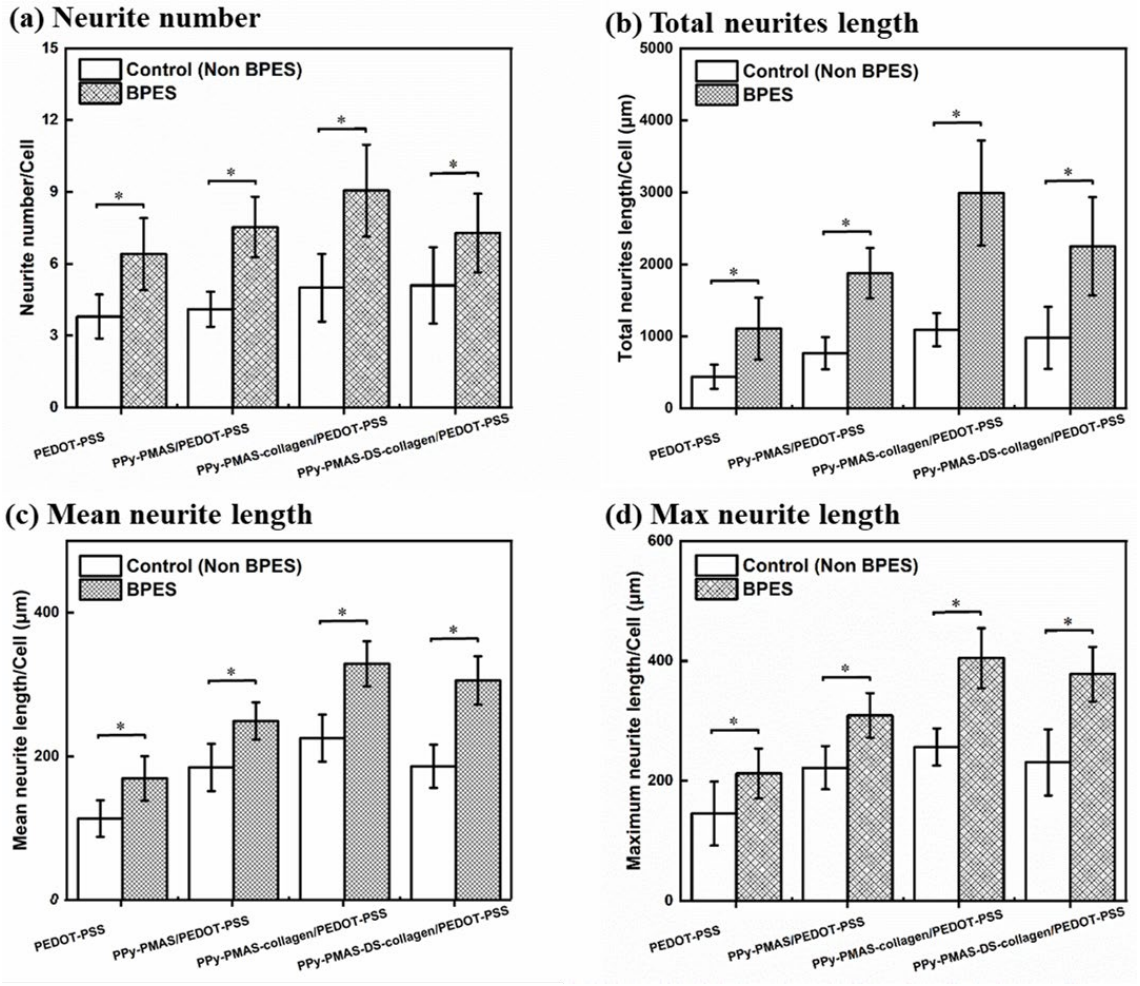

Figure 5.11 Assessments of neurite number and neurite growth of cells, including (a) the total neurite number per cell, (b) the total length of neurites per cell, (c) mean neurite length per cell, and (d) maximum neurite length per cell. PC 12 Cells were cultured on soft CPs templates as bipolar electrodes. BPES: Cells were stimulated on

day 2 for 8 h per day in continuous three days, then standard cultured in the following three days after stimulation finished. Control (Non BPES): cells were standard cultured with no BPES. Statistical analysis used one-way ANOVA. Data are represented as mean ± standard deviation (SD) and "*" ($P < 0.05$) was used to indicate significance.

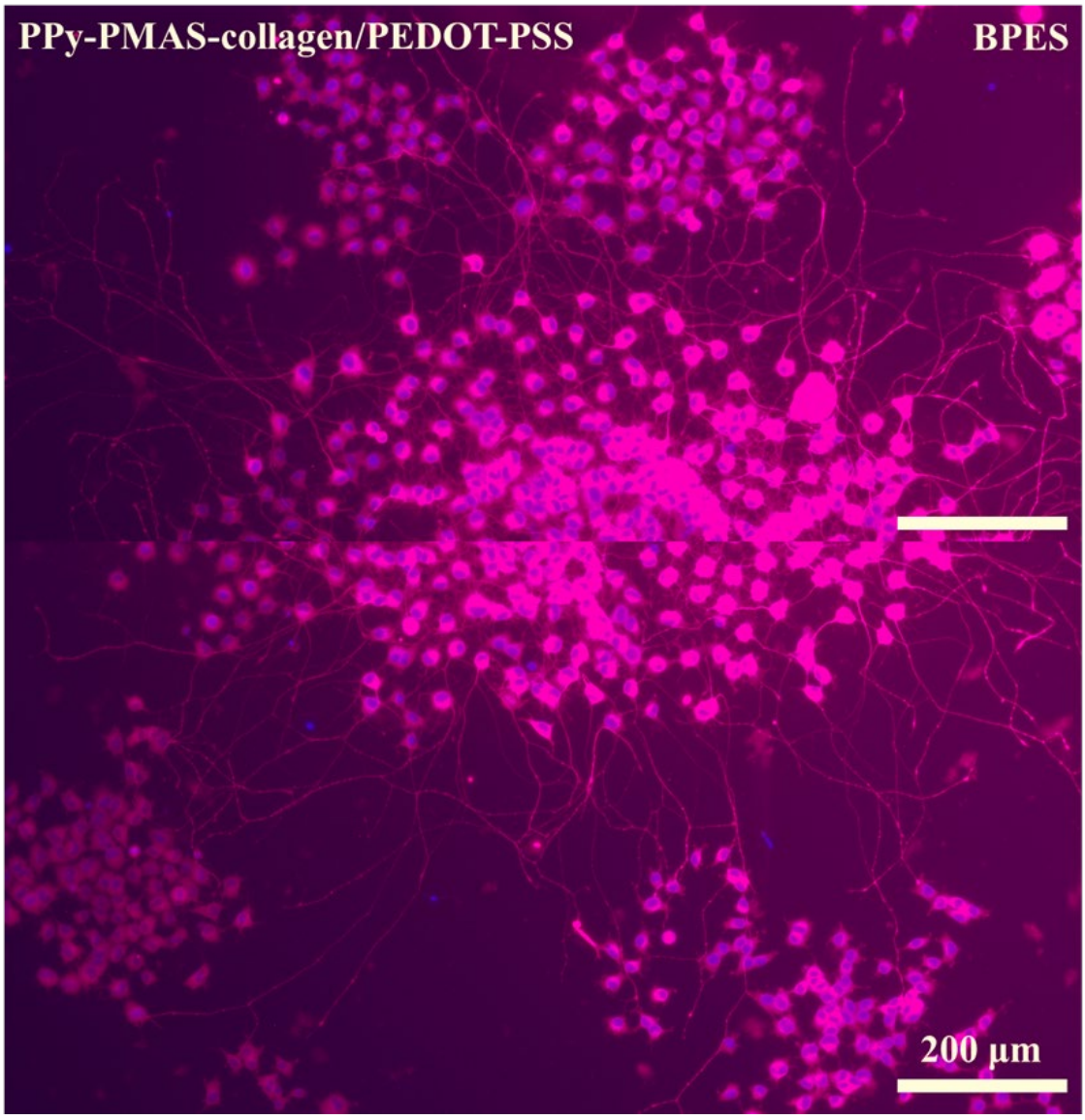

Figure 5.12 Highlights of enhanced PC 12 cell behaviour on soft PPy-PMAS-collagen/PEDOT-PSS template as a bipolar electrode with BPES. Immunofluorescent staining images of PC 12 cells on PPy-PMAS-DS-collagen/PEDOT-PSS film with BPES. BPES: Cells were stimulated on day 2 for 8 h per day in continuous three days,

followed by standard culture for 3 more days. β-tubulin III (red) labels microtubule-associated protein 2, and DAPI (blue) labels nucleus.

The neuronal differentiation of PC 12 cells cultured on the rigid bipolar electrode (PPy-PMAS-collagen/FTO) and the soft bipolar electrode (PPy-PMAS-collagen/PEDOT-PSS) were investigated over a one-week period. Both bipolar electrodes support the differentiation of cells when exposed to wireless electrical stimulation. Under BPES, typical morphological changes of cells cultured on the two substrates are observed with conspicuous neurites outgrowth. This was further visualised by immunostaining of β(III)-tubulin, a widely used neuronal marker. As illustrated in Figure 5.17a, cells on both rigid and soft bipolar electrodes showed expression of β(III)-tubulin. Compared to the cells cultured on the rigid bipolar substrates, at day 7, PC 12 cells on the soft bipolar electrode displayed extensive neurites formation as well as extensive networks of cells. Quantitatively, the neurites number and lengths of cells cultured on the rigid and soft bipolar electrodes at day 7 were measured. In the presence of BPES, though no striking difference in the number of neurites was shown between these two types of bipolar electrodes, both the lengths of total and mean neurite of the cells cultured on the soft bipolar electrode were significantly longer than those on the rigid bipolar electrode (Figure 5.17b). Specifically, when PC 12 cells were cultured on the soft PPy-PMAS-collagen/PEDOT-PSS bipolar electrode, as shown in Figure 5.17c, the number of neurites was nearly 2-fold compared to that without BPES treatment. A more variable trend was observed for the total and mean neurite lengths. These results highlight the advantages of soft CPs templates as bipolar electrodes for stimulating neurite extension of biological cells.

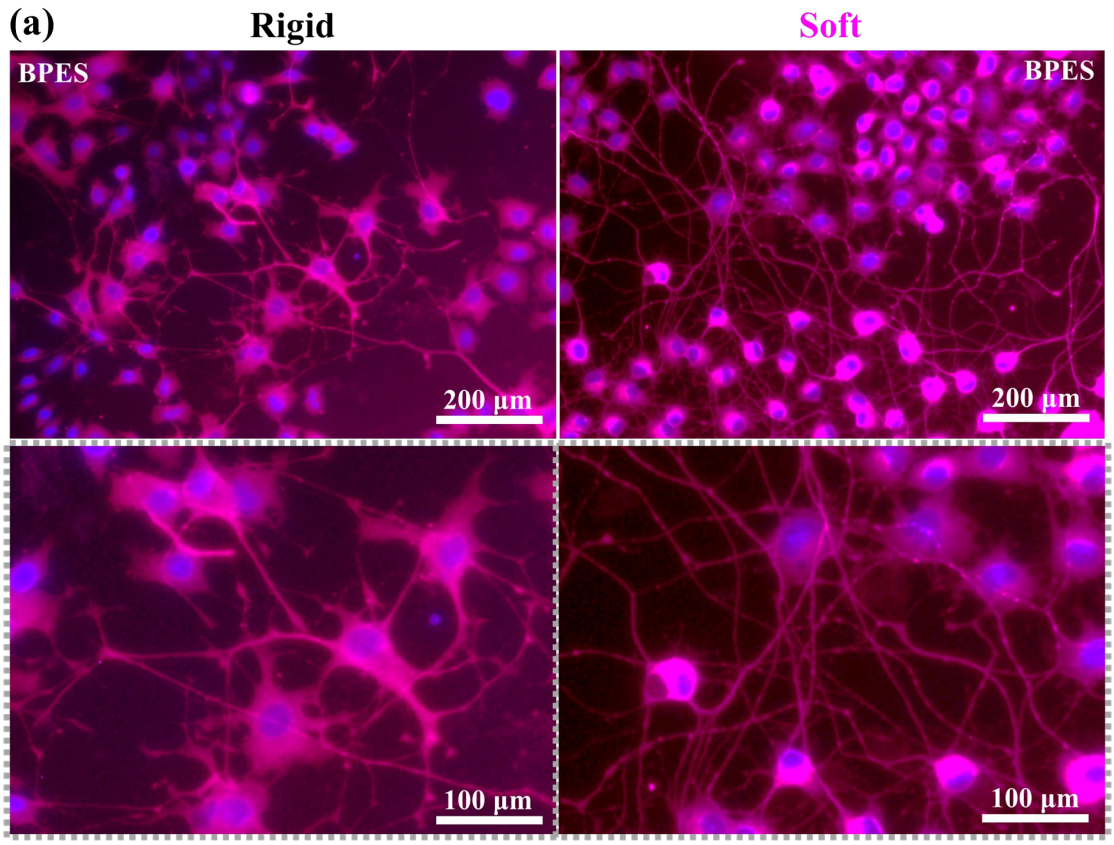
(a)
Rigid
Soft
BPES
BPES
200 µm
200 µm
100 µm
100 µm

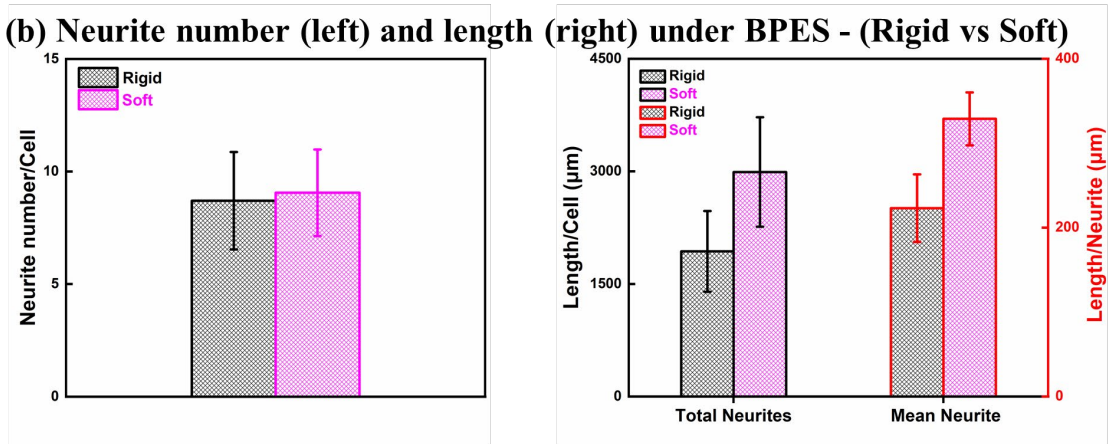
(b) Neurite number (left) and length (right) under BPES - (Rigid vs Soft)
Neurite number/Cell
Rigid
Soft
Length/Cell (µm)
Length/Neurite (µm)
Rigid
Soft
Rigid
Soft
Total Neurites
Mean Neurite

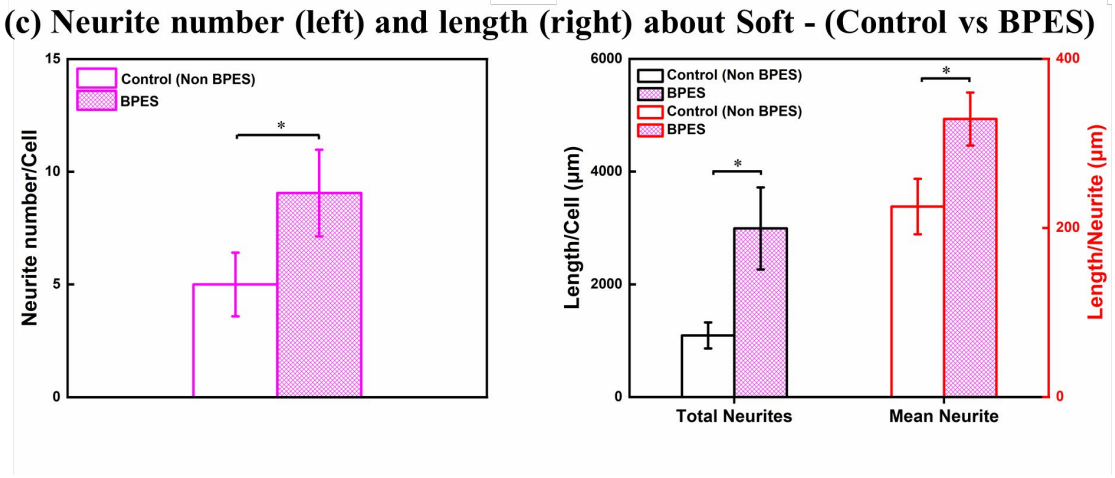
(c) Neurite number (left) and length (right) about Soft - (Control vs BPES)
Neurite number/Cell
Control (Non BPES)
BPES
Length/Cell (µm)
Length/Neurite (µm)
Control (Non BPES)
BPES
Control (Non BPES)
BPES
Total Neurites
Mean Neurite

Figure 5.13 (a) Immunofluorescent staining images of PC 12 cells. (b-c) Assessments of neurite number and neurite growth of cells, including the total neurite number per cell, the total length of neurites per cell, mean neurite length. Cells were cultured on the rigid bipolar electrode (PPy-PMAS-collagen/FTO) and soft bipolar electrode (PPy-PMAS-collagen/PEDOT-PSS). BPES: Cells were stimulated on day 2 for 8 h per day in continuous three days, then standard cultured in the following three days after stimulation finished. Control (Non BPES): cells were standard cultured with no BPES. β-tubulin III (red) labels microtubule-associated protein 2, and DAPI (blue) labels nucleus. Statistical analysis used one-way ANOVA. Data are represented as mean ± standard deviation (SD) and "*" ($P < 0.05$) was used to indicate significance.

5.3.4 Development and evaluation of human cell differentiation under BPES

To broaden the application, a human neuroblastoma cell line, SH-SY5Y has been explored. This cell line is often used for a multitude of neurobiology experiments to investigate Schizophrenia, Parkinson's and Alzheimer's disease because of their stable karyotypes [22–26]. SH-SY5Y cells were seeded on the soft bipolar electrode (PPy-PMAS-collagen/PEDOT-PSS) and cultured in growth media for two days. On day 3, cells were cultivated with fresh differentiation media and then subjected to electrical stimulation with pulse mode for 8 h per day continuously for four days. Cells were stained on day 7 to evaluate the human cell behaviour with BPES. Phase-contrast images of SH-SY5Y cells (Figure 5.18) reveal that the human neuroblastoma cells differentiated in a time-dependent manner under the BPES protocol. Prior to BPES treatment, undifferentiated SH-SY5Y cells contained both neuroblast-like and epithelial-like morphologies, appearing to be non-polarised, with very few and short projections extending outward. Cells differentiated gradually into more neuroblast-like,

round states with a view towards to mature neurons after BPES treatment. These differentiated human cells exhibit extended and branched neurites.

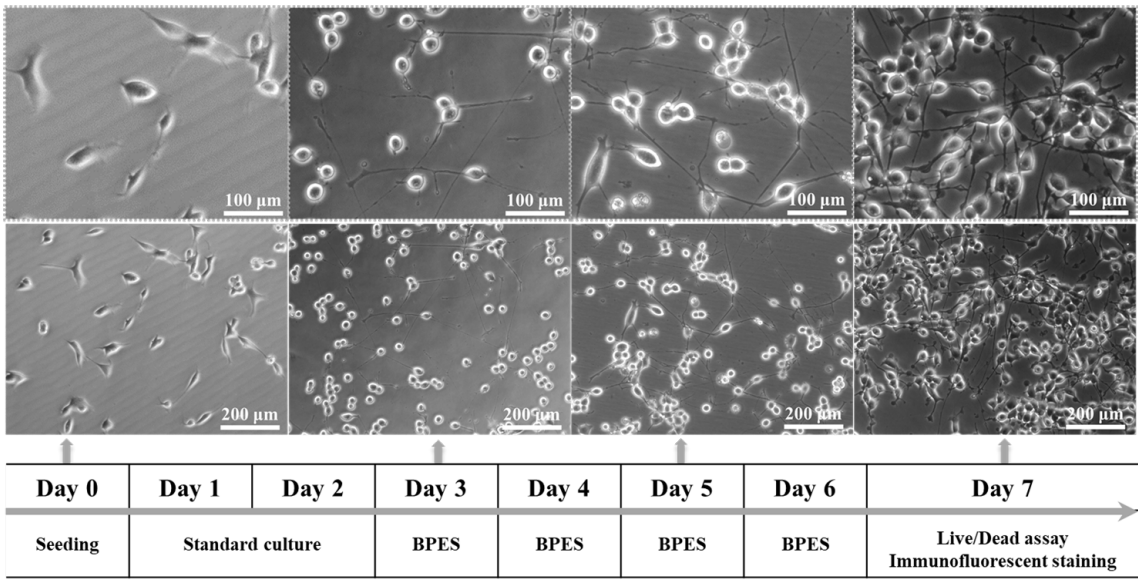

Figure 5.14 Phase-contrast images of human neuroblastoma SH-SY5Y cells differentiation process under-developed BPES protocol. SH-SY5Y cells were cultured on soft bipolar electrode (PPy-PMAS-collagen/PEDOT-PSS) in differentiation media over total one week with BPES treatment. BPES: Cells were standard cultured in the first two days before subjected to electrical stimulation with pulse mode for 8 h per day continuously for four days.

To obtain more information for evaluation of BPES on human cell differentiation, SH-SY5Y cells were monitored by both live/dead staining and tubulin staining. Figure 5.19a shows highly viable cells for both group with and without BPES treatment. Distinctive elongated projections were observed for the group treated with BPES. Further supported by β-tubulin (III) staining (Figure 5.19b), our BPES protocol enabled human SH-SY5Y cells to differentiate into a neuronal phenotype, including neurites or

processes and growth cones. These neurons make connections with other cells, with terminals ending on cells or processes irrespective of BPES treatment or not. Compared to the control group, the cells with BPES treatment demonstrated a much more extensive network of neurites. Representative results have fully illustrated our BPES protocol promoted the formation of neuroblast-like cells, and enhanced expression of specific neuronal microtubule-associated protein 2 of mature human neurons. Therefore, all these fundamental findings indicate that this soft CP-based BPES system works on human cells differentiation, which offers a reliable way to advance this wireless cell stimulation technology with a translational model from animal cells to human neural cells.

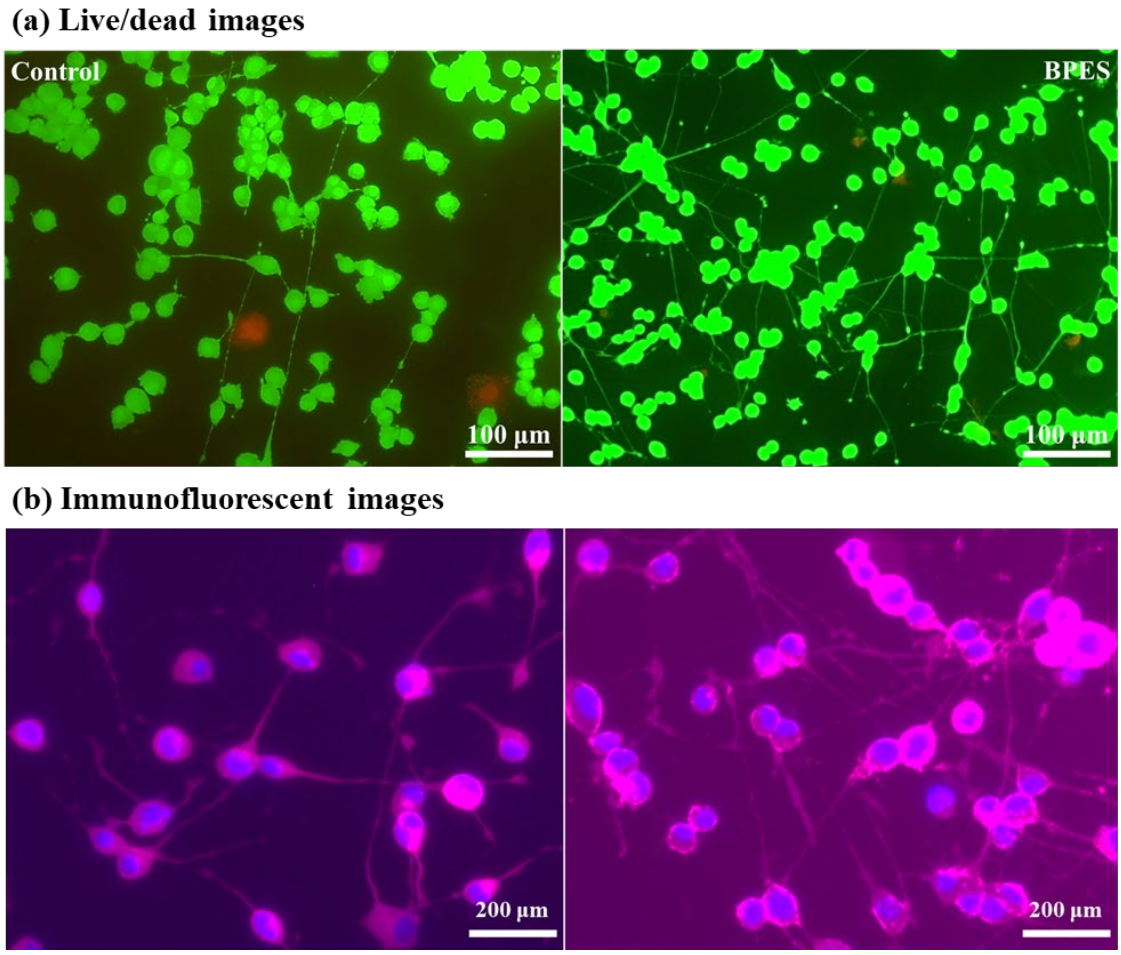

Figure 5.15 (a) Fluorescent images on day 7 via live/dead assay using calcein AM

(green: live) and PI (red: dead) staining indicate the high SH-SY5Y cells viability. (b) Immunofluorescent images illuminate neuronal features of fully differentiated SH-SY5Y cells on day 7. SH-SY5Y cells were cultured on soft bipolar electrode (PPy-PMAS-collagen/PEDOT-PSS) in differentiation media over total one week without (Control) or with BPES treatment. BPES: Cells were standard cultured in the first two days before subjected to stimulated on day 3 for 8 h per day in continuous four days. Control: cells were standard cultured with no BPES. Initial seeding density of 5000 cells/cm^2. Markers of neuronal differentiation: β-tubulin III (red) labels microtubule-associated protein 2, revealing the neuronal soma and proximal portion of neurites. DAPI (blue) labels nucleus.

5.4 Conclusions

In summary, soft and free-standing CPs templates (PPy-PMAS/PEDOT-PSS, PPy-PMAS-collagen/PEDOT-PSS and PPy-PMAS-DS-collagen/PEDOT-PSS films) have been developed where PEDOT-PSS provides physical and mechanical support. The resultant templates are flexible, cytocompatible and highly bipolar electroactive, which may enable *in vivo* applications of wireless electrical stimulation. Improved PC 12 cells proliferation and differentiation are demonstrated using these CPs templates as soft bipolar electrodes in the BPES system. To compare with the rigid bipolar electrode, PPy-PMAS-collagen/PEDOT-PSS film is the preferred soft substrate for stimulating PC 12 cells in this study. Using this soft bipolar electrode, the ability of BPES treatment to work on human neuroblastoma SH-SY5Y cells differentiation process has been evaluated. The results show enhanced formation of neuroblast-like cells, and enhanced expression of specific neuronal proteins of mature human neurons. This opens up new avenues and a potential platform to build wireless, bioactive and bipolar electroactive

based BPES systems as a variety of *in vitro* and *in vivo* applications as disease models and medical implants.

Further work requires more in-depth study using human primary cells and transformation of the bipolar systems from 2D to 3D to better imitate the structure and function of tissues or organs. The creation of 3D culture models to optimise the response of cell-biomaterials interfacing and mimic the native environment is extremely exciting by making our BPES system more suitable for implantation. For instance, hydrogels and 3D printed scaffolds could be taken into account with the benefit of the increasing development of bioinks formation and bioprinting techniques. Furthermore, additional work on the mechanism of BPES is critical, to improve the understanding and its further development into in vivo applications. Overall, the work presented provides worthy information, which is especially significant and relevant to translational models of human infections, mental disorders diseases.

5.5 References

[1] A.M. Rajnicek, Z. Zhao, J. Moral-Vico, A.M. Cruz, C.D. McCaig, N. Casañ-Pastor, Controlling Nerve Growth with an Electric Field Induced Indirectly in Transparent Conductive Substrate Materials, Adv. Healthc. Mater. (2018). https://doi.org/10.1002/adhm.201800473.

[2] C. Qin, Z. Yue, Y. Chao, R.J. Forster, F. Maolmhuaidh, X.F. Huang, S. Beirne, G.G. Wallace, J. Chen, Bipolar electroactive conducting polymers for wireless cell stimulation, Appl. Mater. Today. 21 (2020). https://doi.org/10.1016/j.apmt.2020.100804.

[3] L. Zhang, B. Gupta, B. Goudeau, N. Mano, A. Kuhn, Wireless Electromechanical Readout of Chemical Information, J. Am. Chem. Soc. 140 (2018) 15501–15506. https://doi.org/10.1021/jacs.8b10072.

[4] Y.S. Hsiao, Y.H. Liao, H.L. Chen, P. Chen, F.C. Chen, Organic Photovoltaics and Bioelectrodes Providing Electrical Stimulation for PC12 Cell Differentiation and Neurite Outgrowth, ACS Appl. Mater. Interfaces. 8 (2016) 9275–9284. https://doi.org/10.1021/acsami.6b00916.

[5] P. Sanjuan-Alberte, F.J. Rawson, A. Jain, A. Shaw, S. Abayzeed, R. Rafael Fuentes Dominguez, M.E. Alea-Reyes, M. Clark, M.R. Alexander, R.J.M. Hague, L. Perez-Garcia, Wireless Nanobioelectronics for Electrical Intracellular Sensing, ACS Appl. Nano Mater. (2019). https://doi.org/10.1021/acsanm.9b01374.

[6] Z.A. Fattah, Applications of bipolar electrochemistry : from materials science to biological systems, 2013.

[7] L. Koefoed, S.U. Pedersen, K. Daasbjerg, Bipolar electrochemistry—A wireless approach for electrode reactions, Curr. Opin. Electrochem. 2 (2017) 13–17.

https://doi.org/10.1016/j.coelec.2017.02.001.

[8] R. Gao, Y.L. Ying, Y.X. Hu, Y.J. Li, Y.T. Long, Wireless Bipolar Nanopore Electrode for Single Small Molecule Detection, Anal. Chem. 89 (2017) 7382–7387. https://doi.org/10.1021/acs.analchem.7b00729.

[9] C. Qin, Z. Yue, Y. Chao, R.J. Forster, F. Maolmhuaidh, X.F. Huang, S. Beirne, G.G. Wallace, J. Chen, Data on the bipolar electroactive conducting polymers for wireless cell stimulation, Data Br. 33 (2020) 106406. https://doi.org/10.1016/j.apmt.2020.100804.

[10] and M.R.A. Pouria Fattahi , Guang Yang , Gloria Kim, A Review of Organic and Inorganic Biomaterials for Neural Interfaces, Adv. Mater. 24 (2018) 10300–10305. https://doi.org/10.1002/chem.201801499.

[11] P. Jastrzebska-Perfect, S. Chowdhury, G.D. Spyropoulos, Z. Zhao, C. Cea, J.N. Gelinas, D. Khodagholy, Translational Neuroelectronics, Adv. Funct. Mater. 30 (2020) 1–31. https://doi.org/10.1002/adfm.201909165.

[12] W. Zhang, G. Dong, H. Feng, S. Shan, L. Huang, F. Yuan, B. Bao, L. Yan, Z. Xia, T. Lawson, J. Chen, J. Qu, Y. Liu, Wearable Corneal Biosensors Fabricated from PEDOT Functionalized Sulfur-Doped Graphene for Use in the Early Detection of Myopia, Adv. Mater. Technol. 5 (2020) 1–7. https://doi.org/10.1002/admt.202000682.

[13] Y. Liu, S. Zhang, Y. Zhou, M.A. Buckingham, L. Aldous, P.C. Sherrell, G.G. Wallace, G. Ryder, S. Faisal, D.L. Officer, S. Beirne, J. Chen, Advanced Wearable Thermocells for Body Heat Harvesting, Adv. Energy Mater. 10 (2020) 1–10. https://doi.org/10.1002/aenm.202002539.

[14] S. Zhang, Y. Liu, J. Hao, G.G. Wallace, S. Beirne, J. Chen, 3D-Printed Wearable Electrochemical Energy Devices, Adv. Funct. Mater. 2103092 (2021) 1–33.

https://doi.org/10.1002/adfm.202103092.

[15] S. Inagi, Fabrication of gradient polymer surfaces using bipolar electrochemistry, Polym. J. 48 (2016) 39–44. https://doi.org/10.1038/pj.2015.73.

[16] Y. Ishiguro, S. Inagi, T. Fuchigami, Gradient doping of conducting polymer films by means of bipolar electrochemistry, Langmuir. 27 (2011) 7158–7162.

[17] Y. Wu, Y. Peng, H. Bohra, J. Zou, V.D. Ranjan, Y. Zhang, Q. Zhang, M. Wang, Photoconductive Micro/Nanoscale Interfaces of a Semiconducting Polymer for Wireless Stimulation of Neuron-Like Cells, ACS Appl. Mater. Interfaces. 11 (2019) 4833–4841. https://doi.org/10.1021/acsami.8b19631.

[18] L. Sordini, F.F.F. Garrudo, C.A. V. Rodrigues, R.J. Linhardt, J.M.S. Cabral, F.C. Ferreira, J. Morgado, Effect of Electrical Stimulation Conditions on Neural Stem Cells Differentiation on Cross-Linked PEDOT:PSS, Front. Bioeng. Biotechnol. 9 (2021) 1–13. https://doi.org/10.3389/fbioe.2021.591838.

[19] Y. Liu, B. Weng, J.M. Razal, Q. Xu, C. Zhao, Y. Hou, S. Seyedin, R. Jalili, G.G. Wallace, J. Chen, High-Performance Flexible All-Solid-State Supercapacitor from Large Free-Standing Graphene-PEDOT/PSS Films, Sci. Rep. 5 (2015) 17045. https://doi.org/10.1038/srep17045.

[20] D.G. Harman, R. Gorkin, L. Stevens, B. Thompson, K. Wagner, B. Weng, J.H.Y. Chung, M. In Het Panhuis, G.G. Wallace, Poly(3,4-ethylenedioxythiophene):dextran sulfate (PEDOT:DS) - A highly processable conductive organic biopolymer, Acta Biomater. 14 (2015) 33–42. https://doi.org/10.1016/j.actbio.2014.11.049.

[21] A. Inoue, H. Yuk, B. Lu, X. Zhao, Strong adhesion of wet conducting polymers on diverse substrates, Sci. Adv. 6 (2020) 1–11. https://doi.org/10.1126/sciadv.aay5394.

[22] X.F. Huang, X. Song, Effects of antipsychotic drugs on neurites relevant to schizophrenia treatment, Med. Res. Rev. 39 (2019) 386–403. https://doi.org/10.1002/med.21512.

[23] M. Hu, P. Zheng, Y. Xie, Z. Boz, Y. Yu, R. Tang, A. Jones, K. Zheng, X.F. Huang, Propionate protects haloperidol-induced neurite lesions mediated by neuropeptide Y, Front. Neurosci. 12 (2018) 1–10. https://doi.org/10.3389/fnins.2018.00743.

[24] Y. Huang, S. Tsubota, N. Nishio, Y. Takahashi, K. Kadomatsu, Combination of tumor necrosis factor-α and epidermal growth factor induces the adrenergic-to-mesenchymal transdifferentiation in SH-SY5Y neuroblastoma cells, Cancer Sci. 112 (2021) 715–724. https://doi.org/10.1111/cas.14760.

[25] Y. Shang, M. Liu, T. Wang, L. Wang, H. He, Y. Zhong, G. Qian, J. An, T. Zhu, X. Qiu, J. Shang, Y. Chen, Modifications of autophagy influenced the Alzheimer-like changes in SH-SY5Y cells promoted by ultrafine black carbon, Environ. Pollut. 246 (2019) 763–771. https://doi.org/10.1016/j.envpol.2018.12.080.

[26] H. Xicoy, B. Wieringa, G.J.M. Martens, The SH-SY5Y cell line in Parkinson's disease research: a systematic review, Mol. Neurodegener. 12 (2017) 1–11. https://doi.org/10.1186/s13024-017-0149-0.

Chapter 6

Conclusion and Perspectives

6.1 General conclusion

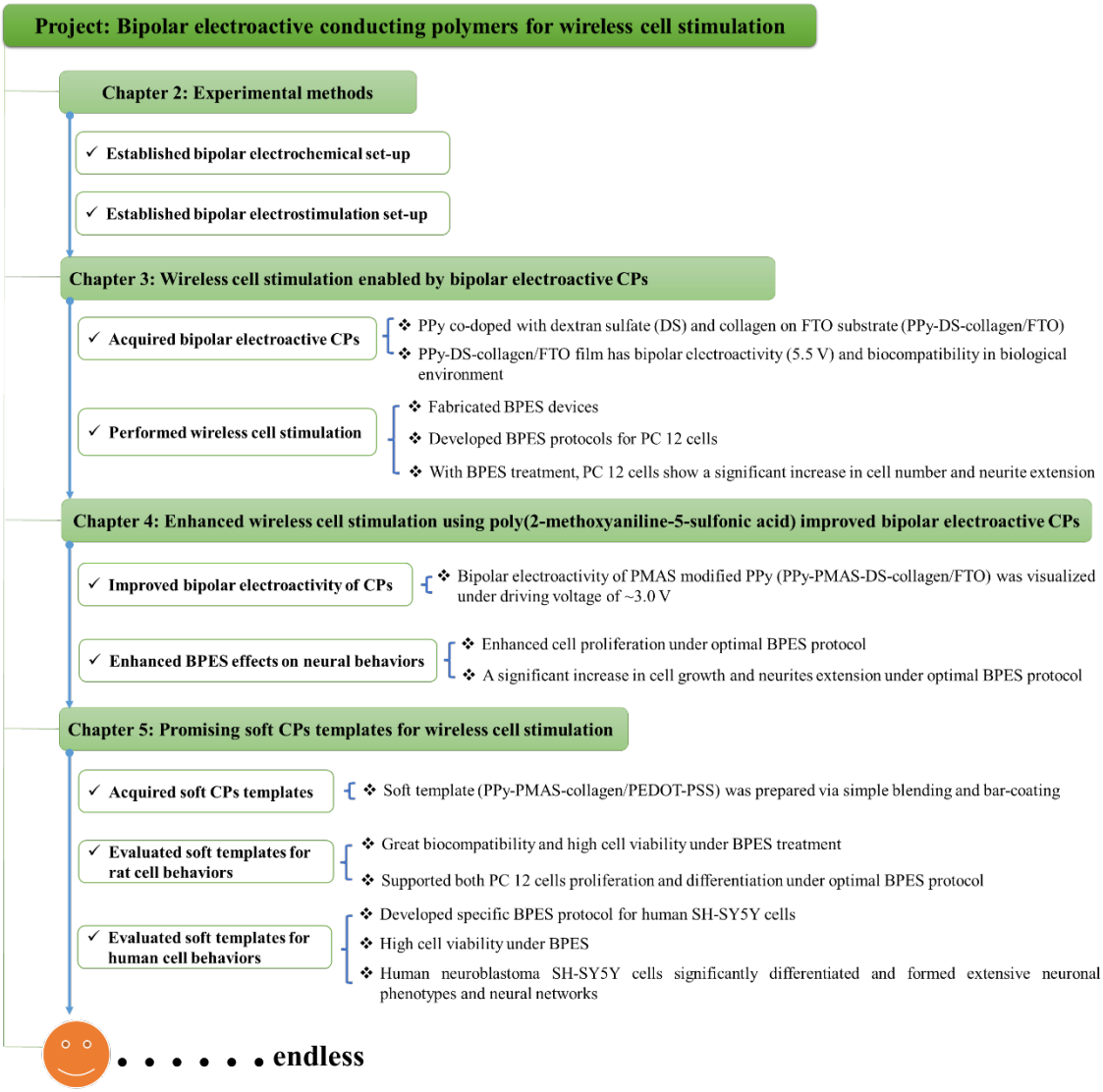

Figure 6.1 Illustration of Thesis outline and conclusions.

The thesis worked out and conclusions were generated step by step as demonstrated in below (Figure 6.1). This work includes synthesising, modifying, and characterising

bipolar electroactive, biocompatible conducting polymers (CPs: PPy-DS-collagen/FTO, PPy-PMAS-DS-collagen/FTO), extending to soft template (PPy-PMAS-collagen/PEDOT-PSS), and efficiently apply these CPs substrates for wireless PC 12 cells stimulation in combination of bipolar electrochemistry (BPE). Rapid and efficient nerve cell proliferation and differentiation were observed, displaying increased cell numbers, extensive neurites growth and network formation. Finally, soft, free-standing PPy-PMAS-collagen/PEDOT-PSS film was acquired and used in bipolar electrochemical stimulation (BPES) system for human SH-SY5Y cells differentiation. This will provide a degree of control hither to unattainable, which will greatly facilitate new opportunities for diagnosing and treating biomedical diseases with a new vision.

6.2 Perspectives

Although current work has many merits in wireless cell stimulation, there are still unavoidable weaknesses. First, the 2D structure of the CP film is different from the 3D structure of tissues and organs. Second, the entire CP-based BPES system is constrained in a 2D model, which is different from a 3D culture model, making it hard to completely mimic the native environment. Also, the soft CP-based BPES system on human cell stimulation should be investigated in more depth and expanded to *in vivo* application. Last but not the least, it is necessary to thoroughly comprehend the interfacing reactions of the cell-bipolar CP electrode and to totally standardize the CPs based BPES system. Together with such fundamental understanding, advances in bipolar electroactive CPs bioelectronics with engineering of various properties and design parameters will progress hand-in-hand with breakthroughs in material modification, thus boosting the refinement of the wireless BPES system, and eventually benefiting each other. The following section will focus on how to complete bipolar materials/devices

transformation elaborately and integrate BPES with 3D culture models with the help of advanced 3D bioprinting techniques and nanotechnologies.

6.2.1 Materials transformation

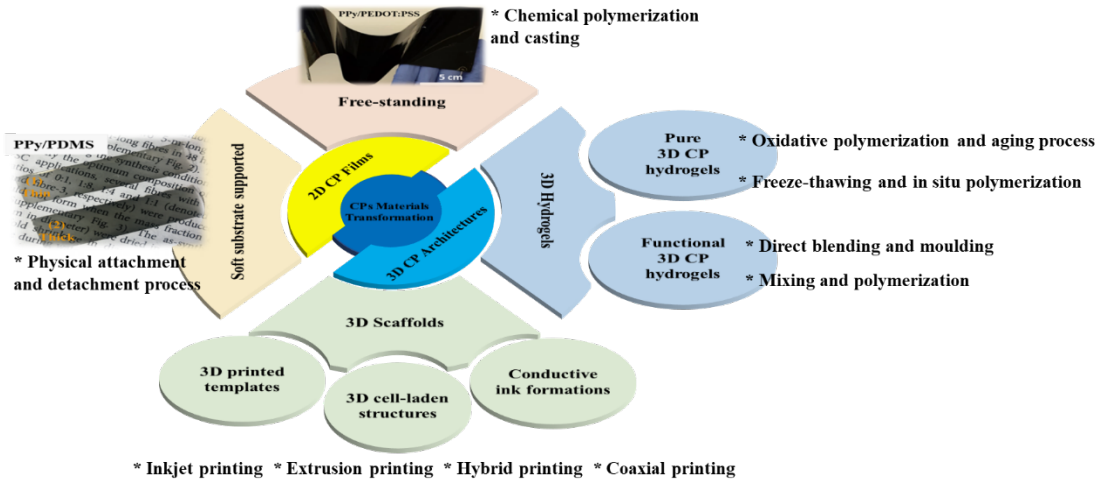

Figure 6.2 Overview of our proposed methods for bipolar electroactive CPs materials transformation.

6.2.1.1 Pure or functional/multifunctional 3D CPs hydrogels

Hydrogels have been commonly used to transfer 2D cell cultures to 3D models due to their ease of synthesis and flexibility in processing [1]. A kind of hydrogels prepared from natural polymers has seen a lot of use in tissue engineering over the past decade due to their safe nature, biocompatibility, hydrophilic properties, and biodegradable nature. Typically, the collagen type I, it has been demonstrated the ability to expand and differentiate into multiple neurons, astrocytes and oligodendrocytes with functional synapse and neuronal circuit formation under optimal cell density and collagen concentration [2,3]. Other naturally derived hydrogels, such as polysaccharide-based hydrogels (hyaluronic acid, alginate, chitosan, and cellulose) and DNA-based hydrogels

are inert biomaterials that can be tailored for 3D neural tissue engineering by varying composition and crosslink density [4]. As the field progresses dramatically, many researchers are looking for ways to address the concerns on inherent reproducibility and culture duration caused by naturally derived hydrogels [5]. Synthetic hydrogels have been created to modify natural ones, preserving the beneficial properties of the natural hydrogels while offering additional functionality [6,7]. One approach is to incorporate the specific biomolecules like growth factors for functionalization [8,9]. Others center around the use of tight control over chemical and physical cues based on different polymerisation methods that endows synthetic hydrogels with electrochemical, magnetoelectric, piezoelectric and thermoelectric properties, as well as better mechanical compatibility and structural tenability as well [10]. Previous work has investigated the effect of traditional ES on cell behaviour when cortical cells were cultured on PPy modified 3D interdigitated electrodes using 3D collagen culture medium (Figure 6.3A) [11,12]. This electroactive CP promotes neurite outgrowth and synaptogenesis in primary cortical neurons in 3D when compared to 2D, which more closely resembles the in vivo biological system and provides a possible diagnostic platform for neurite deficits in neurodevelopmental diseases. The use of synthetic CP hydrogels with chemical definition and controllable matrix has been extensively explored for neural tissue engineering [12-14].

The porous structures of hydrogels provide an opportunity to mechanical interlocking of hydrogel coatings. Pure CP hydrogels can have the interconnected networks using the volatile additive solvents into aqueous CP solutions, followed by controlled dry-annealing and rehydration, ensuring a low interfacial impedance because of the coexistence of ionic and electrical conduction [13,14]. This attributed to not only the

increased interfacial area, but also the numerous locked snap-fits at the microscale created. Deficient oxidative polymerisation of monomer followed by long-term aging allows electroconductive pure CP hydrogel to self-organize, and its mechanical and electrical properties are improved via second aging process for further aggregation formation [15]. While existing methods primarily add polymer monomer into other non-conductive 3D polymer architectures to create the supportive 3D bioarchitectures [16,17]. A porous PVA gel produced by the freeze-thawing method offers a valid ion channel for Py monomer and oxidant molecules penetration, as well as *in situ* polymerisation to form PPy in both external and internal PVA. Thus, 3D porous PPy/PVA could be proposed.

While the pure 3D CP hydrogels with high electronic conductivity, pure 3D CP with non-conducting polymer template hydrogels, like PPy/PVA hydrogels have been demonstrated superior biocompatibility, mechanical stability and elasticity, but poor electronic conductivity and volumetric capacitance after successfully synthesised using the self-assembly and addition of crosslinkable moieties. This is generated from the non-conducting polymer template (such as PVA architecture) component, which cannot be ineluctable to impact on electrical properties because of its inherently insulating character. To solve this restriction, more research into how to improve the electroactivity of CP is needed to be widely explored.

Incorporation of a sulfonated polyaniline, poly (2-methoxyaniline-5-sulfonic acid) (PMAS), as a dopant into PPy matrix previously produced a highly electroactive material with multiple redox centres [18,19]. This material is cytocompatible and effective in providing electrical stimulation to living cells [20,21]. Co-dopants are

proposed to be added in the form of biologically active protein like nerve growth factor (NGF) or polysaccharide, including collagen, alginate, ulvan, dextran sulfate or chondroitin sulfate. The formation of these compositions could be via *in situ* electrochemical oxidation of pyrrole in the presence of the sulfonated polyaniline and the bioactive polymer. In addition, selective in-growth of CPs into conductive metal or carbon hydrogel patterning to obtain high electroconductive implant electrodes have been applied in the field of bioelectronics [11,22]. Likewise, physical and chemical stimulus could be adopted in the same way to functionalize the CP hydrogels with incorporation of silver nanowires, gold nanoparticles, and carbon nanotubes etc. Composite 3D CP hydrogels with nanomaterials are capable of being applied in wireless ES system due to the endowed magnetoelectric, piezoelectric and optoelectric properties.

Except the electrochemical doping, direct blending of CPs power with other functional materials and moulding or mixing of polymer monomer with other functional materials and chemical oxidation polymerisation, both provide a straightforward and simple route to form functional/multifunctional 3D CP composite materials. For example, magnetic nanoparticles like Fe, Ni, Co, Gd, Er, CdTe and several oxide forms of them have demonstrated various paramagnetic and superparamagnetic properties, facile surface modification and biocompatibility, allowing them to become mostly promising candidates in biomedical fields like cellular therapy, drug delivery and magnetic resonance imaging (MRI) [23]. To make the magnetic nanoparticles exceptional bipolar electroactivity, they could be coated with bipolar active CP chemical vapor-phase polymerisation. With the electric and magnetic responsive CP-magnetic composites, researchers could apply external electric field, magnetic field, or/and both to activate the

wireless stimulation. The potential use of functional/multifunctional 3D CP composites in living beings should have turned true for investigating the bioimaging.

6.2.1.2 3D CP scaffolds/architectures via 3D printing

Similar to natural and synthetic hydrogels, diverse 3D scaffolds with mechanical and morphological stability and pore interconnectivity have been prepared with the benefit of bioprinting technique. The advancement of 3D printing technologies has opened up new possibilities to best integrate CPs with hydrogels in a spatially controlled manner, overcoming the limitations in conventional approaches for engineering electroactive biological systems. The umbrella term 3D printing refers to an array of technologies that involve automated distribution of (multi)materials in successive layers into predesigned 3D structures. Bioprinting deals with living cells and represents a special class of 3D printing. 3D printing improves our capability in engineering functional complex structures to meet the requirements for realising both physical and biological functions. An inventory of inks has been developed including electroactive inks for printing 3D scaffolds and biopolymer inks for printing various cell types. Examples include water-dispersible CPs for inkjet printing of conductive films and for extrusion printing of interdigitated microelectrodes, and the biodegradable composite ink, graphene/polycaprolactone, for fused filament fabrication [22,26,27]. For cell printing, 3D printed functional neural-tissue like structures have been demonstrated using polysaccharide-based bioinks (Figure 6.3B) [24,28,29]. The 3D printed structures support *in situ* expansion and differentiation of human neural stems, and differentiated neurons form synaptic contacts, establish networks, are spontaneously active [29]. Further developed co-axial and hybrid printing protocols that fabrication of complex cellular constructs are both mechanically robust and biologically optimised (Figure

6.3C) [25,30]. In addition, the development of 3D models of human brain has been tremendous progressed in tandem with the organoid technology that is largely a cell-driven, bottom-up approach [31].

Special attention is paid to pristine intrinsically CPs and their composites with other organic and inorganic components, well-defined micro- and nanostructures, and enhanced surface areas [32–34]. CP hydrogels have emerged as a promising material candidate for the next-generation bioelectronic interfaces, due to their similarities to biological tissues and versatility in electrical, mechanical, and biofunctional engineering [35]. Their porous structures and crosslinked polymer networks infiltrated with water, provide the space to mount the loading volume of chemical, biochemical and biological molecules. Moreover, their ease of tailor, structural tenability, and flexibility in processing allows various CP scaffolds formation with the help of 3D bioprinting techniques [36,37]. The soft and flexible nature of CP hydrogels, CP scaffolds ensures minimization of mechanical mismatch with biological tissues.[38] All these properties renders innovative CPs a one-of-a-kind link between the synthetic and biological worlds.

(A) 3D electrical stimulation on 3D primary cortical neuronal cultures

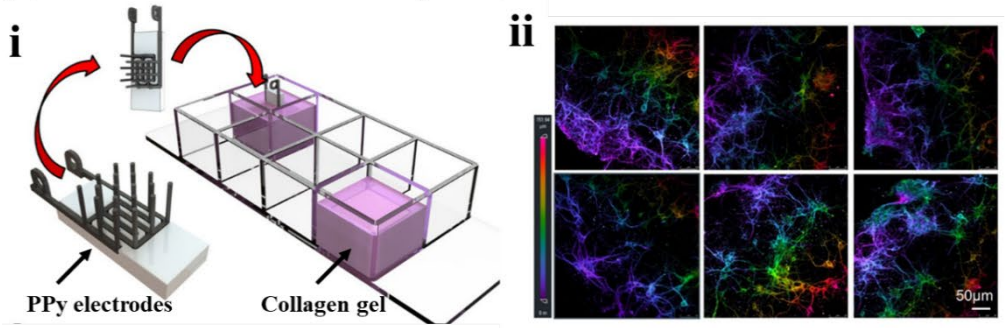

(B) Extrusion printed 3D cell-laden scaffolds

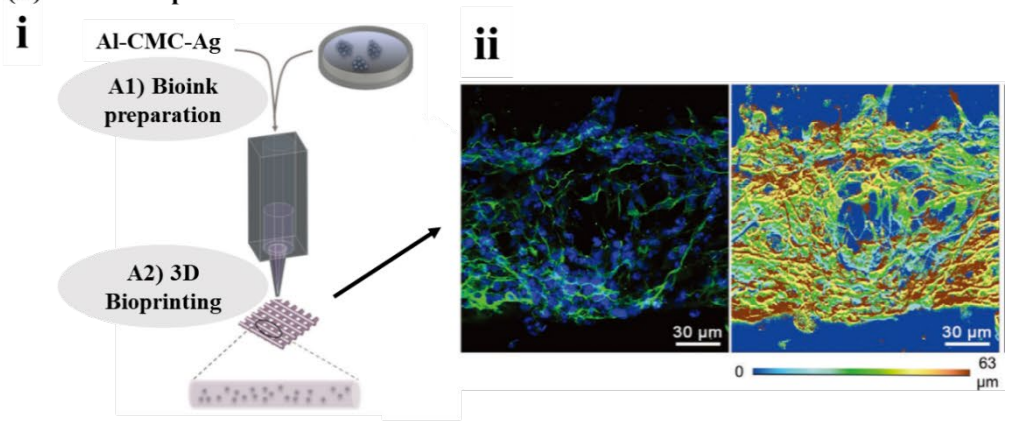

(C) Hybrid printing hydrogels for improved structural integration

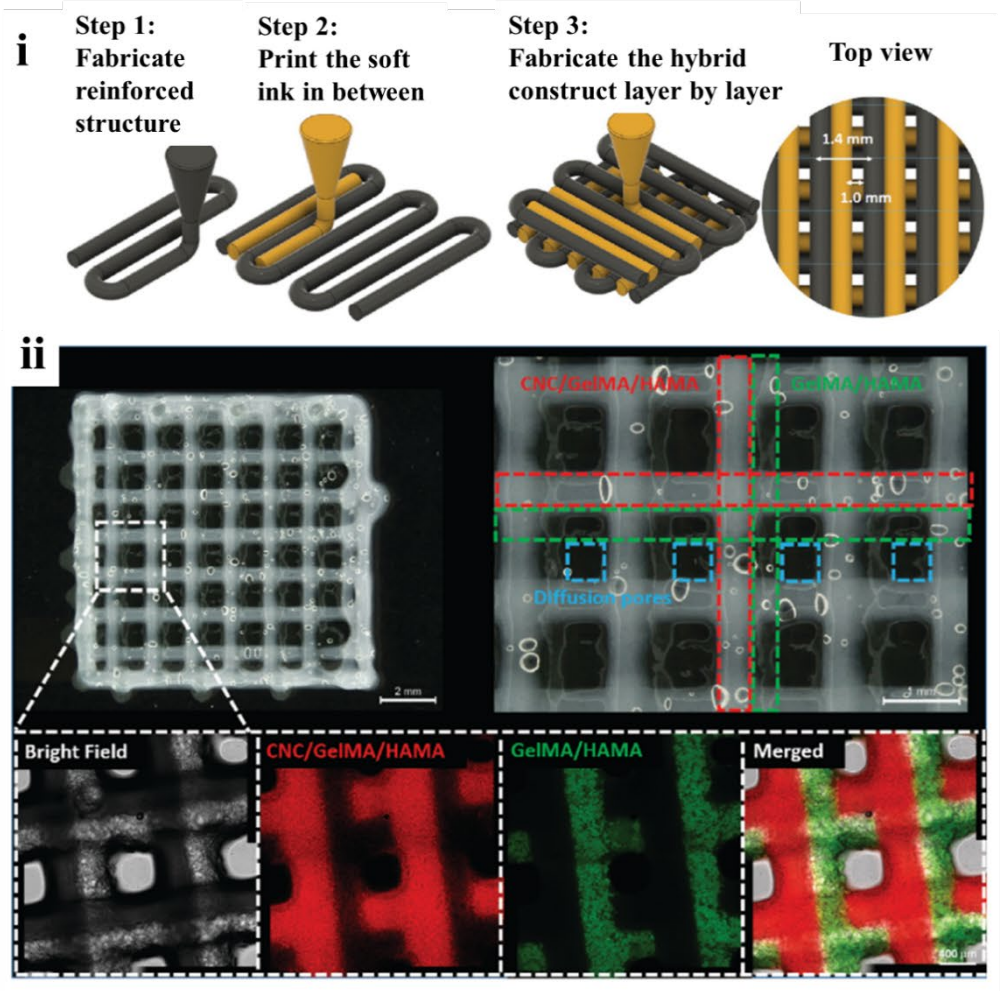

Figure 6.3 (A) 3D interdigitated electrical stimulation on 3D primary cortical neuronal cultures. (i) Schematic illustration of the 3D interdigitated electrodes and cell culture setup; (ii) 3D immunofluorescence images of the 3D primary neuronal cultures in collagen. Scale bar: 50 μm [11]. (B) Extrusion printed 3D induced pluripotent stem cells (iPSCs) laden scaffolds for 3D culture and differentiation. (i) Bioink is prepared by suspending iPSCs with clinically amenable polysaccharides alginate (Al, 5% w/v), carboxymethyl-chitosan (CMC, 5% w/v), and agarose (Ag, 1.5% w/v), followed by bioprinting and ionic-crosslinking for gelation. (ii) Immunophenotyping of 3D bioprinted human iPSCs 40 days postprinting including 30-37 day of neural induction and differentiation. Cells stained with DAPI and expressed pan-neuronal marker MAP2 revealing neural processes extending throughout constructs [24]. (C) Hybrid printing hydrogels for improved structural integration. (i) Illustration of the hybrid printing procedure. (ii) Optical and confocal microscopic observation of the hybrid printed construct. The structure fabricated by the cellulose nanocrystal (CNC) reinforced ink and gelatin methacryloyl and hyaluronic acid methacrylate (GelMA/HAMA) ink were defined in the optical microscopic image by red dotted lines and green dotted lines, respectively. The pores formed were defined by the blue dotted lines. Fluorescence in the confocal images comes from the fluorescence labeled GelMA in the CNC reinforced ink or GelMA/HAMA ink. Red: rhodamine-labeled GelMA; green: FITC-labeled GelMA [25].

Together with the rapid development of 3D bioprinting techniques, patterning of well-dispersed functional CPs composite represents a more spatially controlled strategy other than direct mixing or *in situ* polymerisation. Chemically induced polymerisation of the lead composition established above to form dispersions that are printable using

approaches similar to those developed by us previously for other ink formulations. Where appropriate, the effects of incorporating conductive constitute (such as PEDOT-PSS, edge functionalised graphene) and/or bioplymeric consitituent (such as alginate, gellan gum) as rheological modifier and/or binder to improve the viscosity and printability of conductive inks for extrusion printing should be examined, while retaining the bipolar electrochemical properties. The printability of the conductive inks could be characterised using a 3D-Bioplotter and following a method by Ouyang et al [39]. 3D cell-laden structures will be developed using the conductive inks developed in combination with innovative printing methods such as coaxial printing as described by us previously [40] with the conductor as the core in individually printed struts. Alternatively, a hybrid printing system as described by us previously [41] will be used to print the cell-laden components alongside the bipolar electroactive component. Besides, to design and fabricate bipolar electrochemically active 3D structures containing CP materials, 3D printed hydrogels, e.g., 3D printed gelatin or collagen methacryolyl (GelMA or ColMA) could be utilised to provide a 3D template. The CP compositions developed will be introduced into the 3D structures by means of physical adsorption followed by chemical polymerisation [6]. Lastly, a GelMA or ColMA macromer solution will be prepared and optimised for neural-related cell encapsulation, and then introduced to the said 3D conductive structure for wireless BPES.

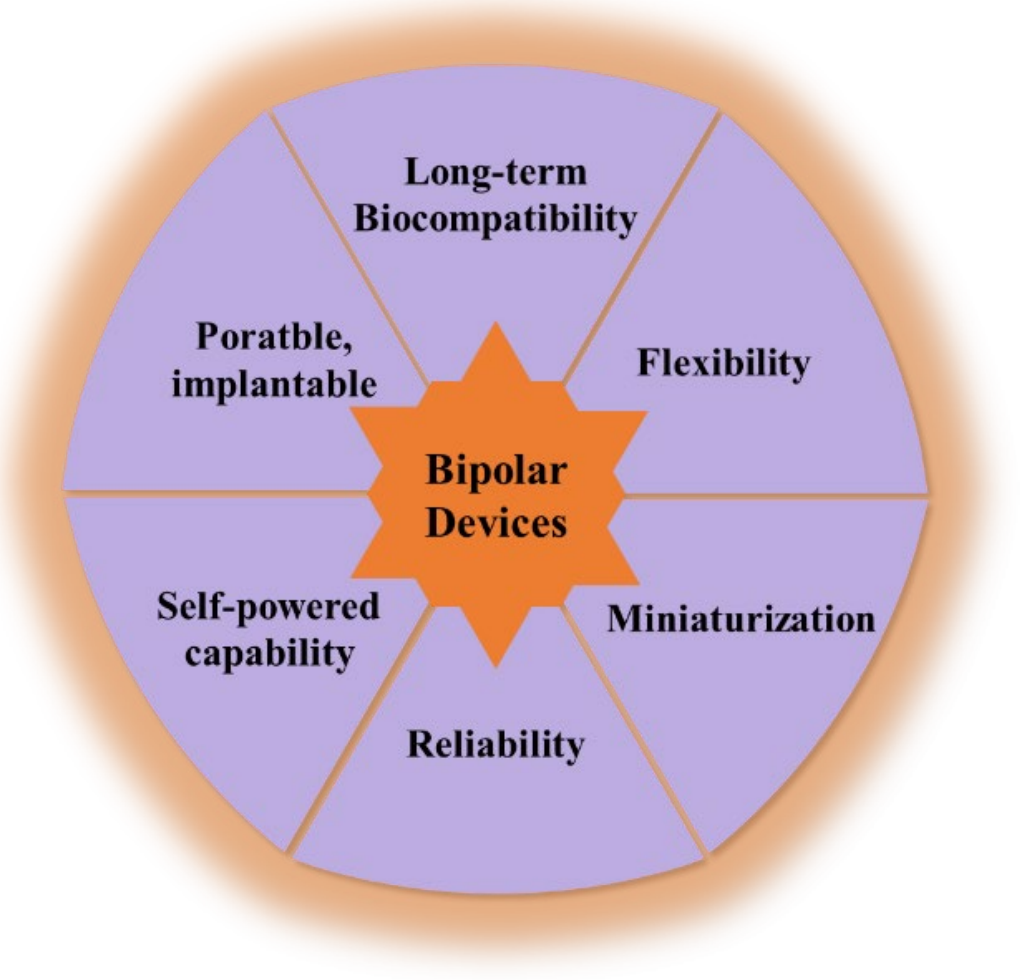

Figure 6.4 Overview of our proposed properties for bipolar devices.

6.2.2 Devices transformation

With the possibility of soft bipolar electroactive CPs materials that promote the BPES from *in vitro* to *in vivo* and even clinic, the bipolar devices (Figure 6.4) should adjust to match the applications. In modern electrical therapeutics, bipolar devices are of great necessity in long-term biocompatibility, flexibility, miniaturization, reliability, and self-powered capability. For implanted devices, maintaining a long-term biocompatibility is a critical issue. Generally, the long-term implantation would have chronic side effects such as inflammation due to long-time exposure to ES signals, toxicity because of

nanoscale or microscale debris from the device, biofouling on the device surface, and interference in normal organ functions [42]. So, gaining a better knowledge of them and improving their long-term biocompatibility, as well as minimizing the potential adverse effects become particular significant and urgent. Furthermore, attachment of big components to movable tissue surfaces during routine laboratory and clinic procedures may require stitches to secure the device and prevent migration under dynamic operating settings. It needs to be considered flexible and miniatured devices with reduced size and foldable shapes that can help to minimize invasiveness and alleviate discomfort in patients. Despite the fact that BPES devices are activated via wireless external field, the power source remains the key challenge for bipolar devices in terms of achieving maximum reduction and flexibility. Occasionally, package of tiny batteries will not be able to satisfy the long-time powering need. If the biomechanical energy could be harvested and converted appropriately and adequately, it would be an “infinite” energy source for powering the implanted devices. And it might be a creative way to deal with the problem.

6.2.3 Potential applications of 3D bipolar electroactive CP architectures based BPES

BPES systems combine bipolar electrochemistry with biology and constitute a unique and wireless tool with great potential in both the clinic and basic research. Despite the multiple challenges in their bipolar electroactive materials selection and modification, bipolar electrochemical devices design and fabrication due to the need to integrate expertise in cell culture, ES, and future translation and implantation, BPES systems offer numerous advantages over traditional wired or wireless ES systems and can translate into unique therapeutic opportunities (Figure 6.5). In the next section, we illustrate step by step and propose several examples that showcase the possibility in

advancing the state-of-art of various forms of bipolar electroactive CP electrodes used for integrated 3D BPES models.

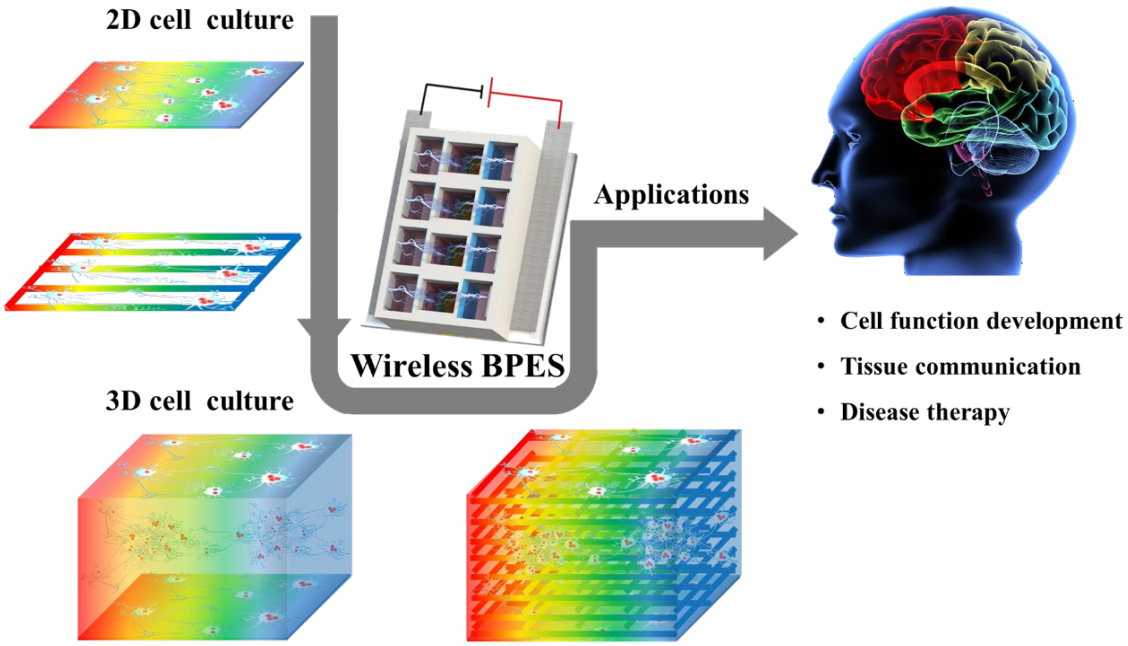

Figure 6.5 Prospects of future bipolar electroactive CPs architectures for wireless BPES towards practical applications.

6.2.3.1 Development of 3D wireless BPES protocols

To bring new concepts in BPES prototype, updated 3D wireless protocols should be developed not only in neural cell types PC 12, but also human neural stem cells, then primary cortical neurons obtained from normal and disease model mice (in wild-type and NRG1-KO mice). Key operational parameters, such as applied DC voltage under different continuous or pulse mode, will be optimised based on the BPES prototype that developed previously for wireless and programmable cell stimulation.[43,44] Three to five independent experiments in each BPES mode (for example, programmed pulse mode), will be conducted in parallel to comprehensively investigate cell functional

activities including proliferation, cell differentiation, cell migration, cell orientation and cell connectively over a period of one week in order to guarantee the accuracy of obtained experimental data. Specially, the effect of 3D electrical stimulation from 3D improved bipolar electroactive CPs electrodes on neurite outgrowth and synaptogenesis, and direction change should be explored from normal culture model to disease model. It is also needed to compare the differential effect of 3D electrical stimulation not only between 2D and 3D cell culture models, but also between wireless 3D BPES and wired 3D ES systems.

6.2.3.2 Studies on synergistic effects of 3D BPES with growth factors

Sustained neurotrophic support at the site of implanted electrodes is essential to maintain intimate interaction between electrode and cells. The incorporation of growth factors such as neurotrophins (NT3) or brain-derived neurotrophic factor (BDNF) in 2D have been identified previously that they can further amplify the effects of electrical stimulation, using spiral ganglion neuron (SGN) explants from rat cochleae [9]. Furthermore, a synergistic effect of delivering both NT-3 and BDNF simultaneously has shown to encourage neurite outgrowth of the cochlear neural explants [45]. In preliminary experiments each of the growth factors will be introduced into the gel environment immediately prior to electrical stimulation. Then to investigate the effect of sustained release of growth factors into the gel, they will first be encapsulated in micro gels to be injected into the gel, after the cell proliferation period. The masses of growth factors incorporated and released from the 3D CPs matrix could be calculated using the specific activity of the radiolabeling. Afterwards, bipolar electroactive 3D CPs matrix contained optimised volume of growth factors are subjected to electrical stimulation for wireless cell stimulation according to the above mentioned and verified 3D BPES

protocols. In this study, the multiplex, synergistic effect of 3D BPES with spatial and temporal presentation of growth factors on neuron survival and neurogenesis will be investigated. Comprehensive and statistical data that are qualitatively and quantitatively tracked and acquired using IncuCyte technology, immunofluorescence staining, and molecular biology techniques. This study will provide the feedback into the previous steps for further improvements in the design of the different kinds of wireless biomedical systems. For instance, it has the potential to be used as a treatment for traumatic nerve injury via delivery of compounds to the peripheral nervous system.

6.2.3.3 Design of wearable, implantable 3D BPES device

Given their outstanding advantages of flexible stretchable and biocompatible properties, wearable bioelectronic devices have been investigated in many biomedical applications from biophysical signals and biochemical analytes detection to specific closed-loop drug delivery, electrotherapy nerve recovery and tissue engineering. Progress in structures of wearable bioelectronics devices has enabled self-powered systems to achieve long-term continuous biomedical therapy chronic diseases. Recently, Yao et al present a triboelectric nanogenerators (TENGs)-activated ES device that can effectively treat alopecia [46]. This wearable device depends on an omnidirectional TENG to generate the electric pulse and a pair of interdigitated dressing electrodes to provide spatially distributed electrical fields. Such self-powered wearable ES could serve as an effective hair regeneration strategy without any known adverse side effects. Functional CP composites can be printed to construct such interdigitated dressing electrodes due to the ease of tailoring and flexibility of processing. Moreover, it is effortless to propel these interdigitated CP electrodes remotely because of the bipolar activity under lower driving voltage by means of bipolar electrochemistry. Thus, a wearable BPES patch

could be applied to external injury to stimulate cell proliferation and differentiation in field of wound healing.

Comparable to the development of wearable and portable BPES devices for onsite therapy, the implantable devices have been gone after indispensable medical purpose synchronously. Specifically, the implantable devices have played a dramatic role in drug delivery systems (DDS) that are externally triggered to localized and controlled release drugs, which hold considerable promise for improving the treatment of many diseases by minimizing nonspecific toxicity and enhancing the efficacy of therapy. In a recently notable study [47], researchers have devised such a drug delivery device that is wirelessly controlled and bioresorbable. Electrochemically triggered crevice corrosion to activate valves to open to allow release of pre-stored drugs. Evaluations in the treatment of cancerous tissues by release of the drug doxorubicin in cell cultures and the control of blood glucose levels by timed delivery of insulin in live-animal models, have completely demonstrated the efficacy of this implantable drug delivery device. Therefore, we envisage the bipolar electroactive, bioresorbable and biodegradable CP composites could be the entrapment matrix used for drug loading and storage. And moreover, in BPES operation process, the redox capability of the charging/discharging promote the uptake or expulsion of drugs from the CP backbone, accompanying mechanical expansion and contraction of the polymer matrix itself. It is concluded that the implantable 3D CP-based BPES systems hold great promise in drug delivery where the dose can be adjusted through external stimulus, thus optimising benefit to side effect ratio while simultaneously ensuring patient adherence.

6.3 Conclusion

Overall, besides taking advantage of wireless nature of bipolar electrochemistry, BPES models benefit from the electrical conductivity, useful mechanical, optical and biological properties as well as good environmental stability of CPs. CP-based BPES system offers opportunities to modulate the biological activities remotely, which builds up a better understanding of the effects of wireless stimuli on cell behaviour, including ES applied to cells via electrochemical changes in the bipolar electroactive CP. To date, such models in this direction are confined to a very new field, with no attempts made yet (to best of our knowledge) to manipulate physical and chemical stimuli with bipolar electrochemistry. Thus, it is necessary to gain knowledge of cell state with spatial resolution inside the 3D construct to develop new concepts for nonplanar platforms. Going forward, the integration with the nonnegligible advent of 3D printing technology for fabrication of scaffolds with/without living cells with a predesigned geometry also provides a simple and versatile route to build up various types of 3D CP-based BPES devices, as well as facilitate the biological integration of the cells and organs at the device fabrication stage. The bioengineering of CP composites compatible with additive manufacturing techniques provide new opportunities to make the integrated 3D CP-based BPES models become one of the flourishing next-generation bioelectronic devices as they should ideally have integrated, wearable, portable, implantable, miniaturized, and self-powered to eliminate the need for an external power supply and bulky wires. Therefore, the soft and flexible CP-based BPES systems are now showing tremendous potential in terms of revolutionizing electroceutical therapeutics through a novel wireless ES manner. As long as fully addressing the limitations/challenges, this technology is foreseeable to transform the developments in the fields of biomaterials, biomedical engineering and particularly electrotherapy with a bright future.

6.4 Reference

[1] S.S.D. Carter, X. Liu, Z. Yue, G.G. Wallace, Three-dimensional neuronal cell culture: In pursuit of novel treatments for neurodegenerative disease, MRS Commun. 7 (2017) 320–331. https://doi.org/10.1557/mrc.2017.96.

[2] A. Sorushanova, L.M. Delgado, Z. Wu, N. Shologu, A. Kshirsagar, R. Raghunath, A.M. Mullen, Y. Bayon, A. Pandit, M. Raghunath, D.I. Zeugolis, The Collagen Suprafamily: From Biosynthesis to Advanced Biomaterial Development, Adv. Mater. 31 (2019) 1–39. https://doi.org/10.1002/adma.201801651.

[3] Z. Yue, X. Liu, P.J. Molino, G.G. Wallace, Bio-functionalisation of polydimethylsiloxane with hyaluronic acid and hyaluronic acid - Collagen conjugate for neural interfacing, Biomaterials. 32 (2011) 4714–4724. https://doi.org/10.1016/j.biomaterials.2011.03.032.

[4] Z. Shi, X. Gao, M.W. Ullah, S. Li, Q. Wang, G. Yang, Electroconductive natural polymer-based hydrogels, Biomaterials. 111 (2016) 40–54. https://doi.org/10.1016/j.biomaterials.2016.09.020.

[5] Q. Shi, H. Liu, D. Tang, Y. Li, X.J. Li, F. Xu, Bioactuators based on stimulus-responsive hydrogels and their emerging biomedical applications, NPG Asia Mater. 11 (2019). https://doi.org/10.1038/s41427-019-0165-3.

[6] C. Wang, S.S. Rubakhin, M.J. Enright, J. V. Sweedler, R.G. Nuzzo, 3D Particle-Free Printing of Biocompatible Conductive Hydrogel Platforms for Neuron Growth and Electrophysiological Recording, Adv. Funct. Mater. 2010246 (2021) 1–10. https://doi.org/10.1002/adfm.202010246.

[7] S. Vandghanooni, M. Eskandani, Electrically conductive biomaterials based on natural polysaccharides : Challenges and applications in tissue engineering, Int. J.

Biol. Macromol. 141 (2019) 636–662. https://doi.org/10.1016/j.ijbiomac.2019.09.020.

[8] X. Liu, Z. Yue, M.J. Higgins, G.G. Wallace, Conducting polymers with immobilised fibrillar collagen for enhanced neural interfacing, Biomaterials. 32 (2011) 7309–7317. https://doi.org/10.1016/j.biomaterials.2011.06.047.

[9] R.T. Richardson, B. Thompson, S. Moulton, C. Newbold, M.G. Lum, A. Cameron, G. Wallace, R. Kapsa, G. Clark, S. O'Leary, The effect of polypyrrole with incorporated neurotrophin-3 on the promotion of neurite outgrowth from auditory neurons, Biomaterials. 28 (2007) 513–523. https://doi.org/10.1016/j.biomaterials.2006.09.008.

[10] H. Palza, P.A. Zapata, C. Angulo-pineda, Electroactive Smart Polymers for Biomedical Applications, Materials (Basel). 12 (2019) 227.

[11] Q. Zhang, S. Beirne, K. Shu, D. Esrafilzadeh, X.F. Huang, G.G. Wallace, Electrical Stimulation with a Conductive Polymer Promotes Neurite Outgrowth and Synaptogenesis in Primary Cortical Neurons, Sci. Rep. 8 (2018) 1–10. https://doi.org/10.1038/s41598-018-27784-5.

[12] Q. Zhang, D. Esrafilzadeh, J.M. Crook, R. Kapsa, E.M. Stewart, E. Tomaskovic-Crook, G.G. Wallace, X.F. Huang, Electrical stimulation using conductive polymer polypyrrole counters reduced neurite outgrowth of primary prefrontal cortical neurons from NRG1-KO and DISC1-LI mice, Sci. Rep. 7 (2017) 1–8. https://doi.org/10.1038/srep42525.

[13] B. Lu, H. Yuk, S. Lin, N. Jian, K. Qu, J. Xu, X. Zhao, Pure PEDOT:PSS hydrogels, Nat. Commun. 10 (2019). https://doi.org/10.1038/s41467-019-09003-5.

[14] D.G. Harman, R. Gorkin, L. Stevens, B. Thompson, K. Wagner, B. Weng, J.H.Y.

Chung, M. In Het Panhuis, G.G. Wallace, Poly(3,4-ethylenedioxythiophene):dextran sulfate (PEDOT:DS) - A highly processable conductive organic biopolymer, Acta Biomater. 14 (2015) 33–42. https://doi.org/10.1016/j.actbio.2014.11.049.

[15] C. Yu, C. Wang, X. Liu, X. Jia, S. Naficy, K. Shu, M. Forsyth, G.G. Wallace, A Cytocompatible Robust Hybrid Conducting Polymer Hydrogel for Use in a Magnesium Battery, Adv. Mater. 28 (2016) 9349–9355. https://doi.org/10.1002/adma.201601755.

[16] Y. Fang, L. Meng, A. Prominski, E.N. Schaumann, M. Seebald, B. Tian, Recent advances in bioelectronics chemistry, Chem. Soc. Rev. 49 (2020) 7978–8035. https://doi.org/10.1039/d0cs00333f.

[17] Y. Lu, Y. Wang, J. Zhang, X. Hu, Z. Yang, Y. Guo, Y. Wang, In-situ doping of a conductive hydrogel with low protein absorption and bacterial adhesion for electrical stimulation of chronic wounds, Acta Biomater. 89 (2019) 217–226. https://doi.org/10.1016/j.actbio.2019.03.018.

[18] S. Little, S.F. Ralph, C.O. Too, G.G. Wallace, Solvent dependence of electrochromic behaviour of polypyrrole: Rediscovering the effect of molecular oxygen, Synth. Met. 159 (2009) 1950–1955.

[19] Y. Yang, C. Wang, S. Ashraf, G.G. Wallace, Polypyrrole doped with redox-active poly(2-methoxyaniline-5-sulfonic acid) for lithium secondary batteries, RSC Adv. 3 (2013) 5447–5452. https://doi.org/10.1039/c3ra40406d.

[20] X. Liu, K.J. Gilmore, S.E. Moulton, G.G. Wallace, Electrical stimulation promotes nerve cell differentiation on polypyrrole/poly (2-methoxy-5 aniline sulfonic acid) composites, J. Neural Eng. 6 (2009) 65002.

[21] K.J. Gilmore, M. Kita, Y. Han, A. Gelmi, M.J. Higgins, S.E. Moulton, G.M.

Clark, R. Kapsa, G.G. Wallace, Skeletal muscle cell proliferation and differentiation on polypyrrole substrates doped with extracellular matrix components, Biomaterials. 30 (2009) 5292–5304. https://doi.org/10.1016/j.biomaterials.2009.06.059.

[22] C.Y. Lee, S. Sayyar, P.J. Molino, G.G. Wallace, A robust 3D printed multilayer conductive graphene/polycaprolactone composite electrode, Mater. Chem. Front. 4 (2020) 1664–1670. https://doi.org/10.1039/c9qm00780f.

[23] M.G. Christiansen, A.W. Senko, P. Anikeeva, Magnetic Strategies for Nervous System Control, Annu. Rev. Neurosci. 42 (2019) 271–293. https://doi.org/10.1146/annurev-neuro-070918-050241.

[24] Q. Gu, E. Tomaskovic-Crook, G.G. Wallace, J.M. Crook, 3D Bioprinting Human Induced Pluripotent Stem Cell Constructs for In Situ Cell Proliferation and Successive Multilineage Differentiation, Adv. Healthc. Mater. 6 (2017) 1–11. https://doi.org/10.1002/adhm.201700175.

[25] Y. Fan, Z. Yue, E. Lucarelli, G.G. Wallace, Hybrid Printing Using Cellulose Nanocrystals Reinforced GelMA/HAMA Hydrogels for Improved Structural Integration, Adv. Healthc. Mater. 9 (2020) 1–11. https://doi.org/10.1002/adhm.202001410.

[26] B. Weng, X. Liu, M.J. Higgins, R. Shepherd, G. Wallace, Fabrication and characterization of cytocompatible polypyrrole films inkjet printed from nanoformulations cytocompatible, inkjet-printed polypyrrole films, Small. 7 (2011) 3434–3438. https://doi.org/10.1002/smll.201101491.

[27] Y. Liu, B. Zhang, Q. Xu, Y. Hou, S. Seyedin, S. Qin, G.G. Wallace, S. Beirne, J.M. Razal, J. Chen, Development of Graphene Oxide/Polyaniline Inks for High Performance Flexible Microsupercapacitors via Extrusion Printing, Adv. Funct.

Mater. 28 (2018) 1–12. https://doi.org/10.1002/adfm.201706592.

[28] R. Lozano, L. Stevens, B.C. Thompson, K.J. Gilmore, R. Gorkin, E.M. Stewart, M. in het Panhuis, M. Romero-Ortega, G.G. Wallace, 3D printing of layered brain-like structures using peptide modified gellan gum substrates, Biomaterials. 67 (2015) 264–273. https://doi.org/10.1016/j.biomaterials.2015.07.022.

[29] Q. Gu, E. Tomaskovic-Crook, R. Lozano, Y. Chen, R.M. Kapsa, Q. Zhou, G.G. Wallace, J.M. Crook, Functional 3D Neural Mini-Tissues from Printed Gel-Based Bioink and Human Neural Stem Cells, Adv. Healthc. Mater. 5 (2016) 1429–1438. https://doi.org/10.1002/adhm.201600095.

[30] C.D. O'Connell, S. Konate, C. Onofrillo, R. Kapsa, C. Baker, S. Duchi, T. Eekel, Z. Yue, S. Beirne, G. Barnsley, C. Di Bella, P.F. Choong, G.G. Wallace, Free-form co-axial bioprinting of a gelatin methacryloyl bio-ink by direct in situ photo-crosslinking during extrusion, Bioprinting. 19 (2020) e00087. https://doi.org/10.1016/j.bprint.2020.e00087.

[31] M.L. Lovett, T.J.F. Nieland, Y.T.L. Dingle, D.L. Kaplan, Innovations in 3D Tissue Models of Human Brain Physiology and Diseases, Adv. Funct. Mater. 30 (2020) 1–27. https://doi.org/10.1002/adfm.201909146.

[32] R. Ravichandran, S. Sundarrajan, J.R. Venugopal, S. Mukherjee, S. Ramakrishna, Applications of conducting polymers and their issues in biomedical engineering, J. R. Soc. Interface. 7 (2010). https://doi.org/10.1098/rsif.2010.0120.focus.

[33] Y. Liu, P. Yin, J. Chen, B. Cui, C. Zhang, F. Wu, Conducting Polymer-Based Composite Materials for Therapeutic Implantations: From Advanced Drug Delivery System to Minimally Invasive Electronics, Int. J. Polym. Sci. 2020 (2020). https://doi.org/10.1155/2020/5659682.

[34] S.S. Nair, S.K. Mishra, D. Kumar, Recent progress in conductive polymeric

materials for biomedical applications, Polym. Adv. Technol. 30 (2019) 2932–2953. https://doi.org/10.1002/pat.4725.

[35] D. Ohayon, S. Inal, Organic Bioelectronics: From Functional Materials to Next-Generation Devices and Power Sources, Adv. Mater. 32 (2020) 1–29. https://doi.org/10.1002/adma.202001439.

[36] B. Weng, J. Diao, Q. Xu, Y. Liu, C. Li, A. Ding, J. Chen, Bio-Interface of Conducting Polymer-Based Materials for Neuroregeneration, Adv. Mater. Interfaces. (2015). https://doi.org/10.1002/admi.201500059.

[37] C. Puckert, E. Tomaskovic-Crook, S. Gambhir, G.G. Wallace, J.M. Crook, M.J. Higgins, Electro-mechano responsive properties of gelatin methacrylate (GelMA) hydrogel on conducting polymer electrodes quantified using atomic force microscopy, Soft Matter. 13 (2017) 4761–4772. https://doi.org/10.1039/c7sm00335h.

[38] E. Zeglio, A.L. Rutz, T.E. Winkler, G.G. Malliaras, A. Herland, Conjugated Polymers for Assessing and Controlling Biological Functions, Adv. Mater. 31 (2019). https://doi.org/10.1002/adma.201806712.

[39] L. Ouyang, R. Yao, Y. Zhao, W. Sun, Effect of bioink properties on printability and cell viability for 3D bioplotting of embryonic stem cells, Biofabrication. 8 (2016). https://doi.org/10.1088/1758-5090/8/3/035020.

[40] X. Liu, S.S.D. Carter, M.J. Renes, J. Kim, D.M. Rojas-Canales, D. Penko, C. Angus, S. Beirne, C.J. Drogemuller, Z. Yue, P.T. Coates, G.G. Wallace, Development of a Coaxial 3D Printing Platform for Biofabrication of Implantable Islet-Containing Constructs, Adv. Healthc. Mater. 8 (2019) 1–12. https://doi.org/10.1002/adhm.201801181.

[41] J.H.Y. Chung, J.C. Kade, A. Jeiranikhameneh, K. Ruberu, P. Mukherjee, Z. Yue,

G.G. Wallace, 3D hybrid printing platform for auricular cartilage reconstruction, Biomed. Phys. Eng. Express. 6 (2020). https://doi.org/10.1088/2057-1976/ab54a7.

[42] Y. Long, J. Li, F. Yang, J. Wang, X. Wang, Wearable and Implantable Electroceuticals for Therapeutic Electrostimulations, Adv. Sci. 2004023 (2021) 1–22. https://doi.org/10.1002/advs.202004023.

[43] C. Qin, Z. Yue, Y. Chao, R.J. Forster, F. Maolmhuaidh, X.F. Huang, S. Beirne, G.G. Wallace, J. Chen, Bipolar electroactive conducting polymers for wireless cell stimulation, Appl. Mater. Today. 21 (2020). https://doi.org/10.1016/j.apmt.2020.100804.

[44] C. Qin, Z. Yue, Y. Chao, R.J. Forster, F. Maolmhuaidh, X.F. Huang, S. Beirne, G.G. Wallace, J. Chen, Data on the bipolar electroactive conducting polymers for wireless cell stimulation, Data Br. 33 (2020) 106406. https://doi.org/10.1016/j.apmt.2020.100804.

[45] B.C. Thompson, R.T. Richardson, S.E. Moulton, A.J. Evans, S. O'Leary, G.M. Clark, G.G. Wallace, Conducting polymers, dual neurotrophins and pulsed electrical stimulation - Dramatic effects on neurite outgrowth, J. Control. Release. 141 (2010) 161–167. https://doi.org/10.1016/j.jconrel.2009.09.016.

[46] G. Yao, D. Jiang, J. Li, L. Kang, S. Chen, Y. Long, Y. Wang, P. Huang, Y. Lin, W. Cai, X. Wang, Self-Activated Electrical Stimulation for Effective Hair Regeneration via a Wearable Omnidirectional Pulse Generator, ACS Nano. 13 (2019) 12345–12356. https://doi.org/10.1021/acsnano.9b03912.

[47] J. Koo, S.B. Kim, Y.S. Choi, Z. Xie, A.J. Bandodkar, J. Khalifeh, Y. Yan, H. Kim, M.K. Pezhouh, K. Doty, G. Lee, Y.Y. Chen, S.M. Lee, D. D'Andrea, K. Jung, K.H. Lee, K. Li, S. Jo, H. Wang, J.H. Kim, J. Kim, S.G. Choi, W.J. Jang,

Y.S. Oh, I. Park, S.S. Kwak, J.H. Park, D. Hong, X. Feng, C.H. Lee, A. Banks, C. Leal, H.M. Lee, Y. Huang, C.K. Franz, W.Z. Ray, M. MacEwan, S.K. Kang, J.A. Rogers, Wirelessly controlled, bioresorbable drug delivery device with active valves that exploit electrochemically triggered crevice corrosion, Sci. Adv. 6 (2020). https://doi.org/10.1126/sciadv.abb1093.